The magnetocrystalline anisotropy of dysprosium and terbium-scandium alloys

Welford, J.

THE MAGNETOCRYSTALLINE ANISOTROPY OF DYSPROSIUM AND TERBIUM-SCANDIUM ALLOYS

by

J. Welford, B.Sc.

Presented in Candidature for the Degree of

Doctor of Philosophy

May 1974

Table of Contents

	Page
Table of Contents	i
Abstract	v
List of Tables and Illustrations	vi
CHAPTER 1 - INTRODUCTION	
1.1 Aims of this Investigation	1
1.2 Some Basic Properties of the Rare Earths, Yttrium and Scandium	1
1.2.1 Electronic Structures	2
1.2.2 Ionic and Atomic Magnetic Moments	3
1.2.3 Crystal Structures	4
1.2.4 Ionic Dimensions	6
1.2.5 Alloying Properties	6
CHAPTER 2 - SOME BASIC CONCEPTS AND DEFINITIONS	
2.1 Units	8
2.2 Varieties of Magnetic Behaviour	10
2.2.1 Diamagnetism	10
2.2.2 Paramagnetism	11
2.2.3 Ferromagnetism	14
2.2.4 Antiferromagnetism	17
2.2.5 Ferrimagnetism	18
2.2.6 Helical Antiferromagnetism	19
2.2.7 Metamagnetism	20
2.3 Demagnetising Fields	22
2.3.1 The Use of Demagnetisation Factors in Reading Magnetisation Curves	22
CHAPTER 3 - MAGNETOCRYSTALLINE ANISOTROPY	
3.1 Anisotropy Energy	24
3.2 Expressions for the Anisotropy Energy	25
3.3 Origins of Magnetocrystalline Anisotropy	27
3.3.1 The Two-Ion Model	28
3.3.2 The One-Ion Model	30
3.4 Magnetostriction and its Contribution to Magnetocrystalline Anisotropy	32
3.5 Variation of Anisotropy with Temperature	37
3.5.1 Qualitative Discussion	37
3.5.2 Temperature Variation of Anisotropy of Single-Ion Origin	39
3.5.3 Temperature Variation of Anisotropy of Two-Ion Origin	42

3.6 Variation of Magnetostriction with Temperature 46

3.7 Temperature Variation of Magnetostriction or Anisotropy as an Indication of the Fundamental Mechanism Involved 47

CHAPTER 4 - MAGNETIC ORDERING IN THE RARE EARTHS

4.1 Varieties of Magnetic Ordering in the Rare Earth Metals 48

4.2 Interactions Causing Magnetic Ordering 49

4.2.1 Indirect Exchange 49

4.2.2 The Effect of Magnetostriction and Magneto-crystalline Anisotropy on Magnetic Ordering in the Heavy Rare Earths 53

4.3 Anisotropy and Related Measurements in Terbium 56

4.4 Anisotropy and Related Measurements in Dysprosium 59

4.5 The Effects on the Magnetic Orderings of Heavy Rare Earths of Alloying with Yttrium 61

4.6 The Effects on the Magnetic Ordering of Heavy Rare Earths of Alloying with Scandium 63

CHAPTER 5 - METHODS OF DETERMINING ANISOTROPY CONSTANTS

5.1 Anisotropy Constants from Magnetisation Curves 66

5.2 Anisotropy Constants from Torque Measurements 67

5.3 Anisotropy Studies Using Ferromagnetic Resonance 71

5.4 Anisotropy Studies Using Inelastic Neutron Scattering 74

5.5 Other Methods of Measuring Anisotropy Energy 74

5.6 Choice of Method of Determining Anisotropy Constants 75

CHAPTER 6 - THE APPARATUS

6.1 General Description and Principles of Operation 76

6.2 The Crystal Specimens 79

6.3 Setting up the Apparatus 79

6.3.1 Etching and Mounting the Crystal Specimens 79

6.3.2 Orientation of the Crystals on the Magnetometer 81

6.3.3 Replacement and Adjustment of the Suspension 82

6.4 Further Details of the Apparatus and its Use 85

6.4.1 Temperature Control and Measurement 85

6.4.2 The Optical System 86

6.4.3 The Amplifier 87

6.4.4 Arrangements for Automatic Recording 89

6.4.5 The Electromagnet 90

6.5 Stability Considerations in the Design of the Magnetometer 92

CHAPTER 7 - CALIBRATION OF THE MAGNETOMETER

7.1 Calibrations Using Flux Meters 96

7.2 Calibration Using a Torsion Fibre 98

7.3 Calibration Using a Current Carrying Solenoid of Known Dimensions 100

CHAPTER 8 - ANALYSIS OF TORQUE CURVES

8.1 General Features of the Curves 102

8.2 Calculations of the Amplitudes and Phases of Components of the Torque Curves 105

8.3 The Determination of the Easy Axis from Phase Angles 109

8.3.1 The Sign of K_4 110

8.4 Method of Reading the Torque Curves 110

8.5 Errors in Reading Torque Curves 111

8.6 Shearing of the Torque Curves 112

8.7 Correction for Shear 116

8.8 Phase Difference Between Fourier Components of Clockwise and Anti-Clockwise Curves 118

8.9 Distortion of the Curves due to Variable Hysteresis Torques and its Correction 119

8.10 Estimate of Errors 120

CHAPTER 9 - RESULTS AND DISCUSSION

9.1 The $Tb_{0.695}Sc_{0.305}$ Basal Plane Disc 122

9.1.1 Orientation of the Specimen 122

9.1.2 The Torque Measurements 122

9.2 The $Tb_{0.825}Sc_{0.175}$ Basal Plane Disc 123

9.2.1 Orientation and Determination of the Easy Axis of Magnetisation 123

9.2.2 Obtaining the Curves 124

9.2.3 The Results 124

9.2.4 Extrapolation to Infinite Fields 124

9.2.5 Variation in the Amplitude of the $\sin 2\phi$ Component 127

9.2.6 Variation in Rotational Hysteresis 127

9.2.7 Comparison of the Results with Theory 128

9.3 The $Tb_{0.89}Sc_{0.11}$ Basal Plane Disc 130

9.3.1 The Results 130

9.3.2 Comparison with Theory 131

9.4 Terbium Basal Plane Disc 132

9.5 Terbium-Scandium Alloys and Terbium: Conclusions 133

9.6 Dysprosium Basal Plane Ellipsoid 134

9.6.1 The Results 134
9.6.2 Discussion: Results, 77 to 100K 136
9.6.3 Discussion: Results Above 136K 139
9.6.4 Temperature Variation of K_4 for Dysprosium 146

9.7 Dysprosium: Conclusions 147

9.8 Suggestions for Further Work 148

Acknowledgements 150

References 151

Appendix I Programme for the Analysis of the Torque Curves 158

Appendix II Table of Normalised Hyperbolic Basal Functions 161

Abstract

The constant K_4 for the hexagonal magnetocrystalline anisotropy of the basal plane has been measured at various temperatures between 77K and 180K for alloys of Terbium and Scandium of compositions

$$Tb_xSc_{1-x} \quad \text{where } x = 0.695,\ 0.825 \text{ and } 0.89$$

using a torque magnetometer with automatic balancing and recording.

Simple methods were devised for setting up the instrument and for analysing torque curves so as to correct for shearing and distortions introduced by rotational hysteresis. Instability in the magnetometer was cured by increasing the speed of response. Three methods of calibration were compared.

The variation of K_4 with temperature for the Tb/Sc alloys indicates that the anisotropy is of single ion origin and due to the second order magnetostriction of hexagonal symmetry. Analysis of the results of P.H. Bly (1967, Ph.D. thesis, University of Durham, unpublished) leads to the same conclusion for pure Terbium. Estimates of K_4 at absolute zero indicate that the hexagonal anisotropy contributes significantly to the driving energy to ferromagnetism in pure Terbium and the Terbium rich alloys.

Reported changes in the easy axis of Dysprosium have been investigated. Those below 80K are associated with hysteresis in the movement of the domain walls and are not reproducible. Those above 130K may be explained by the existence of fan-like spin structures but could also be due to the uncertainty associated with determinations of easy axis using a torque magnetometer with an unsaturated specimen.

List of Tables and Illustrations

Table 1.1	The Rare Earth Metals, Yttrium and Scandium: General Data	Opposite page 2
Table 1.2	The Rare Earth Metals: Magnetic Moment Data	" " 4
Table 4.1	Magnetic Ordering in the Rare Earths	" " 48
Table 6.1	The Crystal Specimens	Page 79
Table 7.1	Calibration of Magnetometer by the Fluxmeter Method	Page 98
Table 7.2	Calibration with a Torsion Wire	Page 99
Table 8.1	Errors Due to Ill-fitting Graticules	Page 111
Table 8.2	The Effect of 'Shear' on the Computed Amplitudes of the Sixfold Components of Torque Curves	Page 114
Table 8.3	The Effect of 'Shear' on the Amplitudes of the Sixfold Component of the Torque Curves and its Second Harmonic	Page 115
Table 9.1	K_4 Values for $Tb_{0.695}Sc_{0.305}$	Opposite page 122
Table 9.2	K_4 Values for $Tb_{0.825}Sc_{0.175}$	" " 124
Table 9.3	K_4 and Single-Ion Functions for $Tb_{0.825}Sc_{0.175}$	" " 128
Table 9.4	$Tb_{0.89}Sc_{0.11}$ K_4 Values	" " 130
Table 9.5	$Tb_{0.89}Sc_{0.11}$ K_4 Values and Single-Ion Functions	" " 131
Table 9.6	Terbium: K_4 Values and Single-Ion Functions	" " 132
Table 9.7	Dysprosium: Characteristics of Torque Curves at 77K Illustrating Hysteresis	" " 134
Table 9.8	Dysprosium: K_4 Values from Feron (1969) and Single-Ion Functions	" " 147
Fig.2.1	Variation of $\frac{1}{\chi_m}$ with Temperature for a Paramagnetic Substance	Opposite page 11
Fig.2.2	A Typical Magnetisation Curve for a Ferromagnetic Substance	" " 15
Fig.2.3	Movement of Domain Boundaries during the Magnetisation Process	" " 15
Fig.2.4	Production of Spontaneous Magnetisation with a High Value of N_w	" " 16
Fig.2.5	Variation of χ_m for Antiferromagnetic Material	" " 17

		Opposite page
Fig.2.6	Exchange Interactions in Helical Antiferromagnetism	19
Fig.2.7	Magnetisation Curve for a Typical Helical Antiferromagnet. H $\perp$ to the Screw Axis	20
Fig.2.8	Perspective View of Sinusoidal Spin Arrangement	21
Fig.2.9	Determination of Magnetisation for a Specimen of Given Demagnetisation Factor	23
Fig.3.1	To Illustrate the Cause of the Temperature Variation of Anisotropy Energy	37
Fig.4.1	Varieties of Spin Structure in Rare Earth Metals	48
Fig.4.2	Basal Plane Anisotropy of Terbium Compared with Theory	58
Fig.4.3	Dysprosium: Bly's Results for Changes of Easy Axis	61
Fig.5.1	To Illustrate $L = +\frac{\delta E_a}{\delta \phi}$	69
Fig.5.2	Variation of Normal Mode Frequency with Applied Field, Basal Plane hcp Specimens, H parallel to a hard axis	72
Fig.6.1	The Torque Magnetometer movement	76
Fig.6.2	Cross-section of the Torque Magnetometer case.	76
Fig.6.3	The Torque Magnetometer: Principles of Operation	77
Fig.6.4	Orientation of the Specimen on its holder.	80
Fig.6.5	Orientation Relative to the Magnet Scale	82
Fig.6.6	The Upper Suspension	83
Fig.6.7	Heating Current Control Circuit	85
Fig.6.8	The Optical System	86
Fig.6.9	The Amplifier Circuit	87
Fig.6.10	The Magnet: Calibration Curve.	91
Fig.6.11	Stability of Torque Magnetometer	94
Fig.7.1	Calibration: Output Versus Twist in the Wire	99
Fig.7.2	Calibration: General Arrangement of Test Coil	100
Fig.7.3	Calibration: Output Versus Current in Test Coil	100
Fig.8.1	Ideal Basal Plane Torque Curve for an hcp Crystal	102
Fig.8.2	Terbium Basal Plane Torque Curve Showing Shearing away from the Easy Axis	112
Fig.8.3	Relationship between the Magnetic Vectors in a Crystal Disc	113

		Opposite page
Fig.8.4	Illustrating the Method of Producing Artificially Sheared Curves	115
Fig.8.5	Reading with an Inclined Graticule	116
Fig.8.6	The Effect of Correction for Shearing	118
Fig.8.7	Improvement to Computer Fit after Exchanging First and Last 12 Readings of each Curve	120
Fig.8.8	Further Illustrating the Computer Fit	120
Fig.9.1	Measured K_4' Values for $Tb_{0.695}Sc_{0.305}$	122
Fig.9.2	Critical Field Versus Temperature for Three Tb/Sc Alloys	123
Fig.9.3	Measured K_4' Values for $Tb_{0.825}Sc_{0.175}$ Versus Applied Field	124
Fig.9.4	Extrapolation of K_4' to Infinite Field for $Tb_{0.825}Sc_{0.175}$	126
Fig.9.5	ΔK_4 as a Function of Temperature	126
Fig.9.6	Amplitude of $\sin 2\phi$ Components at Various Applied Fields	127
Fig.9.7	Variation of Rotational Hysteresis with Applied Field	127
Fig.9.8	$Tb_{0.825}Sc_{0.175}$ K_4 Versus Single-Ion Functions, logarithmic plot	128
Fig.9.9	$Tb_{0.825}Sc_{0.175}$ Temperature Variation of K_4	129
Fig.9.10	$Tb_{0.825}Sc_{0.175}$ Log K_4 Versus log m_T	129
Fig.9.11	$Tb_{0.89}Sc_{0.11}$ Measured K_4 Values Versus Applied Field	130
Fig.9.12	" " " " " "	130
Fig.9.13	" Extrapolation of K_4 Values to Infinite Field	131
Fig.9.14	" " " " " "	131
Fig.9.15	" " " " " "	131
Fig.9.16	" K_4 Values Versus Single-Ion Function, logarithmic plot	131
Fig.9.17	" Temperature Variation of K_4	131
Fig.9.18	Terbium: K_4 Versus Single-Ion Functions logarithmic plot	132
Fig.9.19	Terbium: Temperature Variation of K_4	132
Fig.9.20	Variation of Magnetostriction Energy for Terbium Scandium Alloys	133
Fig.9.21	Dysprosium: Variation of K_4 with Applied Field at 77K	134

		Opposite page
Fig.9.22	Dysprosium: Changes in Sign of K_4, the Amplitude of the sin6ϕ Component of Torque Curves	135
Fig.9.23	Dysprosium: Established Apparent Changes of Easy Axis	140
Fig.9.24	Dysprosium: Apparent Change of Easy Axis may be Caused by Fanlike Spin Structure	140
Fig.9.25	Dysprosium: To Illustrate a Possible Cause for a Change of Apparent Easy Axis	140

CHAPTER 1

INTRODUCTION

1.1 Aims of this investigation

In the heavy Rare Earth metals the magnetic ordering is strongly influenced by magnetostriction and magnetocrystalline anisotropy energies; both help to precipitate the onset of ferromagnetic behaviour and the latter energy determines the direction of the spontaneous magnetisation in the ferromagnetic state and the detailed form of the periodic antiferromagnetic structures.

The aims of this investigation were:

(1) to measure the basal plane anisotropy coefficients of a series of Terbium-Scandium alloys as a contribution to an understanding of the striking effect of dilution with Scandium on the magnetic ordering of the Rare Earth;

(2) to examine further the changes of easy axis in Dysprosium reported by Bly et al. (1969);

(3) to examine the possibility of determining the origin of the basal plane anisotropy from the temperature variation of the coefficients for the alloys, pure Terbium and Dysprosium.

1.2 Some basic properties of the Rare Earths, Scandium and Yttrium

The Rare Earths or Lanthanides are the 15 metallic elements having the atomic numbers 57 to 71 inclusive. A list, together with some of their relevant physical properties, is given in Table 1.1. Similar

Table 1.1 The Rare Earth Metals, Scandium and Yttrium, General Data

Element		Z	Atomic volume cm^3/mole	Crystal structure	Electronic structure of the neutral atom	Normal valency	Normal ion	Lattice Parameters					Transition temperatures		Radius of atom in metal nm	Radius of 3+ ion nm	Density gm cm^{-3}	Melting point °C
								hcp and d-hex			fcc	bcc	fcc above °C	bcc above °C				
								'c' nm	'a' nm	c/a or c/2a	'a' nm	'a' nm						
Lanthanum	La	57	22.53	d-hex	(Xe) - $5d^1\ 6s^2$	3	(Xe)	1.2144	0.3772	1.61	0.530	0.426	310	861	0.1877	0.122	6.166	920
Cerium	Ce	58	20.69	fcc	(Xe)$4f^2$ - $6s^2$	3/4	(Xe)[$4f^1$]	1.1802	0.3673	1.607	0.516*	0.412	-70	762	0.1824	0.118	6.771	798
Praseodymium	Pr	59	20.81	d-hex	(Xe)$4f^3$ - $6s^2$	3	(Xe) $4f^2$	1.1833	0.3672	1.611		0.413		795	0.1828	0.116	6.772	931
Neodymium	Nd	60	20.60	d-hex	(Xe)$4f^4$ - $6s^2$	3	(Xe) $4f^3$	1.1799	0.3659	1.612		0.413		855	0.1822	0.115	7.003	1018
Promethium	Pm	61		d-hex	(Xe)$4f^5$ - $6s^2$	3	(Xe) $4f^4$	1.165	0.365	1.60							7.26	
Samarium	Sm	62	19.95	Sm type	(Xe)$4f^6$ - $6s^2$	3	(Xe) $4f^5$	2.6178	0.3626	1.605		0.407		924	0.1802	0.113	7.537	1072
Europium	Eu	63	28.93	bcc	(Xe)$4f^7$ - $6s^2$	2	(Xe) $4f^7$	-	-			0.458		stable	0.1983	0.113	5.253	822
Gadolinium	Gd	64	19.91	hcp	(Xe)$4f^7$ $5d^1$ $6s^2$	3	(Xe) $4f^7$	0.5781	0.3634	1.591		0.405		1260	0.1801	0.111	7.898	1311
Terbium	Tb	65	19.30	hcp	(Xe)$4f^9$ - $6s^2$	3	(Xe) $4f^8$	0.5698	0.3604	1.581		0.402		1287	0.1785	0.109	8.234	1360
Dysprosium	Dy	66	19.03	hcp	(Xe)$4f^{10}$ - $6s^2$	3	(Xe) $4f^9$	0.5655	0.3593	1.574		0.398		1384	0.1775	0.107	8.54	1409
Holmium	Ho	67	18.78	hcp	(Xe)$4f^{11}$ - $6s^2$	3	(Xe) $4f^{10}$	0.5626	0.3578	1.572		0.396		1428	0.1767	0.105	8.781	1470
Erbium	Er	68	18.49	hcp	(Xe)$4f^{12}$ - $6s^2$	3	(Xe) $4f^{11}$	0.5595	0.3560	1.572					0.1758	0.104	9.045	1522
Thulium	Tm	69	18.14	hcp	(Xe)$4f^{13}$ - $6s^2$	3	(Xe) $4f^{12}$	0.5558	0.3537	1.571					0.1747	0.104	9.314	1545
Ytterbium	Yb	70	24.82	fcc	(Xe)$4f^{14}$ - $6s^2$	2	(Xe) $4f^{14}$	-	-		0.5485	0.444		792	0.1938	0.100	6.972	824
Lutetium	Lu	71	17.79	hcp	(Xe)$4f^{14}$ $5d^1$ $6s^2$	3	(Xe) $4f^{14}$	0.5553	0.3505	1.584					0.1735	0.099	9.855	1656
Scandium	Sc	21	15.04	hcp	(A) - $3d^1\ 4s^2$	3	(A)	0.5268	0.3309	1.592				1335	0.1641	0.081	2.989	1539
Yttrium	Y	39	19.95	hcp	(Kr) - $4d^1\ 5s^2$	3	(Kr)	0.5741	0.3650	1.575		0.408		1479	0.1803	0.106	4.457	1523

* Ce has another fcc phase below 77K (approximately) with a = 0.485 nm

information for Scandium and Yttrium is added to the list. These two elements are also members of group IIIA of the periodic table and have many properties in common with the rare earths.

The chemical properties of the rare earth metals are very similar and this made the separation of the pure elements extremely difficult before the development of the ion-exchange method. All are active reducing agents although they are moderately stable in dry air. Europium is attacked most easily by moist air and so too are Lanthanum, Cerium, Praseodymium and Neodymium in order of decreasing activity. Samarium, the heavy rare earths, Scandium and Yttrium are more stable, Dysprosium and Terbium among the rare earths being least affected by a moist atmosphere while Scandium is not attacked rapidly even by water.

Of special relevance to this investigation are the electronic configurations, the crystal structures and the alloying properties of these metals. A survey of their general properties is given by Taylor (1970).

1.2.1. Electronic Structures

The similarity of chemical properties in the Rare Earths arises from the similarity of their outer electron structures. The distribution of electrons in the neutral atom is as follows:

$$1s^2\ 2s^2\ 2p^6\ 3s^2\ 3p^6\ 3d^{10}\ 4s^2\ 4p^6\ 4d^{10}\ 4f^n\ 5s^2\ 5p^6\ 5d^{(1)}\ 6s^2$$

This is the Xenon structure with the addition of a variable number of 4f electrons (up to the maximum of 14) a possible 5d electron and two 6s electrons. In the description of atomic and ionic electron structures in Table 1.1, only the additional electrons are listed.

The ions are formed by the loss of the 6s electrons and the 5d electron (if it exists) or of one electron from the 4f shell. An exception to this is Cerium which sometimes loses both 4f electrons giving the ion the stable Xenon structure and a valency of four. Other exceptions are Europium and Ytterbium which are usually divalent, losing only the two 6s electrons and leaving intact the stable half-full and completely-full 4f shells respectively. In all the ions the outermost electrons are the two 5s and the 6 5p electrons, differences being only in the number of 4f electrons.

The elements are conveniently grouped into the Light rare earths (La to Eu) with zero to seven 4f electrons and the Heavy rare earths (Gd to Lu) with seven to fourteen 4f electrons.

The angular momenta, disposition and small spatial extension of the 4f electrons are of interest because they are responsible for the unique range of magnetic properties found in the rare earths.

1.2.2. Ionic and atomic magnetic moments

The magnetic moments of the Rare Earth elements are due to the resultant angular momentum of the 4f electrons. The filling of the 4f shell is in accordance with Hund's rules, i.e. so that the resultant spin angular momentum S is a maximum and that the resultant orbital angular momentum L has the highest value consistent with that value of spin and with Pauli's exclusion principle.

When the 4f shell is less than half filled the resultant angular momentum is given by

$$J = L - S \qquad (1.1)$$

Element	Number of 4f electrons	Trivalent ion S	L	J	Saturation moment $n_{sat}=m_{sat}/m_B$ calc. gJ	obs.	Effective moment $n_{eff}=m_{eff}/m_B$ calc. $g\sqrt{J(J+1)}$	V-V	obs. 3+ion	metal
						(b)			(a)	(b)
La	0	0	0	0	0		0	0		
Ce	1	$\frac{1}{2}$	5	$2\frac{1}{2}$	2.14		2.54	2.56	2.52	2.51*
Pr	2	1	5	4	3.20		3.58	3.62	3.6	3.56*
Nd	3	$1\frac{1}{2}$	6	$4\frac{1}{2}$	3.27		3.62	3.68	3.5	3.45*
Pm	4	2	6	4	2.40		3.68	2.83		
Sm	5	$2\frac{1}{2}$	5	$2\frac{1}{2}$	0.72		0.85	1.55		1.74[a] *
Eu	6	3	3	0	0	>3	0	3.40		8.3 [a] *
Gd	7	$3\frac{1}{2}$	0	$3\frac{1}{2}$	7.0	7.55	7.94	7.94	7.8	7.98
Tb	8	3	3	6	9.0	9.34	9.72	9.70	9.74	9.71
Dy	9	$2\frac{1}{2}$	5	$7\frac{1}{2}$	10.0	10.33	10.64	10.6	10.5	10.64
Ho	10	2	6	8	10.0	10.34	10.6	10.6	10.6	11.2
Er	11	$1\frac{1}{2}$	6	$7\frac{1}{2}$	9.0	9	9.58	9.6	9.6	9.9
Tm	12	1	5	6	7.0	7.14	7.56	7.6	7.1	7.6
Yb	13	$\frac{1}{2}$	3	$3\frac{1}{2}$	4.0		4.53	4.5	4.4	0
Lu	14	0	0	0	0		0	0		0

(a) Data from Chikazumi (1964)

(b) Data from Rhyne, page 129 et. seq. of Elliott (1972)

* n_{eff} data for the light rare earths is complex. These values should be regarded with caution.

Table 1.2 The Rare Earth metals: magnetic moment data

When the shell is half filled or more, then

$$J = L + S \qquad (1.2)$$

Except for Samarium and Europium the measured effective magnetic moments of the Rare Earth trivalent ions in salts agree quite well with the moments calculated from the expression

$$m_{eff} = g\, m_B \sqrt{J(J+1)}$$

where g is the Landé splitting factor, m_B is the Bohr magneton and J is obtained from equations 1.1 or 1.2. Values are given in Table 1.2.

Sm^{3+} and Eu^{3+} ions give values of m_{eff} higher than that obtained from the theoretical expression above. This was explained by Van Vleck by taking into account the transfer of some ions to the first excited state which has a larger value of J and lies close to the ground state for these two elements.

In the heavy rare earths with the exception of Ytterbium, the effective magnetic moments in the metallic state are close to those of the ions in salts, the slight differences being attributable to polarisation of the conduction electrons in the metal; this is taken as confirmation that the 4f electrons are localised even in the metals. A résumé of this and other evidence for the small spatial dimensions of the 4f shell is given by de Gennes (1962). Neutron scattering experiments indicate that the mean radii of the 4f shells are of the order of 10% of the interatomic distance.

1.2.3. Crystal structures

In the rare earths and Scandium and Yttrium, close packed crystal structures predominate. In a close packed arrangement the

atoms may be visualised as spheres packed in planes, which for ease of description may be imagined to be horizontal. The arrangement of spheres within one plane is unique but one plane may be stacked on another in either of two alternative positions. The positions of atoms in the first plane and of other atoms lying vertically over them may be called "A" sites. Similarly the alternative positions of atoms in the second layer define the positions of "B" and "C" sites.

The stacking sequence A B A B A B or A C A C A C gives the hexagonal close packed structure, denoted by "hcp" in Table 1.1. Similarly the sequences A B A C A B A C, and A B C A B C A B C give the double hexagonal close packed and face centred cubic structures, denoted by d-hcp and fcc respectively.

Samarium has a stacking sequence peculiar to itself, namely,

A B A B C B C A C.

Except for Europium, which already has a body centred cubic structure, and Pm, Er, Tm and Lu for which there is no certain data, all the metals change to a body centred cubic form at temperatures approaching their melting points. This is not a close packed form.

In addition, Lathanum changes to a face centred cubic form at temperatures above 533K and Cerium has a double hexagonal close packed structure below 200K and a further change to a face centred cubic form below 77K.

Dysprosium on entering the ferromagnetic phase is distorted so much by magnetostriction that its crystal structure can then be described as orthorhombic. Evidence exists (Bucher et al. 1970) that high purity Ytterbium, as normally prepared, is a mixture of hcp and fcc phases and

that a change to 100% hcp can be produced by cooling to 77K. This phase persists on warming up to room temperatures but may be entirely removed by annealing at 150K.

1.2.4. Ionic dimensions

Apart from the two normally divalent elements, it can be seen from Table 1.1 that the dimensions of the Rare Earth ions decrease with increasing atomic number. This is the well known Lanthanide contraction. The metallic interatomic distances (given roughly by the length 'a' for the hcp crystals) hardly alter at all across the series, an indication that the ion core does not play a large part in the binding. This applies a fortiori to the 4f orbitals which are much nearer to the nuclei. The ratio c/a or c/2a is given in Table 1.1 for the hexagonal structures. This departs from the value 1.633 which it would have for the perfect packing of geometrical spheres and has important consequences for the anisotropy energy.

1.2.5. Alloying properties

The Rare Earths form among themselves and with other elements a vast array of intermetallic compounds of definite stoichiometry. These exhibit a great variety of properties and are the objects of much interest and investigation. A review is given by Taylor (1971).

The heavy Rare Earths with the exception of Ytterbium form continuous solid solutions with each other and with various other metals such as Thorium, Yttrium and Scandium.

Yttrium and Scandium have similar outer electron configurations to the Rare Earths but are non-magnetic. They also have the hcp crystal structure and so do their alloys with hcp Rare Earth metals. They form

therefore ideal diluants for altering the magnetic and other properties of the Rare Earths in a controlled manner and so gaining an insight into the magnetic interactions involved.

The volume of the Yttrium atom is very close to that of Gadolinium and dilution of the heavy Rare Earth metals with Yttrium does not alter the lattice parameters greatly. Dilution with Scandium, in contrast, causes a reduction of the lattice parameters. For Tb/Sc alloys, Chatterjee and Corner (1971) have shown that there is a linear relationship between the "c" axis lattice parameter and the atomic percentage of one constituent, while there is a nearly linear relationship for the "a" axis lattice parameter.

The effects of dilution with Yttrium and Scandium on the magnetic properties of Rare Earth metals are considered in Chapter 4 following the introduction of some fundamental magnetic concepts and definitions in Chapters 2 and 3.

CHAPTER 2

SOME BASIC CONCEPTS AND DEFINITIONS

2.1 Units

S.I. units are used throughout. The magnetisation or magnetic polarisation, which is the magnetic moment per unit volume, is symbolised by M and is related to the flux density (B) and the magnetic field strength (H) thus:

$$B = \mu_o(H + M) \qquad (2.1)$$

The units of M are therefore Am^{-1}.

This convention, usually attributed to Sommerfeld (1964, page 89) differs from that used in many standard works but is embodied in the Symbols, Units and Abbreviations report of the Royal Society (1969) and is the one accepted by the International Union of Pure and Applied Physics. It is also associated with methods of developing the theory of magnetism in which prominence is given to current loops rather than to the concept of magnetic poles.

The maximum torque on a current loop of area A carrying a current I in a field of flux density B is B A I. The Sommerfeld convention allows the product AI to represent the magnetic moment (m) of the current loop so that

$$\text{Maximum torque} = Bm \qquad (2.2)$$

The small 'm' is used to represent magnetic moments. Thus the Bohr magneton is represented as 'm_B'.

For a current loop where m = Al, the relationship (2.2) above holds both in free space and in isotropic homogeneous magnetic fluids,

provided that the fluid is allowed to penetrate the loop. A permanent magnet, provided that it has a very high coercive force, can be represented by a system of currents but is only equivalent to them in vacuo. The magnetic moment is then defined by equation (2.2).

In a homogeneous isotropic magnetic fluid the bar magnet is equivalent to a system of current loops from which the fluid has been excluded and the maximum torque is then (Whitworth and Stopes-Roe, 1971) given by:

$$\text{Maximum torque} = \mu_o Hm \qquad (2.3)$$

Jouguet (1972) points out that neither (2.2) or (2.3) above can be applied directly in all cases. They are identical in free space and become so in a magnetic fluid when account is taken of the change in magnetic polarisation produced when a bar magnet displaces the fluid. As a result of (2.3) the maximum torque on an atomic spin is

$$\text{Maximum torque} = \mu_o HJgm_B \qquad (2.4)$$

where g is the Landé 'g' factor and J is the angular momentum quantum number.

The work done per unit volume in magnetising a body is

$$W = \mu_o \int_0^M H \, dM \qquad (2.5)$$

M(T) denotes the magnetisation at a temperature T. The reduced magnetisation, here denoted by m_T, is given by $m_T = \frac{M(T)}{M(0)}$, where M(0) is the magnetisation at absolute zero. In describing experimental results, field strengths are given as $\mu_o H(=B_o)$ and in units of Tesla rather than in Am^{-1}. The quantity B_o is called variously 'Applied flux density', 'External flux

density', or less rigorously 'Field Strength' (Bates 1970). Comparison with other work is then facilitated by the easy numerical relationship.

$$B_o/\text{Tesla} = B_o/10^4 \text{ Oersted} \qquad (2.6)$$

Comparison of specific magnetic moment (σ) is also easy

$$\sigma/\text{Am}^2\text{kg}^{-1} = \sigma/\text{e.m.u. gm}^{-1} \qquad (2.7)$$

2.2 Varieties of magnetic behaviour

For an isotropic material, or for a particular direction in an anisotropic material, the magnetic susceptibility χ_m is defined by the relationship

$$\underset{\sim}{M} = \chi_m \underset{\sim}{H} \qquad (2.8)$$

Since M and H have the same dimensions in the Sommerfeld convention, χ_m is a dimensionless quantity as in the c.g.s. system. Because of rationalisation however, χ_m of unity in S.I. units is equivalent to a volume susceptibility of $1/4\pi$ when M and H are measured in c.g.s. units.

χ_m is not in general a constant and its value and variations with magnetic field strength and temperature can be used to distinguish varieties of magnetic behaviour.

2.2.1. Diamagnetism

For diamagnetic substances χ_m is negative, small, (of the order of 10^{-5} for solids) nearly independent of applied field strength and usually independent of temperature also. The bulk magnetisation of magnetic materials is due to the orbital and spin angular momenta of electrons. In solids however the degeneracy of the orbitals which allows the motion of electrons from one orbital to another may be removed by

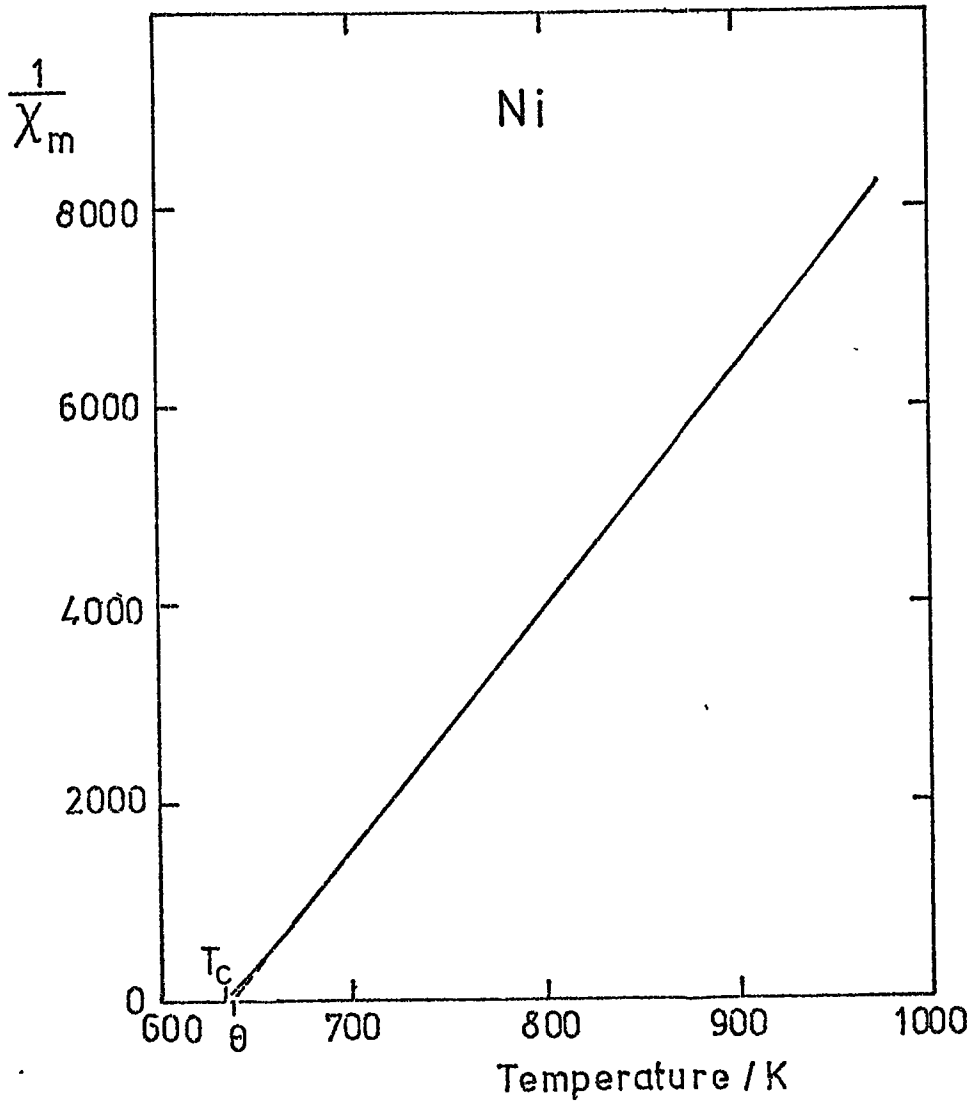

Figure 2.1 The variation of $1/\chi_m$ with temperature for a Paramagnetic substance (Nickel above 631 K)

bonding and the orbital angular momentum of unpaired electrons may be partly or wholly quenched. Magnetic effects are then due to spins only. In diamagnetic substances the electrons are paired so that their resultant angular momenta are zero. The effect of an applied magnetic field may be understood in classical terms as causing precession of orbits and spins about the field direction in such a sense as to produce a magnetic moment in the opposite direction to the applied field. The effect occurs in all materials including those described as 'non-magnetic', but is masked in all magnetic materials by the larger magnetic polarisation due to the atoms having resultant magnetic moments.

2.2.2. Paramagnetism

In paramagnetic substances χ_m is positive, of the order of 10^{-3}, is independent of applied field strength and varies with temperature according to the Curie law

$$\chi_m = \frac{C}{T} \qquad (2.9)$$

or the Curie-Weiss law

$$\chi_m = \frac{C}{T-\theta} \qquad (2.9a)$$

in which C and θ are constants, θ being known as the paramagnetic or asymptotic Curie temperature, see Fig.2.1. Paramagnetic behaviour at ordinary temperatures can be accounted for by regarding the elementary moments as randomly orientated due to thermal motion. When a magnetic field is applied, orientations more nearly parallel to the field have a lower potential energy and the fraction of the elementary moments having those orientations increases in accordance with the Boltzman law.

$$\frac{dN}{d\omega} \propto \exp(-W/kT) \qquad (2.10)$$

$\frac{dN}{d\omega}$ is the number of moments per unit solid angle orientated at a given angle to the field and W is their potential energy. There is thus a resultant bulk magnetic polarisation M(T) parallel to the applied field at a given temperature.

If J is the total angular momentum quantum number of the atoms, g is the Landé splitting factor and m_B is the value of the Bohr magneton then the maximum component of the atomic moments parallel to the field, known also as the saturation moment, is

$$m_{sat} = J\, g\, m_B \qquad (2.11)$$

$Jg = n_{sat}$, the number of Bohr magnetons in the saturation moment.
The lowest value of potential energy of an individual magnetic ion is

$$-Jg\, m_B\, \mu_o H$$

The hypothetical maximum value of magnetic polarisation M(0) will be obtained at absolute zero of temperature when the atomic moments are undisturbed by thermal vibrations. All the moments are then parallel to the applied field and

$$M(0) = N_L J g m_B \qquad (2.12)$$

N_L is the number of atoms in unit volume and the quantity Jg is known as the saturation moment per ion (units of Bohr magnetons). It can be shown (Chikazumi 1965, page 63) that

$$M(T) = M(0)\left\{\left(\frac{2J+1}{2J}\right)\coth\left(\frac{2J+1}{2J}\right)a - \frac{1}{2J}\coth\left(\frac{a}{2J}\right)\right\} \qquad (2.13)$$

where $a = \frac{gJm_B\mu_o H}{kT}$. The quantity in curly braces is the Brillouin function $B_J(a)$.

As H and hence a tend to infinity then

$$B_J(a) \rightarrow 1$$

In the classical case where spins may assume any orientation, J as a measure of the number of possible orientations is effectively infinite so that

$$B_J(a) \rightarrow \text{Coth } a - \frac{1}{a} \qquad (2.14)$$

The quantity on the right hand side of 2.14 is the Langevin function, denoted usually by $\mathcal{L}(a)$.

When $a \ll 1$

$$B_J(a) \rightarrow \left(\frac{J+1}{3J}\right)a$$

and

$$M(T) = \frac{N_L g^2 J(J+1) m_B^2 \mu_o H}{3kT}$$

and

$$\chi_m = \frac{M}{H} = \frac{N_L g^2 J(J+1) m_B^2 \mu_o}{3kT} \qquad (2.15)$$

Thus for a given material $\chi_m \propto \frac{1}{T}$ which is the Curie law. (The quantity $g\sqrt{J(J+1)}\ m_B$ which appears squared in 2.15 is called the <u>effective</u> atomic moment and $g\sqrt{J(J+1)} = n_{eff}$ is its measure in Bohr magnetons). The Curie-Weiss law (equation 2.9a) can be explained if it is further assumed that there is an internal molecular field due to the partial orientation of the atomic moments. Each atomic moment is not only under the influence of the external applied field H but of an internal field proportional to the magnetic polarisation. The resultant field H' is given by

$$H' = H + N_\omega M(T) \qquad (2.16)$$

where N_ω is the Weiss molecular field constant.

From equation 2.15 above we have

$$M(T) = \frac{C'H}{T} \qquad (2.17)$$

where $C' = \frac{N_L g^2 J(J+1) m_B^2 \mu_o}{3k}$ and is a constant.

Putting $H + N_\omega M(T)$ for H

we have $M(T) = \frac{C'}{T}(H + N_\omega M(T))$

and hence $\chi_m = \frac{M}{H} = \frac{C'}{T - C'N_\omega} \qquad (2.18)$

in which C' and $C'N_\omega$ may be identified with C and θ respectively in the Curie-Weiss law. (2.9a).

2.2.3. Ferromagnetism

Ferromagnetic materials have values of χ_m which are positive, very large (of the order of 10^4 to 10^5) and depend on the field strength, the temperature and the previous magnetic history of the specimen. The bulk magnetic polarisation shows an approach to saturation at moderate field strengths (10^{-6} to 10^{-1}T) whereas paramagnetic substances show a tendency to saturate only at very low temperatures ($\sim$ 4K) and high applied fields (5T).

This behaviour is explained by the existence within crystals of the ferromagnet of regions called Domains, a name due to Weiss, in each of which all the atomic moments are parallel save for the effects of thermal vibration. The value of magnetic polarisation within the domains is called the spontaneous magnetisation (M_s) and is usually not much less than the saturation magnetisation at OK (M(O)). Domains are separated by boundaries or Bloch Walls, regions through which the direction of

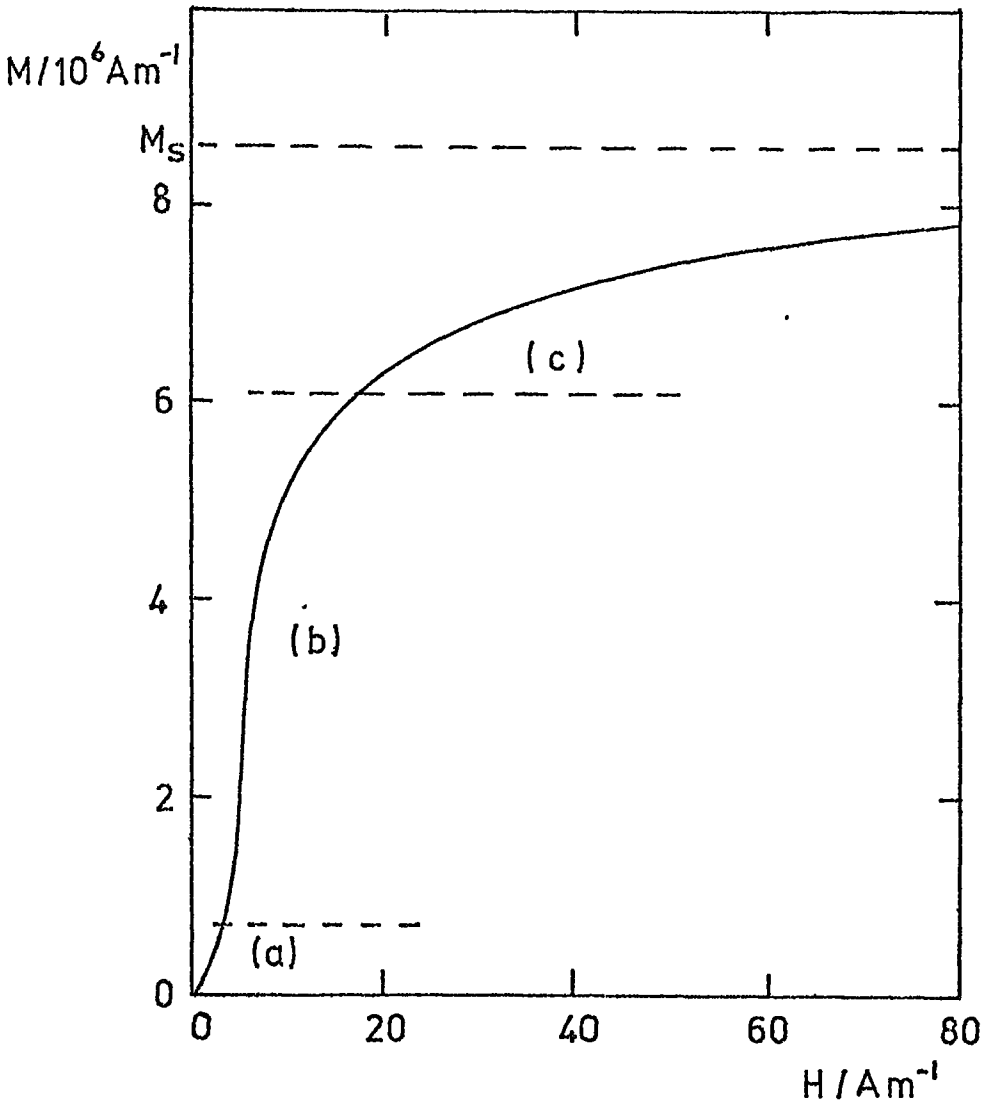

Figure 2.2. A typical magnetisation curve for a ferromagnetic substance.

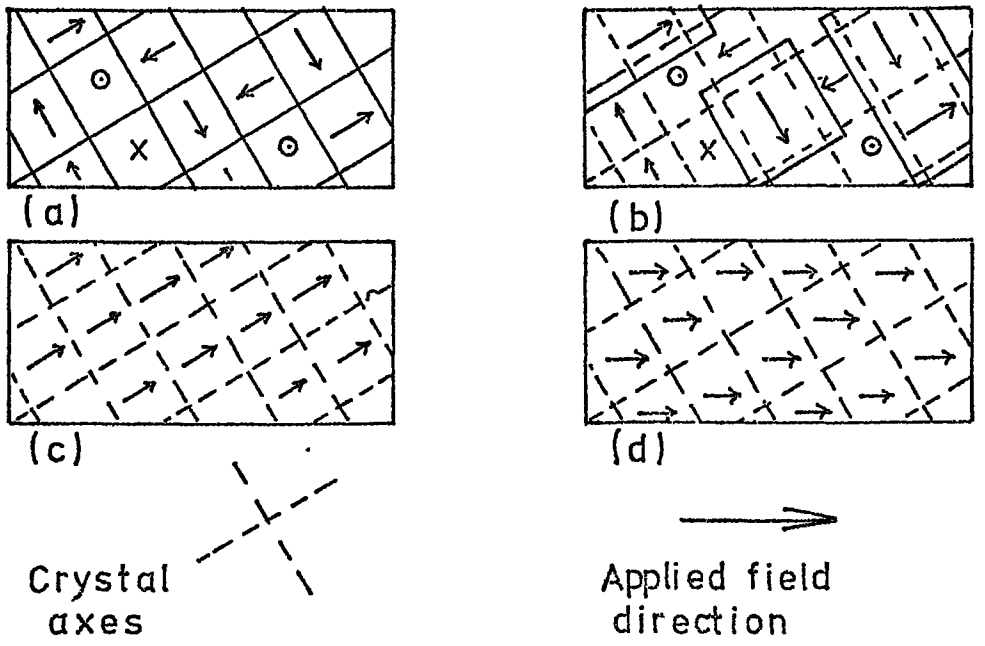

Figure 2.3 The movement of domain boundaries during the magnetisation process. (Schematic)

the atomic moments changes gradually. Domains form so as to minimise the total of magnetostatic energy and wall energy and in the absence of an applied field the resultant moments of the domains are randomly distributed among a set of easy directions in the crystal. The resultant bulk magnetisation may therefore be small or zero.

Magnetisation of a specimen proceeds not by orientation of individual magnetic moments but by rearrangement of domains. Figure 2.2 shows a typical magnetisation curve. At (a), the instep of the curve, the applied field moves domain boundaries nearly reversibly. Those domains in which the magnetic polarisation is more nearly parallel to the applied field grow at the expense of the others, (Fig.2.3a,b). At (b) in Figure 2.2 the directions of the spontaneous magnetisation within each domain change irreversibly till they are all parallel to the easy direction nearest to the direction of the applied field. When this stage is completed the crystals are effectively single domains and further increase of the applied field causes reversible rotation of the magnetic moments as a whole more nearly into alignment with itself. The bulk magnetisation approaches asymptotically the value of M_s of the spontaneous magnetisation. M_s therefore also denotes the saturation value of magnetisation.

If the applied field is removed, in general the magnetisation of a ferromagnetic specimen does not fall to zero, i.e. it exhibits hysteresis. Energy is needed to move the domain boundaries which form again spontaneously. However, even in a specimen which is magnetised beyond the knee of the magnetisation curve and in which there are no domain boundaries, if the specimen is rotated in a magnetic field, thermodynamically

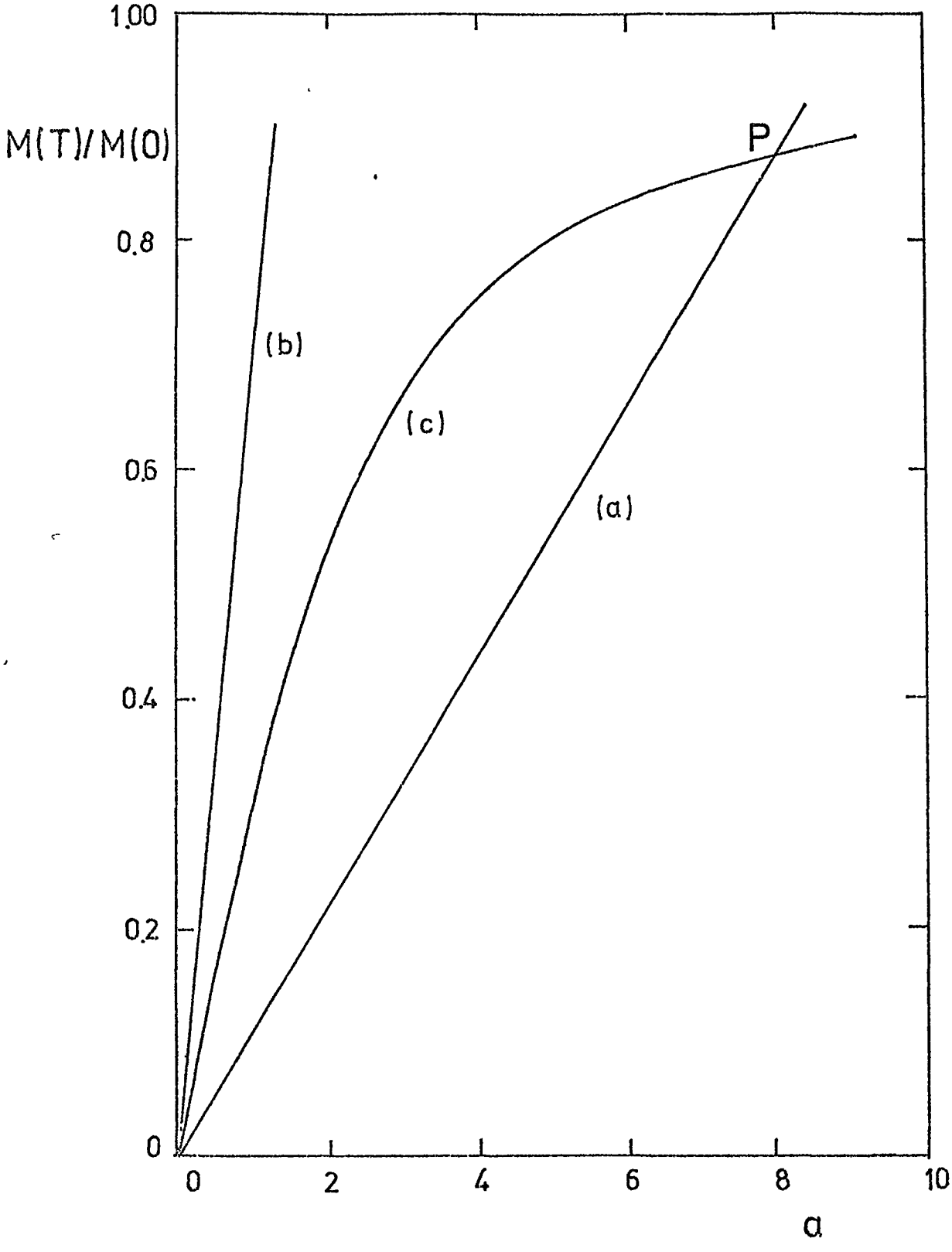

Figure 2.4 The production of spontaneous magnetisation when N_W has a high value.

(a) $M(T) = \frac{a.kT}{gJm_B N_W}$ versus a for large N_W

(b) The same with a small value of N_W so that the slope exceeds the initial slope of graph (c)

(c) $M(T) = M(0)B_J(a)$ versus a

irreversible jumps in the direction of the magnetisation take place (between one easy direction and another) and work must be done to maintain the rotation. This rotational hysteresis was observed in all specimens used in this investigation.

The spontaneous alignment of the atomic moments within the domains of a ferromagnetic material may be comprehended by an extension of the Weiss theory of paramagnetism.

For a paramagnetic material from equation 2.13

$$M(T) = M(0)B_J(a) \qquad (2.19)$$

Where $a = gJm_B\mu_o H/kT$ From Eq.(2.16) in the absence of any external field $H = N_\omega M(T)$. The value of M(T) can be found in principle by plotting:

$$M(T) = M(0)B_J(a) \text{ versus } a \qquad (2.20)$$

and

$$M(T) = \frac{a.kT}{gJm_B\mu_o N_\omega} \text{ versus } a \qquad (2.21)$$

If the value of N_ω is large then the line represented by 2.21 crosses the curve represented by 2.20 at two points as shown in the Figure 2.4.

The solution M(T) = 0 is unstable since any slight local alignment of the atomic moments will increase the molecular field and the alignment will further increase. A stable solution is the value of M(T) at the point P in Fig.2.4.

Experimentally, for a ferromagnetic material $\frac{M(T)}{M(0)} = B_J(a)$ at the point P might be 0.85. This corresponds approximately to a value of $\underline{a}$ of 7, and a value of molecular field H of the order of 200 or 300T. Such a large internal field cannot arise from the ordinary Lorentz field

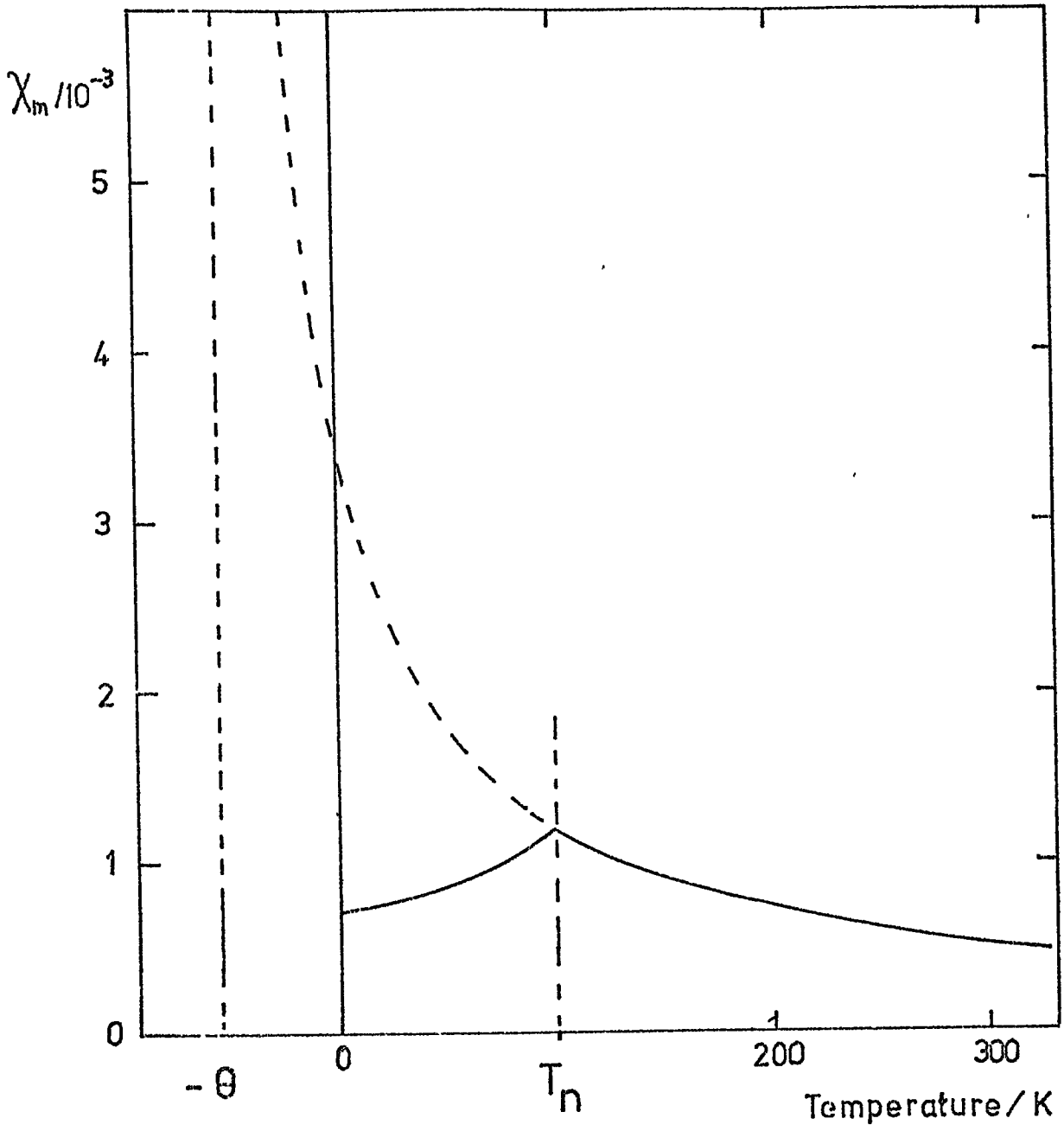

Figure 2.5 The characteristic variation of χ_m with temperature for an antiferromagnetic substance.

of the surrounding magnetic dipoles and Heisenberg suggested that the internal field causing the alignment of the elementary moments is a quantum mechanical exchange force. The potential energy between two atoms having spins $\underset{\sim}{S}_i$ and $\underset{\sim}{S}_j$ is

$$\omega_{ij} = -2\mathcal{J}\underset{\sim}{S}_i \cdot \underset{\sim}{S}_j \qquad (2.22)$$

where $\mathcal{J}$ is the exchange integral. If $\mathcal{J}$ is positive, the energy is least when $\underset{\sim}{S}_i$ and $\underset{\sim}{S}_j$ are parallel. The exchange forces are basically electrostatic and $\mathcal{J}$ is related to the overlap of the charge distributions of the atoms i and j. If the two spins are parallel, the spatial part of the wave functions must be antisymmetric under exchange of the electrons, and if the spins are antiparallel, the spatial part of the wave functions must be symmetric. The different wave functions, representing different distributions of charge, have different Coulomb energies of the correct order of magnitude to account for the alignment.

When a ferromagnetic material is heated to the ferromagnetic Curie temperature (T_c) the spontaneous alignment of the spins within each domain disappears and often the material then shows paramagnetic behaviour, beginning to obey the Curie Weiss law a few degrees above T_c.

2.2.4. Antiferromagnetism

The characteristic variation of χ_m with temperature for an anti-ferromagnetic material is shown in Figure 2.5. χ_m is positive, of the order of 7×10^{-4} and increases with temperature up to the Néel temperature, T_N, above which it varies with temperature according to

$$\chi_m = \frac{C}{T + \theta} \qquad (2.23)$$

i.e. the material becomes paramagnetic with a negative paramagnetic Curie temperature.

These properties may be explained by the existence of an ordered spin state below the Néel temperature in which adjacent spins are anti-parallel, the exchange integral $\mathcal{J}$ being negative. Increasing temperature weakens the negative interaction so that χ_m rises until the spins become disordered at the Néel temperature. The existence of this type of ordering was first shown by Shull in 1949 using neutron diffraction techniques, since when the technique has become standard for investigating magnetic structures. Comparison of X-ray and neutron diffraction patterns, or comparison of neutron patterns above and below the transition temperatures, shows additional neutron reflections in the magnetically ordered states. In the case of the antiferromagnet MnO, the magnetic unit cell is found to be twice the size of the crystallographic unit cell since alternate (111) planes of Mn^{++} ions have their magnetic moments in opposite directions.

2.2.5. Ferrimagnetism

An antiferromagnetic arrangement of spins may be regarded as two interleaved arrays of spins each of which alone is ferromagnetic. Because the spins in each array are of equal magnetic moment, the resultant susceptibility tends to zero with falling temperature. If the spins in the two sublattices are not equal or opposite there is a resultant spontaneous magnetisation which will be smaller than in a typical ferromagnet. Domain structures may exist and the specimen may give magnetisation curves similar in all respects to those of a ferromagnet. Such ferrimagnetic substances resume paramagnetic behaviour when heated above a characteristic Curie temperature.

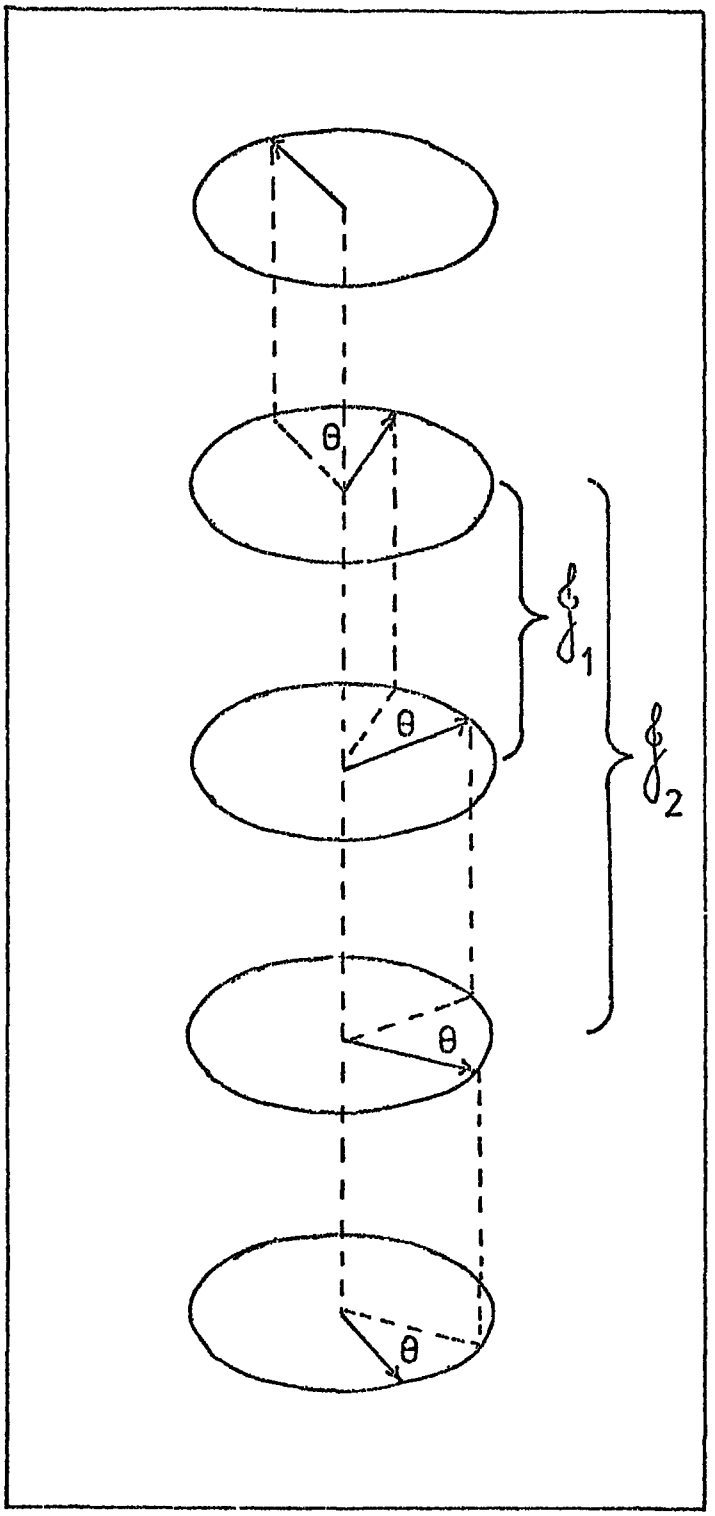

Figure 2.6 Exchange interactions in helical antiferromagnetism.

2.2.6. Helical Antiferromagnets

Yafet and Kittel (1952) proposed a triangular arrangement of spins to explain an anomalously small value of spontaneous magnetisation in certain ferrites. Yoshimori (1959) proposed a helical arrangement of spins for MnO_2 and J. Villain (1959) a similar arrangement for antiferromagnetic $MnAu_2$. Herpin et al (1959) investigated the magnetic structure of tetragonal $MnAu_2$ by neutron diffraction, observing the production of two satellites to each Bragg reflection when the material was in the antiferromagnetic state. The spacing and intensities of these satellites were consistent with a structure in which all the atoms of manganese in the same plane have their moments parallel to each other and normal to the 'c' axis; the common directions of the spins in consecutive planes being advanced by a fixed angle. The vectors representing a series of spins lying in a row parallel to the 'c' axis then form a helix; the 'c' axis of the crystal is the axis of the helix or the screw axis, and the angle between the spins in one plane and the next is known as the interlayer turn angle.

From the variation in the spacing of one satellite ($00\bar{2}$) from the main reflection Herpin et al calculated that the interlayer turn angle varied between 46° at 125K to 51° at 300K.

To show in principle how this simple helical arrangement can arise, consider a single row of spins as shown in Fig.26. If $\oint_1$ is the exchange integral between adjacent spins in the row and $\oint_2$ that between next nearest neighbours then the arrangement is stable when the energy $u = -2(\oint_1 \underset{\sim}{S}_p \cdot \underset{\sim}{S}_{p+1} + \oint_2 \underset{\sim}{S}_p \cdot \underset{\sim}{S}_{p+2})$ is a minimum (taking the interactions only as far as next nearest neighbours). In terms of the interlayer turn angle θ this means that the quantity $\oint_1 \cos\theta + \oint_2 \cos 2\theta$ must be a minimum.

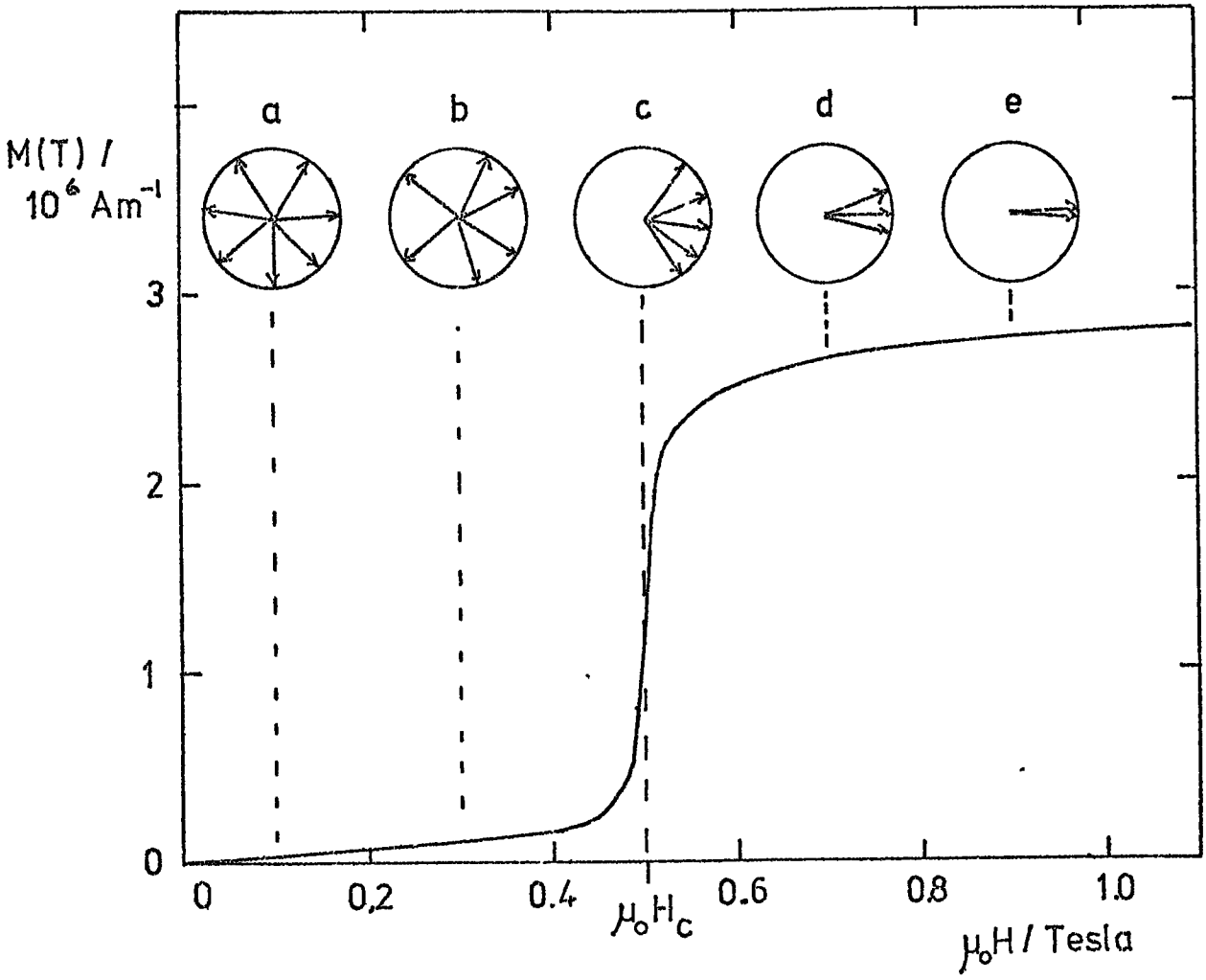

Figure 2.7 A magnetisation curve for a typical helical antiferromagnetic material. H ⊥ to the screw axis.

This occurs when

$$\cos\theta = -\frac{\mathcal{J}_1}{4\mathcal{J}_2} \qquad (2.24)$$

and $< |4\mathcal{J}_2|$

If $\mathcal{J}_2$ is negative and $\mathcal{J}_1$ is positive, then neighbours in a layer will couple ferromagnetically and the helical arrangement described will result. In any real crystal the exchange energies $\mathcal{J}_1$, $\mathcal{J}_2$ must be replaced by effective exchange interactions appropriate to the crystal symmetry and which are functions of the exchange integrals for pairs of spins on various sites. Equation 2.24 then holds for the interlayer turn angle. This simple treatment ignores magnetostriction and magneto-crystalline anisotropy energy. Their influence is considered in Chapter 4. Helical and other forms of period magnetic structure occur in the rare earths and their alloys (Child et al 1966, 1968; Koehler 1961, 1965; Spedding et al 1970) and are further described in Chapter 4. Koehler (1961, 1965) lists the patterns obtained from the various structures and outlines the techniques used in the study of magnetic structures by neutron diffraction.

2.2.7. Metamagnetism

This is the name given originally by Becquerel and van den Handel (1939) to the behaviour of those magnetic materials which can be changed from antiferromagnetic (including helical forms) to ferromagnetic by means of an applied field or a change of temperature. The change from antiferromagnetism to ferromagnetic behaviour is called the meta-magnetic transition and the value of applied field where it occurs is called the Critical Field (H_c). Figure 4.3 shows the variation of H_c with temperature for Dysprosium. Figure 2.7 shows the variation of the magnetisation with applied field for a typical metamagnetic transition

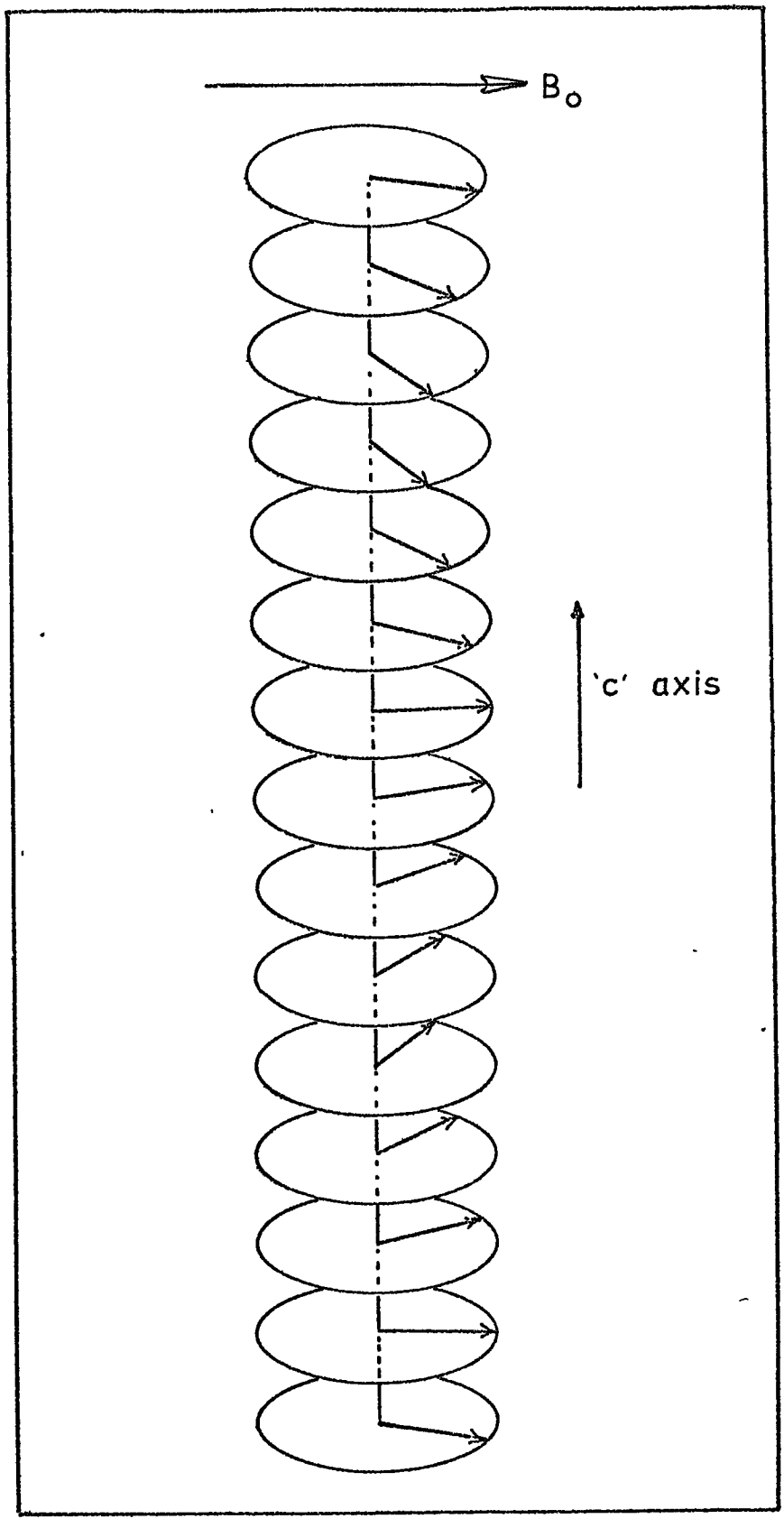

Figure 2.8 Perspective view of a sinusoidal spin arrangement.

in a helical antiferromagnet and the inset diagrams represent schematically the behaviour of one row of spins according to the theory of Enz (1960), Nagamiya et al (1962) and Kitano and Nagamiya (1964). The spins are viewed along the screw axis, which is perpendicular to the direction of magnetisation. At low values of applied field the helix distorts and a small magnetisation is produced in the direction of the field. At the critical field the helix changes into a sinusoidal arrangement of moments, (Fig. 2.7c,d), in which all the individual spins have a component parallel to the field (Fig.2.8). At a higher field, H_f approximately $2H_c$, this fan structure collapses to a normal ferromagnetic arrangement, the transition being first or second order depending on the anisotropy and magnetostriction energies which are discussed later. Another effect of these energies is to lower both H_f and H_c, increasing anisotropy lowering H_f more than H_c so that they coincide and the fan phase is eliminated. Theoretical studies of these processes are discussed by Cooper (1972).

The materials used in this investigation, Dysprosium, Terbium and the Terbium rich Terbium/Scandium alloys are all helical antiferromagnetic in some temperature range, having the screw axis parallel to the 'c' crystallographic axis, and they show metamagnetic transitions under suitable applied fields. Measurements were made with the applied fields perpendicular to the 'c' axis and of magnitude H_c and above, so that the collapse of the helical structure shown in Fig.2.7 was a significant feature of the work.

2.3 Demagnetising Fields

The resultant field (B_r) inside a magnetised body is the applied field B_o reduced by a quantity $\mu_o N_d M$, the demagnetising field which is proportional to M and opposite in direction. N_d is strictly defined only for ellipsoids uniformly magnetised parallel to an axis. Values are given by Brailsford (1966) for ellipsoids with axes in various ratios.

Standard texts explain the demagnetising field in terms of free magnetic poles at the surface of the body. Coleman (1971) has shown that an explanation in terms of a current loop model does not present any very great difficulty, so that a consistent development of the subject is possible within the Sommerfeld convention and making no use of the concept of free poles.

2.3.1. The use of demagnetisation factors in determining the magnetisation of specimens

Graphs of specific magnetisation for materials are commonly available plotted against the resultant field B_r rather than against the applied field B_o. Given a demagnetisation factor N_d for a specimen, the problem of determining the magnetisation in a given applied field is that of solving simultaneously two equations

$$\sigma = fn(B_r) \tag{2.25}$$

and

$$B_r = B_o - \mu_o \sigma \rho N_D \tag{2.26}$$

where ρ is the density of the material.

These may be solved graphically by plotting graphs of each to the same scale and noting the point of intersection. The graph of Eq.2.25 is simply the magnetisation curve which is already available.

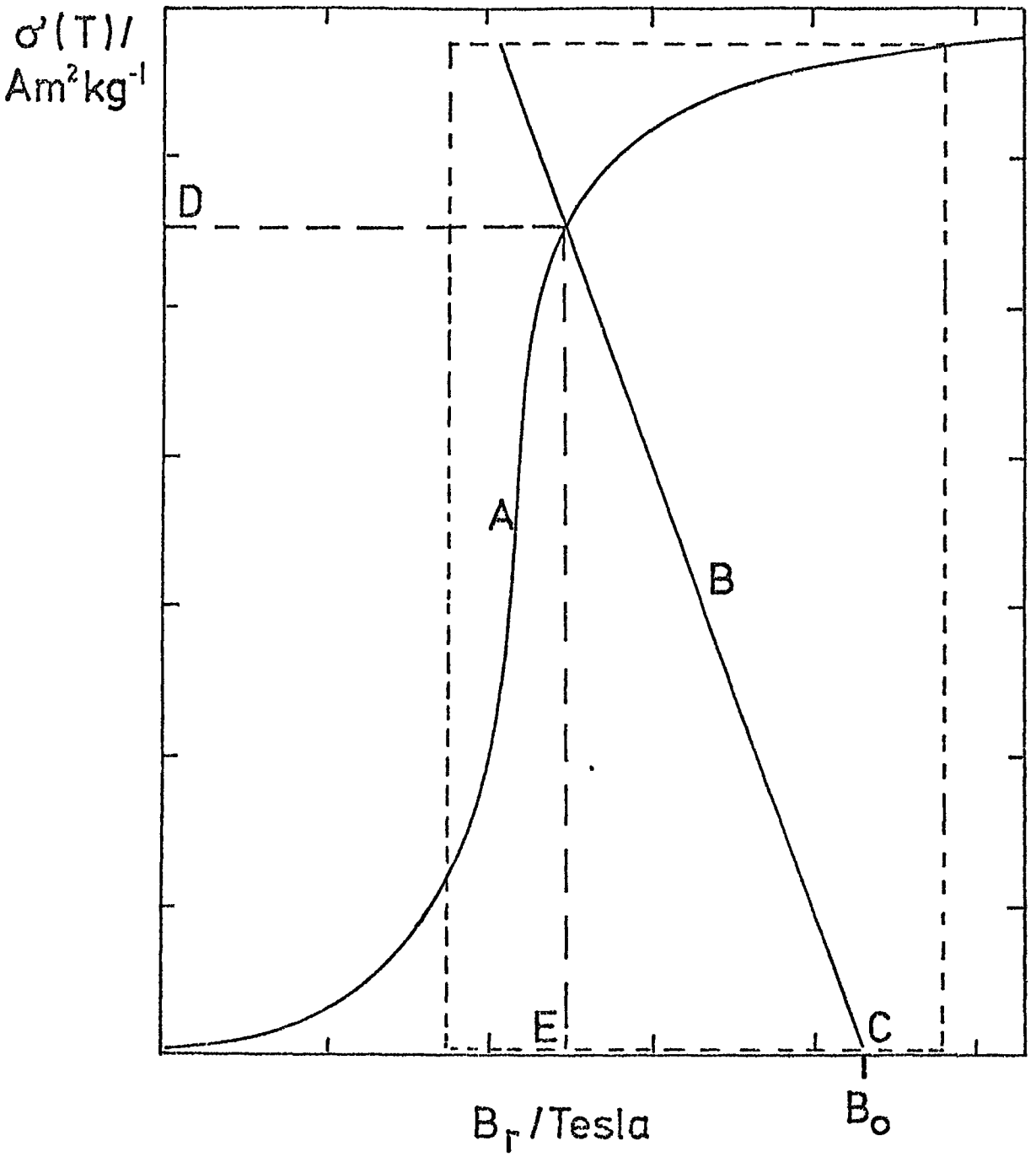

Figure 2.9 The determination of the magnetisation of a specimen of given demagnetisation factor.
A is the magnetisation curve for the material.
B is a line of slope $-1/\mu_0 N_d$ on a transparent overlay
C is the end of the line B which is placed on B_o, the given value of applied field.
D indicates the required magnetisation and
E is the resultant field.

Rearranging (2.26) we have

$$\sigma = \frac{B_o - B_r}{\mu_o \rho N_D}$$

Plotting σ against B_r gives a straight line, the slope of which is $\frac{-1}{\mu_o N_D \rho}$ and the intercept on the B axis is the value B_o. It is convenient in practice to draw the graph of the second equation on a piece of transparent graph paper. Sliding this graph over the magnetisation curve allows determination of magnetisation (and also of B_r) for any given value of B_o. The process is illustrated in Figure 2.9.

CHAPTER 3

MAGNETOCRYSTALLINE ANISOTROPY

3.1 Anisotropy Energy

The work done on a body per unit volume to raise the magnetisation from zero to its saturation value is given by

$$W = \mu_o \int_o^{M_s} \underset{\sim}{H}.d\underset{\sim}{M} \qquad (3.1)$$

Some of this energy is lost in irreversible magnetisation processes and part is stored as a potential energy of magnetisation (E), the value of which may depend on the direction in which the material is magnetised. This variation of magnetisation energy with direction may be produced by applying mechanical stress to a material, it may be due to the shape of the specimen or it may be produced in polycrystalline materials by cold working or by heat treatment in a magnetic field. When these three types of anisotropy, known respectively as magnetostrictive, shape and induced magnetic anisotropy, are eliminated by suitable shaping and mounting of a single crystal specimen the magnetisation energy may still depend on the direction of the magnetisation with respect to the crystallographic axes.

This anisotropy, due solely to crystal symmetry is known as Magnetocrystalline Anisotropy. In this case, the difference between the energy of magnetisation in an arbitrary direction and its value along a selected crystal axis is known as the Magnetocrystalline Anisotropy Energy (E_a). E_a is a free energy and increases when work is done on the system. Directions within a crystal in which E_a is a maximum or minimum are called hard and easy directions of magnetisation

respectively. The direction of the spontaneous magnetisation within a ferromagnetic domain is along an easy axis if no magnetic field is applied. Although easy directions and hard directions usually do coincide with a crystallographic axis, they need not necessarily do so, e.g. in Gadolinium below about 240K the easy direction is specified by the surface of a cone of varying half angle, (Corner et al 1962).

3.2 Expressions for the Magnetocrystalline Anisotropy Energy

The variation of the anisotropy energy E_a can be expressed as a series involving constants and functions of the angles between M_s and the crystallographic axes. Symmetry considerations can be used to simplify the expressions. Thus the variation for a cubic crystal can be represented adequately by

$$E_a(T,\infty) = K_1(\alpha_1^2\alpha_2^2 + \alpha_2^2\alpha_3^2 + \alpha_3^2\alpha_1^2) + K_2\alpha_1^2\alpha_2^2\alpha_3^2 + \ldots \quad (3.2)$$

(Brailsford 1966,p.121)

In principle terms of higher order could be added but in practice they are usually unnecessary. K_1 and K_2 are functions of temperature only and α_1, α_2, α_3 are the direction cosines of M_s with respect to the crystal axes.

The energy of a hexagonal crystal is best expressed in polar co-ordinates. The expression originally derived by Mason (1954) is

$$E_a(T,\infty) = K_1\mathrm{Sin}^2\theta + K_2\mathrm{Sin}^4\theta + K_3\mathrm{Sin}^6\theta + K_4\mathrm{Sin}^6\theta\mathrm{Cos}^6\phi \quad (3.3)$$

where θ and ϕ are the angles between M_s and the $< 0001 >$ or 'c' axis and the $< 11\bar{2}0 >$ or 'a' axis respectively. K_1, K_2 etc. are constants at any one temperature. In this expression K_3 and K_4 are generally small

compared with K_1 and K_2; the K_4 term represents a modulation of the uniaxial anisotropy with the symmetry of the basal plane. It can be shown (Zijlstra,1967 , p.170) that if K_1 is positive the easy axis is the 'c' axis and if $K_1 < -2K_2$ the easy axis is perpendicular to the 'c' axis. If $-2K_2 < K_1 < 0$ the easy axis lies on a cone of half angle Ψ given by

$$\mathrm{Sin}\Psi = \sqrt{-\frac{K_1}{2K_2}} \qquad (3.4)$$

Where the easy axis lies in the basal plane and is parallel to the $< 10\bar{1}0 >$ or 'b' axis, the energy minimum occurs where $\phi = 90^o$ and $\theta = 90^o$ i.e. where the $\sin 6\theta \sin 6\phi$ term is a minimum. K_4 is therefore positive as in Terbium. Where the easy axis parallel to the $< 11\bar{2}0 >$ or 'a' axis, K_4 is negative as in Dysprosium.

It is important to note that the energy E_a is defined for magnetisation at constant stress. Due to magnetostriction part of the free energy is stored as elastic strain in the crystal. Methods of supporting crystals during measurements of anisotropy energy must therefore allow the development of these strains and yet not introduce any stresses. It is also important to note that E_a is defined for saturation magnetisation of the crystal. Measurements at finite values of applied field give values of the anisotropy constants K_1 etc. which vary with the field value and are distinguished by primes thus: K_1', K_2' etc. Methods of obtaining infinite field or saturation values of the constants are discussed in Section 9.2.4.

Zener (1954) showed that the temperature dependence of the anisotropy energy in his theory could be stated more simply if the anisotropy energy is expressed as a series of surface harmonics of appropriate symmetry thus:

$$E_a = \sum_n E_n S_n(\alpha_1\alpha_2\alpha_3) \qquad (3.5)$$

where S_n is a surface harmonic of degree n. (This form also has the advantage of allowing direct comparison with crystal field terms in a one-ion theory of anisotropy.) This practice is followed widely with a variety of symbols for the coefficients. For example Feron (1969) has for hexagonal symmetry

$$E_a = V_2^{\,o}P_2(\mathrm{Cos}\theta) + V_4^{\,o}P_4(\mathrm{Cos}\theta) + V_6^{\,o}P_6(\mathrm{Cos}\theta) + V_6^{\,6}\mathrm{Sin}^6\theta\mathrm{Cos}6\phi \qquad (3.6)$$

Where $P_1(\mathrm{Cos}\theta)$ is the Legendre polynomial of degree 1. Similarly Rhyne (1972) has

$$E_a = K_2 Y_2^{\,o}(\theta,\phi) + K_4 Y_4^{\,o}(\theta,\phi) + K_6 Y_6^{\,o}(\theta,\phi) + K_6^{\,6}\mathrm{Sin}^6\theta\mathrm{Cos}6\phi \qquad (3.7)$$

where the $Y_1^{\,m}(\theta,\phi)$ are spherical harmonics, which being normalised to unity for $\theta = \phi = 0$, reduce to the Legendre polynomials.

The E_n, the $V_1^{\,m}$ and the K_1 are linear combinations of the constants K_1 in equation (3.3). $K_6^{\,6}$ and $V_6^{\,6}$ are to be identified with Mason's K_4.

The use of the older phenomenological equations continues (e.g. Miyahara 1971, Novac 1971) and following Callen and Callen (1966), to avoid confusion the symbol K will be used when expansion of E_a in spherical harmonics is implied. The coefficient of the term representing the hexagonal anisotropy of the basal plane will be most frequently given as K_4.

3.3 Origins of Magnetocrystalline Anisotropy

The greater part of the magnetisation energy arises from the Heisenberg exchange interaction which produces the molecular field and is of the form (Eq. 2.22)

$$U_{ij} = -2\oint \underset{\sim}{S}_i . \underset{\sim}{S}_j$$

This quantity is an invariant under a rotation of the co-ordinates and it therefore gives a free energy which is independent of the direction of magnetisation and cannot account for the anisotropy. Models to account for the anisotropy are of two main kinds: the first, the "two-ion" model, traces the anisotropy to a dependence of the exchange energy between pairs of magnetic ions on their orientation relative to the line joining them. Two-ion mechanisms include both anisotropic exchange and true dipole-dipole interaction. The second model, the "single-ion" model, traces the anisotropy to the interaction between individual magnetic ions and the anisotropic field produced by the other ions and conduction electrons. The models are not mutually exclusive. For example, both one-ion and two-ion mechanisms have been combined to account for the temperature dependence of the magnetostriction coefficient λ^{γ} in Gadolinium (Callen and Callen, 1965).

3.3.1. The Two-Ion Model

The pair or two-ion model is due largely to Van Vleck (1937 and 1956). The classical electromagnetic coupling between two spins gives a potential energy

$$\frac{\mu_o g^2 m_B^2}{4\pi \underset{\sim}{r}_{ij}^3}\left(\underset{\sim}{S}_i . \underset{\sim}{S}_j - \frac{3(\underset{\sim}{S}_i . \underset{\sim}{r}_{ij})(\underset{\sim}{S}_j . \underset{\sim}{r}_{ij})}{r_{ij}^2}\right) \qquad (3.8)$$

where g is the Landé splitting factor for the spins. $g \sim 2$ in most cases because of the quenching of orbital angular momentum in the crystal lattice.

$\underset{\sim}{r}_{ij}$ is the distance between the Spins $\underset{\sim}{S}_i$ and $\underset{\sim}{S}_j$

This expression, which represents the true dipole-dipole interaction, is of the correct form but gives values which are too low to account for observed values of anisotropy energy. An expression of the following form was sought

$$C_{ij}(r_{ij})\left(\underset{\sim}{S}_i.\underset{\sim}{S}_j - \frac{3(\underset{\sim}{S}_i.\underset{\sim}{r}_{ij})(\underset{\sim}{S}_j.\underset{\sim}{r}_{ij})}{r_{ij}^2}\right) \qquad (3.9)$$

where C_{ij} is a function of $\underset{\sim}{r}_{ij}$ much larger than the classical constant and dying away more rapidly with increasing $\underset{\sim}{r}_{ij}$.

By superposing the spin-orbit coupling on the exchange energy in a second order perturbation calculation an interaction of the form given in (3.9) was obtained with C_{ij} of the order of magnitude of $\mathcal{J}(g-2)^2$, where $\mathcal{J}$ is the exchange integral.

Qualitatively the origin of the interaction is the effect of magnetic spin-orbit coupling between any unquenched orbital angular momentum and the spins responsible for the magnetic moment. Part of the orbital rotates with the spins and the overlap and hence the electrostatic energy of neighbouring orbitals is thereby altered. The dependence of the anisotropy on the existence of unquenched orbital angular momentum is clearly indicated in the factor (g-2) since complete quenching of the orbital angular momentum leaves only the intrinsic angular momenta of the electrons for which g = 2.

The coupling represented by the expression 3.9 above is known as the pseudo-dipolar interaction or anisotropic exchange.

Where the fourth order effect of the spin-orbit interaction is included in the perturbation calculation a potential energy of the following type is obtained,

$$D_{ij}(\underset{\sim}{S}_i \cdot \underset{\sim}{r}_{ij})^2(\underset{\sim}{S}_j \cdot \underset{\sim}{r}_{ij})^2 \qquad (3.10)$$

where $D_{ij} \approx \oint (g-2)^4$.

D_{ij} falls off very rapidly with increase of $\underset{\sim}{r}_{ij}$ and by considering only the coupling between nearest neighbours it is possible to obtain energies large enough to account for typical measured anisotropy energies. D_{ij} is of the same order of magnitude as K_1 for cubic crystals. This interaction is called "pseudo-quadrupolar".

The pseudo-dipolar interaction averages to zero in b.c.c. lattices since it is proportional to $(1-3\cos^2\theta_{ij})$ and the average value of $\cos^2\theta_{ij}$ is 1/3 in this case for parallel spins. The pseudo-quadrupolar interaction can only occur if the spins S_i are 1 or greater. Van Vleck found that if a second order calculation is made of the effect of the pseudo-dipolar energy on the isotropic exchange an anisotropy energy is obtained of the same order of magnitude as for the pseudo-quadrupolar i.e.

$$\oint (g-1)^4$$

Exact calculations are not easy on this model. For example, in uniaxial crystals the first order pseudo-dipolar interaction does not average to zero and gives calculated values of anisotropy energy much higher than those measured. Only qualitative explanations are possible, thus one may regard the uniaxial crystals as slightly distorted cubic crystals where the interaction is zero.

3.3.2. The One-Ion Model

For ions such as Fe^{3+} and Mn^{2+} in non-metallic ferromagnetic crystals the degeneracy of the 3d orbitals is completely removed, the orbital angular momentum is nearly completely quenched and the Landé g factor is very close to 2. Thus the anisotropic exchange, which is

proportional to $(g-2)^4$, cannot account for the magnetocrystalline anisotropy. In this case the spins are not coupled to the orbitals and may be viewed as free. They are sited in an electric field, (the crystal field) due to the other ions, which possesses the symmetry of the crystal lattice. Wolf (1957) showed how, on this view, the anisotropy energy could be calculated in terms of parameters entering the spin Hamiltonian for a single ion. The form of the Hamiltonian depends on the symmetry of the surroundings as well as the magnitude of the spin. For spins in a lattice of cubic symmetry with axial distortion

$$\mathcal{H} = g\mu_o m_B \underset{\sim}{H} . \underset{\sim}{S} + \frac{1}{6}a(S_x^4 + S_y^4 + S_z^4) + DS_\alpha^2 + fS_\alpha^4 \qquad (3.11)$$

constant terms having been dropped. S_x, S_y, S_z and S_α are the components of S (the total spin of the ion) parallel to the x, y, z axes and α the direction of the axial distortion. Of the three parameters, a, D and f, f represents the amount of axial distortion. H is the molecular field used to represent the exchange energy, and here assumed to be isotropic. The expressions obtained for the free energy involve H and hence the relative magnetisations of the sublattices on which the ions are placed. This makes it possible to predict the temperature dependence of the anisotropy from the temperature dependence of the magnetisation.

The single-ion model can also be expected to apply to the Rare Earth elements in the metallic state since the unpaired electrons responsible for the magnetic moments of the ions belong to the 4f shell. The mean radius of the 4f shell being small compared with the interionic distance, the magnetic ions may be regarded as isolated. Spin-orbit coupling is strong and the crystalline field tends to align the non-spherical 4f charge cloud as a unit relative to the crystal axes. For the hexagonal case, the potential energy of a single 4f electron can be expressed

in spherical harmonics (Elliott, 1961 and 1972, p.156),

$$V = A_2^{\,o} r^2 Y_2^{\,o}(\theta,\phi) + A_4^{\,o} r^4 Y_4^{\,o}(\theta,\phi) + A_6^{\,o} r^6 Y_6^{\,o}(\theta,\phi) + A_6^{\,6} r^6 [Y_6^{\,6}(\theta,\phi) - Y_6^{\,-6}(\theta,\phi)] \qquad (3.12)$$

where r, θ and ϕ are the spherical co-ordinates of the electron, the $A_l^{\,m}$ are crystal field potentials calculated from the distributions of positive ions and the screening effect of the electrons in the 5s and 5p orbitals. In terms of the total angular momentum quantum number J of the ions this may be written, (Elliott and Stevens, 1953)

$$V = A_2^{\,o} \langle r^2 \rangle \alpha Y_2^{\,o}(J) + A_4^{\,o} \langle r^4 \rangle \beta Y_4^{\,o}(J) + A_6^{\,o} \langle r^6 \rangle \gamma Y_6^{\,o}(J) + A_6^{\,6} \langle r^6 \rangle \gamma [Y_6^{\,6}(J) + Y_6^{\,-6}(J)] \qquad (3.13)$$

where the factors $\langle r^l \rangle \alpha_l Y_l^{\,o}(J)$ represent the dipole, quadrupole etc. moments of the 4f charge cloud.

3.4 Magnetostriction and its Contribution to Magnetocrystalline Anisotropy

Ignoring shape effects, the free energy of a crystal may be written as

$$F = F_{\text{exchange}} + F_{\text{crystal field}} + F_{\text{spin-orbit coupling}} + F_{\text{elastic}} \qquad (3.13A)$$

As the magnetisation vector in an unstressed crystal changes direction, changes in $F_{\text{crystal field}}$ and $F_{\text{spin-orbit coupling}}$ occur. These energies depend on interionic distances and changes in these are therefore accompanied by distortions of the crystal lattice. Changes in F_{elastic} occur to keep the total free energy a minimum, the changes in dimensions of the crystal being known as magnetostriction.

The single-ion theory, as described above, pictures an ion orientated within an anisotropic but constant electrostatic field produced by the other ions in an unstrained lattice. Anisotropy measurements are however carried out under conditions of constant stress so that magnetostrictive strains are allowed to develop and modulate the crystal field. We can therefore regard measured values of anisotropy coefficient as containing two parts (Brooks, 1972).

$$\mathcal{K}_1^m = {}_o\mathcal{K}_1^m + \Delta\mathcal{K}_1^m \qquad (3.14)$$

where $\mathcal{K}_1^m$ is the measured value, ${}_o\mathcal{K}_1^m$ is the anisotropy coefficient due to the unstrained crystal and $\Delta\mathcal{K}_1^m$ is the contribution from the magnetostriction. It is the ${}_o\mathcal{K}_1^m$ which scale with the factors $A_1^m < r^1 > \alpha_1$ of equation 3.13.

In the hcp crystals used in this investigation the magnetic moments are confined to the basal plane, i.e. $\mathcal{K}_2^o$ is large and negative. From symmetry considerations, the elastic (F_e) and magnetoelastic (F_{me}) free energies can be written (Cooper, 1968 II)

$$F_e = \tfrac{1}{2}c^\gamma[(\epsilon_1^\gamma)^2 + (\epsilon_2^\gamma)^2] \qquad (3.15)$$

$$F_{me} = \epsilon_1^\gamma[2C_1(\alpha_1^2 - \alpha_2^2) - C_2 + 8C_2\alpha_1^2\alpha_2^2] + \epsilon_2^\gamma[4C_1\alpha_1\alpha_2 + 4C_2\alpha_1\alpha_2(\alpha_1^2 - \alpha_2^2)] \qquad (3.16)$$

where α_1 and α_2 are the direction cosines of the magnetisation with respect to the "a" and "b" axes respectively. C_1 and C_2 are constants giving the magnitude of the first and second order magnetoelastic energies.

$$\epsilon_1^\gamma = \tfrac{1}{2}(\epsilon_{aa} - \epsilon_{bb}) \quad \text{and}$$

$$\epsilon_2^\gamma = \epsilon_{ab}$$

are the irreducible strains appropriate to the symmetry.

$$\epsilon_{ij} = \frac{\partial r_i}{r_j}$$

c^{γ} is the elastic stiffness constant related to the Cartesian stiffness constants c_{11}, c_{12} by

$$c^{\gamma} = 2(c_{11} - c_{12})$$

The energy due to magnetostriction is the sum of F_e and F_{me}

$$F_{ms} = F_e + F_{me} \tag{3.17}$$

Differentiating the energy with respect to ϵ_1^{γ} and ϵ_2^{γ} in turn and setting the result equal to zero gives the minimum energy when

$$\bar{\epsilon}_1^{\gamma} = -\frac{1}{c^{\gamma}}\left[2C_1(\alpha_1^2 - \alpha_2^2) + 8C_2\alpha_1^2\alpha_2^2 - C_2\right] \tag{3.18}$$

and

$$\bar{\epsilon}_2^{\gamma} = -\frac{1}{c^{\gamma}}\left[4C_1\alpha_1\alpha_2 + 4C_2\alpha_1\alpha_2(\alpha_1^2 - \alpha_2^2)\right] \tag{3.19}$$

Mason (1954) gives the following expression for the magnetostriction in a hexagonal crystal

$$\begin{aligned}\lambda = \frac{\Delta l}{l} &= A[2\alpha_1\alpha_2\beta_1 + (\alpha_1^2 - \alpha_2^2)\beta_2]^2 \\ &+ B\alpha_3^2[(\alpha_1\beta_1 + \alpha_2\beta_2)^2 - (\alpha_1\beta_2 - \alpha_2\beta_1)^2] \\ &+ C[(\alpha_1\beta_1 + \alpha_2\beta_2)^2 - (\alpha_1\beta_2 - \alpha_2\beta_1)^2] \\ &+ D(1 - \alpha_3^2)(1 - \beta_3^2) \\ &+ \text{etc.}\end{aligned} \tag{3.20}$$

The A, B, C etc. are constants, β_1, β_2, β_3 are the direction cosines made by the direction in which $\frac{\Delta l}{l}$ is measured with the 3 crystal axes and α_1, α_2, α_3 are the direction cosines of the magnetisation with respect to

the crystal axes a, b, c respectively. When the magnetisation is confined to the basal plane, $\alpha_3 = 0$, and when $\frac{\Delta l}{l}$ is measured parallel to the "b" axis, $\beta_1 = \beta_3 = 0$ and $\beta_2 = 1$ hence,

$$\left[\frac{\Delta l}{l}\right]_b = A(\alpha_1^2 - \alpha_2^2)^2 + C(\alpha_2^2 - \alpha_1^2) + D \qquad (3.21)$$

When $\frac{\Delta l}{l}$ is measured parallel to the "a" axis $\beta_1 = 1$ and $\beta_2 = \beta_3 = 0$ and

$$\left[\frac{\Delta l}{l}\right]_a = A(2\alpha_1\alpha_2)^2 + C(\alpha_1^2 - \alpha_2^2) + D \qquad (3.22)$$

$\lambda^{\gamma,2}$ is defined as the change in $\left[\frac{\Delta l}{l}\right]$ when the magnetisation rotates from being parallel to the "a" axis to the "b" axis. In the first case $\alpha_1 = 1$ and $\alpha_2 = 0$ and in the second, $\alpha_1 = 0$ and $\alpha_2 = 1$ therefore

$$\lambda^{\gamma,2} = \left[\frac{\Delta l}{l}\right]_a^o - \left[\frac{\Delta l}{l}\right]_a^{90} = 2C \qquad (3.23)$$

Since $\left[\frac{\Delta l}{l}\right]_a = \epsilon_{aa}$

and $\left[\frac{\Delta l}{l}\right]_b = \epsilon_{bb}$

we have, from 3.21, 3.22 and the definition of ϵ_1^{γ} on page 33

$$\epsilon_1^{\gamma} = \tfrac{1}{2}\{A[(2\alpha_1\alpha_2)^2 - (\alpha_1^2 - \alpha_2^2)^2] + 2C[\alpha_1^2 - \alpha_2^2]\}$$

and since $\alpha_1^2 = 1 - \alpha_2^2$

$$\epsilon_1^{\gamma} = \tfrac{1}{2}\{A(8\alpha_1^2\alpha_2^2 - 1) + 2C(\alpha_1^2 - \alpha_2^2)\}$$

Comparing terms with equation 3.18 we have, with equation 3.23

$$C_1 = -\frac{c^{\gamma}C}{2} = -\frac{c^{\gamma}\lambda^{\gamma}}{4} \qquad (3.24a)$$

and $$C_2 = -\frac{c^{\gamma}A}{2} \qquad (3.24b)$$

Substituting the values of the minimum strains $\bar{\epsilon}_1^{\gamma}$ and $\bar{\epsilon}_2^{\gamma}$ in equations 3.15, 3.16 and 3.17 for the magnetostriction energy, the expressions simplify to

$$\bar{F}_{ms} = -\left[\frac{c^{\gamma}(\lambda^{\gamma})^2}{8}\right](\alpha_1^2 + \alpha_2^2)^2 + \frac{c^{\gamma}\lambda^{\gamma}}{4} A\cos 6\phi \qquad (3.25)$$

where $\phi = \cos^{-1}\alpha_1$

The first term has cylindrical symmetry since $\alpha_1^2 = 1 - \alpha_2^2$ and therefore it does not contribute to anisotropy in the basal plane. The second term has hexagonal symmetry and writing 1 = m = 6 in equation 3.14 it is possible to make the identity

$$\Delta K_6^6 = \frac{c^{\gamma}\lambda^{\gamma}A}{4} \qquad (3.26)$$

ΔK_6^6 being the contribution to the planar anisotropy from magnetostriction. The magnitude of this contribution can be calculated. Values of c^{γ} being obtained from the longitudinal and shear elastic wave velocities and the constants A and C and hence λ^{γ} being obtained from the variation of basal plane magnetostriction as follows:

In equation 3.22 we let $\alpha_1 = \cos\phi$ and $\alpha_2 = \sin\phi$. Taking as a reference the position where M_s is parallel to the "a" axis and $\alpha_1 = 1$ and $\alpha_2 = 0$,

$$\frac{\delta l}{l} = \left[\frac{\Delta l}{l}\right]_a - \left[\frac{\Delta l}{l}\right]_a^o = A\{(2\alpha_1\alpha_2)^2\} + C\{(\alpha_1^2 - \alpha_2^2) - 1\}$$

$$= A\,\sin^2 2\phi + C\{(1-2\sin^2\phi) - 1\}$$

$$= A\sin^2 2\phi - 2C\sin^2\phi \qquad (3.27)$$

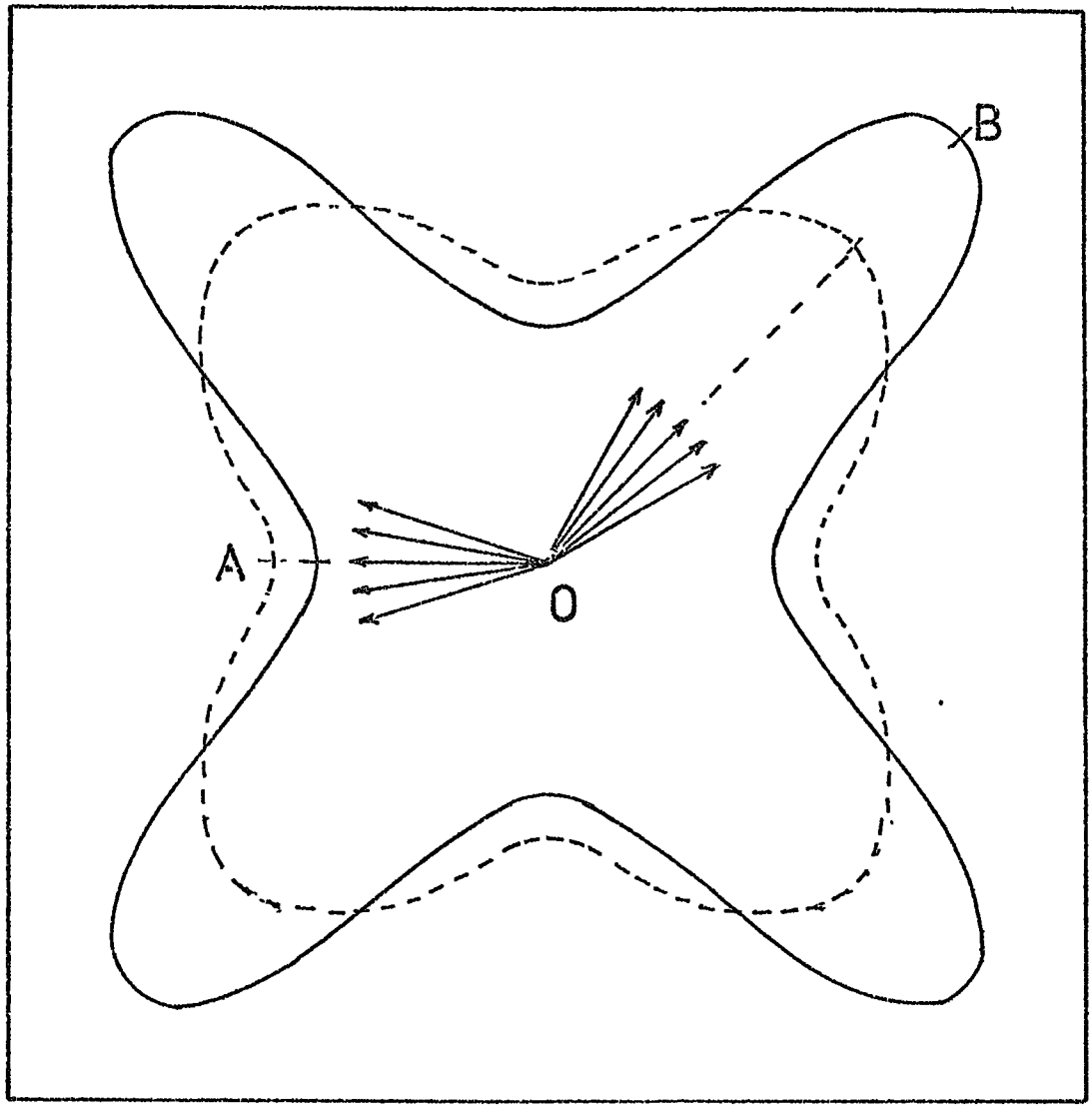

Figure 3.1 To illustrate the cause of the temperature variation of anisotropy energy (adapted from Callen and Callen 1960)

Measurements of $\frac{\delta l}{l}$ at various values of ϕ suffice to give A, C and λ^{γ}.

3.5 Variation of Anisotropy with Temperature

3.5.1. Qualitative Discussion

The measured anisotropy coefficients are found to fall rapidly with increase of temperature. This cannot be attributed to a weakening of the microscopic mechanism causing the anisotropy since for example in Nickel the spin-orbit coupling as indicated by the value of the Landé 'g' factor remains virtually constant with changes of temperature. Satisfactory explanations of the temperature variation of anisotropy are all based on the following general idea, illustrated in Figure 3.1.

The solid line represents the energy density of a single elementary moment for various orientations in the (010) plane of a cubic crystal. This curve is independent of the temperature. At absolute zero of temperature all the elementary moments or spins would be parallel to each other and would have the same energy density. The average energy density of N spins would then be equal to that for a single spin and the mean energy density curve would have the same form as the solid line. At a finite temperature however, when the macroscopic magnetisation is parallel to a hard axis OB, many spins have less than the maximum value of potential energy because thermal vibrations cause them to be distributed in a cone around OB as a mean direction. The mean energy density is then less than the energy density for a single spin aligned along OB. Similarly when the macroscopic magnetisation is parallel to an easy direction OA, those spins which are not parallel to OA have more than the potential energy appropriate to that axis so that the mean energy density is higher than

it would be at absolute zero. The overall result is shown in the dotted curve which is clearly less anisotropic than the solid line.

The elementary moment may be the magnetic moment of a single ion or a coupled pair or a small region containing several magnetic ions, so that the general idea may be applied to one-ion, two-ion and cluster models.

From Figure 3.1 it may be inferred qualitatively that the dotted curve will become circular and the anisotropy will fall to zero when the mean deviation of the spins from the magnetisation direction is about 22 degrees although the resultant magnetisation may still be quite large. This is in accordance with experience that the anisotropy falls to zero much more rapidly than the magnetisation. In the hexagonal case, the diminution of the six-fold component of the anisotropy would occur even more rapidly. The problem of calculating the temperature variation of the anisotropy energy consists of averaging the anisotropy energy of the spins at various temperatures. Since the macroscopic magnetisation also depends on the distribution of the spins about the average direction it is convenient to express the anisotropy energy in terms of the reduced magnetisation

$$m_T = \frac{M_s(T)}{M_s(0)} \quad \text{or} \quad \frac{\sigma_T}{\sigma_0}$$

where $M_s(T)$ is the saturation magnetisation at temperature T and $M_s(0)$ is the value at absolute zero. A history of the methods of performing the averaging and the variety of results obtained are given by Callen and Callen (1966) and a full explanation of the mathematical background is given by Birss (1964, page 162 et. seq.). A brief account of the relationships which have been established is now given.

3.5.2. Temperature Variation of Anisotropy of Single Ion Origin

At absolute zero of temperature, N spins in a domain or a saturated crystal might be supposed to be parallel, and the anisotropic part of the macroscopic free energy would be N times the anisotropy energy of one spin. The anisotropy coefficients K_1 would take the value of $K_1(0)$. It is permissible therefore to express the energy density of a single spin in terms of these coefficients. Following Callen and Callen,

$$e(S)_A = \sum_1 K_1(0)\, \mathcal{S}_1(S) \tag{3.28}$$

where $\mathcal{S}_1(S)$ is a normalised polynomial of the 1th degree in either the spin operators or a unit vector along the spin axis. $\mathcal{S}_1(S)$ has a symmetry imposed by the crystal lattice and is conveniently written as a linear series of spherical harmonics.

$$\mathcal{S}_1(S) = \sum_m a_1^m\, Y_1^m(S) \tag{3.29}$$

where the constants a_1^m are fixed by the crystal symmetry.

The anisotropy energy per unit volume of a system of spins is

$$E_A = \sum_1 K_1(0) \sum_m a_1^m < Y_1^m(S) > \tag{3.30}$$

where $< Y_1^m(S) >$ is an average value computed assuming the magnetisation itself to be isotropic.

By changing the polar axis to the direction of the resultant magnetisation, Callen and Callen obtain

$$E_A = \sum_1 K_1(0) < Y_1^o(S') > \mathcal{S}_1(\alpha) \tag{3.31}$$

where α is a unit vector parallel to the magnetisation and S' is the spin unit vector referred to this direction. By comparison with equation 3.28, the quantity

$$K_1(0) < Y_1^0(S') >$$

may be recognised as the temperature dependent anisotropy coefficient $K_1(T)$ and also

$$\frac{K_1(T)}{K_1(0)} = \frac{< Y_1^0(S') >_T}{< Y_1^0(S') >_0} \qquad (3.32)$$

The temperature variation of the anisotropy coefficients is reduced to an evaluation of the right hand side of equation 3.32. Several separate cases are treated.

(a) At low temperature. Quantum mechanical treatment

Using the fact that

$$\frac{< Y_1^0 >_T}{< Y_1^0 >_0} = \frac{M(T)}{M(0)} = m_T \qquad (3.33)$$

Callen and Callen obtain

$$\frac{K_1(T)}{K_1(0)} = (m_T)^{\frac{1(1+1)}{2}} \qquad (3.34)$$

(b) Extension to arbitrary temperatures

The averages of equation 3.32 were calculated in this case using a Boltzman distribution function for the deviations of the spins from the mean direction. This gives

$$\frac{K_1(T)}{K_1(0)} = \hat{I}_{1+\frac{1}{2}}(Z) \qquad (3.35)$$

where Z is a parameter which can be eliminated by the use of the relationship

$$m_T = \hat{I}_{3/2}(Z) \tag{3.36}$$

Here $\hat{I}_{1+\frac{1}{2}}$ is a normalised Hyperbolic Bessel function of order 1 and $\hat{I}_{3/2}(Z)$ is the Langevin function $\mathcal{L}(Z)$. Normalised hyperbolic Bessel functions are related to the hyperbolic Bessel functions ($I_{1+\frac{1}{2}}$) thus:

$$\hat{I}_{1+\frac{1}{2}}(Z) = \frac{I_{1+\frac{1}{2}}(Z)}{I_{\frac{1}{2}}(Z)}$$

At low temperatures only, where m_T is nearly 1 and X is large, a series expansion for $\hat{I}_{1+\frac{1}{2}}(X)$ and $\hat{I}_{\frac{1}{2}}(X)$ gives

$$\frac{\mathcal{K}_1(T)}{\mathcal{K}_1(0)} = (m_T)^{\frac{1(1+1)}{2}} \tag{3.37}$$

in agreement with the quantum mechanical treatment. This is the well known $\frac{1(1+1)}{2}$ power law enunciated by Zener (1954). Zener's proof of the law is classical, allowing the spins any orientation in an applied field, and makes the same basic assumption i.e. the sole effect of temperature is to introduce local fluctuations in the direction of the magnetisation vector. His theory does not specify that the microscopic local moment is a single spin or atom. He obtains a similar expression to 3.32 above

$$\frac{\mathcal{K}_1(T)}{\mathcal{K}_1(0)} = \frac{\langle P_1(\mathrm{Cos}\theta) \rangle_T}{\langle P_1(\mathrm{Cos}\theta) \rangle_0} \tag{3.38}$$

where $P_1(\mathrm{Cos}\theta) = Y_1^{\,o}(\theta,\phi)$ replaces $Y_1^{\,o}(S')$.

He makes a second assumption, namely that the deviation θ of the local magnetisation is the resultant of a large number of small deviations

in random directions and the probability of a deviation within a certain range is given by a random walk function. This leads to

$$\frac{K_1(T)}{K_1(0)} = (m_T)^{\frac{1(1+1)}{2}} \qquad (3.39)$$

This agrees with equations 3.34 and 3.37 for low temperatures but does not agree with equation 3.35 for higher temperatures. Keffer (1955) points out that this is due to Zener's use of a random walk distribution function rather than the Boltzman distribution, the latter function implying a field of force tending to restore the spins to parallelism.

Wolf (1957) calculated the anisotropy energy of a cubic lattice in terms of the reduced magnetisation (m_T) using explicit quantum mechanical expressions for the energy of a single spin in the crystal field and assuming a Boltzman distribution of spins between the various levels. His results for 1 = 2 and 4 and for spins 1, 3/2, 5/2 and 7/2 were adapted by Callen and Callen (1965) who showed that the values converge very rapidly to those given by the hyperbolic Bessel functions for the classical approximation.

3.5.3. Temperature variation of anisotropy of two-ion origin

The temperature dependence of anisotropy resulting from pseudo-dipolar and pseudo-quadrupolar interactions is caused by the statistical deviations of the pairs of spins S_i and S_j from the direction of the macroscopic magnetisation. The form of the theoretical temperature variation depends very much on the degree of correlation between the spins, that is on how far they maintain parallel alignment with each other. Only the two limits of complete correlation and no correlation can be treated with any confidence.

(a) The case of complete correlation

Keffer (1955) showed that Zener's 10th power law (for $l = 4$) applies to the pseudo-quadrupolar interaction in cubic crystals in the case of complete correlation and Keffer and Oguchi (1960) established the same result for the pseudo-dipolar interaction. In this limit the theoretical temperature variation of the anisotropy is the same whether calculated from expressions for the energy of interaction between neighbouring spins or from expressions involving single spins in a crystalline field.

If S_i and S_j move always parallel to each other then the two spins can be treated as one spin of magnitude 2S and the averaging of the anisotropy energy can be carried out by the same methods as for the single ion case. Thus for complete correlation at low temperatures equation 3.34 also holds and $|\kappa_1$ is proportioned to the $\frac{l(l+1)}{2}$ power of m_T.

For the pseudo quadrupolar term this may be regarded as a replacement of the term

$$< (\underset{\sim}{S}_i . \underset{\sim}{r}_{ij})^2 (\underset{\sim}{S}_j . \underset{\sim}{r}_{ij})^2 >$$

by

$$< (\underset{\sim}{S}_i . \underset{\sim}{r}_{ij})^4 >$$

i.e. $\underset{\sim}{S}_i$ becomes the same as $\underset{\sim}{S}_j$ through correlation.

This situation can hold only where the lowest states of the two spin complex are occupied since in these the spins remain parallel. The condition is that

$$1 - m_T \ll \frac{1}{S}$$

This correlation can also be regarded as breaking down at temperatures where the wavelength of thermally generated spin waves is of the same order of magnitude as the range of the given two-ion mechanism.

(b) The case of no correlation

In this case the spin averages transform separately, so that for the pseudo-quadrupolar terms the expression

$$< (S_i \cdot r_{ij})^2 (S_j \cdot r_{ij})^2 >$$

is replaced by

$$< S_i \cdot r_{ij} >^2 < S_j \cdot r_{ij} >^2$$

and the average of $< Y_2^o(S_i) >^2$ rather than $< Y_4^o(S_i) >$ is found. Thus Van Vleck (1937) obtained a $(\frac{1(1+1)}{2})^2$ law (=6th power law for the two-fold component) for the pseudo-quadrupolar interaction at low temperatures, since his use of the molecular field approximation was equivalent to the assumption of no correlation.

Callen and Callen (1965) performed a cluster theory calculation for 1 = 2, for several spin values and for several ratios of $\mathcal{J}_1/\mathcal{J}_2$ where $\mathcal{J}_1$ and $\mathcal{J}_2$ are the exchange integrals for nearest and next-nearest neighbours. They show that an m_T^2 law holds over practically the whole range of values of m_T, and only at the very low temperature limit is $\mathcal{K}_2$ again proportional to m_T^3. This distinguishes the two-ion variation from that due to the single ion mechanism for which the approximation

$$\frac{\mathcal{K}_2(T)}{\mathcal{K}_2(0)} = \hat{I}_{5/2}(z) \approx (m_T)^3$$

is valid over nearly the whole temperature range. They state (1966) that in general for two-ion interactions at high temperatures,

$$\frac{\mathcal{K}_1(T)}{\mathcal{K}_1(0)} = (m_T)^1 \qquad (3.40)$$

Yang (1971) obtained expressions for the temperature variation of the anisotropy constants K_1 and K_2 in equation 3.3 for hexagonal crystals which included terms representing two-ion interactions with no correlation. Since her coefficient K_1 is a linear combination of $\mathcal{K}_2$ and $\mathcal{K}_4$ the single ion terms are as follows:

$$\frac{K_1(T)}{K_1(0)} = a\hat{I}_{5/2}(Z) + b\hat{I}_{9/2}(Z) \qquad (3.41)$$

$$\frac{K_2(T)}{K_2(0)} = c\hat{I}_{9/2}(Z) \qquad (3.42)$$

where $Z = \mathcal{L}^{-1}\left(\frac{M(T)}{M(0)}\right) = \hat{I}^{-1}_{3/2}(m_T)$ as before.

With the addition of the two-ion terms the expressions are

$$\frac{K_1(T)}{K_1(0)} = a'\hat{I}_{5/2}(Z) + b'\hat{I}_{9/2}(Z) + a''(m_T)^2 + b''(\hat{I}_{5/2}(Z))^2 \qquad (3.43)$$

and $$\frac{K_2(T)}{K_2(0)} = c'\hat{I}_{9/2}(Z) + c''(\hat{I}_{5/2}(Z))^2 \qquad (3.44)$$

The coefficients a', b', a", b" etc. involve quantities which are not known with any precision and Yang treats them as constants which can be adjusted to fit the experimental results. Thus any theoretical relationship between the coefficients is lost and it may be said simply that each single-ion term in $\hat{I}_{9/2}(Z)$ is supplemented by a term of the form $(\hat{I}_{5/2}(Z))^2$ representing the two-ion interaction and similarly each single-ion term $\hat{I}_{5/2}(Z)$ has added to it a proportion of $(\hat{I}_{3/2}(Z))^2$. (Equivalent to $(m_T)^2$). Yang was able to represent very closely indeed the temperature variation of K_1 and K_2 for both Gadolinium and Cobalt with expressions of this form. Yang et al. (1973) have applied the theory

to cubic crystals and have obtained good fits to the temperature variation of K_1 for Iron and Nickel. They point out that fitting with four adjustable constants is not a very critical test but the expression is superior to previous expressions for nickel, (e.g. that of W.J. Carr quoted in Chikazumi 1964, p.152) at least in that it has a theoretical justification. A complete check of the theory must wait until knowledge of the microstructure of the metals allows a calculation of the coefficients.

3.6 Variation of Magnetostriction with Temperature

Kittel and Van Vleck (1960) extended the classical theory of the temperature variation of anisotropy energy to include the magnetoelastic constants. They used expressions derived by Becker and Doring on symmetry considerations for the magnetoelastic energy of a cubic crystal and regrouped the terms so that they formed homogeneous surface harmonics of order 2 and 4. The temperature dependent coefficients of these terms were shown to be proportional to $< P_2(\mathrm{Cos}\theta) >$ and $< P_4(\mathrm{Cos}\theta) >$ which correspond exactly to the averages appearing in the temperature variation of anisotropy. Callen and Callen extended this work to crystals of other symmetry and pointed out that the thermal averages involved in calculating magnetostrictive strains are identical to those in the theory of anisotropy so that the temperature variation of anisotropy coefficients of order 1 should be the same as anisotropy coefficients of the same order. For example the coefficient λ^{γ} for which $1 = 2$ should vary as $\hat{I}_{5/2}(Z)$ if it is of single-ion origin. For Dysprosium the proportionality is found to hold over three orders of magnitude (Clarke et al., 1965).

3.7 The Temperature Variation of Magnetostriction or Anisotropy as an Indication of the Fundamental Mechanism Involved.

In the case of Gadolinium, Callen and Callen (1965) found that magnetostriction data obtained from Coleman was fitted very well by the expression

$$\lambda^{\gamma} = 351 \times 10^{-6}\, \hat{I}_{5/2}(Z) - 243 \times 10^{-6}\, m^{2}_{T,H} \qquad (3.45)$$

The first term indicates a single-ion mechanism and the second a two-ion mechanism of comparable strength. The relatively small single-ion contribution is entirely consistent with the S ground state of Gadolinium.

Similarly it should be possible in principle to distinguish contributions to the hexagonal anisotropy from magnetostriction and the crystal field by their different temperature dependence. The contribution from magnetostriction $\Delta K_6^{\,6}$ is given (section 3.4) by equation (3.26).

$$\Delta K_6^{\,6} = \frac{C^{\gamma}\lambda^{\gamma}A}{4}$$

C^{γ} does not vary greatly with temperature, while λ^{γ} and A, for which l = 2 and l = 4, if of single-ion origin, vary as $\hat{I}_{5/2}(Z)$ and $\hat{I}_{9/2}(Z)$.

Therefore
$$\frac{\Delta K_6^{\,6}(T)}{\Delta K_6^{\,6}(0)} = \hat{I}_{5/2}(Z).\hat{I}_{9/2}(Z) \qquad (3.46)$$

This is in contrast to the crystal field contribution for which l = 6 and

$$\frac{{}_{o}K_6^{\,6}(T)}{{}_{o}K_6^{\,6}(0)} = \hat{I}_{13/2}(Z) \qquad (3.47)$$

Combining (3.46) and (3.47)

$${}_{s}K_6^{\,6}(T) = {}_{o}K_6^{\,6}(T) + \Delta K_6^{\,6}(T) = {}_{o}K_6^{\,6}(0)\hat{I}_{13/2}(Z) + \Delta K_6^{\,6}(0)\hat{I}_{9/2}(Z).\hat{I}_{5/2}(Z) \qquad (3.48)$$

Element	Temperatures			Comments on the antiferromagnetic phase.
	Néel K	Transition K	Curie K	
Co	12.5			Ferrimagnetic planes, moments parallel to the 'c' axis.
Pr	25			Adjacent layers antiparallel. Sinusoidal modulation of ferromagnetic structure in each plane. Magnetic ordering is not found in single crystals.
Nd	19	7.5		Sinusoidal modulation as for Pr. Hexagonal sites order at 19K and cubic sites at 7.5K with a different modulation wave vector.
Sm	14	106		Spins on hexagonal sites order antiferromagnetically at 106K. Cubic sites order ferromagnetically at 14K.
Eu	89			Helical structure as for Dy with spins parallel to a cube face and the screw axis perpendicular to a cube face.
Gd			292.7(g)	Has no antiferromagnetic phase.
Tb	230.2(a)		219.6(f)	
Dy	176 (a)		88.3(f)	
Ho	130 (a)		19 (b)	
Er	85 (c)	53(d)	19.5(b)	The 'squaring up' to the form (d) of figure 4.1 proceeds gradually and is not complete when T_c is reached.
Tm	57.2(c)	40(c→e)	32 (e)	

Table 4.1 Magnetic Ordering in the Rare Earths (Data from Koehler in Elliott(1972) page 81 et. seq.)

Figure 4.1 Varieties of spin structure in Rare Earth metals.
Adapted from Koehler (1965)

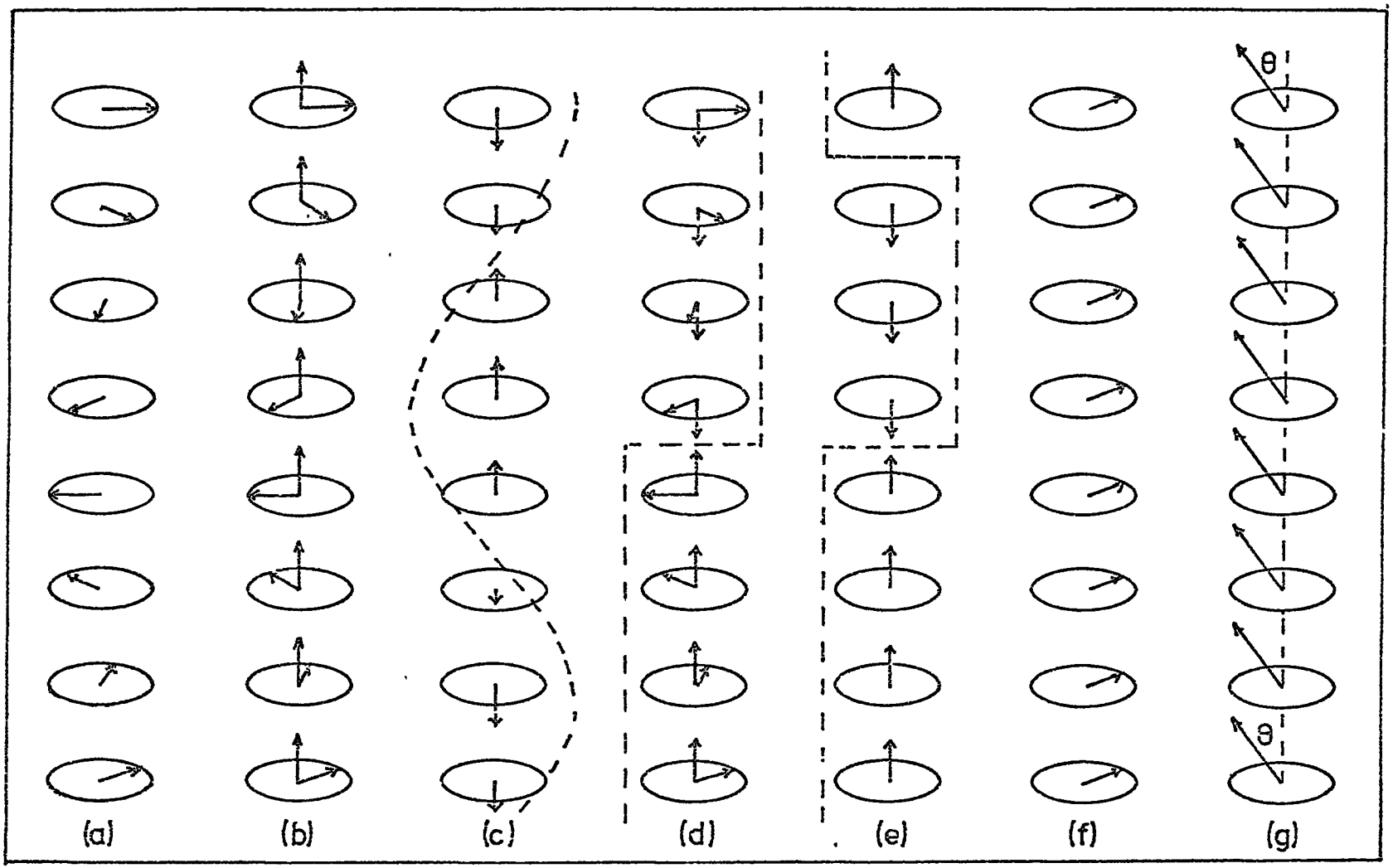

CHAPTER 4

MAGNETIC ORDERING IN THE RARE EARTHS

4.1 Varieties of Magnetic Ordering in the Rare Earth Metals

Table 4.1 gives the various ordering temperatures. Small letters in parentheses refer to the sections of Figure 4.1 where the various types of magnetic ordering are illustrated. The symbols represent the orientations of spins in consecutive planes parallel to the basal plane.

Figure 4.1(a) represents the helical spin arrangement described in section 2.36 and found in Terbium, Dysprosium and Holmium. The temperature range over which this periodic structure exists in Terbium is quite narrow and the application of a small magnetic field (about 0.1T) destroys the periodic structure. It is not absolutely certain that the structure is helical but such a structure is expected on theoretical grounds and measurements on alloys with Yttrium, which are expected to have the same structure, seem to confirm this.

In the arrangement of Figure 4.1(b) each spin is shown resolved into two components. One set of components aligns ferromagnetically parallel to the c axis while the other set forms the planar spiral arrangement as in Figure 4.1(a). The unresolved moments evidently lie on a cone which has its axis parallel to the "c" axis.

Figure 4.1(c) illustrates a sinusoidal variation of the "c" axis component of the individual moments. The other components of the moments which are parallel to the basal plane are randomly orientated and produce no overall effect; they are therefore not shown in the diagram.

In Figure 4.1(d) components of the atomic moments parallel to the basal plane form a planar spiral while components parallel to the "c" axis align antiferromagnetically.

Figure 4.1(e) shows the ferrimagnetic ordering peculiar to Thulium in which the bulk magnetic moment results from the alternation of 4 planes having spins parallel to the "c" axis with 3 planes having oppositely directed spins.

Figure 4.1(f) shows the ferromagnetic ordering in Terbium and Dysprosium while Figure 4.1(g) shows the ferromagnetic ordering in Gadolinium where the angle marked θ changes with temperature, becoming zero above 240K (Corner et al., 1962)

Periodic structures are repeated throughout the crystal with a wavelength which varies with temperature and is in general not commensurate with the interlayer spacing of the crystal.

4.2 Interactions Causing Magnetic Ordering (With particular reference to the heavy Rare Earths)

4.2.1. Indirect Exchange

The exchange interaction giving rise to the co-operative phenomena encountered in the Rare Earths must be indirect in view of the small spatial extent of the 4f orbital. It must also be oscillatory, i.e. change sign with the separation of the pairs of ions, in order to explain the spiral and other periodic structures observed (section 2.36). The small value of Hc, needed to produce the metamagnetic transition in, for example, Terbium (less than 0.08T) compared to the magnitude of the Heisenberg field points to the existence of ferromagnetic interactions alongside the antiferromagnetic interactions which reduce the difference in energy between the ferromagnetic and antiferromagnetic states. The existence of magnetic ordering in alloys containing as little as 5% of magnetic Rare-Earth in a non-magnetic diluant such as Lanthanum or Yttrium indicates that the interaction is of greater range than the distance between nearest neighbours in a lattice.

The usual explanation of these facts has been on the basis of a model, used orginally by Rudermann and Kittel in connection with Nuclear Magnetic Resonance investigations, subsequently applied by Kasuya to the magnetic ordering in Gadolinium and by Yosida to Copper Manganese alloys, now known as the Rudermann-Kittel-Kasuya-Yosida or simply RKKY interaction. In this model the exchange interaction between the 4f electrons of one ion and the conduction electrons in the metals results in a polarisation of the latter which in turn couples with a more distant 4f shell. The exchange integrals are difficult to evaluate from first principles and it is found adequate for a phenomenological theory to represent the interactions as scalar couplings of the form

$$H_i = \Gamma \underset{\sim}{S}_i . \underset{\sim}{S}_c \qquad (4.1)$$

where Γ is a constant.

This leads to a polarisation of the conduction electrons

$$P_i(\underset{\sim}{r}) = \frac{9\pi Z^2 \Gamma}{4V^2 E_f} \underset{\sim}{S}_i F(2k_f . \underset{\sim}{r}) \qquad (4.2)$$

where Z is the number of conduction electrons per atom, V is the atomic volume, E_f if the Fermi energy, k_f the wave-vector of the electrons at the Fermi surface and F(x) is a function

$$F(x) = \frac{(\sin x - x\cos x)}{x^4} \qquad (4.3)$$

F(x) has the necessary properties of alternating in sign and dying away slowly with distance. The interaction of this polarisation with a second spin has the same form as equation (4.1) above and this leads to an interaction of the form

$$H_{ij} = \frac{-9\pi Z^2\Gamma^2}{4V^2E_f} \sum_{i\neq j} F(2k_f \cdot r_{ij}) S_i \cdot S_j \qquad (4.4)$$

de Gennes (1962) showed that in order to take account of the spin-orbit coupling when applying the above result to the Rare Earths it was necessary to replace S_i and S_j by $(g-1)J_i$ and $(g-1)J_j$, the projections of the spins on the direction of J.

The theory in broad outline is very successful. In the molecular field approximation it leads to an expression for the paramagnetic Curie temperature θ_p,

$$k\theta_p = \frac{3\pi Z^2\Gamma^2(g-1)^2J(J+1)}{V^2E_f} \sum_{i\neq j} F(2k_f \cdot r_{ij}) \qquad (4.5)$$

The factor $(g-1)^2J(J+1)$, is known as the de Gennes function and is found to be closely proportional to the average values of θ_p for Rare Earths. For the case where there are three conduction electrons per atom de Gennes obtained a minimum exchange energy when the interlayer turn angle in a helical spin structure is about 60^o; this is not far above typical values actually observed. Theoretical expressions also predict correctly that the exchange energy in the helical state is not very different from that in the ferromagnetic state, a fact which gives magnetostriction and anisotropy energies a decisive role in determining the ordered state of the metals. (Section 4.2.2).

The polarisation of the conduction electrons which is an essential feature of the model is observed as an enhancement of the magnetic moments of the Rare Earth atoms in the metallic state.

Many sweeping assumptions are made in performing calculations on the RKKY model. The Fermi surface is assumed to be spherical and the conduction electrons are all assumed to be of an 's' character. The theory does not account at all for the variation of the interlayer turn angle with temperature and the expression for θ_p breaks down for various Rare Earth intermetallic compounds (Levy 1970, Becle et al 1970) Campbell (1972) points out many inconsistencies in deductions based on the model and shows that many of them would be removed by a different indirect mechanism having positive exchange between 4f and 5d electrons in the same atom and direct 5d-5d interactions between different atoms. This proposed interaction is however of short range and alone cannot account for the phenomena in the Rare Earths. The main features of the RKKY theory are still accepted while modifications are made to achieve consistency (Taylor 1971, Levy 1970).

The exchange function may be determined experimentally from spin-wave spectra excited by inelastic neutron scattering and is usually given in terms of the Fourier transform function

$$\mathcal{J}(\underset{\sim}{q}) = \sum_{i \neq j} \mathcal{J}(\underset{\sim}{r}_{ij}) e^{i\underset{\sim}{q}\cdot\underset{\sim}{r}} \qquad (4.6)$$

where $\underset{\sim}{q}$ is a reduced wave vector $2\pi/\lambda\underset{\sim}{c}$ (Mackintosh and Bjerrum Møller (1972)). If a maximum in the graph of $\mathcal{J}(\underset{\sim}{q})$ against $\underset{\sim}{q}$ occurs where $\underset{\sim}{q} = 0$, the initial ordering is ferromagnetic as in the case of Gadolinium; but if there is a maximum at $\underset{\sim}{q} = \underset{\sim}{q}_{max}$, the ordering should then be periodic with a wave-vector $\underset{\sim}{Q}$ equal to $\underset{\sim}{q}_{max}$, and may be helical, sinusoidal or some other form. If $\underset{\sim}{q}_{max} = 1$ then normal antiferromagnetism should result.

4.2.2. The effect of magnetostriction and magnetocrystalline anisotropy on magnetic ordering in the heavy Rare Earths

Although spiral structures will not occur without the long range oscillatory type of exchange interaction with a maximum in $\mathcal{J}(\underset{\sim}{q})$ at some non-zero value of $\underset{\sim}{q}$, the existence of this type of exchange does not necessarily produce a periodic structure. Thus experimental results for $\mathcal{J}(\underset{\sim}{q})$ for Dysprosium at 78K show a definite maximum displaced from the origin, yet at this temperature Dysprosium is ferromagnetic. The explanation of this is that the system of spins takes up the state with the lowest free energy and reductions in the total free energy due to magnetostriction and anisotropy in the ferromagnetic state may more than compensate for an increase in exchange energy.

In the heavy Rare Earths magnetocrystalline anisotropy largely controls the form of the periodic structures. In the particular materials studied in this investigation (Dysprosium, Terbium and Terbium-Scandium Alloys) the "c" axis is very "hard" magnetically and spin moments are confined to the basal plane in both the ferromagnetic and the antiferromagnetic state so that the latter is helical. Details of the following discussion therefore mainly refer to the transition from helical to parallel spin arrangements although the principles are of wider applicability. The ideas involved were developed by Elliott (1961, 1971) and Cooper (1968, I and II) and are fully described in Chapter 2 of Elliott (1972).

The components of the free energy which should be taken into account are as follows:-

(i) The isotropic indirect exchange energy described by the RKKY theory ($F_{iso.ex}$).

(ii) Anisotropic exchange energy ($F_{an.ex}$). Since two-ion interactions are not significant in these materials this energy is neglected.

(iii) Crystal field anisotropy (F_{cf}) due to the undistorted lattice.

(iv) Elastic strain energy (F_e).

(v) Magnetoelastic energy (F_{me}) coupling the spins to the strains.

(vi) In the presence of a magnetic field there will also be the Zeeman energy (F_z).

The change to ferromagnetism will occur when

$$F_{ex.hel} \geq F_{ex.fm} + F_{me} + F_e + F_{cf} + F_z \qquad (4.6)$$

or when

$$F_{ex.hel} - F_{ex.fm} - F_z \geq F_{ms} + F_{cf} \qquad (4.7)$$

The equality holding at the critical field for each temperature. $F_{ex.hel}$ and $F_{ex.fm}$ represent the exchange energy in the helical a.f.m. and f.m. states respectively, and F_{ms} is the free energy due to the equilibrium magnetostriction, equal to the sum of F_e and F_{me}. Expressions for the values of F_{ms} and F_{cf} are already known. From equation (3.25) we have

$$F_{ms} = -\frac{c\gamma(\lambda\gamma)^2}{8} + \frac{c\gamma_\lambda\gamma_A \cos 6\phi}{4} \qquad (4.8)$$

Omitting all terms concerned with the axial anisotropy from equation (3.7), since the spins do not leave the basal plane,

$$F_{cf} = \mathcal{K}_6^{\,6} \cos 6\phi \qquad (4.9)$$

The sum of F_{ms} and F_{cf} is always negative since the first term for F_{ms} is negative and the spins orientate themselves so as to make the sum of $\frac{c\gamma_\lambda \gamma_A}{4} \cos 6\phi$ and $\mathcal{K}_6^{\,6} \cos 6\phi$ negative, ϕ being either 30° or 0° depending on whether or not the sum of $\frac{c\gamma_\lambda \gamma_A}{4}$ and $\mathcal{K}_6^{\,6}$ is positive.

The energies F_{ms} and F_{cf} therefore reduce the free energy in the ferromagnetic state so that the system may become ferromagnetic even when the exchange energies favour the helical spin arrangement. Their sum

$$F_d = F_{ms} + F_{cf} \qquad (4.10)$$

may be regarded as a driving energy to ferromagnetism. A numerical test of equation (4.7) above is described by Cooper for Dysprosium. The quantities on the left hand side of the equation were obtained from the analysis of Elliott (1961) and the quantity F_d was calculated assuming that the magnetostriction and anisotropy are of single-ion origin, and that the constant A is negligible for this metal. Therefore

$$F_d = -\frac{c\gamma}{8} \left\{ \lambda^\gamma \hat{I}_{5/2}(z) \right\}^2 + \mathcal{K}_6^{\,6} \left\{ \hat{I}_{13/2}(z) \right\} \qquad (4.11)$$

where as before,

$$m_T = \hat{I}_{3/2}(z)$$

Although the two terms contributing to F_d are of roughly equal magnitude at absolute zero, the hexagonal anisotropy dies away more rapidly with increasing temperature and is only about 20% of F_d at the Curie temperature. Satisfactory numerical agreement was obtained, thus supporting the general validity of the concepts and also that the driving energy to ferromagnetism in Dysprosium consists mainly of the cylindrically symmetrical magnetostriction energy.

The onset of ferromagnetism with reduction of temperature can be understood easily on this model. The driving energy F_d depends on $(\hat{I}_{5/2}(Z))^2$ and on $\hat{I}_{13/2}(Z)$ both of which factors increase more rapidly than the exchange energy as the temperature falls.

The hexagonal anisotropy determines the direction of the moment when ferromagnetism occurs and may determine whether the collapse of the helical spin structure at the critical field is a second or first order transition. A knowledge of the magnitude of this anisotropy energy is therefore of some importance in understanding the magnetic ordering of a particular material, and a knowledge of its temperature variation is also of use in giving an indication of its origin.

4.3 Anisotropy and Related Measurements in Terbium

A complete series of magnetisation measurements on single crystals of Terbium is given by Hegland et al (1963) together with some data from specific heat, neutron diffraction and electrical resistivity measurements confirming the phase changes found. The antiferromagnetic order between 220 and 230K can be overcome with a field less than 0.08T. They also reported the very much smaller susceptibility parallel to the "c" axis compared with directions in the basal plane, the enormous anisotropy making it necessary to restrain the specimen with chains during measurements parallel to the "c" axis at lower temperatures. From the lack of saturation along the "a" axis they deduced that the "b" axis is the easy axis at all temperatures.

Rhyne and Legvold (1965) measured the magnetostriction of Terbium single crystals between 4 and 350K in fields up to 3T, computed the values of the constants A and C in equation (3.27) and compared the temperature

variation with the predictions of the single ion theory (Section 3.5). Since A is a coefficient of a term of the fourth degree and C of a term of the second degree, it was expected that

$$\frac{C(T)}{C(0)} = \hat{I}_{5/2}(\hat{I}^{-1}_{3/2}(m_T)) \qquad (4.12a)$$

and

$$\frac{A(T)}{A(0)} = \hat{I}_{9/2}(\hat{I}^{-1}_{3/2}(m_T)) \qquad (4.12b)$$

where C(T) and A(T) denote the values of C and A at temperature T while C(0) and A(0) are their values at absolute zero. Both of these relationships were very well satisfied by the results over the whole temperature range.

In order to measure the enormous anisotropy energy when the specimen is magnetised parallel to a "c" axis, Rhyne and Clark (1967) used a torque magnetometer in which the counter torque was provided by a current in a coil fastened to the specimen and suspended with it in the applied field. Fields up to 14T were used and it was found that fields of 10T were able to move the magnetisation less than 10^{o} out of the basal plane. Using magnetisation data to calculate the actual orientation of the magnetisation and the first term in equation 3.7 they found that the temperature variation of K_2 followed the single-ion theory well i.e.

$$\frac{K_2(T)}{K_2(0)} = \hat{I}_{5/2}(\hat{I}^{-1}_{3/2}(m_T)) \qquad (4.13)$$

with a value of $K_2(0)$ equal to 6.65×10^3 J Kg^{-1}. In contrast K_6^6, the basal plane anisotropy constant deduced from the magnetostriction data, did not fit the corresponding one-ion function $\hat{I}_{13/2}(Z)$, at all closely.

$$K_6^6(0) = 29.25 \text{ J Kg}^{-1}$$

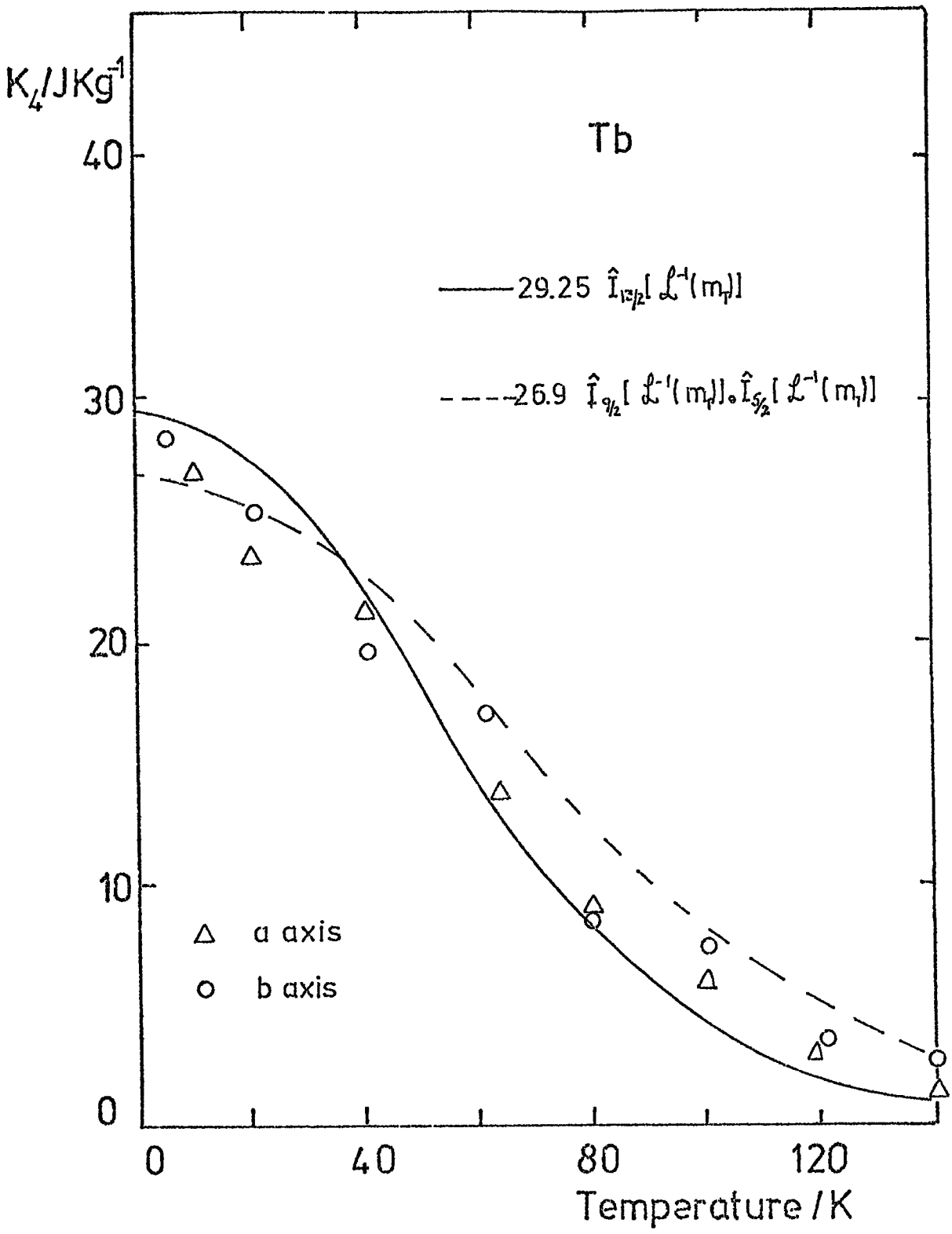

Figure 4.2 The basal plane anisotropy of Terbium compared with theory. Adapted from Cooper (1968 I)

Bly et al (1968) measured the anisotropy constant K_1 for Terbium in the paramagnetic region and also K_4 ($\equiv \kappa_6^6$) in the ferromagnetic range. The results agreed well with those of Rhyne and Clarke, and confirm the poor fit of the single-ion function, $\hat{I}_{13/2}(Z)$.

Feron (1969) measured the magnetocrystalline anisotropy of Terbium using the magnetisation curve method (Section 5.1) and found a satisfactory agreement between the variation of κ_4^o and the corresponding single-ion function but a much poorer agreement for the variation of κ_2^o. This he felt would be improved by taking magnetostriction into account. His value of $\kappa_2(0)$ is only 3% greater than that of Rhyne and Clarke. Microwave absorption experiments at 9.44 GHz by Bagguley and Liesegang (1966) on a basal plane crystal disc of Terbium allowed an estimate to be made of the hexagonal anisotropy field. This quantity was found to be proportional to $(m_T)^6$ in the temperature interval 140 to 220K. This is a smaller power law than expected on the single-ion theory, whether the anisotropy is of crystal field origin or not.

Cooper (1968,I) considered the contribution to the hexagonal anisotropy of Terbium from the second order magnetostriction effects which should vary (Equation 3.46) with temperature as the product,

$$\hat{I}_{9/2}(Z).\hat{I}_{5/2}(Z) \qquad m_T = \hat{I}_{3/2}(Z)$$

He showed that this function did not provide a significantly improved fit to the results of Rhyne and Clarke (1967) (Figure 4.2).

From inelastic neutron scattering experiments, Nielsen et al (1970) were able to show that the variations of $h\omega(0)$ with field and temperature for a Terbium/10% Holmium crystal could be fitted to theoretical expressions only if the parameter representing the crystal field

anisotropy is near zero. They concluded that the hexagonal anisotropy is entirely accounted for by magnetoelastic effects. Because of the similarity between the anisotropy properties of Terbium and Holmium, and because the proportion of Holmium in the sample was small, they felt that the same conclusion could be drawn for pure Terbium.

4.4 Anisotropy and Related Measurements in Dysprosium

The magnetic properties of Dysprosium in various crystallographic directions were determined by Behrendt et al (1958) and interpreted by Liu et al (1959) who determined the axial and the basal plane anisotropy constants by fitting theoretical expressions for the magnetisation to the experimental curves. K_4 varied as $(m_T)^{21}$ and K_1 as $(m_T)^3$ in accordance with Zener's theory. They found no anisotropy in the basal plane between 110K. and the Néel temperature. This was not expected for a normal antiferromagnetic material. Neutron diffraction experiments (Wilkinson et al 1961) showed that the antiferromagnetic structure is helical with a further slight modulation below 140K possibly due to the basal plane anisotropy. Clark et al (1963, 1964, 1965) studied the magnetostriction, which is extremely large, $\frac{\delta l}{l}$ reaching 6×10^{-3} parallel to an "a" axis with an applied field parallel to the "b" axis. The high value allows measurement over a wide range of temperature, and the variation of $\lambda^{\gamma,2}$ was found to follow the single ion function $\hat{I}_{5/2}(Z)$ over three decades.

Experiments carried out by Rhyne and Clark at the same time as those on Terbium indicate similar values for $\mathcal{K}_2^{\,o}(0)$. This was to be expected from the identical values of the quantity $< r^2 > \alpha\, Y_2^{\,o}(J)$ for the two metals in the expression for the anisotropy energy in equation

(3.13). $\kappa_6^6(0)$ is of the order of 100 J kg^{-1}. Rhyne et al (1968) continued magnetisation measurements on Dysprosium and Terbium in static fields up to 14T and in pulsed fields of the order of 40T. Fields above 6T applied along the "c" axis produced permanent changes in the crystals. From the magnetisation curves at lower fields, values of $\kappa_2^0(0)$ were deduced some 20% lower than those obtained in torque measurements.

Feron (1969) using magnetisation curves obtained values of κ_2^0 and κ_6^6 in substantial agreement with the torque methods. The anisotropy coefficient κ_6^6 obeys the single-ion relationship equation (3.35) quite closely. Thus

$$\frac{\kappa_6^6(T)}{\kappa_6^6(0)} = \hat{I}_{13/2}(Z) \quad \text{where } Z = \hat{I}_{3/2}(m_T)$$

confirming the single-ion crystal field origin of the anisotropy.

Changes of easy axis in Dysprosium were observed by Bly (1967,1969) in experiments with a torque magnetometer. The easy axis changes are summarised in Figure 4.3, which is taken, with modifications from Bly's thesis (1967). A point on the graph represents one temperature and applied field value. The lines join points where the easy axis of magnetisation changes and K_4 changes sign. The broken line joins points obtained from the torque measurements while the solid lines mark changes of easy axis deduced by Bly from the magnetisation measurements of Jew and Legvold (1963). The regions of the diagram bounded by these lines are marked with Roman numerals and the easy axis in each region is shown by small letters placed close to the lines. The dotted line shows the critical field at each temperature.

The original version of this diagram contains an error which has the effect of exchanging 'a' for 'b'. The correction was made in Bly's

Figure 4.3 Dysprosium: Bly's results for changes of easy axis.

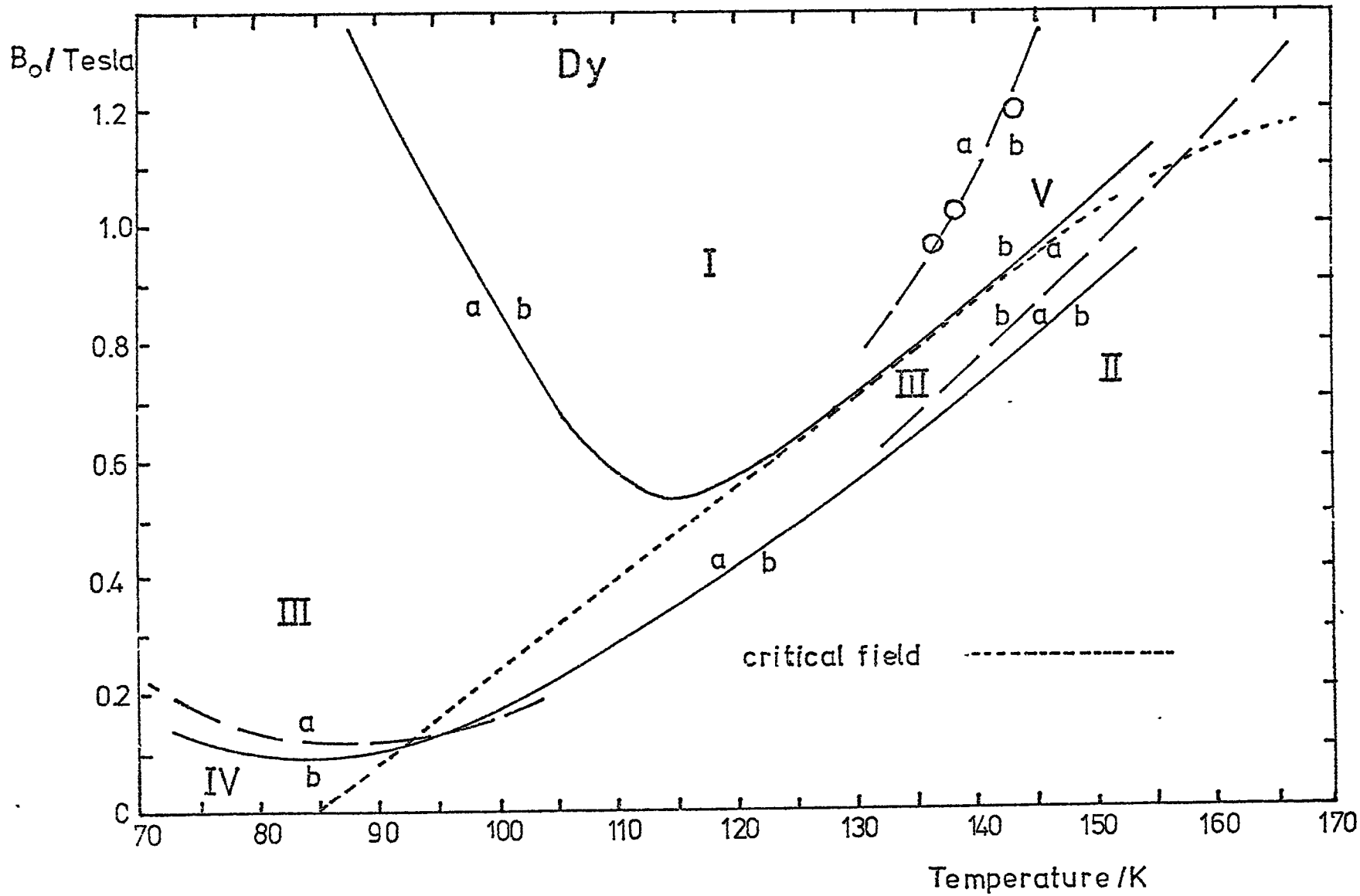

1969 paper and is incorporated in Figure 4.3. Also in the 1969 paper Bly pointed out that the changes of easy axis lie very close to a line of constant magnetisation where

$$\sigma = 236 \ Am^2kg^{-1}$$

There are several discrepancies between the torque-curve and the magnetisation results. For example in the regions I and II they indicate different easy axes.

4.5 The Effects on the Magnetic Ordering of Heavy Rare Earths of Alloying with Yttrium

Alloys of Gadolinium and Lanthanum with Yttrium were investigated by Thorburn et al (1958) and alloys of Terbium, Dysprosium, Holmium, Erbium and Thulium with Yttrium were investigated by Child et al (1965) by neutron diffraction techniques. The results confirmed and extended previous work (e.g. Weinstein et al 1963) and are reviewed and discussed by Koehler (1965).

Increasing percentages of Yttrium lower the Néel point but lower the Curie temperature even more, thus widening the ranges of temperatures over which the alloy has an antiferromagnetic structure. The ferromagnetic phase in Terbium disappears with less than 25 atomic percent of Yttrium and in Dysprosium it disappears with less than 5 At% of Yttrium.

Within the limits of resolution of the method the antiferromagnetic structures in the alloys are found to be the same as those in the pure Rare Earth.

Gadolinium alloys remain purely ferromagnetic with up to 34 At% of Yttrium; with 34 to 40 At% of Yttrium they show both ferromagnetic and antiferromagnetic behaviour, while more dilute alloys exhibit only an

antiferromagnetic phase, probably of a helical kind.

The overall effect of dilution with Yttrium seems to be to produce magnetic behaviour characteristic of the Rare Earth elements further down the list and to stabilise the helical structures at the expense of the ferromagnetic ones. Ordered structures are found with quite small concentrations of the magnetic Rare Earth, e.g. 5% Terbium or 10% Holmium. Relationships similar to those obtaining for the inter-Rare Earth alloys (Bozorth et al 1966) are found between the Néel temperatures, the initial inter-layer turn angle and the average de Gennes function. The latter quantity is defined as

$$\bar{G} = \Sigma C_i (g-1)^2 J_i (J_i + 1)$$

where C_i is the fraction of the ith. component in the alloy and

$$G_1 = (g-1)^2 J_i (J_i + 1)$$

is the square of the effective spin, i.e. the projection of the spin on J.

The Néel temperatures are proportional to the 2/3 power of the de Gennes function. This relationship holds, with the same constant of proportionality, for all percentage compositions of all the inter-Rare Earth and Yttrium-Rare Earth binary alloys tested. More remarkably, the Curie temperatures of the ferromagnetic Gadolinium alloys also fit the relationship.

The interlayer turn angles just below the Néel point (θ_i) when plotted against the average de Gennes function lie quite close to a single smooth curve. This curve extrapolates to $\theta_i = 50^o$ for small values of $\bar{G}$.

The value of θ_i falls to zero for G = 11.5, corresponding quite closely to the composition first showing ferromagnetic behaviour in the Gadolinium alloys.

4.6 The Effects on the Magnetic Ordering of Heavy Rare Earths of Alloying with Scandium

Measurements of χ_m for Scandium (Chechernikov et al 1963, Ross et al 1969) show paramagnetic behaviour with a negative value of θ_p the paramagnetic Curie temperature. This indicates antiferromagnetic coupling between nearest neighbours. There are uncertainties in the value of χ_m and in the slight anisotropy. Ross gives $\chi_m \approx 90 \times 10^{-6}$ with $\chi_{\perp c} - \chi_{\parallel c} \approx 4 \times 10^{-6}$. This anisotropy is drastically affected by small amounts of magnetic impurities. Wohlleben (1968) explains the field dependence of the magnetisation in alloys containing 0.1% of Gadolinium by (a) the existence of an antiferromagnetic interaction, (b) the existence in Scandium of unquenched angular momentum in the d-orbitals and (c) ready polarisation of the d electrons.

Neutron diffraction experiments (Child et al 1966, 1968) on alloys of Terbium, Holmium and Erbium with Scandium indicate some similarities to the alloys with Yttrium. The ordered structures are of the same kind as in the pure Rare Earth and the initial value of the inter-layer turn angle (θ_i) is a single valued function of $\bar{G}$ with a limiting value of 50^o. There are several significant differences however. The Néel temperatures do not follow a $\bar{G}^{2/3}$ law and Scandium lowers the Néel temperatures more for a given dilution. Magnetic ordering vanishes for quite high percentages of magnetic Rare Earth, e.g. about 25 At% of Terbium, 18At% of Holmium, and 39 At% of Erbium, even for temperatures as low as 1.3K.

Magnetic measurements on Gadolinium-Scandium alloys (Nigh et al 1964) show that ferromagnetic behaviour persists up to approximately 30 At% of Scandium. At about 31 At% of Scandium the alloys show both ferromagnetic and antiferromagnetic behaviour while alloys with more Scandium are antiferromagnetic only.

The polarisation of the Scandium matrix is shown by the rise in m_{eff} with decreasing Gadolinium concentration and a similar rise in m_{sat} for the ferromagnetic alloys. Salamon (1971) using electron spin resonance found that the effective moment of Gd in Scandium was enhanced and varies with direction.

Measurements of the lattice parameters, magnetisation, thermal expansion and magnetostriction of a series of Terbium Scandium alloys were made by Chatterjee and Corner (1971). The Néel temperatures appear to vary as $\bar{G}^{4/3}$ and θ_p as $(\bar{G})^2$. Magnetostriction measurements for two of the richer alloys show that the constant $\lambda^{\gamma,2}$ follows the single-ion theory well. In addition the sharp fall in the Curie temperature with increasing Scandium content correlates well with the fall in the cylindrically symmetrical magnetostriction energy $E_{ms} = \frac{1}{8} c^{\gamma}(\lambda^{\gamma})^2$. This is approximately 2K/Atom for Terbium but falls to 1.25 K/Atom for $Tb_{0.89}Sc_{0.11}$ and 0.8 K/Atom for $Tb_{0.825}Sc_{0.175}$. This suggests the idea that cylindrically symmetrical magnetostrictive energy is responsible for "driving" the spin from a helical to a ferromagnetic structure in Terbium as for Dysprosium but takes no account of hexagonally symmetrical magnetostriction.

The existence of helical structures in the alloys indicates that the exchange interactions are still long range and oscillatory. The entire absence of ordering with more than 70 to 80 At% of Scandium indicates considerable weakening of the interaction. The Scandium atoms have a volume about 25% smaller than those of Yttrium and this could be the cause of the different behaviour. The R.K.K.Y. theory does not help in understanding the effect of such changes on the exchange energy. Wollan (1967) compared certain effects of dilution of Terbium and Gadolinium with

Scandium to the effects of applying high pressures and showed that they were essentially the same.

Isaacs et al (1971) investigating the anisotropy changes produced in a Scandium matrix by quantities of magnetic Rare Earth of the order of 1% showed that Gadolinium changed the easy axis from "a" to "c" at low temperatures, while Dysprosium did not change the easy axis but increases the anisotropy by several orders of magnitude. It thus appears that the solute begins to dominate the anisotropy at very low percentages.

CHAPTER 5

METHODS OF DETERMINING ANISOTROPY CONSTANTS

5.1 Anisotropy Constants from Magnetisation Curves

The work done per unit volume in magnetising a specimen is given by

$$W = \mu_o \int_o^M \underset{\sim}{H}.d\underset{\sim}{M}$$

If the specimen is symmetrical, unstrained, magnetised to saturation, and if in addition corrections are made for demagnetisation fields and irreversible processes, then the work W is the anisotropy energy E_a. The integral may be found graphically as the area between the magnetisation (M/versus H) curve and the M axis. Determinations of E_a in four selected directions should then suffice to determine four anisotropy constants, and from equation 3.3 it should be possible to obtain K_4 from one curve measured in the basal plane parallel to an "a" axis.

To eliminate the contribution of irreversible processes to the integral, a complete hysteresis loop may be plotted for the specimen and a curve constructed, the M co-ordinates of points being unchanged but the H co-ordinates of points being the mean of corresponding pairs of H co-ordinates on the hysteresis curve. Alternatively, each point on the magnetisation curve may be obtained by superimposing on the static field a large alternating field, and gradually reducing the latter to zero. This allows the system to settle in the state of minimum energy for each point.

To eliminate the effect of demagnetising fields the specimen may be made in the form of a picture frame. Otherwise it may be an ellipsoid

of revolution so that the demagnetising field may be calculated. If the specimen is spherical then the work done against the demagnetising field is the same for all directions in magnetising to saturation. It may then be treated as an extra unknown quantity and eliminated by obtaining another magnetisation curve.

The method has several disadvantages. Unless the magnetisation curves are required also, it is very time consuming and requires temperature stabilisation over long periods. There are uncertainties associated with the corrections for demagnetising field which are large compared with the quantity measured and results are also very sensitive to misorientation of the sample. In addition it cannot be applied directly in cases where the fields available are not high enough to saturate the material in the hard direction. This is the case for the axial anisotropy in Dy and Tb where Feron (1969) evaluated the coefficients K_2^o and K_4^o by fitting theoretical expressions involving them to the magnetisation curves.

5.2 Anisotropy Coefficients from Torque Measurements

A single crystal specimen is cut, usually in the form of a disc or oblate spheroid with its minor axis perpendicular to an important crystal plane. It is suspended from a vertical torsion wire or other counter torque device so that the major axes of the disc or ellipsoid are horizontal, and the specimen is situated in a uniform horizontal magnetic field. The torque exerted by the field on the crystal is measured as either the specimen or the magnet is rotated and plotted as a function of the angle between the field lines and a specified crystal axis.

On the assumption that the magnetisation within the crystal is virtually parallel to the applied field, the torque may be obtained in

terms of the anisotropy constants by differentiating the appropriate expressions for magnetocrystalline anisotropy energy. Thus for a hexagonal crystal, from equation (3.3),

$$E_a = K_1 \mathrm{Sin}^2\theta + K_2 \mathrm{Sin}^4\theta + K_3 \mathrm{Sin}^6\theta + K_4 \mathrm{Sin}^6\theta \mathrm{Cos}6\phi \qquad (5.1)$$

If the specimen is cut with a 'c' axis in the plane of the disc then the torque exerted on the crystal by the field is, since ϕ is a constant,

$$L = \frac{\partial E_a}{\partial \theta} = 2K_1 \mathrm{Sin}\theta\mathrm{Cos}\theta + 4K_2 \mathrm{Sin}^3\theta\mathrm{Cos}\theta + 6(K_3 + K_4\mathrm{Cos}6\phi)\mathrm{Sin}^5\theta\mathrm{Cos}\theta \qquad (5.2)$$

Following Corner et al (1962)

$$K_3 + K_4\mathrm{Cos}6\phi = K_3' \qquad (5.3)$$

so that

$$L = (K_1 + K_2 + \frac{15}{16} K_3')\mathrm{Sin}2\theta - \left(\frac{K_2}{2} + \frac{3K_3'}{4}\right)\mathrm{Sin}4\theta + \frac{3}{16} K_3'\mathrm{Sin}6\theta \qquad (5.4)$$

Fourier analysis of the curve allows a determination of the coefficients of sin2θ, sin4θ and sin6θ and hence of K_1 and K_2. To determine K_3 it is necessary to know K_4 and ϕ. ϕ can be determined from X-ray photographs or it can be arranged to cut the crystal so that its plane contains the "a" axis, thus making $\phi = 0^o$. K_4 can be determined from similar measurements on another specimen cut so that its major axes are parallel to the basal plane of the crystal. Since in this case $\theta = 90^o$ the anisotropy energy is

$$E_a = K_1 + K_2 + K_3 + K_4\cos6\phi \qquad (5.5)$$

and the torque is

$$L = \frac{+\partial E_a}{\partial \phi} = -6K_4 \mathrm{Sin}6\phi \qquad (5.6)$$

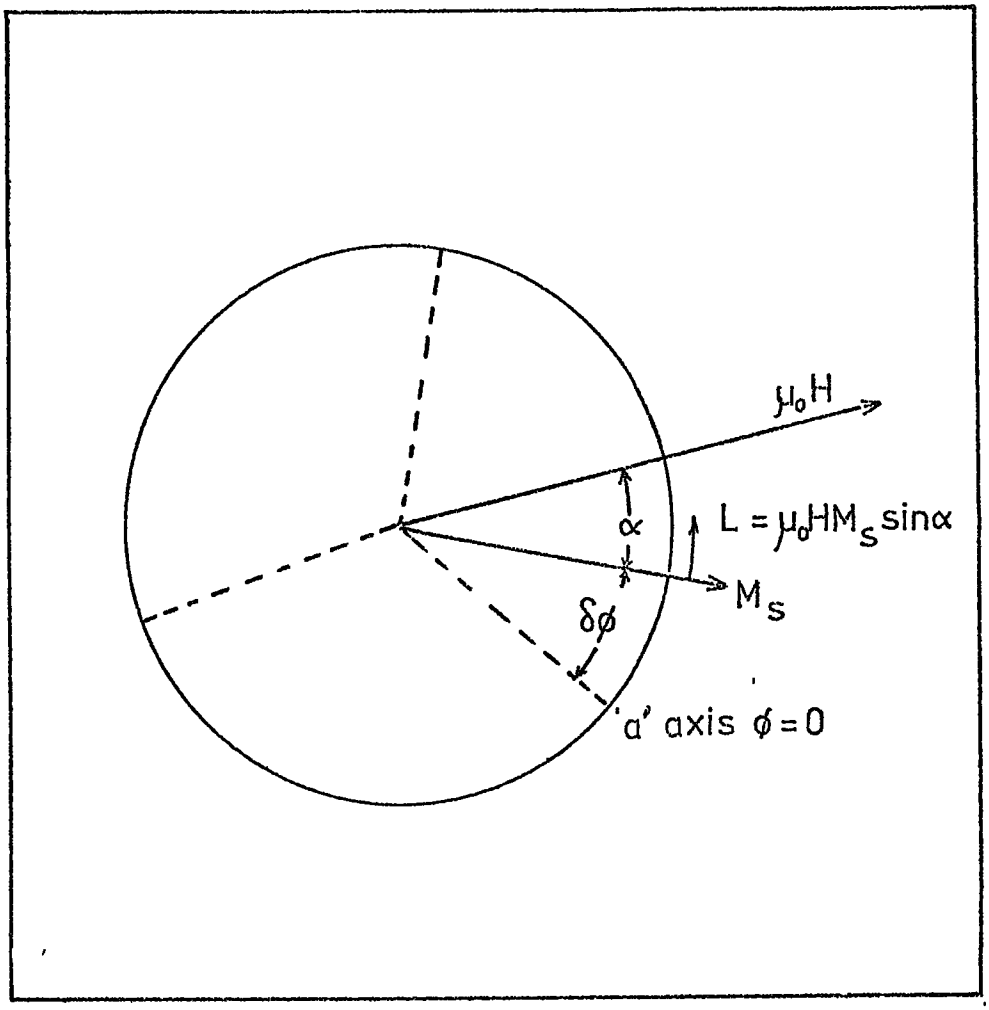

Figure 5.1 To illustrate $L = + \dfrac{\delta E_a}{\delta \phi}$

In general the torque curve obtained will still have other periodic components due to misalignments and Fourier analysis is still needed to give a value for K_4. The coefficients $\mathcal{K}_1$ of equation (3.7) can be found as linear combinations of the coefficients K_n. $\mathcal{K}_6^6$ is identical with K_4.

Birss and Wallis (1964) pointed out the importance of clarity on the sign of $\frac{\delta E_A}{\delta \phi}$ in obtaining expressions for the torque and suggested that failure to observe this point caused disagreements about the sign of K_2 for nickel. Here the positive derivative of E_a is used since it is the torque exerted on the crystal by the field which is considered. Corner et al (1962) use the negative derivative of E_a but clearly specify that they mean the counter-torque provided to keep the specimen from rotating in the applied field. In Figure 5.1 representing a basal plane crystal disc, the applied field $\mu_o H$ has moved the magnetisation vector away from the easy axis, here taken to be the "a" axis, in the direction of increasing ϕ. The energy E_a is increased and the crystal experiences a torque tending to reduce the angle ϕ and hence the energy. This torque tends to rotate the crystal in the positive, anticlockwise direction. It can be clearly seen in this situation that $\delta\phi$, δE_a and the torque L are all positive so that

$$L = + \frac{\delta E_a}{\delta \phi}$$

The torques exerted on the crystal have been measured in a variety of ways.

(i) By the torsional strain produced in the suspension wire.

For stability a stiff suspension is needed (see Section 6.5) and several workers have used a flexible cage to replace the wire. This reduces the sensitivity enormously and methods to measure the distortion of the cage include

1) the use of strain gauges (Tajima 1971),

2) the use of a variable transformer, one coil being fixed and the other attached to the lower end of the cage and hence the rod carrying the specimen (Aldenkamp et al 1960). The varying output from the secondary of the transformer is amplified and is almost directly proportional to the torque on the cage,

3) the use of a variable capacitor, one plate being connected to the upper end of the cage and one end to the lower. The capacitor is connected to a stable oscillator and the variations in frequency are used to indicate torque in the suspension. (Alberts et al., 1971).

(ii) By applying a counter-torque to the crystal to prevent it from rotating. Deviation of the specimen from its position causes a spot of light to alter the output from photoelectric cells. This output controls the counter-torque which may be applied in a variety of ways. The output may be amplified and passed through a coil fixed to the crystal holder and suspended between the poles of a second magnet (Penoyer 1959, Corner et al 1962). The magnitude of this counter-torque current is then proportional to the torque experienced by the crystal in the field. Rhyne and Clarke (1967) placed the specimen inside the counter torque coil and placed both in the main field. Barron et al (1970) used a similar sensor to control a motor which twisted the wire suspension to apply a counter torque, the size of which was indicated by the output of a potentiometer attached to the drive spindle of the motor.

5.3 Anisotropy Studies using Ferromagnetic Resonance

When a steady magnetic field is applied to a ferromagnetic material the individual atomic moments tend to precess about their equilibrium position. This precession is coherent because of the strong exchange forces and the motion can be viewed as a uniform precession of the whole magnetic moment about the direction of the applied magnetic field. This precessional movement can be regarded as a section of a spin wave of wavelength far exceeding the dimensions of the specimen so that the angle between one spin and the next is practically zero.

The angular frequency of a spin wave of wave vector $\underset{\sim}{q}$ is usually denoted $\omega(\underset{\sim}{q})$ and the quantum of energy associated with it is $\hbar\omega(q)$ where $\hbar = \frac{h}{2\pi}$. The quantum of energy in the uniform or normal mode of precession is therefore denoted by $\hbar\omega(0)$. The graph of $\hbar\omega(q)$ versus $\underset{\sim}{q}$ for a given temperature and direction in a material represents the magnon disperson relation and the intercept on the $\underset{\sim}{q} = 0$ axis gives the value of $\hbar\omega(0)$. This is therefore also referred to as the spin-wave or magnon energy gap in the long wavelength limit. It is possible by semi-classical arguments to calculate the normal mode frequency in certain special cases. Thus for hexagonal crystals where the easy direction is in the basal plane and the applied field and magnetisation are parallel to the hard direction in the basal plane, the normal mode quantum energy is

$$\hbar\omega(0) = gm_B\left\{\left[B_o - \frac{36K_4}{M_s} + \mu_o\left(N_{Da} - N_{Db}\right)M_s\right]\left[B_o - \frac{6K_4}{M_s} + \frac{2K_1}{M_s} + \mu_o\left(N_{Dc} - N_{Db}\right)M_s\right]\right\}^{\frac{1}{2}} \qquad (5.7)$$

B_o is the applied field. N_{Da}, N_{Db}, N_{Dc} are demagnetising factors

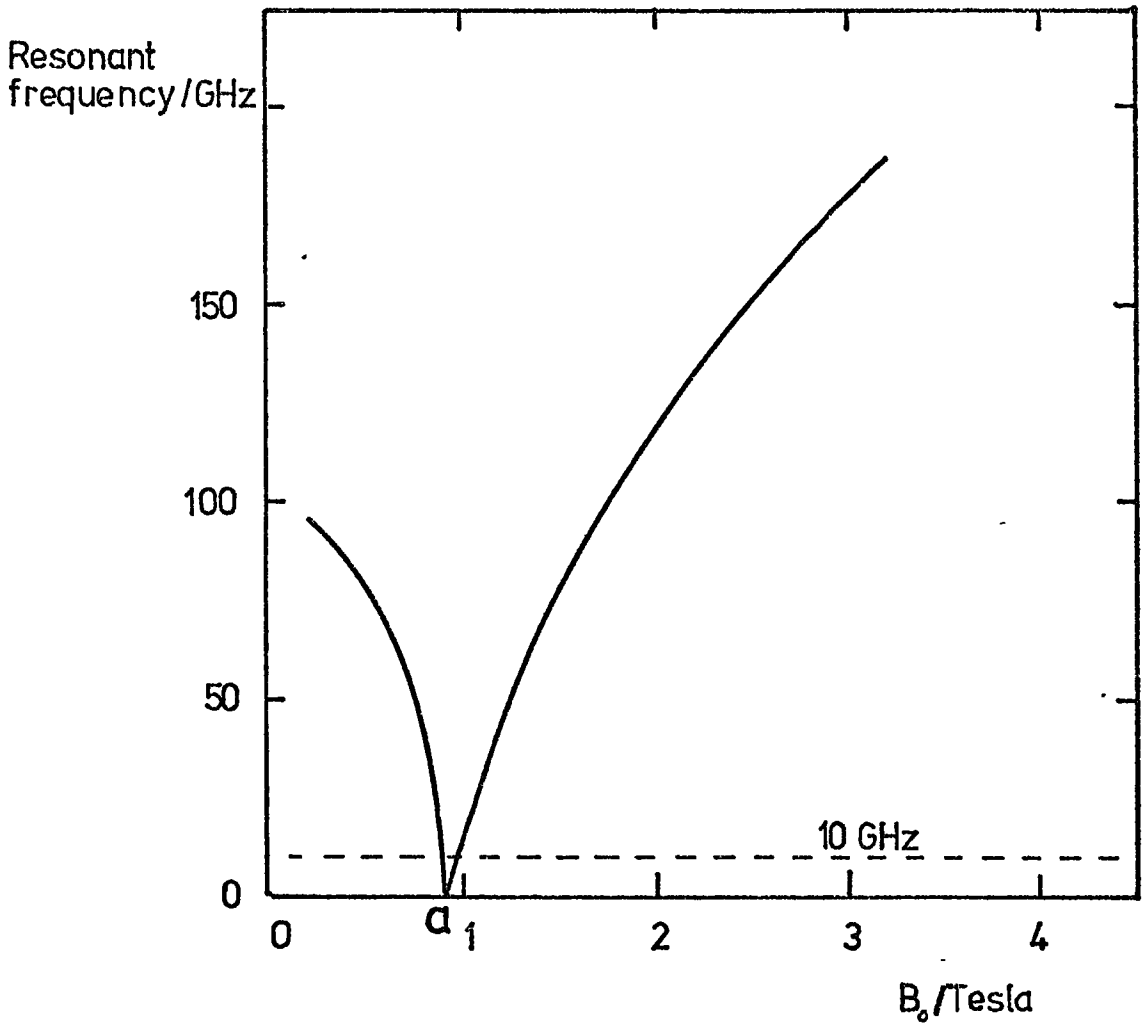

Figure 5.2 Typical Variation of the Normal Mode Frequency with Applied Field for hcp specimens having their easy axis in the basal plane and the applied field parallel to a hard axis in the basal plane.
At the point marked "a" $B_0 = \frac{36K_4}{M_s}$

parallel to the a, b and c axes, the quantity in curly braces representing a geometric mean of effective fields in the basal plane and the plane containing the "c" and "b" axes. Expressions corresponding to equation (5.7) for different orientations of the applied field are given by Bagguley and Liesegang (1967). Expressions for cubic crystals are given in Vonsovskii (1964), Morrish (1965) and other texts.

In the usual experimental arrangements the crystal specimen is cut so as to make the demagnetising factors N_D easily calculable, (or equal, in which case they cancel). The specimen is mounted in a resonant cavity which is supported between the poles of an electromagnet so that the D.C. and radio frequency magnetic fields are mutually perpendicular. Microwaves of fixed frequency are fed to the cavity and as the D.C. magnetic field is altered, dips in the reflected or transmitted microwave amplitude indicate that the normal mode frequency is equal to that of the microwaves. Information concerning the anisotropy constants can be obtained. For the case represented by equation (5.7) Figure 5.2 shows schematically the relationship between resonant frequency and applied field where $N_{Da} = N_{Db}$. A typical microwave frequency (10 GHz) is indicated. Two resonances are observed at values of applied field close to the value $\frac{36K_4}{M_s}$ where the resonance frequency falls to zero. A complete system using a klystron to generate the microwaves is described by Tannenwald (1955). Kyllonen and Mamasse (1972) describe an inexpensive and extremely convenient arrangement where the microwaves are generated by a Gunn diode mounted in the resonant cavity. The tuning of the cavity is not critical and the Dewar vessel with a narrow neck containing coolant and specimen can be inserted into the cavity and rotated conveniently. Reflected amplitudes are observed using a crystal detector connected to the resonant cavity via a directional coupling.

This method, like that following (section 5.4) presents difficulties both in experimentation and interpretation of results. Thus apparent resonances may be due to changes in resistive losses. Resonances obtained at low frequencies ($\sim$ 10GHz in this work) may disappear at high frequencies ($\sim$ 100 GHz) due to changes from free to "frozen" lattice behaviour (Hart and Stanford 1971, Vigren and Liu 1971, 1972). At the higher frequencies the strains in the lattice cannot follow the magnetisation vector and remain at their equilibrium value. This introduces terms representing the magnetoelastic energy into expressions for the uniform mode resonance frequency, which consequently does not fall to zero when $B_o = \frac{36K_4}{M_s}$, and may not fall far enough to give resonance with the radio frequency field applied.

Values of K_4 ($\equiv \mathcal{K}_6^6$) obtained by fitting theoretical expressions for the temperature variation of the resonance frequency to experimental results for Dysprosium and Terbium (Marsh and Sievers 1969) were much higher than those obtained in magnetisation and torque methods. This and other discrepancies can be due to difficulties in deriving the theoretical expressions and in correctly identifying the microscopic parameters with the measured anisotropy coefficients. Thus Egami (1972) attributes differences between static and dynamic results for K_4 for Dysprosium to neglect of the zero point energy introduced by ellipticity of the spin precession caused by the high anisotropy.

The method is exceedingly valuable for the light it throws on microscopic processes by comparison of its results with those from static measurements.

5.4 Anisotropy Studies using Inelastic Neutron Scattering

Spin waves of finite wavelength ($\underset{\sim}{q} > 0$) are excited in the crystal studied by bombardment with monoenergetic neutrons. Using a crystal spectrometer, the wave vectors $\underset{\sim}{k}_1$ and $\underset{\sim}{k}_2$ of the incident and scattered neutrons are determined. The wave vector of the excited spin wave is

$$\underset{\sim}{q} = \underset{\sim}{k}_1 - \underset{\sim}{k}_2 - \underset{\sim}{\tau} \qquad (5.8)$$

where $\underset{\sim}{\tau}$ is a reciprocal lattice vector. The energy transferred to the spin wave is $\hbar\omega(\underset{\sim}{q}) = \hbar^2(\underset{\sim}{k}_1^2 - \underset{\sim}{k}_2^2)$.

Maxima in intensity of scattered neutrons give conjugate pairs of values of $\hbar\omega(\underset{\sim}{q})$ and $\underset{\sim}{q}$ from which the magnon disperson relation can be plotted. Extrapolation to $\underset{\sim}{q} = 0$ gives the value $\hbar\omega(0)$ for which expressions are known involving the anisotropy constants. Values of $\hbar\omega(0)$ may be obtained with applied fields along various crystallographic directions and at various temperatures. This method can only be used with materials having low capture cross section for thermal neutrons. Terbium can be investigated this way and Nielsen et al (1970) were able to show for Tb-Ho 10% alloy, that the variation of $\hbar\omega(0)$ with applied field and temperature could only be explained if the basal plane anisotropy arose from hexagonally symmetrical second order magneto-striction effects.

5.5 Other Methods of Measuring Anisotropy Energy

Rhyne and Clarke (1967) have calculated the basal plane anisotropy coefficient K_4 for Dysprosium and Terbium from the departures of the moment vector from parallelism with the applied field as detected by magnetostrictive strain. Other methods include the remanent torque

magnetometer and torsion pendulum, described by Zjilstra (1967, page 195 et seq). They may be of very high sensitivity (Collette 1962) but have limited application.

5.6 Choice of Method of Determining Anisotropy Constants

The most convenient of the methods described is that using the torque magnetometer with counter-torque feedback. Measurements are direct, and with automatic recording are rapid. The instrument can be adapted for use over a wide range of temperatures and magnetic fields and the sensitivity can be altered conveniently over several orders of magnitude to suit different materials. The method does not give much information in addition to the actual anisotropy energy but it may give this with considerable precision, particularly when a torque curve is dominated by one component as in measurements on basal plane specimens of hexagonal crystals.

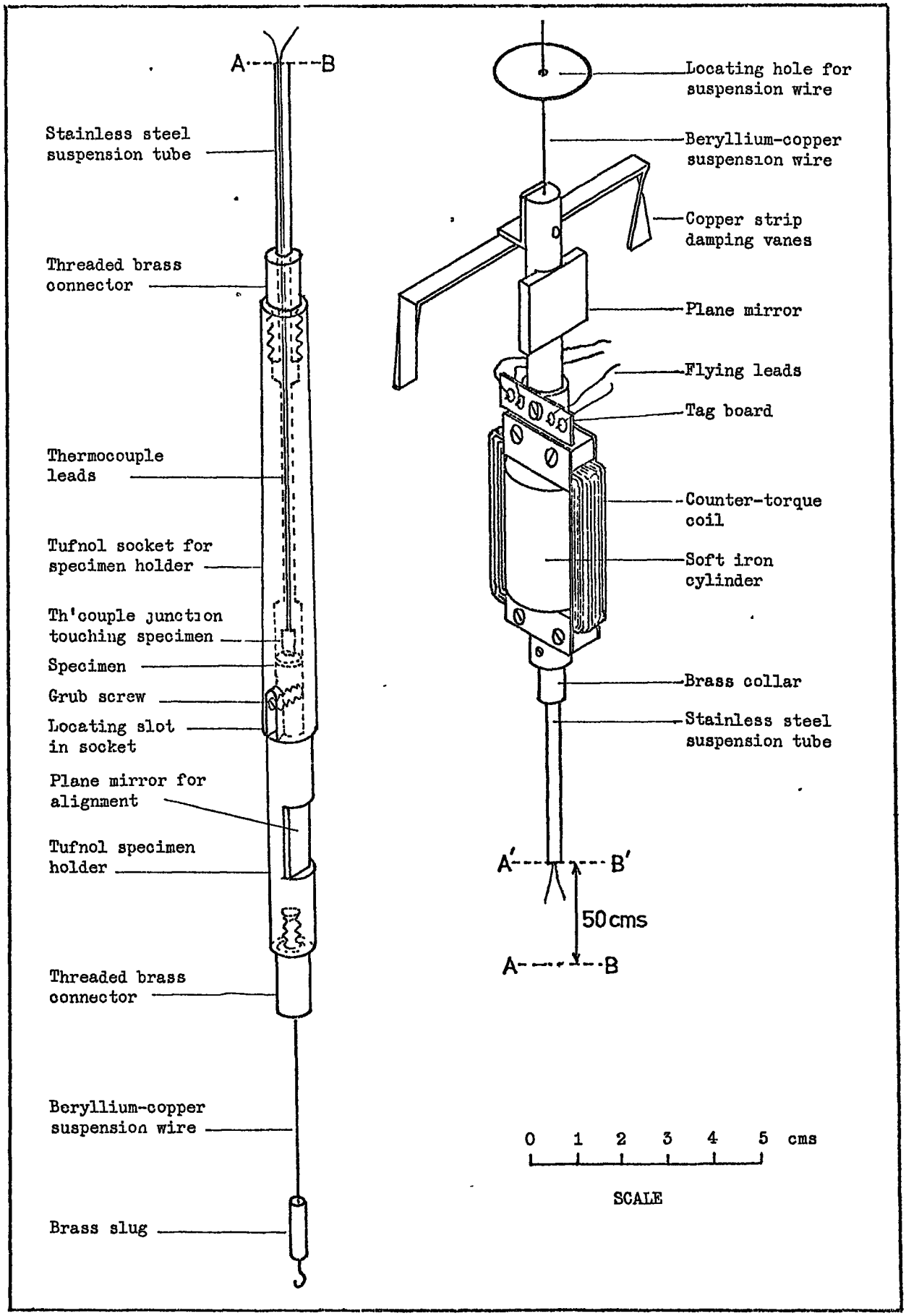

Fig 6.1 The Torque Magnetometer Movement.

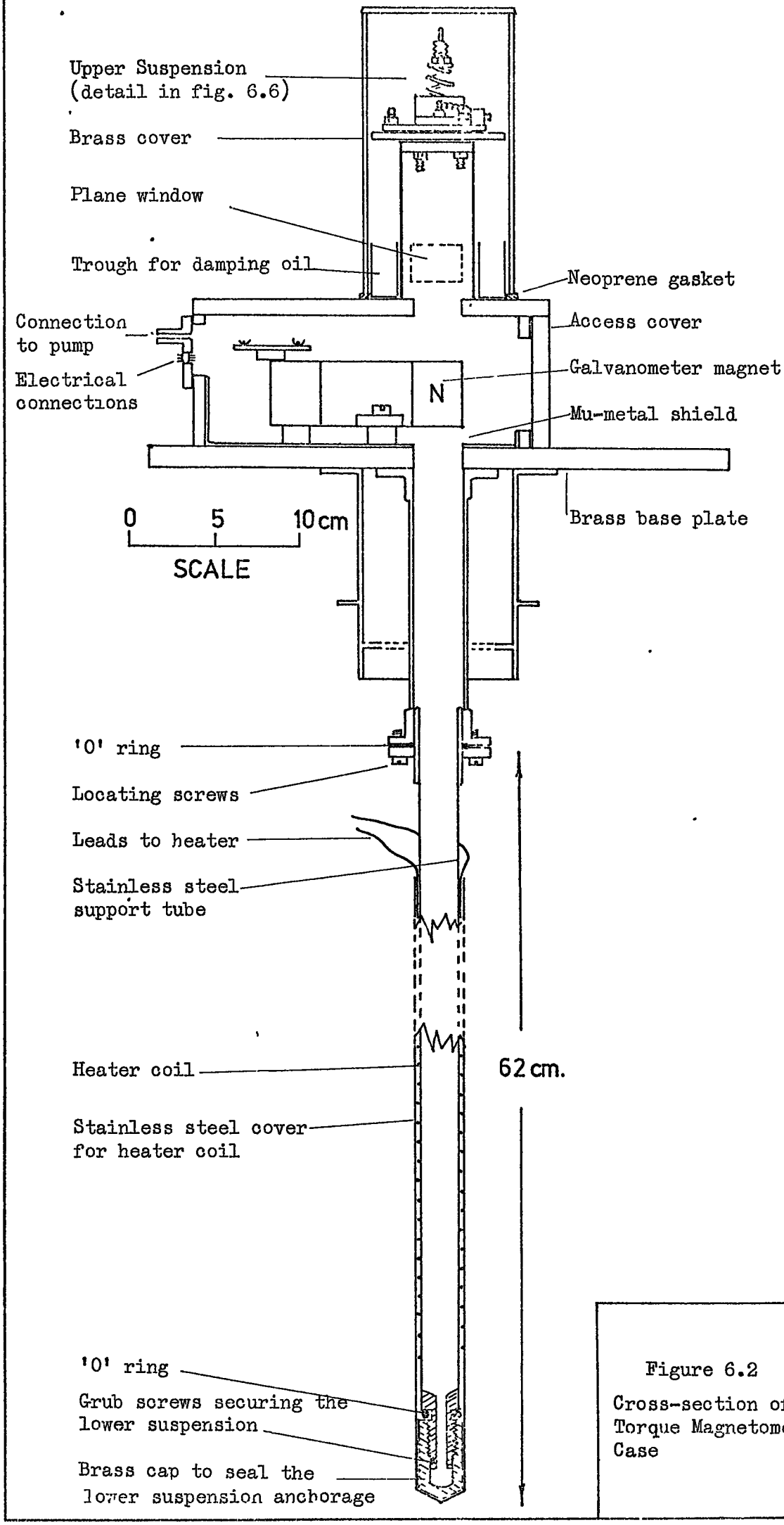

Figure 6.2

Cross-section of the Torque Magnetometer Case

CHAPTER 6

THE APPARATUS

6.1 General Description and Principles of Operation

The principal moving parts of the torque magnetometer are shown in Figure 6.1. The single crystal specimen, with its major axes horizontal, is mounted on a specimen holder of tufnol. This plugs into a tufnol socket which is connected rigidly by a short threaded brass rod to the lower end of a stainless steel tube, 0.6 m long and 5mm in diameter, the upper end of which is fastened to the counter-torque coil. This coil is wound with 150 turns of 30 s.w.g. enamelled wire and moves in the radial field of a large galvanometer magnet.

The whole torque magnetometer movement is suspended by taut beryllium-copper wires, 0.01 inches in diameter, so that it is free to rotate about a vertical axis. The leads from a copper-constantan thermocouple pass up the stainless steel suspension tube to a tag board just above the counter-torque coil. From there they pass to vacuum lead-through pins in the case by means of flexible flying leads. Similar connections carry current to the counter-torque coil, all the flying leads being arranged so as to place minimum constraint on the movement.

A cross section of the case is shown in Figure 6.2. The lower support tube carries the anchorage for the lower suspension wire and a heating coil. The end of this tube is covered by a brass cap which screws down onto a neoprene "O" ring. Similarly the cover over the top suspension and all other joints in the case are sealed with neoprene gaskets so that the apparatus can be evacuated before cooling to liquid nitrogen temperatures. The liquid nitrogen is contained in a Dewar vessel which is suspended from the same framework which supports the magnetometer case. Further details of the construction of the

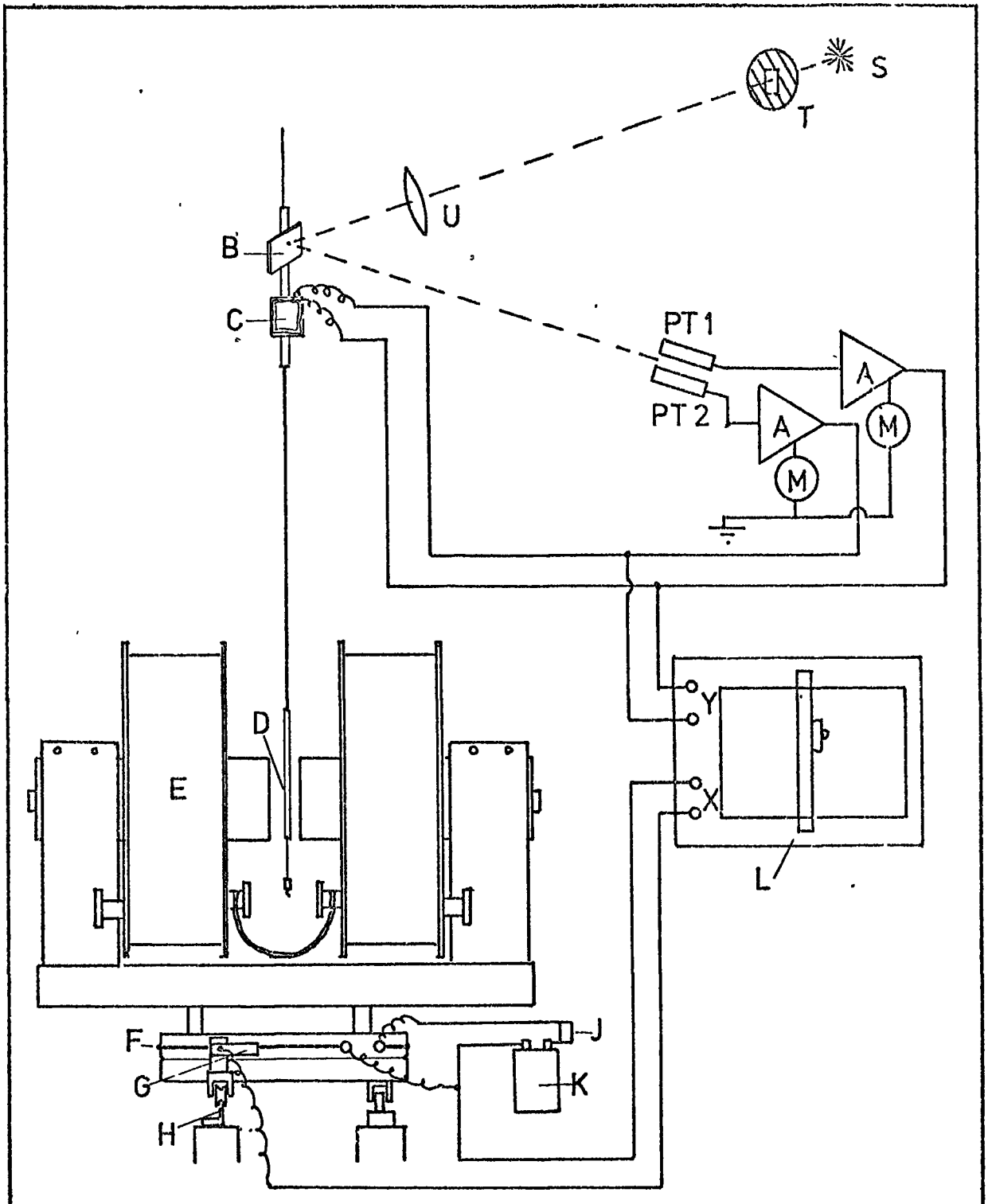

A - Amplifier
B - Plane mirror
C - Counter-torque coil
D - Crystal specimen
E - Electromagnet
F - Slide wire over transparent insulation on magnet scale
G - Sliding contact
H - Rails on which magnet moves
J - Fixed resistor (220 ohms)
K - 2 volt accumulator
L - X-Y recorder
M - Warning meters
PT1, PT2 - Phototransistors
S - Light source
T - Illuminated slit
U - Lens, forming image of T on PT1 and PT2

Figure 6.3 The Torque Magnetometer: Principles of Operation.

apparatus are given in sections 6.3 (page 79) and 6.4 (page 85) which are concerned with the setting up and use of the magnetometer.

Figure 6.3 is a block diagram illustrating the principles of operation of the apparatus. It is arranged so that the crystal specimen is midway between the flat pole faces of an electromagnet in a uniform horizontal magnetic field. Light from a small projector lamp is reflected from the plane mirror, which is fastened to the movement just above the counter-torque coil, and falls on two phototransistors PT1 and PT2. These are connected in a long-tailed-pair amplifier in such a way that the output current is zero when they are equally illuminated and increases as one receives more light than the other, the direction of the current output and the connection to the counter-torque coil being such that the current tends to restore the movement to its central position.

If the specimen in the field experiences any torque, the movement rotates slightly and the current output from the amplifier increases until the rotation is arrested. Damping is provided by means of a bent strip of copper fastened to the movement and having its ends immersed in a trough of oil.

If the torque on the crystal exceeds the maximum counter-torque available then the spot of light may be moved past the phototransistors and the movement will then be twisted violently and may be damaged. Two warning meters were therefore included in the amplifier. When the current is near zero in one meter, this indicates that the counter-torque current is near to its maximum value.

The torque produced by the counter-torque coil is proportional to the current through it and hence to the potential difference across it. This P.D. is recorded as the Y deflection on an XY recorder. The X

deflection of the pen recorder is controlled by a P.D. derived from a slide wire on the base of the electromagnet. This magnet rotates about the same vertical axis as the crystal holder. Rotating the electromagnet slowly therefore produces automatically a graph of the counter-torque or the torque experienced by the specimen versus the angle between the magnetic field and some arbitrary direction in the plane of the crystal disc. With suitable calibration the absolute values of the torques may be found and the anisotropy constants deduced. The electromagnet is mounted on rails and can be moved to one side to facilitate setting up the apparatus. The framework carrying the magnetometer is screwed to the floor and the lamp and phototransistors are carried by an angle iron tower, also bolted to the floor of the laboratory.

In principle the apparatus is the same as that described by Penoyer (1950) but with important modifications introduced by Roe (1961) and Bly (1967). The main parts of the apparatus were already constructed and were as used by Bly. The following items are modifications made for the present investigation.

(a) The use of the XY recorder and the potentiometer system on the base of the magnet.

(b) The use of phototransistors instead of photoresistors to speed the response of the feedback system and so increase stability.

(c) The use of gauges and a sighting device to set up and orientate the specimen.

(d) The use of lenses and plane windows and mirrors to allow more efficient light transmission to the phototransistors.

(e) Modifications to the circuit of the amplifier to increase the counter-torque current available.

(f) The construction of a top suspension with two orthogonal screw adjustments.

(g) The use of a transistor to stabilise the heating current.

6.2 The Crystal Specimens

Table 6.1

Material	Diameter ±0.005 cm	Thickness ±0.002 cm	Shape	Mass ±0.5 mg	Density
Terbium	0.492 cm	0.054 cm	disc	51 mg	8.272
$Tb_{0.89}Sc_{0.11}$	0.497 cm	0.116 cm	disc	90 mg	7.85
$Tb_{0.825}Sc_{0.175}$	0.524 cm	0.064 cm	disc	100.5 mg	7.64
$Tb_{0.695}Sc_{0.305}$	0.515 cm	0.103 cm	disc	153 mg	7.07
Dysprosium	0.493 cm	0.0605 cm	ellipsoid	51 mg	8.536

The experiments were carried out on five single crystal specimens, all having the "c" axis parallel to the short axis of the specimen. Dimensions are given in Table 6.1. The Dysprosium and Terbium specimens were the same as those used by Bly et al (1968) and the Terbium-Scandium alloy specimens were those used by Chatterjee (1972).

6.3 Setting up the Apparatus

6.3.1. Etching and Mounting the Crystal Specimens

The crystals were etched for one or two seconds in the following mixture of acids.

Lactic acid	20 ml
Phosphoric acid	5 ml
Acetic acid	10 ml
Conc. Nitric acid	15 ml
Conc. Sulphuric acid	1 ml

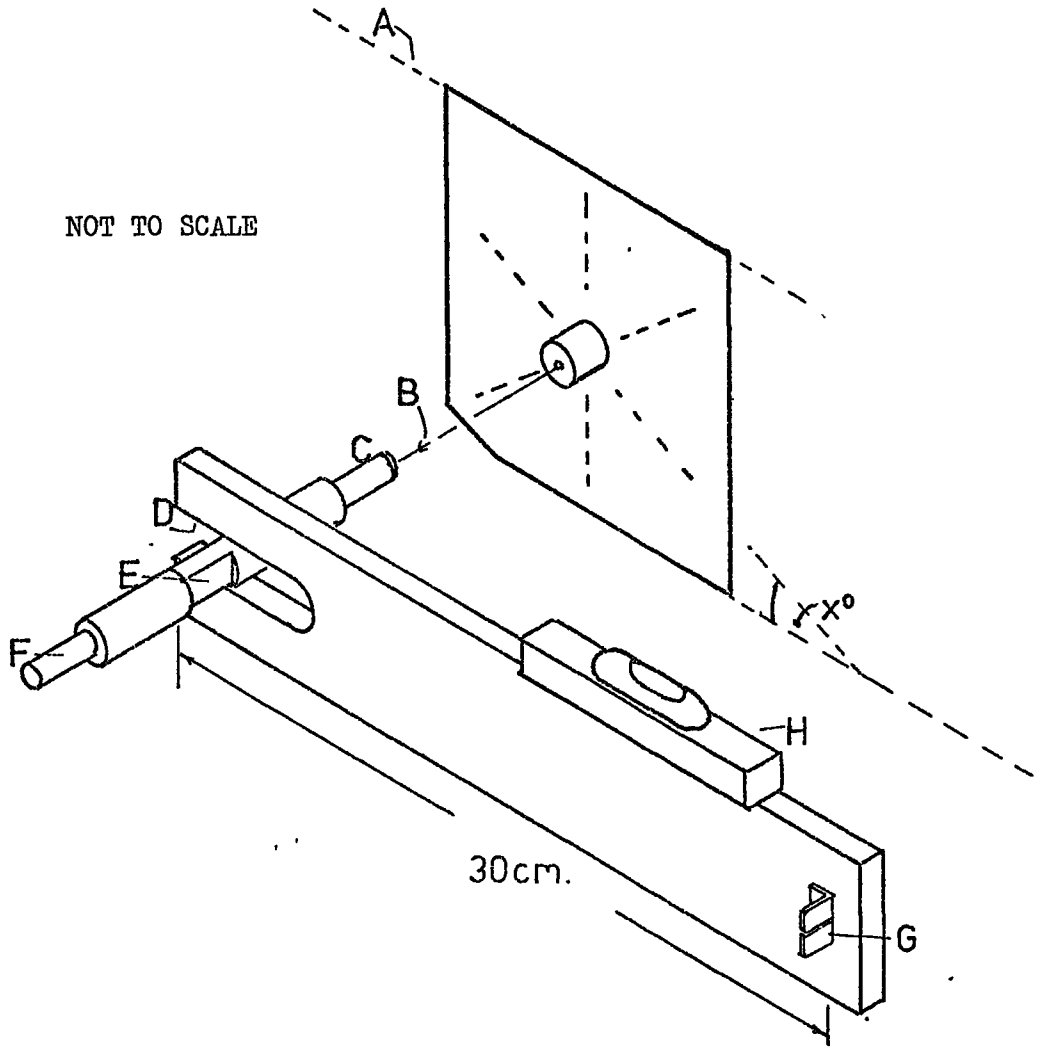

A - Top edge of X-ray film holder. Inclination checked with a spirit level. (Normally horizontal)
B - Path of incident X-ray beam
C - Crystal specimen
D - Slot in gauge to accommodate the specimen holder
E - Plane mirror inset into specimen holder
F - Brass rod screwed into specimen holder in place of the lower suspension ligament and supported in the socket for the collimator tube of a second film holder (not shown)
G - Sighting slit
H - Spirit level used to set the gauge parallel to the edge of the X-ray film
X - The inclination of the 'b' axis of the crystal to one edge the film, measured after developing the film and identification of the axes

Figure 6.4 Orientation of the specimen on its holder

They were then washed in water free acetone, allowed to dry, weighed and mounted on the ends of specimen holders using four strips of sellotape approximately 2mm by 15 mm bound with a similar strip as a collar. This technique has been found to provide a firm attachment which is immune to thermal cycling. Curves obtained from specimens which are attached in this way do not show the distortions which appear when using adhesives to fix the crystal. These distortions are attributed to strains produced in the crystal by differential thermal expansion.

The orientation of the crystals on the holder was determined using the Laue back reflection technique. With the crystals at 3cm from the film, an exposure time of 1.5 hours was adequate using a cobalt anode without a filter and a current of 10 mA at 30 kV. The axes were identified by comparing the films with standard (0001) projections for hcp crystals. The specimen holder has a small piece of plane mirror let into its side for purposes of alignment. The plane of the mirror can be set accurately perpendicular to the axis of a combined gauge and sight (Figure 6.4) by looking through the slit and rotating the specimen holder until the image of the slit appears in the centre of the plane mirror. The gauge was clamped on the X-ray set and its axis made parallel to one edge of the film holder using a spirit level. The specimen holder was screwed onto a threaded brass rod which fitted the aperture in a second spare Laue camera. This method kept the crystal accurately on the axis of the X-ray beam and allowed it to rotate until the mirror was perpendicular to the axis of the gauge. Measurements on the film gave the angle between one of the "b" axes and the normal to the mirror within 1/3 of a degree.

The centre of the pattern on the exposed film was in all cases close to the geometrical centre of the film. The "c" axis of the

crystals was estimated to be within 3 to 5 degrees of the axis of the specimen holder in all cases.

6.3.2. Orientation of the crystals in the magnetometer

The specimen holder is a push fit in the tufnol socket attached to the stainless steel tube (Figure 6.1). The grub screw in the specimen holder slides into a slot in the socket and this was intended to provide precise location of the specimen. No great reliance was placed on this arrangement however and the specimen was not moved after the orientation had been performed. Since the movement is under tension from the suspension, it is necessary to screw up the locating grub screw very gently until it grips the back of the socket.

A heavy brass disc is screwed into the bottom of the specimen holder in place of the suspension wire to load the movement so that it hangs vertically from the upper suspension. The bolts holding the torque magnetometer to its frame are slackened and it is moved until the specimen holder is midway between the pole faces of the electromagnet. This adjustment is aided by the use of the gauge which is a gentle push fit between the magnet poles and has a central slot wide enough to accommodate the specimen holder with a millimetre clearance on each side. This adjustment is made with the magnet pole faces parallel to the rails on which it runs. At the same time the main plate carrying the magnetometer is checked with a spirit level and made horizontal if necessary by the use of shims under the corner bolts. After removing the gauge temporarily as a precaution, the magnet is turned through 90^{o} and moved on its rails until the pole faces are again equidistant from the specimen holder. Clamps are then placed on the rails to mark this position.

Figure 6.5 Orientation relative to the Magnet Scale

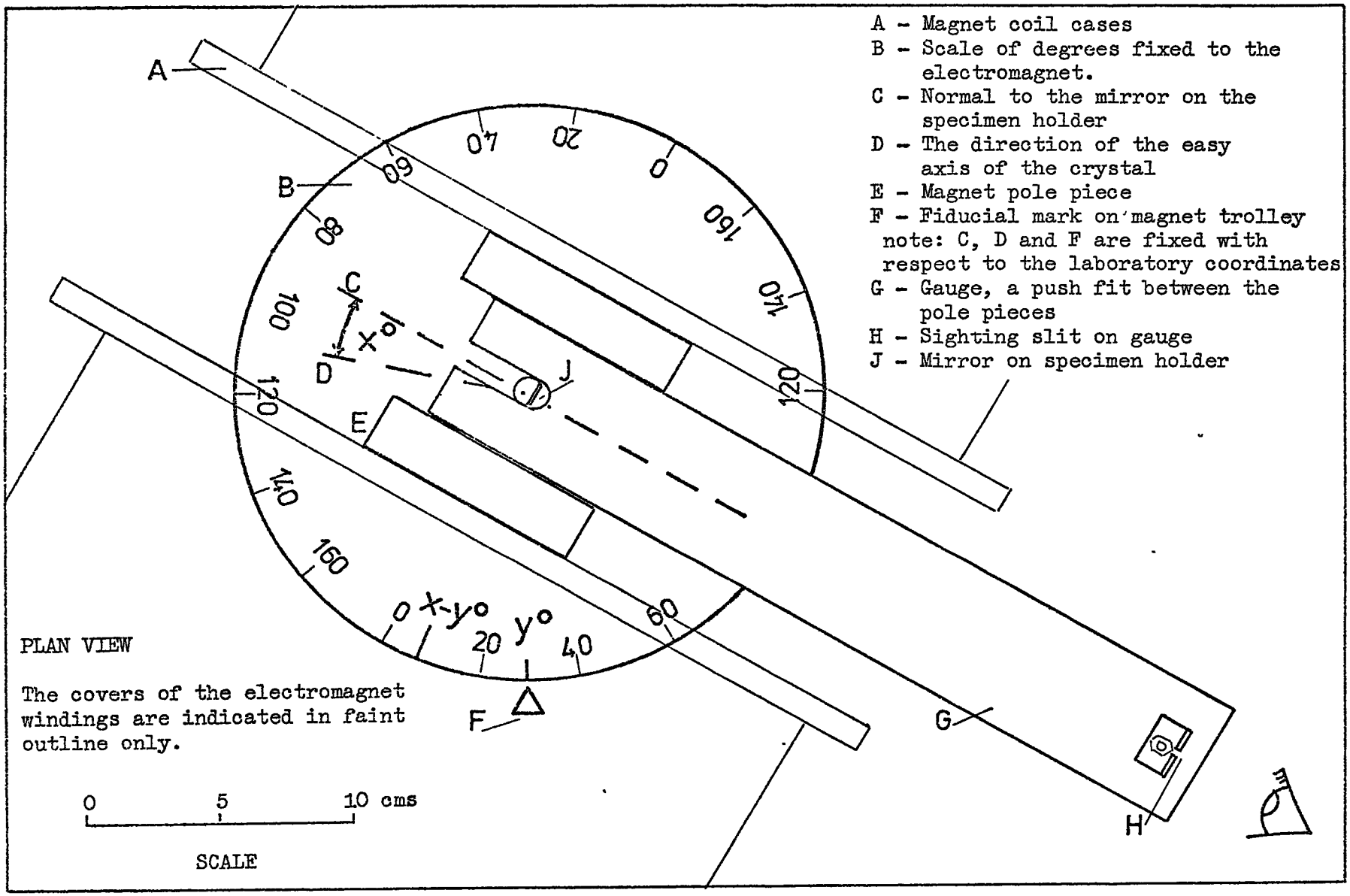

Only one clamp is removed when it is necessary to move the magnet to insert the Dewar vessel; the correct position of the magnet is then easily found with the other.

The movement is turned by hand until the reflected spot of light is seen to fall equally across the two lenses in front of the phototransistors. Without disturbing the movement, the magnet is rotated until the image of the slit on the sight appears in the centre of the mirror on the specimen holder when viewed through the slit. The magnet scale is read at this point and it is then known that the pole faces and the normal to the mirror are parallel. With a small lamp to illuminate the slit, this setting is particularly easy and can be repeated within ¼ of a degree. Figure 6.5 illustrates the procedure. If the reading on the scale is y^{o} and the angle between the mirror normal and a "b" axis is x^{o}, then an anticlockwise rotation of the magnet by x^{o} to $(y-x)^{o}$ makes the pole faces parallel to one "b" axis. The field lines are then parallel to an "a" axis. It is thus possible to determine quickly the angle between the flux lines and the crystal axes with a probable error of less than 1^{o}. Later it was found that the zero of the $\sin 6\theta$ component of the torque curves occurred within one or two degrees of the position of a crystal axis as determined above.

6.3.3. Replacement and adjustment of the suspension

The heavy brass disc is removed from the bottom of the movement and is replaced by the lower suspension wire. The brass slug on the lower end of this wire is fastened to a piece of fine wire which is threaded through the small hole in the support tube to help in pulling it down when the tube is replaced. This tube is pushed back in position

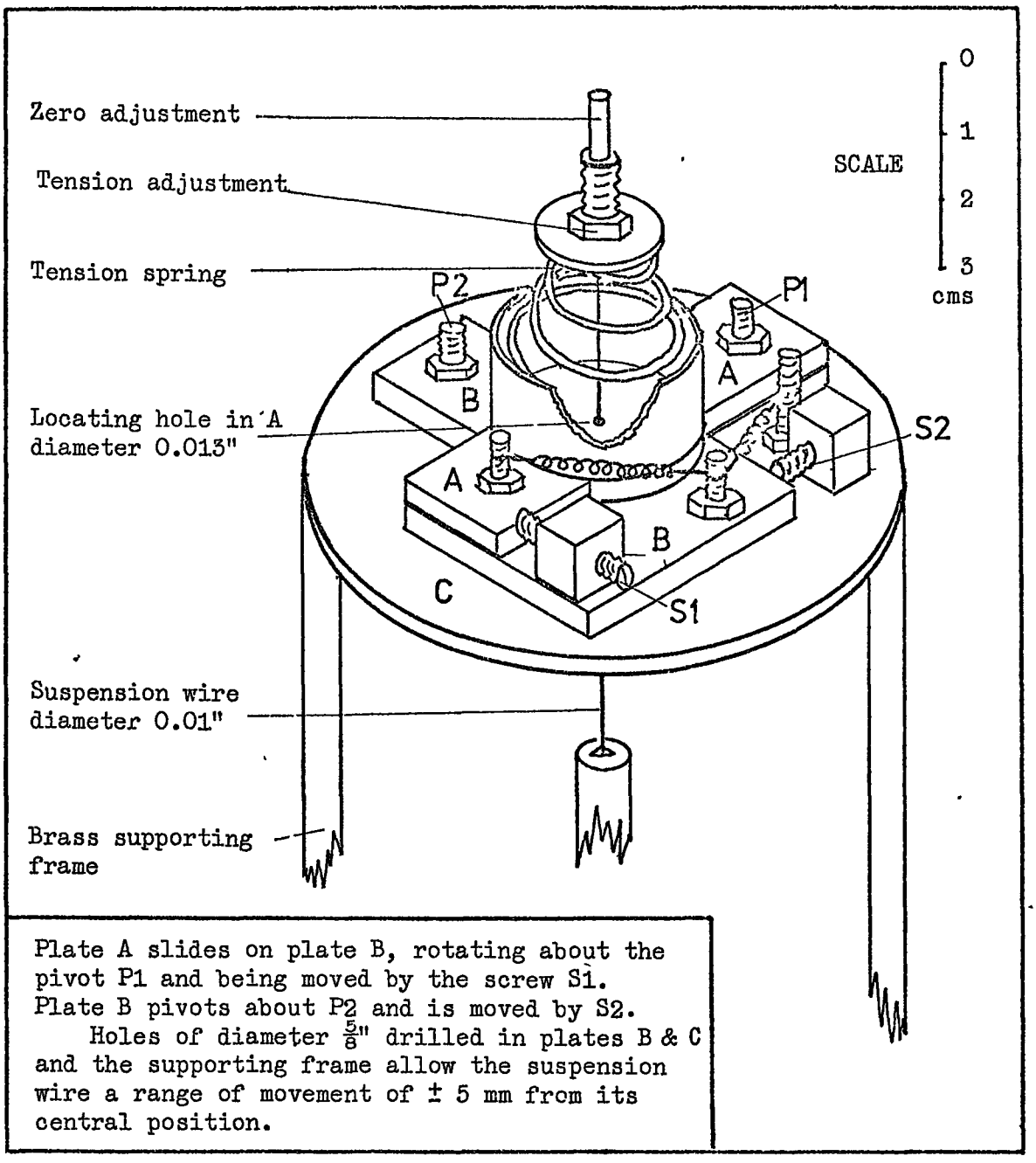

Plate A slides on plate B, rotating about the pivot P1 and being moved by the screw S1. Plate B pivots about P2 and is moved by S2.

Holes of diameter $\frac{5}{8}$" drilled in plates B & C and the supporting frame allow the suspension wire a range of movement of ± 5 mm from its central position.

Figure 6.6 The Upper Suspension

against its "O" ring and the three screws which secure it are tightened gently in turn until the tube is centrally placed between the poles of the electromagnet. Tightening one screw excessively will pull the tube and the specimen away from the centre of the field. To assist in this adjustment another gauge was made, similar to the first but having a slot wide enough to accommodate the support tube. The three screws are adjusted until the tube remains central in the slit in the gauge while the magnet is rotated.

The tensioning nut on the top suspension (Fig.6.6) is screwed down until the spring is about half of its uncompressed height. In this position the upper suspension pulls the counter-torque coil against the lower edge of the soft iron cylinder in the galvanometer magnet. The brass slug on the lower suspension is then pulled down by means of the attached wire until the top edge of the coil touches the top of the soft iron cylinder. It is then allowed to rise 2 mm and fastened with the grub screws in the lower end of the support tube. The vertical adjustment is facilitated by placing a small piece of plastic, 2 mm in thickness and having a small slot, around the brass slug and gripping the latter close to the plastic with a pair of pliers. Removing the plastic and moving the pliers into contact with the case makes the adjustment automatically. The counter-torque coil should then clear the soft iron cylinder by approximately 2 mm at both top and bottom edges. The fine wire is then removed and the brass cap which makes the lower end of the suspension air tight is screwed down firmly onto its "O" ring. The heating coil is covered with its stainless steel sheath and connected to the control circuit.

If there is any damping oil in the trough it is removed so that the magnetometer movement can swing without damping. The amplifier is

switched on and the upper suspension is twisted until the spot of light falls across the phototransistors. The movement should then start to oscillate freely. If it does not, then the adjusting screws on the upper suspension are moved until it does. Then the range of travel of each screw is explored in turn and each is set half-way between the two positions when the movement just begins to stick. Since the two adjusting screws are at right angles, they act independently and the movement is centred by 2 adjustments only. The top suspension wire passes through a hole 0.013 inch in diameter and is therefore precisely located. Until this form of suspension was made, great difficulty was experienced in making the coil move freely even for a short series of readings. The upper suspension ligament can be twisted without disturbing the centring adjustment. This makes it possible, at this stage in setting up, to switch off the amplifier and rotate the movement till the spot of light is centrally placed on the photocells. If this is not done, the counter-torque current has an additional steady component even in the absence of any torque on the crystals.

The damping oil (Shell Spirax E.P. 140) is replaced in the trough and the reflected spot of light settles down firmly and centrally on the two phototransistors. The brass cover is replaced on its "O" ring with a twisting motion and the apparatus is evacuated and is then ready for use. The damping oil is stored in an evacuated vessel. Otherwise outgassing under vacuum causes bubbles to form in the trough. These cause sticking and, in bursting may introduce dribbles of oil into the centre of the magnetometer.

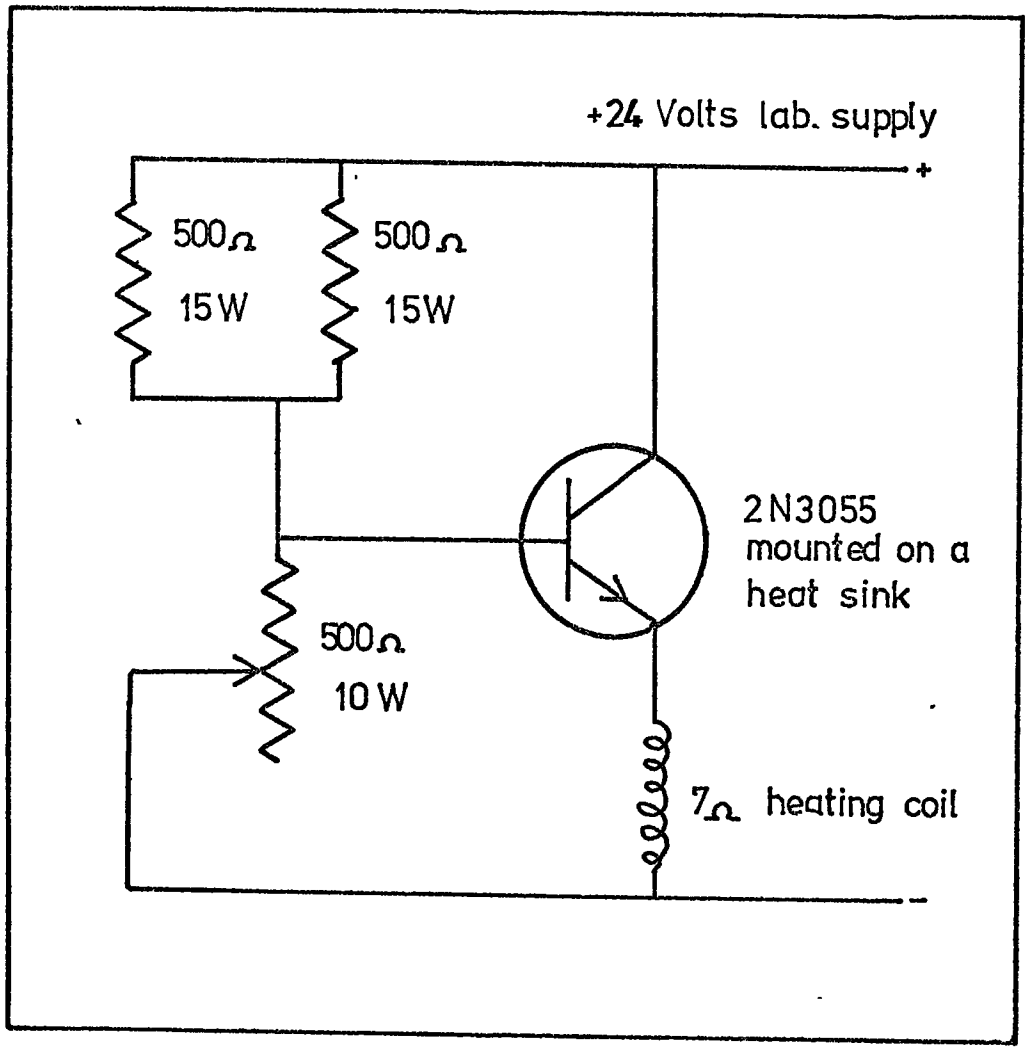

Figure 6.7 Heating Current Control Circuit

6.4 Further Details of the Apparatus and its Use

6.4.1. Temperature control and measurement

Experiments were carried out in the temperature range 77 to 190K and for this range the method used by P.H. Bly was found to be very satisfactory. The support tube is immersed in liquid nitrogen and temperatures above 77K are obtained by passing a current through a heating coil of Kanthal wire wound on a layer of Sellotape on the stainless steel support tube at the level of the specimen. This wire is insulated with a further layer of Sellotape and covered with a stainless steel sheath. The resistance of the coil is 7 ohms and a current of about 1.25 amperes from a transistorised potentiometer (Fig.6.7) was needed to raise the temperature of the specimen to about 190K. At higher temperatures the boiling of the nitrogen occasionally caused waves to appear in the recorded torque curves but these were of uniform amplitude and could easily be allowed for in taking readings from the graphs. The time to reach thermal equilibrium was usually about 10 to 15 minutes and temperatures were then measured with a copper-constantan thermocouple, the reference junction being kept in liquid nitrogen. The thermoelectric e.m.f.'s were measured on a Pye portable potentiometer. It was possible to read the potentiometer to within 0.01 mV (corresponding to 0.5K at the lower temperatures). Measurement of the thermal e.m.f. at three fixed temperatures, (boiling nitrogen, melting acetone and melting ice) gave agreement, within these limits, with the calibration table used. Temperatures are therefore assumed to be within 1K of the measured value. Because of the need to remove the movement from the apparatus, the thermocouple leads were not continuous as far as the potentiometer. Connection was by means of a small gold plated plug and socket. Soldered joints were also discovered in the leads at the vacuum lead-through in the case and on the tag board on the

Figure 6.8 The Optical System

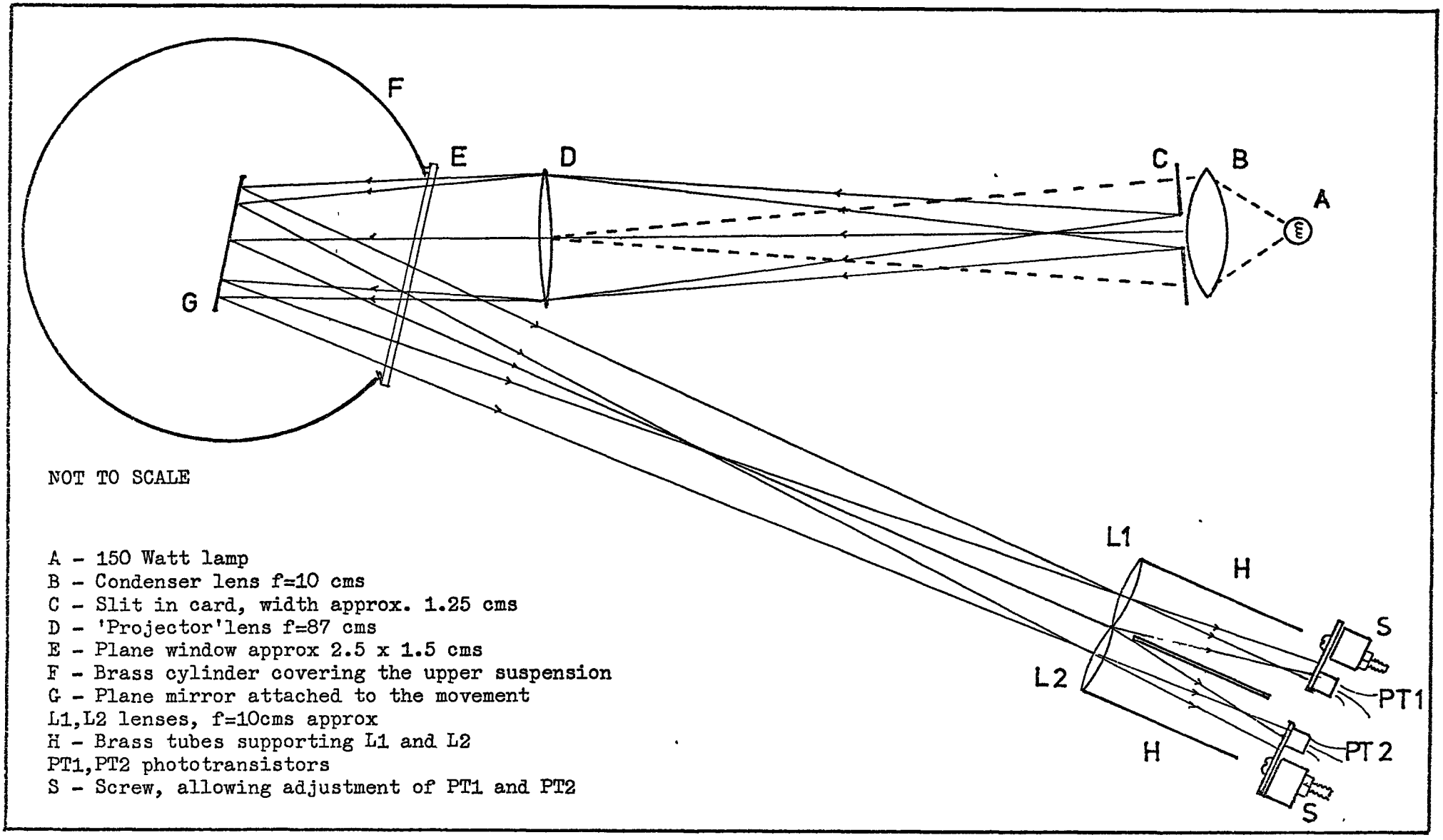

NOT TO SCALE

A - 150 Watt lamp
B - Condenser lens f=10 cms
C - Slit in card, width approx. 1.25 cms
D - 'Projector'lens f=87 cms
E - Plane window approx 2.5 x 1.5 cms
F - Brass cylinder covering the upper suspension
G - Plane mirror attached to the movement
L1,L2 lenses, f=10cms approx
H - Brass tubes supporting L1 and L2
PT1,PT2 phototransistors
S - Screw, allowing adjustment of PT1 and PT2

counter-torque coil. Deliberately introduced temperature differences (for instance by touching one lead with a screwdriver cooled in liquid nitrogen) produced variations in the apparent temperature of only 2 to 3K. It was therefore assumed that normal temperature differences would produce negligible effects, since the connections were physically close together and distant from any sources of heat.

6.4.2. The optical system

The maximum counter-torque available is proportional to the maximum out-of-balance current from the amplifier. This in turn depends on the illumination of the phototransistors. The cylindrical glass dome formerly used on the apparatus had the effect of diffusing the light and the galvanometer mirror formerly used was of a very small area. In order to make better use of the light available the arrangement shown in figure 6.8 was used.

A condenser lens of 10 cm focal length and 5 cm diameter focuses an image of the lamp's filament on the projector lens (87 cm focal length and 3 cm diameter). A slit is placed close to the condenser lens and the projector lens forms a sharp image of this on the lenses on front of the phototransistors, via the plane mirror on the movement and the plane window in the cover of the instrument. The phototransistors have a very small sensitive area and are mounted on adjustable brackets so as to be exactly at the foci of two lenses. Two tubes help to protect the phototransistors from stray light but they were found to be unnecessary since the phototransistors are relatively insensitive to changes in the background illumination. The tubes were mounted as closely as possible but this is not necessary to restrict the rotation of the

Figure 6.9 The Amplifier Circuit

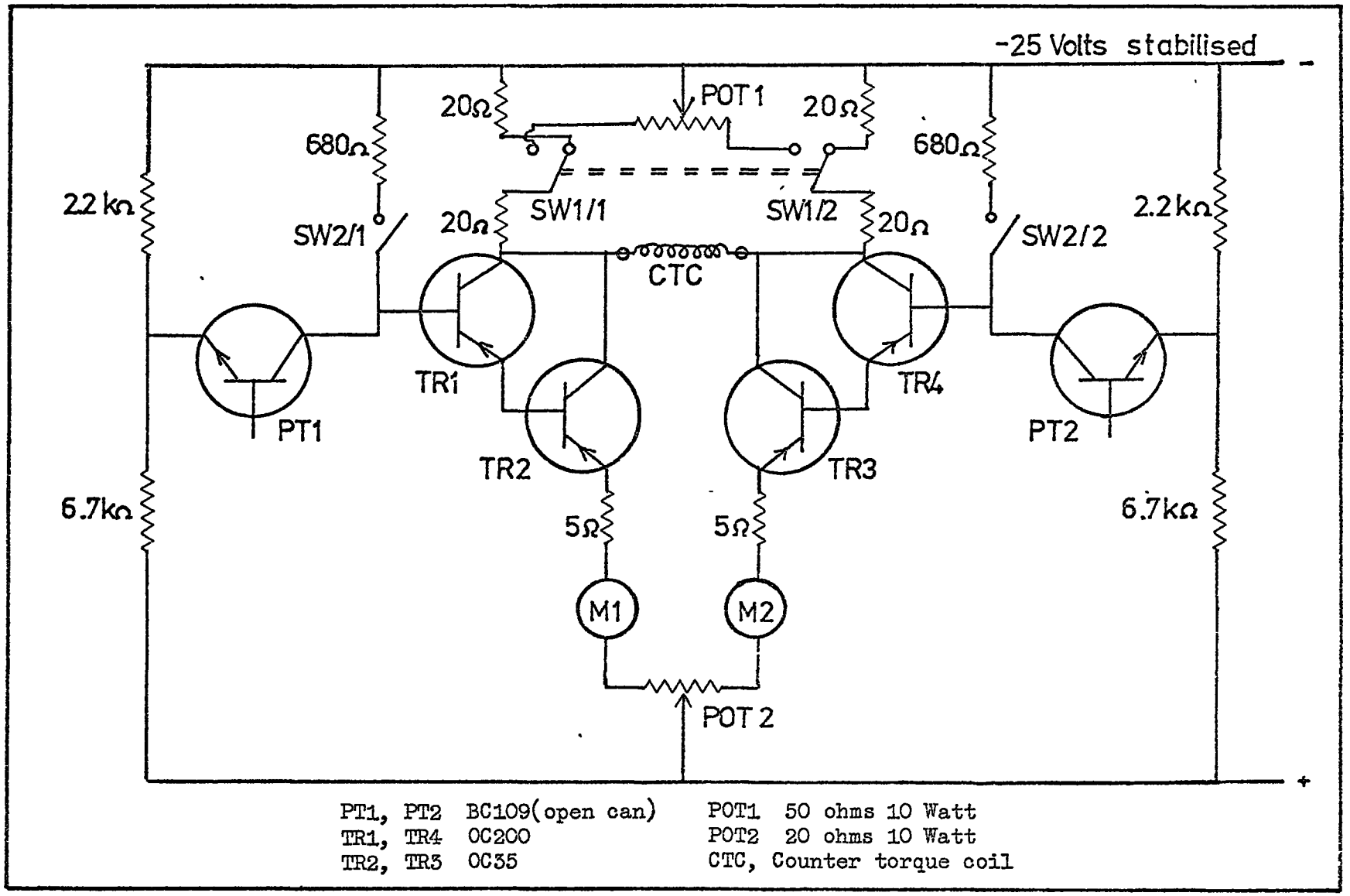

PT1, PT2	BC109(open can)	POT1	50 ohms 10 Watt
TR1, TR4	OC200	POT2	20 ohms 10 Watt
TR2, TR3	OC35	CTC,	Counter torque coil

magnetometer movement since the maximum torque is obtained when the spot of light moves off one phototransistor completely. The width of the slit in the light source is adjusted till the image covers one half of each of the pair of lenses L1 and L2.

Since the distance of the phototransistors from the moving mirror is about 180 cm and the width of the lenses is 2 cm, maximum torque is obtained when the spot moves 1 cm, i.e. when the movement turns through an angle of $\frac{1}{2 \times 180}$ radians, or 0.15 degrees. Calculations with artificially produced displacements in the torque curves show that results are not significantly affected by rotations in the specimen of several times this value. It is therefore permissible to regard the specimen as fixed. In addition, because the rotation of the crystal is so small, torques introduced by twisting of the suspension wires and connecting leads may be neglected.

The lamp, which is an Atlas Truflector A1/184 (21.5V 150 Watt) is fan cooled and may be dimmed by a rheostat to prolong its life when maximum torques are not required.

6.4.3. The Amplifier

The circuit of the amplifier is shown in Figure 6.9. SW1 is a double-pole, double-throw type and SW2 is double-pole, single-throw. Both switches are shown in their normal position. Potentiometers Pot 1 and Pot 2 are set initially with their sliders half way along the track. With the reflected light from the torque magnetometer falling equally on both phototransistors (which are normal BC109 types opened and fixed to transparent windows with Araldite) both OC200's and both OC35 transistors are conducting. The collector terminals of the OC35's (marked X1 and X2) are at the same potential and the current in the counter-torque coil, which is connected between them, is zero.

If the light moves off PT1 and onto PT2 then the currents in TR1 and TR2 fall, while those in TR3 and TR4 increase. The point X2 then becomes positive with respect to X1 and current flows in the coil. This current increases with the distance moved by the light spot and reverses when it moves onto the opposite phototransistor. If the light spot should accidentally move off both phototransistors then all currents fall to zero, and, since the apparatus is sealed, no direct means exists of getting the spot of light back onto the phototransistors. This situation can sometimes be cured by rotating the electromagnet. The crystal usually sets itself with an easy direction of magnetisation parallel to the field and it follows the magnet as it rotates. Otherwise, SW2 is closed producing a large current in both sides of the circuit. The potentiometer Pot 2 is then adjusted to unbalance the circuit and provide a current in the coil sufficient to bring the light back to a central position. SW2 is then opened and the spot of light should remain on the phototransistors.

In plotting a torque curve the restoring torque varies continuously and the variation of current in TR3 and TR4 can be observed on the meters M1 and M2. If it is clear that the current in either is about to fall to zero then the switch SW1 is changed over and the circuit is deliberately unbalanced with potentiometer Pot 1 to raise the current. This allows the measurement of larger torques than would otherwise be possible. The potentiometer Pot 2 can be used to unbalance the circuit even more. This gives output currents up to 440 mA which produce counter-torques of approximately 3.25 Nm. In normal use such a high current would not flow continuously through the counter-torque coil. It was however checked that the coil could tolerate this current for at least two minutes with only slight rise in temperature.

6.4.4. Arrangements for Automatic Recording

To obtain a torque-curve with the apparatus as used by Bly it was necessary to read currents at 36 points as the magnet was rotated and a further 36 points as it was rotated in the opposite direction. With practice a set of readings could be obtained in 15 minutes but the tendency of the magnet to overheat made readings at the highest field strengths impracticable by this method and it became imperative to make the recording automatic. The counter-torque current was recorded by connecting the terminals of the coil directly to the Y terminals of a Hewlett-Packard potentiometric recorder (Type 7030A). The recorder contains an internal voltage reference standard and, using a suitable scale, deflections of the trace can be read off directly as potential differences. To record the angular setting of the magnet a potentiometer wire was stretched over a transparent insulating strip round the scale of degrees on the base of the magnet. One end of this wire and a wiping contact fixed to the magnet trolley were connected to the X terminals on the recorder. A 2 volt cell and a 220 ohms resistance were connected in series with the wire and a scale chosen so that the recorder pen traversed nearly the whole length of the paper for a 180 degree rotation of the magnet. This adjustment was kept constant throughout each series of measurements but no reliance was placed on this. The 0^{o} and 180^{o} positions of the magnet were indicated on each graph by operating the Y set-zero switch on the recorder with the magnet in those positions. If the X set-zero switch was operated with the Y set-zero switch down and the magnet in the appropriate position, the recorder would draw in the horizontal axis on each graph.

A linear relationship was found between the angular displacement of the magnet and the X deflection on the recorder. When this had been established angles were read from the graphs by interpolation between the 0 and 180 degree marks.

The reading of the graphs is described separately. This process took almost as much time as the direct reading of the currents did formerly. Several advantages were obtained by the automatic recording however. It became possible to detect rapidly cases where the apparatus was misbehaving, overheating of the magnet was avoided and in the case of the Dysprosium specimen it was possible to recognise regularities in the behaviour of the material after collecting large numbers of torque curves. Also temperature stabilisation became easier. It is unsafe to analyse a series of numerical results without first plotting them to see if they lie on a smooth curve of the expected form. The selection of the next working temperature or field value often depends on the form of the curve just obtained. The labour of plotting all the curves, including many that will have to be rejected, is avoided. The graphs obtained were stored in a centrally heated environment until required for computing.

6.4.5. The Electromagnet

The electromagnet is the same as that described by Bly (1967) and originally constructed by Roe. Although this magnet had been calibrated carefully there was evidence that the poles had been disturbed and a check was made on the calibration using two specially constructed search coils and two calibrated Grassot Fluxmeters. Differences of up to 3% were observed from the original calibration. This may however indicate merely differences in the instrument used to measure the current through the magnet. For currents under 30 amps a specially shunted AVO

Figure 6.10 The Electromagnet: Calibration Curve

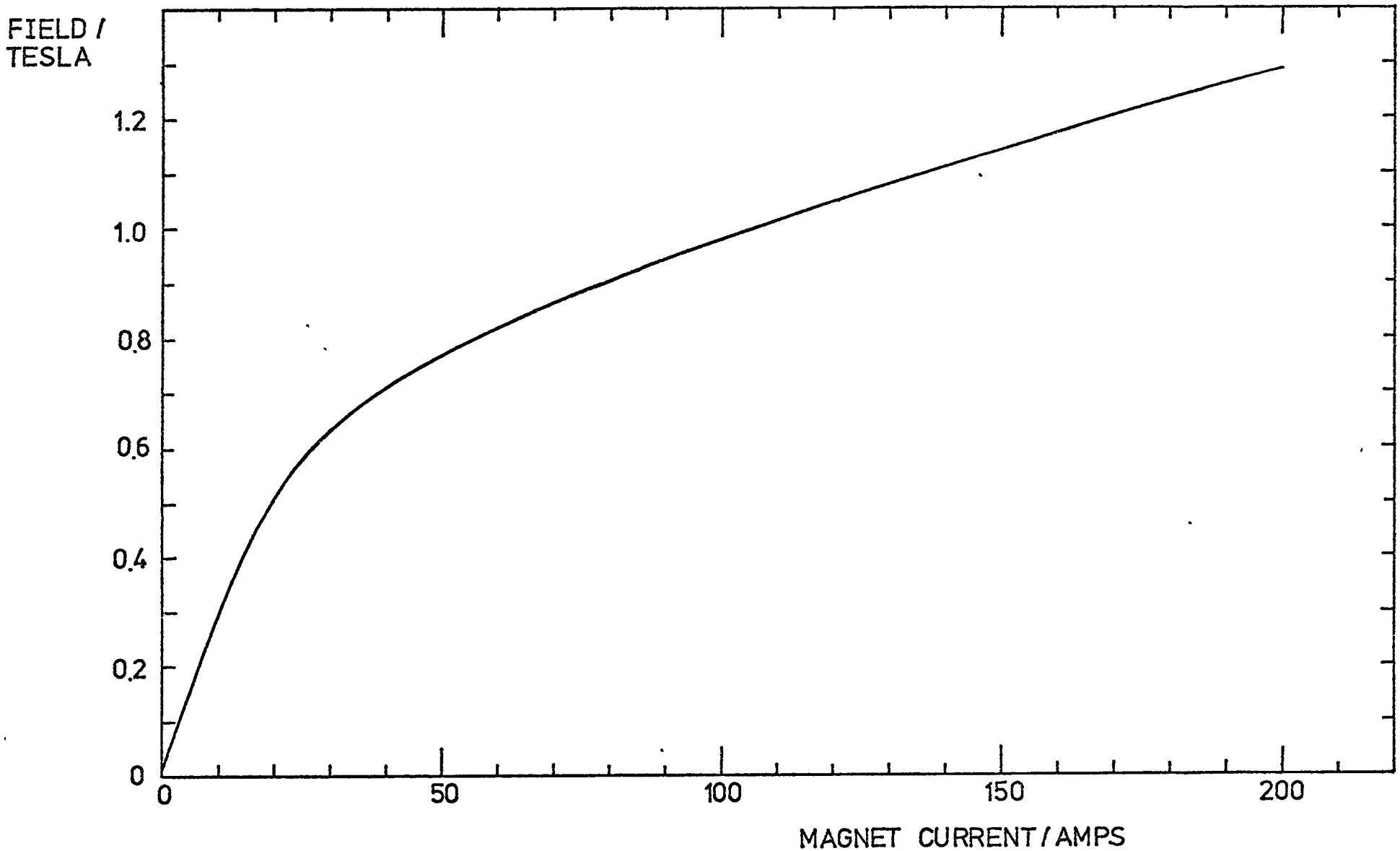

meter was used and for currents above this, the pointer instrument in the control unit of the magnet power supply was used. The strength of the applied field could be determined within 2% between 0.6T and the maximum value. The calibration curve is shown in Figure 6.10. Uniformity of the field was checked using a small Hall probe. No sensible variation in the flux density could be observed over a distance of approximately 0.75 cm from the centre of the space between the poles of the magnet, although the pole faces deviated from being parallel by approximately ¼ degree.

The pole faces are circular and 10 cm in diameter and an average of 4.770 cm apart. The magnet coils are connected in series and have a resistance of 1 ohm. The maximum current supplied by the power unit is 200 amperes at 200 volts. This is unsmoothed D.C. rectified from the mains supply. The current is controlled by means of a motorised variable transformer feeding the input to the P.S.U. The magnet is cooled by means of distilled water pumped from a 40 litre tank through the coils and a heat exchanger. The heat exchanger is cooled by running mains water. The pressure of the water produced by the circulating pump was quite capable of blowing out the rubber gaskets on the magnet and to avoid this the outlet tap from the magnet was opened fully and the inlet tap opened only as far as necessary to keep the magnet cool. A slight electrical leak from one end of the magnet coils to the case makes it safer to observe polarity in connecting the magnet to the D.C. supply, the negative terminal of the supply being earthed.

It was necessary to construct a framework to support the hoses carrying cooling water so that the magnet could rotate freely. The rotation was still limited to about 200 degrees. In obtaining torque curves the magnet was rotated continuously from about 15 degrees before

the zero of the curve to about 15 degrees beyond the 180 degree mark. Analysis was then carried out on readings taken between the 0 and 180 marks.

6.5 Stability Considerations in the Design of the Magnetometer

In all torque magnetometers the specimen is held in equilibrium by opposing the torque due to the magnetic field by an equal restoring torque, and it is the restoring torque which is measured. In simple instruments the restoring torque is provided by a torsion wire and is measured by the angle of twist in the wire. Equality of the torques is however not a sufficient condition for stability. F.W. Harrison (1956) has shown from energy considerations that for any slight rotation of the specimen, the change in torque in the torsion wire must be greater than the change of torque on the specimen due to its changed orientation in the magnetic field. The change in magnitude of both torques must have the same sign. If this condition is not met at some position of the specimen then no measurement can be made. Expressed in Harrison's symbols

$$\tau > V \frac{dL}{d\alpha}$$

Where τ is the torsion constant of the wire,

V is the volume of the specimen,

L is the torque per unit volume of the material of the specimen and

α is the angle between the magnetic flux lines and some direction fixed within the specimen.

For crystal specimens with hexagonal symmetry, in certain circumstances, the torque due to the field may change with rotation at a rate which, if continued, would bring it to its maximum value after 5 degrees. A

torsion wire suspension must be stiff enough in this case therefore to provide its maximum restoring torque for an angle of twist of less than 5 degrees. The movement of the torsion head and therefore the sensitivity of the instrument is small unless special methods are used to measure the angle of twist in the suspension.

In instruments such as the one used here, the maximum restoring torque is produced by a very small deflection of the moving parts and the feedback mechanism can be regarded as constituting a suspension of very high torsion constant. The condition specified by Harrison is therefore easily obtained. A more serious problem however is that of the violent oscillations which can occur with this kind of instrument, and which require some form of damping. Bly (1967) was forced to fix double paddles moving in a closely fitting annular trough filled with high viscosity gear oil. King et al. (1964) used paddles immersed in a 50/50 mixture of paraffin and liquid paraffin. Craft Donahoe and Love (1955) used wires dipping into vacuum oil. Baron and Hoffman (1970) used eddy current damping. However, Roe (1961), apart from a 30 microfarad capacitor connected across the counter-torque coil, had no special provision for damping and neither had Penoyer (1959) or more recently Willey et al. (1972). Penoyer and Willey used air bearings in their apparatus and both used magnetron magnets with the counter torque coil. It may be that some damping was introduced by these means.

In this investigation. the use of close fitting paddles was found to be most unsatisfactory. They tended to jam against the side of the trough after the apparatus had been cooled, so that time was wasted in warming up and opening the apparatus to put the fault right. In any case the damping provided was only barely adequate. Several attempts

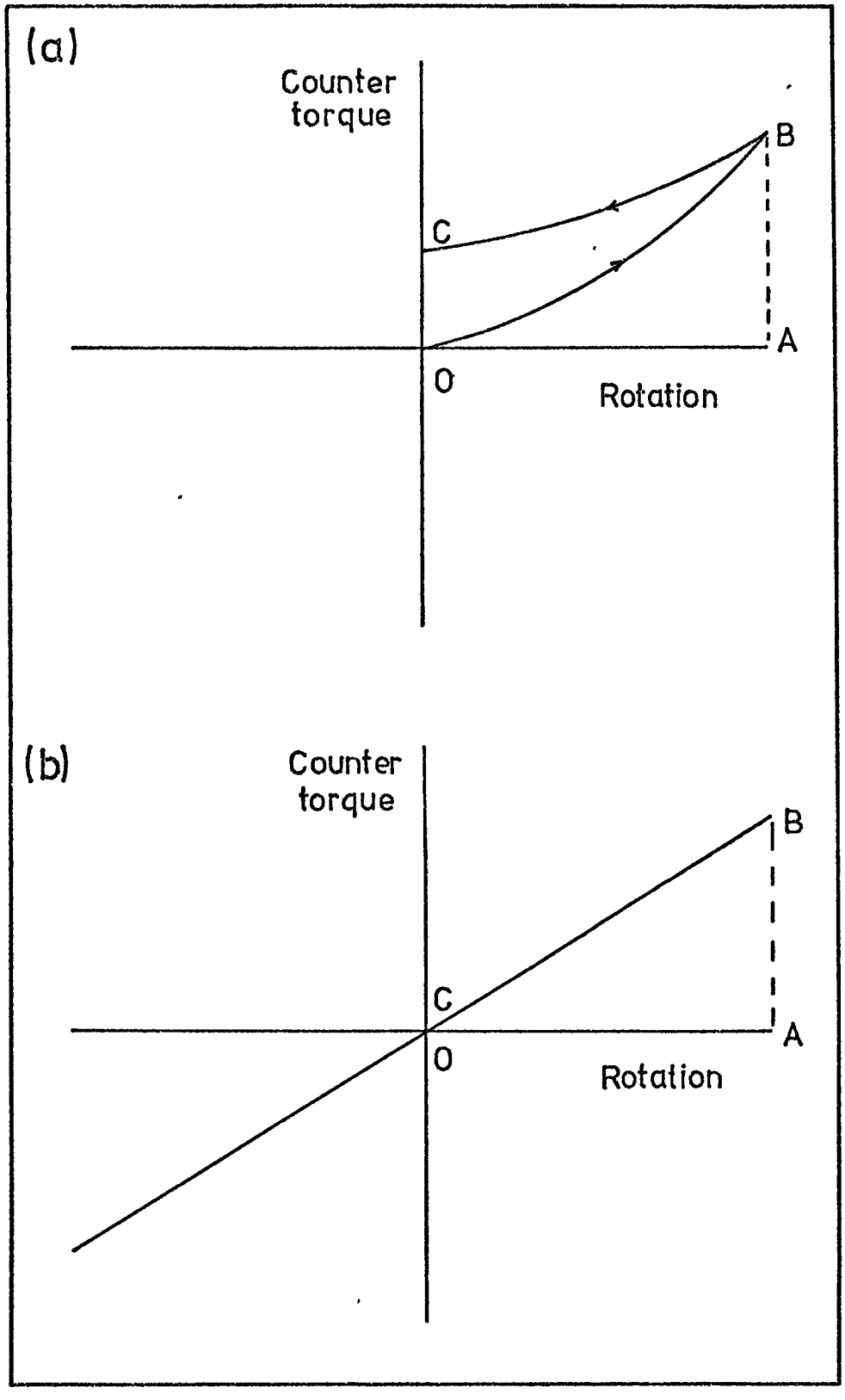

Figure 6.11 The Stability of a Torque magnetometer.
To illustrate the argument of page 94

were made to damp the oscillations electronically but without any success. Multiple paddles gave no more damping and made adjustments virtually impossible.

King et al. (1964) mention the importance of fast response for obtaining stable feedback. The speed of response of this system was therefore examined. The system originally used Cadmium Sulphide photo-resistors as the light sensitive elements. Maximum counter-torque was only obtained from the amplifier when the resistance of one cell fell to about 450 ohms and that of the other rose to 10,000 ohms. These resistances correspond to full illumination and complete darkness respectively and the changes were found to take as much as ¼ of a second to complete. This suggested the following qualitative explanation for the behaviour of the magnetometer. Referring to Figure 6.11a. If a random vibration moves the spot of light away from the central position a counter-torque will be developed and the motion will be reversed. The motion stops at B when the work done by the counter-torque current on the system (represented by the area OAB) equals the rotational kinetic energy of the original random motion. At this point however the counter-torque current (AB) is still high and, as the movement reverses, it falls only to DC because of the slow response of the system. On the reverse journey the movement therefore acquires more kinetic energy from the counter-torque current and makes a much larger excursion in the opposite direction. The area OABC represents the kinetic energy of the movement as it passes through its central position. If the damping system is unable to dissipate the additional energy, represented by OBC, while turning through the angle OA then oscillations will build up. In the ideal case represented by Figure 6.11(b) the speed of response is

imagined to be very high so that for every position of the magnetometer movement there is a unique value of the counter-torque current. The area of the loop OBC is zero, no energy is supplied to the movement from the feedback system and damping is only needed to dissipate the kinetic energy due to random vibrations of the moving parts. Multiple, closely fitting paddles moving in very viscous oil having proved inadequate to dissipate the energy acquired from the feedback system, it was realised that increased speed of response would decrease the ordinate OC in Figure 6.11(a) and hence the energy fed into the system. For this reason phototransistors, which have a response time 2 or 3 orders of magnitude smaller than photoresistors, were used. The feedback mechanism then became very much more stable and sufficient damping was obtained from strips of copper 3 mm wide dipping 8 mm into the heavy oil.

The greater clearances in the trough of oil allowed a greater range of movement to the upper suspension and permanent adjustments could be made quickly. In principle the same result could have been obtained by greatly increasing the gain of the amplifier. This would have greatly added to the cost and complexity of the amplifier and would have made the system extremely sensitive to stray light.

CHAPTER 7

CALIBRATION OF THE MAGNETOMETER

7.1 Calibration using a Flux Meter

The magnetometer was first calibrated by the method described by Roe (1961) and by Bly (1967). In this method a flux meter is connected to the counter-torque coil and the coil is rotated sharply through a small angle by pushing the damping vanes between two stops made of plasticine. The angle turned is calculated from the deflection of the reflected spot of light on a metre rule and the distance of the rule from the mirror on the apparatus. Assuming that the flux density in the gap of the galvanometer magnet is constant over the small angle turned, it is possible to calculate the product BAn from the relationship

$$BAn\delta\theta = \delta\Phi$$

where B is the flux density in the magnet gap (Tesla)

A is the effective area of the counter-torque coil (m^2)

n is the number of turns on the coil

$\delta\theta$ is the angle turned through in radians

$\delta\Phi$ is the change in flux linkages indicated by the fluxmeter (Webers).

Since the torque produced in the coil by passing a current of i amperes through it is τ = BAin (Newton metres), the quantity BAn is the required calibration constant τ/i NmA^{-1}. Since in this case torques were recorded on an XY recorder as potential differences across the counter-torque coil, the method also required an accurate determination of the resistance of the coil and its leads and a check on the accuracy of the XY recorder. The resistance of the coil was found to be

10.115 ± 0.005 ohms at room temperature (approx. 20°C)

The XY recorder has a very high impedance input and was connected directly to a Weston Standard cell. The readings on the 1 volt per inch, 0.5 volt per inch and 0.2 volt per inch scales were measured directly and the 0.1 volt per inch scale was checked by suppressing the zero on the instrument. In all cases the readings agreed with the certificate accompanying the cell, within the limits set by the thickness of the recorder pen trace. The standard cell was checked against another which was available and agreement within 10 microvolts was found. Further successful checks were made with a Mallory cell but these added nothing to the precision.

The results for the determination of the product BAn are given in Table 7.1. Large numbers of readings are necessary because of the low precision of each reading. Three fluxmeters were used and the speed and amplitude of the deflection of the counter-torque were varied. "Slow" in the table indicates a change taking about 0.75 of a second and "fast" one made by flicking the coil rapidly with a pencil and taking perhaps 0.1 to 0.2 of a second. "Small" means a rotation of about 3 degrees while a "large" swing is about 10 degrees.

It can be seen from the table that the results show several unsatisfactory features. Although there is reasonable agreement between the results from the different fluxmeters, mean results for different speeds of rotation of the coil differ between themselves by more than one standard error, indicating the existence of some damping in the fluxmeter. Results for different angles of rotation also differ between themselves, possibly because of variations in the flux density in the magnet gap.

Table 7.1

Calibration of Magnetometer by Fluxmeter Method

Fluxmeter	No. of readings	Type of Displacement	Torque per unit current BAn NmA^{-1}
C453832	14	small, fast	$(6.818 \pm 0.076) \times 10^{-3}$
C554228	15	large, fast	$(7.080 \pm 0.073) \times 10^{-3}$
	17	small, fast	$(7.160 \pm 0.065) \times 10^{-3}$
C755103	12	small, slow	$(6.23 \pm 0.142) \times 10^{-3}$
	13	small, fast	$(6.82 \pm 0.068) \times 10^{-3}$
	20	large, fast	$(7.030 \pm 0.049) \times 10^{-3}$
	7	V. large, fast	$(7.080 \pm 0.104) \times 10^{-3}$

7.2 Calibrations using a Torsion Fibre

A brass wire of round cross section, 0.5 mm in diameter and 0.3m long was soldered centrally into a brass screw which was then screwed into the lower end of the specimen holder in place of the normal lower suspension. The lower end of the brass wire could be twisted by a precision 30:1 worm drive gear clamped to the track on which the magnet ran. The upper suspension was freed and adjusted and the XY recorder set up as if for recording a torque curve. The lower end of the brass wire was twisted in 12 degree steps, each step being the result of turning the worm drive through one complete revolution, and the position of the recorder pen on the paper was marked at each step using the zeroing switch on the X amplifier. The P.D. appearing across the counter-torque coil for unit angular twist of the wire was found from a total of 20 readings on four switched ranges of the recorder.

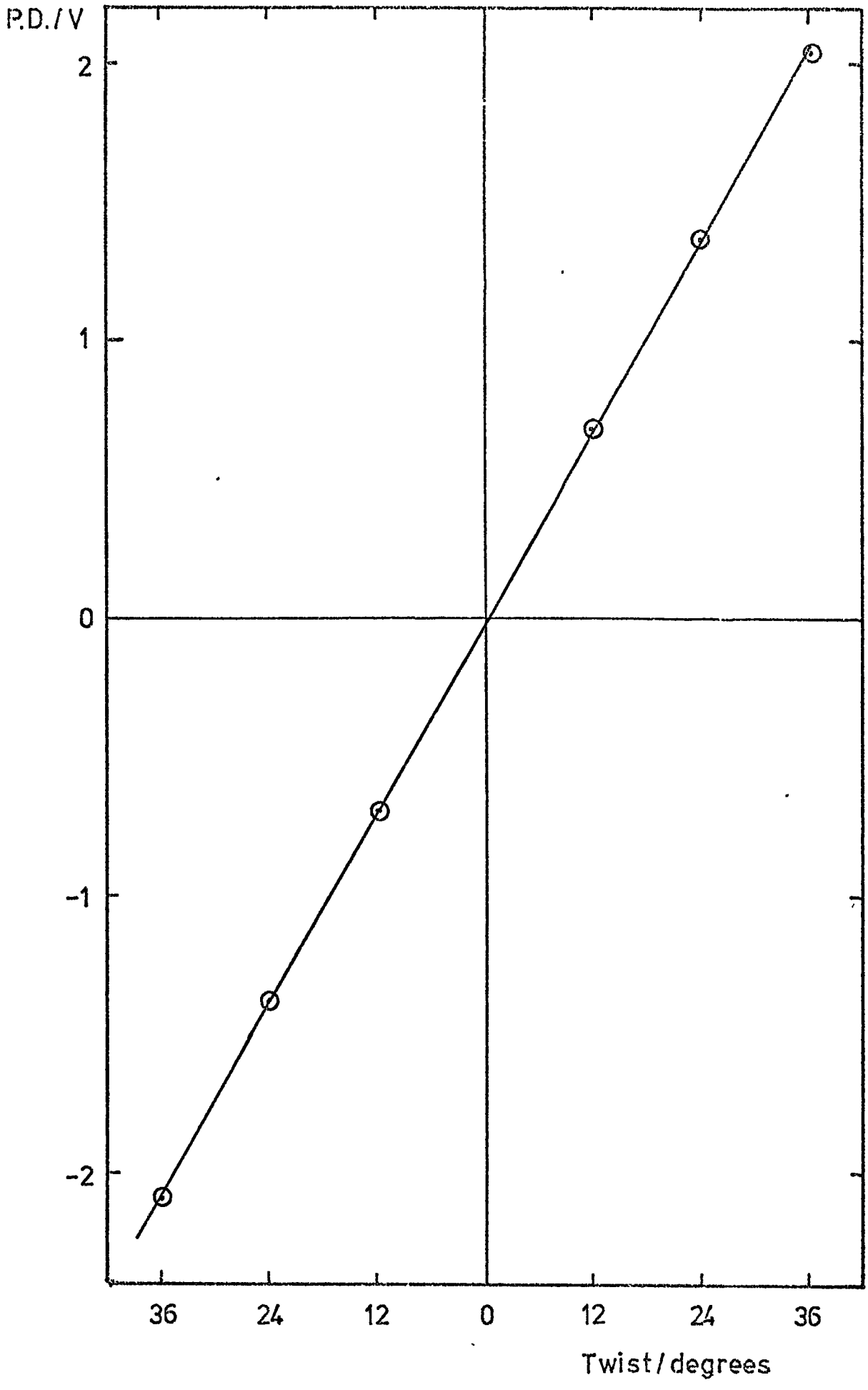

Figure 7.1 Calibration: Output versus twist in calibrating wire

The torque constant of the wire was then determined by suspending from it an accurately machined brass cylinder and measuring its period of oscillation about a diameter through its centre of gravity. The dimensions of the cylinder were found with a travelling microscope and the mass with a chemical balance. Timing was done with a stop watch calibrated against the G.P.O. speaking clock. Results are given in Table 7.2. The linearity of the counter torque system is indicated in Figure 7.1 which shows the P.D. across the counter-torque coil plotted against the angle of twist in the torsion wire. This calibration does not agree with the first within the limits of experimental error and a third method of calibration was used.

Table 7.2

Calibration with a Torsion-Wire

P.D. across counter-torque coil for 12 degree twist in torsion wire	= 0.3499 $\pm$ 0.0017V
Length of brass cylinder	= 12.10(275) $\pm$ 0.001 cm
Diameter of cylinder mean	= 1.58(775) $\pm$ 0.001 cm
Mass of cylinder	= 202.10 $\pm$ 0.03 gm
Time of one oscillation	= 2.81(43) $\pm$ 0.04s
Torque for a P.D. of one volt	= (0.745 $\pm$ 0.008) x 10^{-3} NmV^{-1}

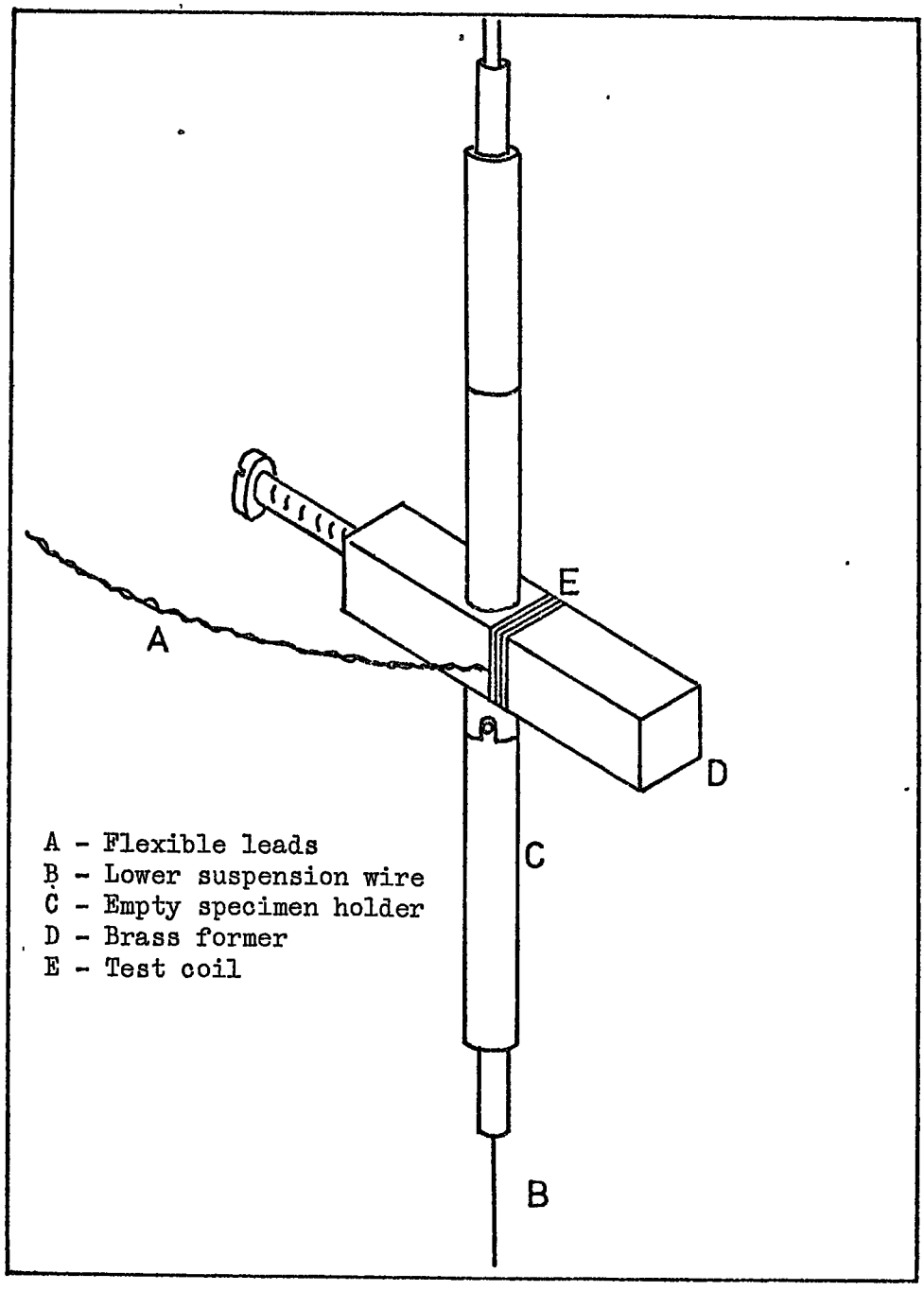

Figure 7.2 Calibration: General Arrangement of the Test Coil

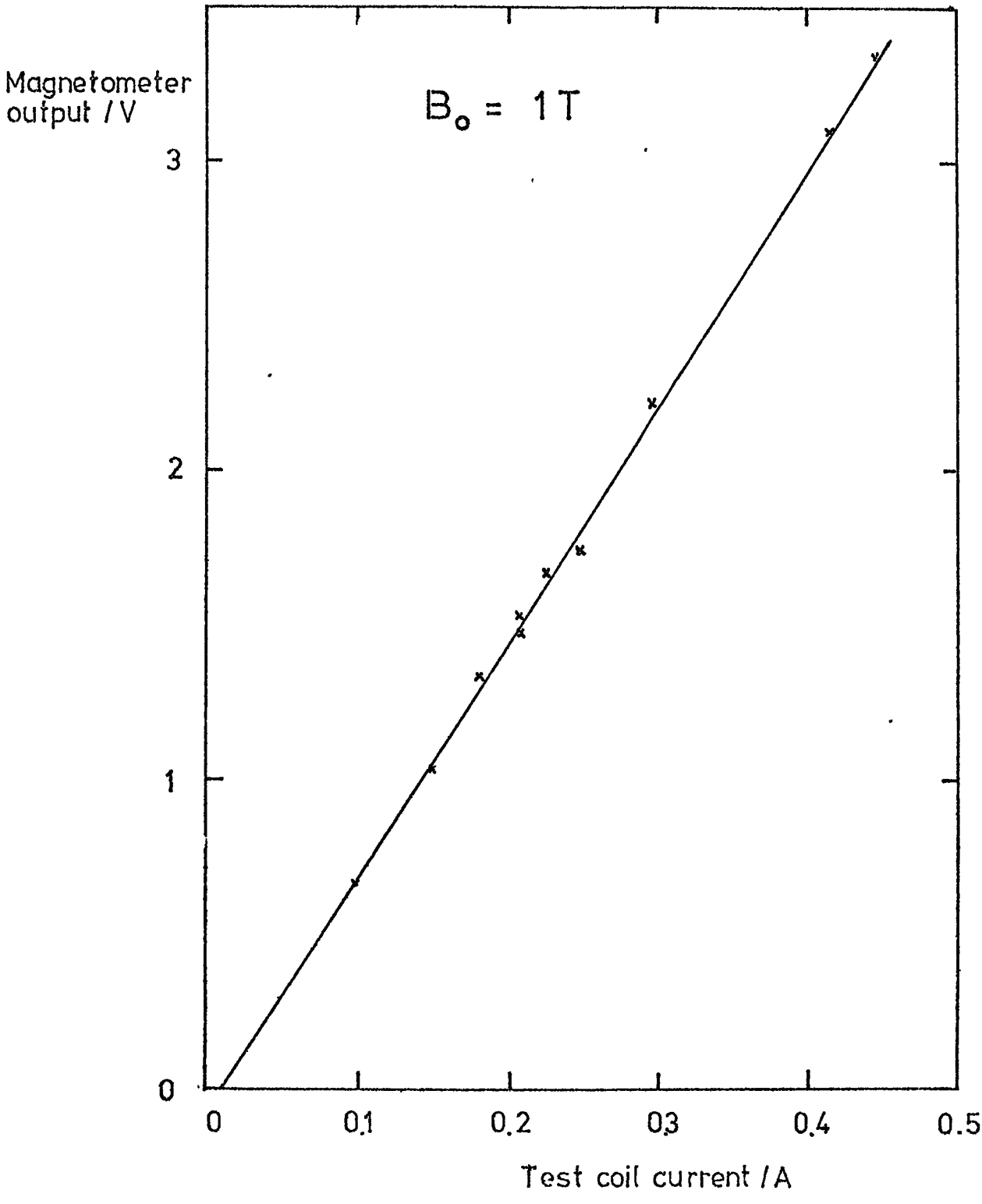

Figure 7.3 Calibration: Output versus current in test coil

7.3 Calibration using a Current carrying Solenoid of known Dimensions

A coil of 31 turns of 40 s.w.g. wire was wound on a square section brass former, drilled and fitted with a grub screw so that the coil could be fastened to the specimen holder at the level normally occupied by the specimen as shown in Figure 7.2. The projecting end of the brass former was of assistance in setting the plane of the coil parallel to the magnetic field of the electromagnet. The lower suspension wire of the magnetometer movement was fastened to a heavy support resting on the yoke of the electromagnet. To avoid direct pulls on the coil due to the effect of the magnetic field on the current in the lead in wires, they were twisted together and made as long and flexible as possible.

Currents between 0.1 and 0.45 amperes were passed through the coil and measured with a sub-standard ammeter. At the same time a field of about 1T was applied and the deflections of the pen on the XY recorder were marked. The quantity $\frac{BAin}{V}$ was found for each value of current and field, where V is the P.D. obtained from the pen recorder.

The mean of 15 determinations is

$$(0.7470 \pm 0.0055) \times 10^{-3}\ \mathrm{NmV^{-1}}$$

This figure agrees quite closely with that obtained from the use of torsion wires. Figure 7.3 shows the P.D. across the counter-torque coil plotted against current in the test coil for an applied field of 1T. The line does not pass through the origin because of constant torques in the suspension.

The results of the calibrations using a fluxmeter do not agree within the limits of experimental error with those obtained by the other two methods. Possible reasons for the discrepancy are (1) The assumption made that the flux density round the counter-torque coil is independent of the

current passing through it. This is questionable since the flux density due to the current in the coil is not negligible compared with that due to the permanent magnet. Exact calculations are not possible but for comparison, the flux density round the counter-torque coil due to the galvanometer magnet is less than 0.03T while the flux density 1 mm away from the coil at maximum counter-torque current is approximately 0.013T, neglecting the effect of the soft iron core. Harnwell (1949) page 426, describes the disturbing effect of current in a dynamo armature, a similar situation.

(2) The fact that the value of flux density varies over the pole faces of the galvanometer magnet and this method determines a quantiy BAn depending on the average value of B while the value required is that at the central rest position of the counter-torque coil.

(3) In deflecting the coil, eddy currents in the brass former would tend to diminish the induced e.m.f. in the coil.

For these reasons the result from the fluxmeter method of calibration was discarded and the weighted mean of the other two results was used in all subsequent calculations. The weighted mean is

$$(0.7463 \pm 0.008) \times 10^{-3} \text{ NmV}^{-1}$$

Figure 8.1 Ideal Basal Plane Torque Curve for an hcp Crystal

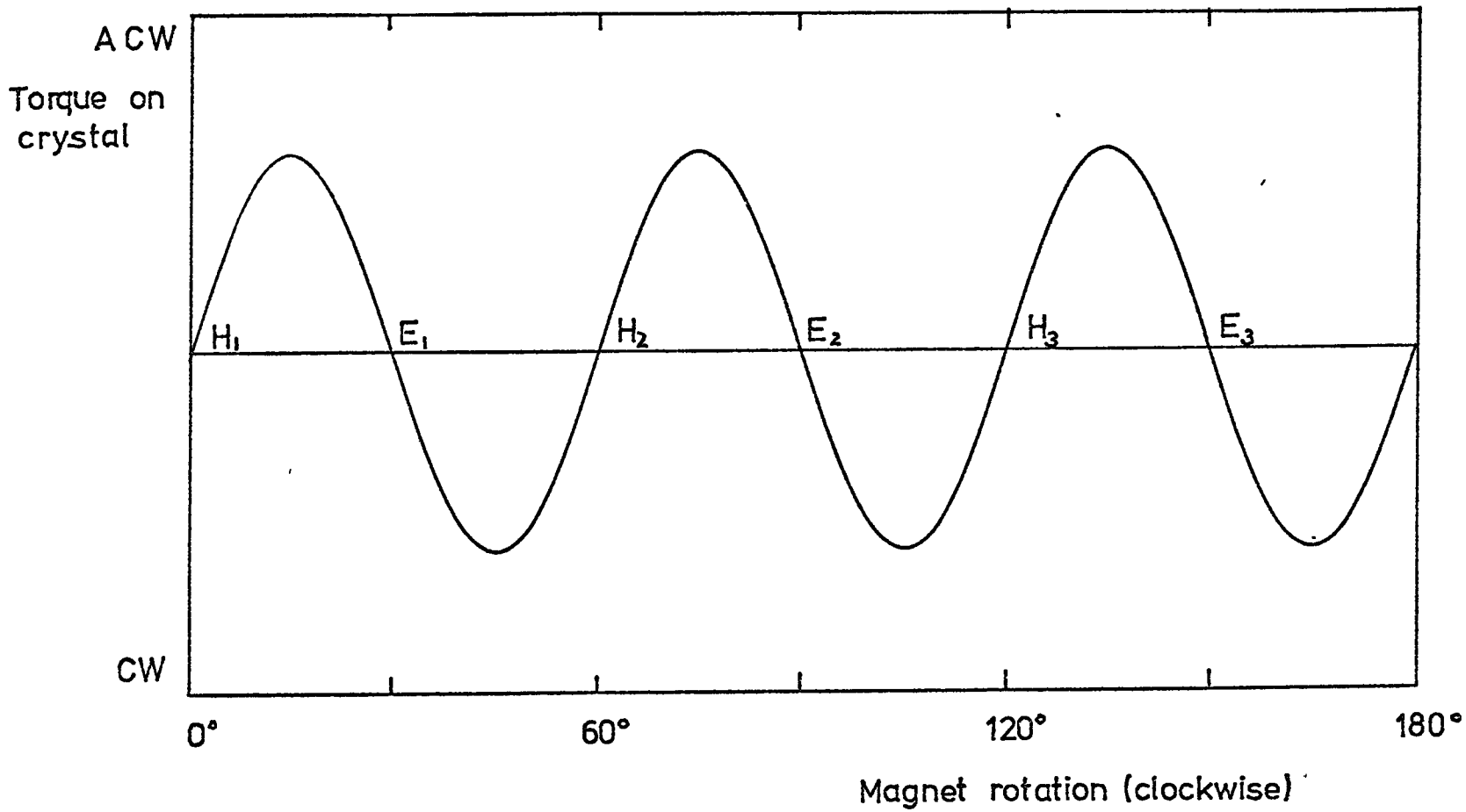

CHAPTER 8

ANALYSIS OF TORQUE CURVES

8.1 General Features of the Torque Curves

An ideal basal plane torque curve for an H.C.P. crystal is shown in Figure 8.1. The sign conventions used are as follows.

(i) The crystal is viewed from above.

(ii) Positive values on the graph represent torques turning the crystal anticlockwise.

(iii) A point on the scale of degrees gives the angle between some horizontal direction (such as the magnetic flux lines, or the magnetisation vector inside the crystal) and a fixed direction in the specimen. Increasing values on this scale indicate a rotation clockwise in the plane of the crystal. The graph in Figure 8.1 shows torque versus rotation of the magnetic field and when the magnetic field turns clockwise towards a direction such as E_1, E_2 or E_3, there is an anticlockwise torque on the crystal, which diminishes, and passes through zero as the field becomes parallel to these directions. E_1, E_2 and E_3 are therefore easy axes of magnetisation in the crystal. The points marked H_1, H_2 and H_3 show the position of the hard axes of magnetisation.

From equation 5.6, in the case of a basal plane disc cut from a hexagonal crystal, with the magnetisation vector in the plane of the disc, the torque exerted by the field on the crystal lattice is

$$L = \frac{\delta E}{\delta \phi} = - 6K_4 \mathrm{Sin}6\phi$$

where L the torque and K_4 may both refer to unit mass and ϕ is the angle between the magnetisation vector and 'a' axis of the crystal.

If ϕ could be measured directly it would be possible to plot L versus ϕ and obtain K_4 from direct measurement of the amplitude of the curve. In practice torque is plotted against the angle of rotation of the applied field and other features occur in the torque curves, which make the analysis for K_4 more complex. These are discussed below.

(i) Phase angles

Zero torque rarely coincides with the origin of the torque curve. The range of angles through which the magnet can be turned is limited by electric current and water connections and the orientation of the axes of the specimen in a horizontal plane is measured only after it has been settled by chance. The effect is to add phase angles to the periodic components of the torque curves.

(ii) Torques varying with the period of 2ϕ

These represent a very large disturbance and may arise from several causes.

a) Non-horizontal mounting of the crystal specimen

b) Non-circular shape of the crystal specimen

c) Misalignment of the crystallographic axes with the geometrical axes of the disc

(a) and (b) above are treated by Phillips and Shephard (1970) who showed that the first disturbance gives a component proportional to the magnetic field strength while the second is independent of it.

The disturbance mentioned in (c) above, was considered by Darby and Taylor (1964). They showed that in order to find the constant K_4 it is strictly speaking necessary to know exactly the orientation of the crystal's axes and the other anisotropy constants K_1, K_2 and K_3.

However in a case where the crystallographic C axis is not more than 5 degrees from the normal to the plane of the specimen and where

$$K_4 \ll K_1 + 2K_2 + 3K_3$$

it is permissible to regard the misorientation as merely adding a term with the period 2ϕ. These conditions were always fulfilled.

(iii) Torques with the period of ϕ

Phillips and Shephard also point out that if the centre of the specimen is mounted off the axis of rotation of the magnetometer and the magnetic field is not uniform then a component proportional to $\sin\phi$ can be expected in the torque curves. This component was not detectable on inspection of the curves and the calculated points could be fitted to the experimental curves without the inclusion of $\sin\phi$ terms.

(iv) Constant torques

These may be due to a slight twist left in the magnetometer suspension after setting it up. In this case both clockwise and anti-clockwise torque curves are displaced vertically in the same direction by a constant amount.

More often the constant torques are due to rotational hysteresis in the specimen and act in the same direction as the rotation of the magnetic field. Clockwise and anticlockwise curves are then displaced vertically away from each other and the area enclosed between the curves and the 0 and 180 degree ordinates is proportional to twice the work done in moving the magnetisation vector through 180 degrees.

(v) Torques with the period of $\sin4\phi$ and $\sin12\phi$

Because of random errors in reading the curves, Fourier analysis will show the presence of second and higher harmonics of the $\sin2\phi$ and

$\sin 6\phi$ components. These $\sin 4\phi$ and $\sin 12\phi$ components may also rise from the structure of the specimen. For instance Bly (1967) found a 12 fold component in the basal plane anisotropy of Holmium. Such components can be recognised by their phase angles which do not vary more than one or two degrees from graph to graph.

The torque curves may be expected to be represented by an expression of the form,

$$L(\phi) = A_o + \sum_{n=1,2,3,6} A_{2n} \sin 2n(\phi + \alpha_{2n})$$

Where A_o is a constant torque due to rotational hysteresis,

A_{2n} is the amplitude of the $\sin 2n\phi$ component and

α_{2n} is its phase angle.

$L(\phi)$ in this case refers to an arbitrary mass W of the material

then $$K_4 = \frac{A_6}{6W}$$

so that Fourier analysis for A_6 should suffice to obtain K4.

It is also useful to know the amplitudes of the other components and their phases.

8.2 Calculation of the amplitudes and phases of components of the torque curves

The torque $L(\phi)$ is given by

$$L(\phi) = A_o + \sum_{n=1,2,3,6} A_{2n} \sin(2n\phi + 2n\alpha_{2n})$$

Expanding this we have

$$L(\phi) = A_o + \sum_{n=1,2,3,6} A_{2n} \sin 2n\phi \cos 2n\alpha_{2n} + \sum_{n=1,2,3,6} A_{2n} \cos 2n\phi \sin 2n\alpha_{2n}$$

Now $$\int_0^{\pi} \sin 2n\phi \, d\phi = \int_0^{\pi} \cos 2n\phi \, d\phi = 0$$

$$\int_0^{\pi} \sin 2n_1\phi \cos 2n_2\phi \, d\phi = 0 \text{ for all } n,$$

$$\int_0^{\pi} \sin 2n_1\phi \sin 2n_2\phi \, d\phi = \begin{cases} 0 \text{ if } n_1 \neq n_2 \\ \pi/2 \text{ if } n_1 = n_2 \end{cases}$$

and $$\int_0^{\pi} \cos 2n_1\phi \cos 2n_2\phi \, d\phi = \begin{cases} 0 \text{ if } n_1 \neq n_2 \\ \pi/2 \text{ if } n_1 = n_2 \end{cases}$$

$$\therefore \quad \int_0^{\pi} L(\phi) \sin 2n\phi \, d\phi = \frac{\pi}{2} A_{2n} \cos\alpha_{2n} = C_{2n} \text{ (say)}$$

and $$\int_0^{\pi} L(\phi) \cos 2n\phi \, d\phi = \frac{\pi}{2} A_{2n} \sin\alpha_{2n} = S_{2n} \text{ (say)}$$

$$\therefore \quad A_{2n} = \frac{2}{\pi} \left(C_{2n}^2 + S_{2n}^2\right)^{\frac{1}{2}}$$

and $$\alpha_{2n} = \tan^{-1}\left(\frac{S_{2n}}{C_{2n}}\right)$$

A_o is simply the mean value of the ordinates over the torque curve.

The integration is performed numerically using the Euler-McLarin expansion (Booth 1957, page 35 and 178).

$$\int_a^{a+m\delta x} f(x)\,dx = \frac{\delta x}{2}\Big[f(a) + 2f(a+\delta x) + 2f(a+2\delta x) + \ldots\ldots\ldots + f(a+m\delta x)\Big]$$

$$- \frac{(\delta x)^2}{12}\Big[f'(a+m\delta x) - f'(a)\Big]$$

$$+ \frac{(\delta x)^4}{720}\Big[f'''(a+m\delta x) - f'''(a)\Big]$$

f(x) is a function which it is desired to integrate over the range (a) to (a + mδx). The range is divided into m equal parts of width δx and values of f(x), f'(x), f"(x) etc. found at x = a, a+δx, a+2δx, etc. where f'(x) indicates the first derivative of the function f(x) and f"(x) the second derivative and so on.

If the function f(x) is periodic and mδx is an exact multiple of its period then

$$f(a) = f(a + m\delta x)$$

$$f'(a) = f'(a + m\delta x)$$

and so on for the other derivatives. The expansion therefore simplifies to the following:

$$\int_a^{a+m\delta x} f(x)dx = \delta x[f(a) + f(a + \delta x) + f(a + 2\delta x) + \ldots\ldots f(a +(m-1)\delta x)]$$

To integrate

$$\int_o^{\pi} L(\phi)\sin 2n\phi d\phi = C_{2n}$$

first let $x = \phi$, $m = 36$, $\delta x = \frac{\pi}{36}$, $a = 0$

then

$$C_{2n} = \frac{\pi}{36}\left[L(0)\sin(0) + L\left(\frac{\pi}{36}\right)\sin 2n\left(\frac{\pi}{36}\right) + L\left(\frac{2\pi}{36}\right)\sin 2n\left(\frac{2\pi}{36}\right)\right.$$

$$\left. + L\left(\frac{3\pi}{36}\right)\sin 2n\left(\frac{3\pi}{36}\right) + \ldots\ldots\ldots L\left(\frac{35\pi}{36}\right)\sin 2n\left(\frac{35\pi}{36}\right)\right]$$

and similarly

$$\int_0^{\pi} L(\phi)\cos 2n\phi\, d\phi = S_{2n} = \frac{\pi}{36}\left[L(0)\cos(0) + L\left(\frac{\pi}{36}\right)\cos 2n\left(\frac{\pi}{36}\right) + \ldots\ldots\right.$$

$$\left. L\left(\frac{35\pi}{36}\right)\cos 2n\left(\frac{35\pi}{36}\right)\right]$$

It is then only necessary to find the torques and trigonometrical functions at 5^{o} intervals and perform the simple numerical summation to obtain an exact value for each of the above integrals.

Readings in centimetres were taken from the torque curves at 5^{o} intervals and the integrals were evaluated for n = 1,2,3,4,5,6. Hence values in centimetres of A_2, A_4, A_6, and A_{12} and α_2, α_4, α_6 and α_{12} were computed for each curve. A_o was found simply as the mean value of the 35 readings. The value of K_4 for each curve was then found after finding the value of A_6 in units of Nm, using the scale factor of the XY recorder and the calibration constant of the torque magnetometer. The value of K_4 obtained at a particular field below saturation is referred to as K_4'. Values of K_4' were obtained separately from clockwise and anticlockwise curves and a mean value computed for each field and temperature value. Calculations were performed on the Northumbrian Universities Multiple Access Computer using mainly the language APL360. This allowed rapid development and modification of programmes and in addition can be used in batch mode. The final version of the programme used is given in Appendix I, and is written in PL1. This programme, in addition to calculating amplitudes, phase angles and a mean value of K_4', causes the computer to print out ordinates calculated from the values of A_o, A_2, A_4, A_6 and A_{12} previously obtained. It also prints out the R.M.S.

difference between the measured and the calculated ordinates. In addition the programme causes the computer to estimate the area between the clockwise and anticlockwise torque curves obtained for each pair of field and temperature values. The values are in arbitrary units but take account of the differences in scale factor between the graphs so that comparison can be made. This area between the curves is proportional to the rotational hysteresis and the values were subsequently used to detect the maximum which occurs in this quantity when the specimen is magnetised near the 'knee' of its magnetisation curve (Bozorth, 1951, page 515).

Other sections of the programme were written to deal with corrections for 'shearing' in the torque curves and also variable hysteresis drag. These are discussed later.

8.3 The Determination of the Easy Axis from Phase Angles

Assuming that the six-fold component of the torque curve is due to magnetocrystalline anisotropy, the phase angle for this component gives the position of a hard axis of magnetisation. Thus a phase angle of (say) +11 degrees would indicate that this component had zero value and a positive slope when the magnetic field was parallel to an axis 11 degrees anticlockwise of the zero of the torque curve; this axis is a hard axis because rotating the magnet clockwise would produce a positive (= anti-clockwise) torque.

Hard axes determined from computed phases always coincided with crystal axes as determined by the orientation procedure described in section 6.3.2. within 3 degrees and very often within 1 degree. Phases found when a component was nearly indistinguishable from the background were often different for the clockwise and anticlockwise curves, and were

not reproducible. This suggests that if a component cannot be seen in the recorded curve then a Fourier analysis for it is not likely to produce a reliable result. Random errors and distortions in the curves will produce spurious components.

8.3.1. The sign of K_4

For a hexagonal crystal magnetised in its basal plane $E_a = K_1 + K_2 + K_3 + K_4 \cos 6\phi$ (Equation 5.5) where ϕ is measured in the plane of the crystal from the 'a' axis. If K_4 is positive, then as the magnetisation moves away from the 'a' axis, $\cos 6\phi$ falls and the system moves to a state of lower energy. Thus the 'a' axis is a hard axis of magnetisation. Similarly if K_4 is negative then the 'a' axis is easy. Since the programme used for calculating K_4 gives a positive value regardless of easy axis, it is necessary to add a negative sign if the 'a' axis is found to be easy from inspection of the phases.

8.4 Methods of Reading the Torque Curves

A set of graticules was prepared on waterproof, transparent graph paper. The scale on the paper was checked against laboratory scales was found to be accurate and more stable dimensionally than the graphs from the XY recorder. All paper sheets were kept as far as possible in the same environment during the course of the experiments and the reading of the values. The graticules consisted of 37 equally spaced parallel lines, the first of which was laid on the 0 degree mark of the graphs and the last of which was made to coincide with the 180 degree mark. The displacement of the torque curve from the axis was then read on the first 36 lines on both clockwise and anticlockwise curves. The 72 values were read into a tape recorder and then taken down on punching forms ready for the preparation of punched cards for computing.

8.5 Errors in Reading Torque Curves

(a) Due to mismatch between graticule and torque curve

The distance between the 0 degree mark and the 180 degree mark varied by 2 or 3 mm between curves obtained on different days and it was feared that a very large number of graticules would be needed to read all the graphs. An analysis was made to determine how closely the graticules used for reading need to match the length of the rotation axis. Values of $\sin 6\phi$ were found at intervals of $5^{o}\ 3.5'$ which corresponds to reading a pure sine curve with a graticule 2 mm too long. These values were analysed as if they were readings from a normal torque curve and the value of A_6 was found to be 0.999. This procedure was repeated with values of $\sin 6\phi$ as they would be read from graticules 2 mm too short, 4 mm too long and 4 mm too short. The results are given in Table 8.1.

Table 8.1

Errors due to ill-fitting Graticules

Graticule misfit	Computed amplitude
2 mm long	0.999
2 mm short	1.001
4 mm long	0.9979
4 mm short	1.001

The greatest error can be seen to occur when the graticule is too long for the graph and is approximately 0.2% for a 4 mm misfit. The computation is very tolerant of errors of the order of 1 mm in the length of the graticule. This made it possible to read all the torque curves with only

Figure 8.2 Terbium Basal Plane Torque Curve Showing Shearing away from the Easy Axis

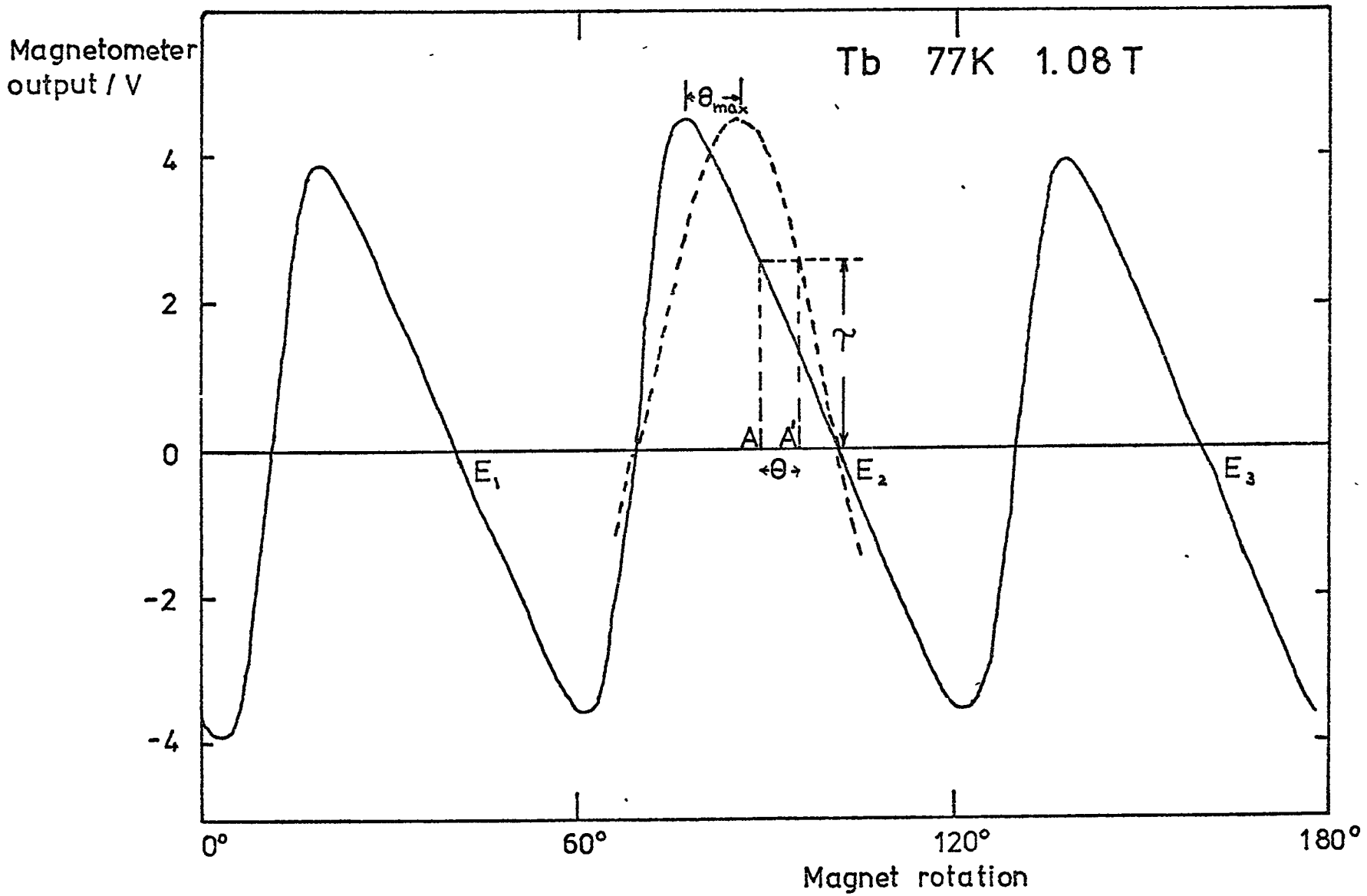

three prepared graticules. Further calculations with $\sin 2\phi$ curves showed that a 4 mm misfit caused an error of 0.5% in this component, but also produced a spurious $\sin 6\phi$ component of about 0.9% of the $\sin 2\phi$ amplitude. Similarly the amplitude of a $\sin 4\phi$ curve read with a graticule short by 4 mm was only changed by 0.3% but a spurious $\sin 6\phi$ component with an amplitude 1.3% of the $\sin 4\phi$ amplitude was produced. Thus a gross mismatch in an extreme case where the $\sin 2\phi$ and $\sin 4\phi$ components have the same amplitude as the $\sin 6\phi$ component introduces an error of 2.5%. In the torque curves which were used, even in the most unfavourable case

$$\frac{A_4}{A_6} < 0.3, \quad \frac{A_2}{A_6} < 2$$

and the mismatch was about 1 mm and occasionally 2 mm. Therefore errors due to this cause are estimated to be less than 0.5% for most readings.

(b) Random errors

Errors due to random faults in reading ordinates vary from curve to curve. A typical mean ordinate might be 20 mm and this might be read with a precision of 1 mm. K_4 values were computed from 72 such readings so that the standard error is approximately 0.6%.

8.6 Shearing of the Torque Curves

Figure 8.2 shows a torque curve for the pure Terbium basal plane specimen. A section of a sine wave is included in the graph for comparison. The torque curve is not sinusoidal, but has the appearance of a sine wave sheared away from the easy axes, the horizontal displacement of a point from the sine curve being approximately proportional to the height of the ordinate at that point.

Figure 8.3 The Relationship between the Magnetic Vectors in a Crystal Disc

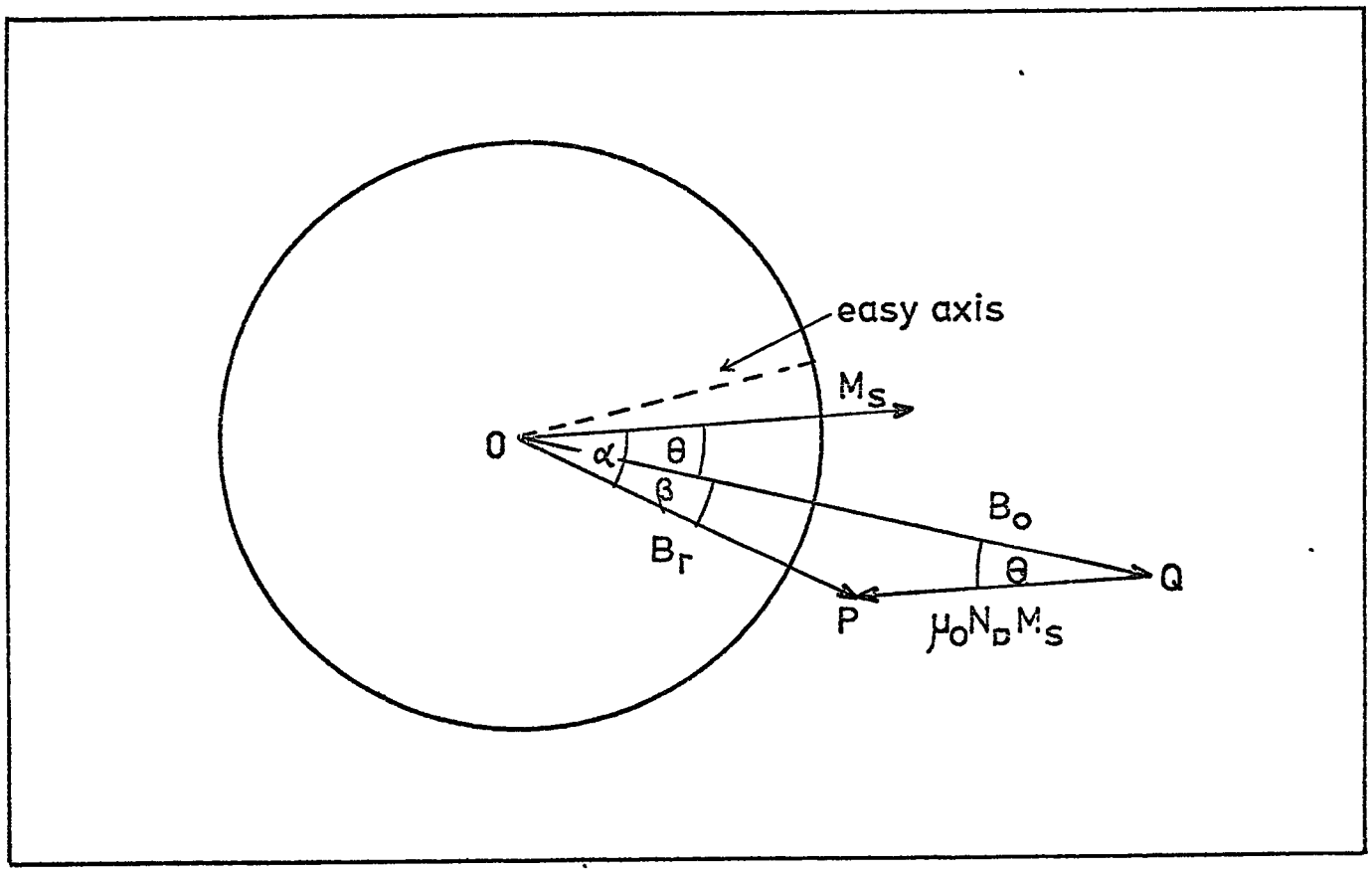

The cause of the shearing is the fact that in finite magnetic fields the magnetisation vector in the crystal does not lie parallel to the applied field except when the torque is zero, but is always directed between the applied field and the nearest easy axis. In Figure 8.2 when the applied field is at an angle A the magnetisation vector is at an angle A' nearer to the easy axis (E_2). The torque τ which is produced when the magnetisation is at this angle is actually recorded at A, further from the easy axis. In Figure 8.3 M_s represents the direction of the saturation magnetisation vector, B_o the direction of the applied magnetic field (assumed to be high enough to saturate the specimen), $\mu_o N_D M_s$ the demagnetisation field antiparallel to M_s and B_r the resultant field. The torque on the crystal is

$$L = B_r M_s \sin\alpha$$

In the triangle OPQ

$$\frac{B_r}{\sin\theta} = \frac{B_o}{\sin(180-(\beta + \theta))} = \frac{B_o}{\sin\alpha}$$

therefore

$$B_r \sin\alpha = B_o \sin\theta$$

$$\text{and} \quad L = B_o M_s \sin\theta$$

$$\text{so} \quad \sin\theta = \frac{L}{B_o M_s}$$

$$\text{and very closely } \theta_{\text{radians}} = \frac{L}{B_o M_s} = \text{const.}L \qquad (8.1)$$

The angle θ is the amount by which the torque ordinate corresponding to this orientation of M_s would be displaced away from the position of the easy axis on the graph. The correction suggested by H.J. Williams, (Bozorth 1954) is to displace each ordinate on the experimental curve

through the appropriate angle θ (Fig 8.2) back towards the nearest easy axis. The value of θ for each ordinate can be found very simply from the above equation 8.1 since the applied field is known and the saturation magnetisation is generally available from other experiments.

When the correction is applied the sinusoidal form is regained, but if the correction is not applied then unwanted harmonics appear in the Fourier expansion of the torque curve and the amplitude of the $\sin 6\phi$ component is seriously affected. To determine the importance of the correction a sine curve of unit amplitude was carefully drawn and deliberately sheared by moving each point side ways through an angle proportional to the height of the ordinate at that point. This artifically sheared curve was then read at 5 degree intervals and analysed as for a normal torque curve. Table 8.2 shows the displacement of the peak value of the distorted curve and the computed value of the $\sin 6\phi$ amplitude

Table 8.2

The effect of 'shear' on computed amplitudes of the sixfold component of torque curves

Maximum value of θ degrees	Computed amplitude $\sin 6\phi$
0	0.999
3	0.975
5	0.9578
7.5	0.916

To perform a more precise test a series of points on a sheared $\sin 6\phi$ curve was obtained by solving numerically the equation

Figure 8.4 Illustrating the Method of Producing Artificially Sheared Curves

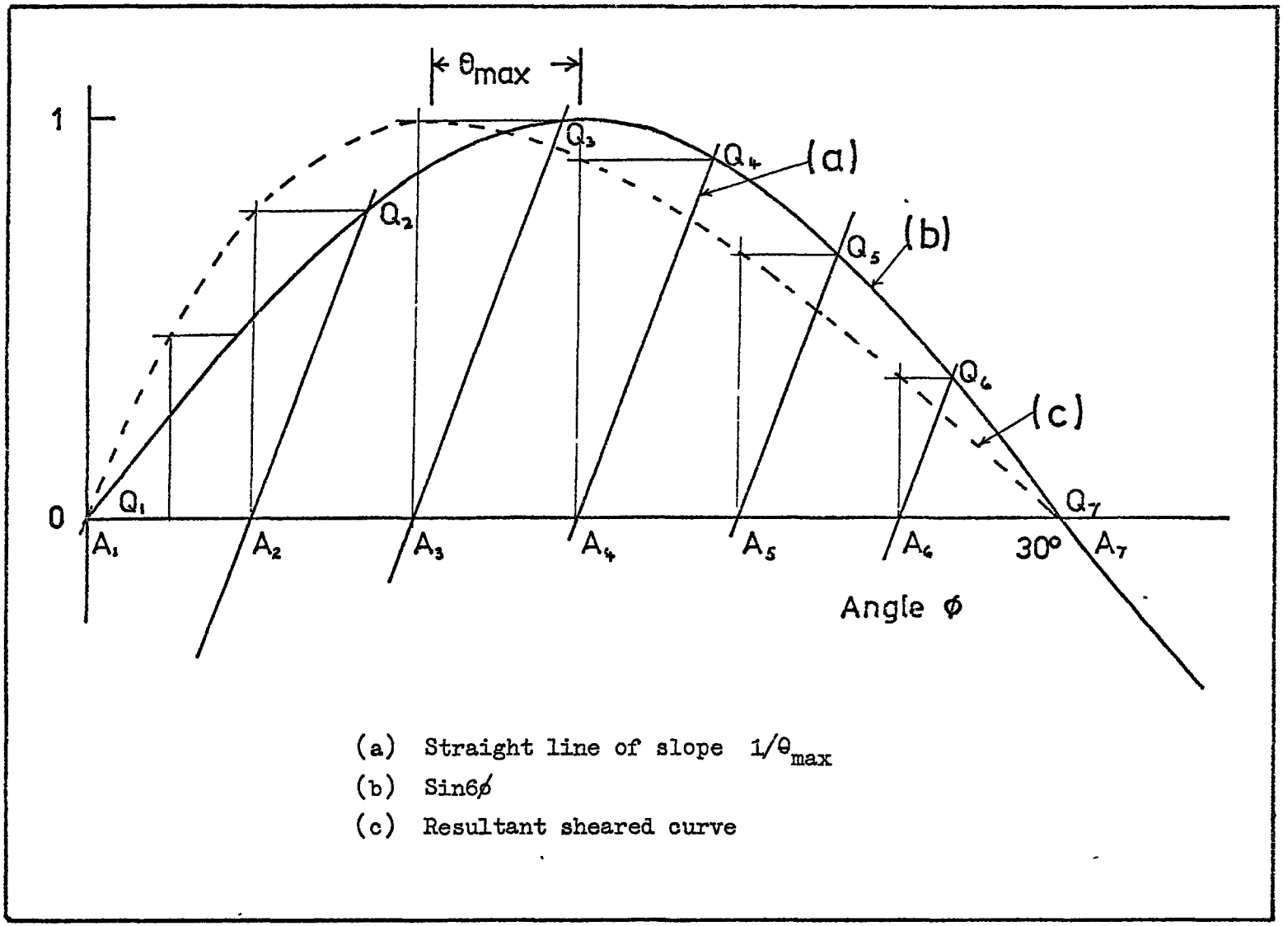

(a) Straight line of slope $1/\theta_{max}$

(b) $\sin 6\phi$

(c) Resultant sheared curve

$$\sin 6\phi = \frac{1}{\theta_{max}} (\phi - A)$$ for values of A at five degree intervals.

θ_{max} is a given maximum displacement of the ordinates from an easy axis. It can be seen (Figure 8.4) that the solutions to these equations represent the ϕ co-ordinates of the points of intersection (Q_1,Q_2, etc.) of a series of sloping lines with the $\sin 6\phi$ curve. If the values of $\sin 6\phi$ at the points Q_1,Q_2 etc. are plotted against the value of A at five degree intervals then a sheared curve is obtained. At the peak of the curve $\sin 6\phi = 1$, and

$$\phi = A + \theta$$

that is, the peak of the curve occurs at an angle θ earlier than the peak of a pure $\sin 6\phi$ curve and the displacement of the other ordinates is proportional to their height. Table 8.3 shows the results of Fourier analysis of the sheared curves for various values of θ_{max}.

Table 8.3

The effect of 'shear' on the amplitudes of the sixfold component of torque curves and its second harmonic

θ_{max} degrees	Amp.$\sin 6\phi$	Amp.$\sin 12\phi$
0	1.0000	
1	0.9979	0.0498
2	0.9952	0.1013
3	0.988	0.1499
5	0.9655	0.2359
8	0.9095	0.3165
10	0.8583	0.3337

Figure 8.5 Reading with an Inclined Graticule

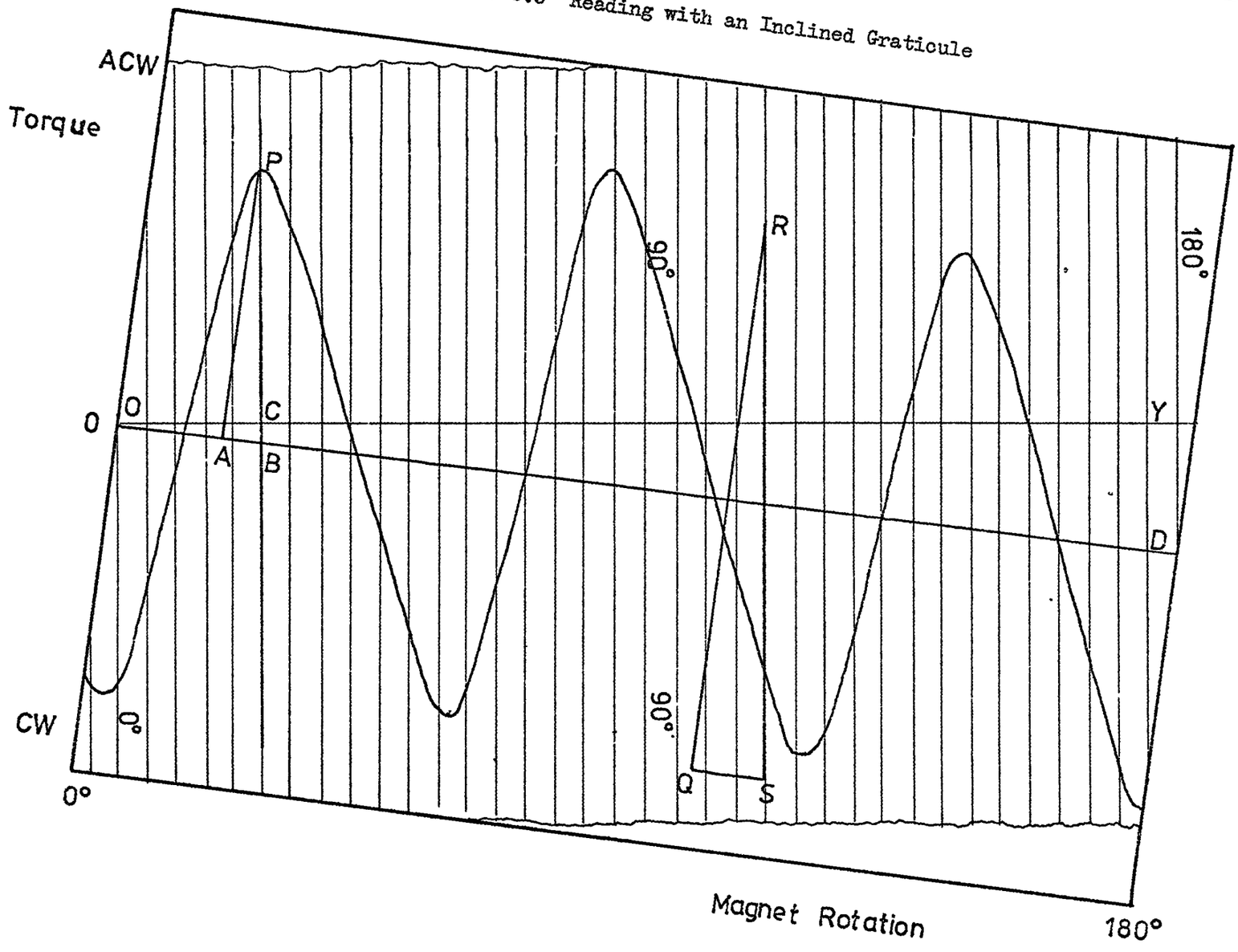

The following conclusions may be drawn concerning the correction for shear.

The error in the amplitude of the $\sin 6\phi$ component rises rapidly once the value of θ_{max} has risen above 2½ degrees, and it is therefore imperative that some correction should be applied if θ_{max} is more than this. It is also clear that even a rough correction can make a great improvement in the accuracy of the results. If the actual maximum angle of shear is say 8^{o} then any correction to θ_{max} between 5.5 and 10.5 degrees will then reduce the error from 9% to 1%.

8.7 Correction for Shear

Where large numbers of torque curves are to be read some automatic method of applying the correction for shearing is needed. Penoyer (1959) achieved this by tapping off a proportion of the output from the torque magnetometer and connecting it in series with the output from the potentiometer which indicated the orientation of his magnet. The angle co-ordinate of each point was thus displaced the appropriate amount towards the easy axis.

In this investigation it was found possible to correct for shear by reading values of torque from the curves with an inclined graticule. The general arrangement is shown in Figure 8.5. Values are read off where the inclined lines cut the experimental curve. E.g. the torque represented by the line AP in the diagram is read where the line PB through the 25 degree mark cuts the curve and is tabulated against this angle. The angle through which each value of torque is moved is proportional to the value.

The inclination of the graticule is found thus. The torque

represented by some arbitrary vertical distance on the graph, say RQ is calculated from the scale factor of the XY recorder and the calibration constant of the torque magnetometer. Suppose this torque is L. The end of the angle axis of the graticule is then tilted up so that the distance QS represents an angle

$$\sin^{-1} \frac{L}{M_s B_o}$$

If DY is the displacement of the angle axis on the graticule from the angle axis on the torque curve at the 175 deg. ordinate, and OY is the distance between the 0 and 175 deg. ordinates on the graticule, then the latter must be tilted until

$$DY = OY \times \frac{QS}{QR}$$

It is inconvenient to read AP directly, since the scales on the graticule are inclined to the axis of the torque curve. Instead, the distance PC is read, and a correction made as follows. Suppose AP' is the n'th ordinate (n = zero for the origin) then

$$AP = (PC + BC) \cos\hat{APB}$$

$$= (PC + n \frac{DY}{35}) \cos(\tan^{-1} \frac{DY}{OY})$$

A section of the programme given in Appendix I causes the computer to make this correction to each reading.

The graticule used has to be chosen so that the inclined distance between the 0 and 180 deg. ordinates fits the length of the experimental curve. At the 0 deg. ordinate the graticule and torque curve axes coincide.

An advantage of this method of correction for shearing the graphs is that a good approximate correction can be made without performing the

Figure 8.6 The Effect of Correction for Shearing.
$Tb_{.89}Sc_{.11}$, 77K, B_o = 0.645 T
(a) Tracing of Recorded Torque Curve
(b) Plot of Readings after Correction for Shear

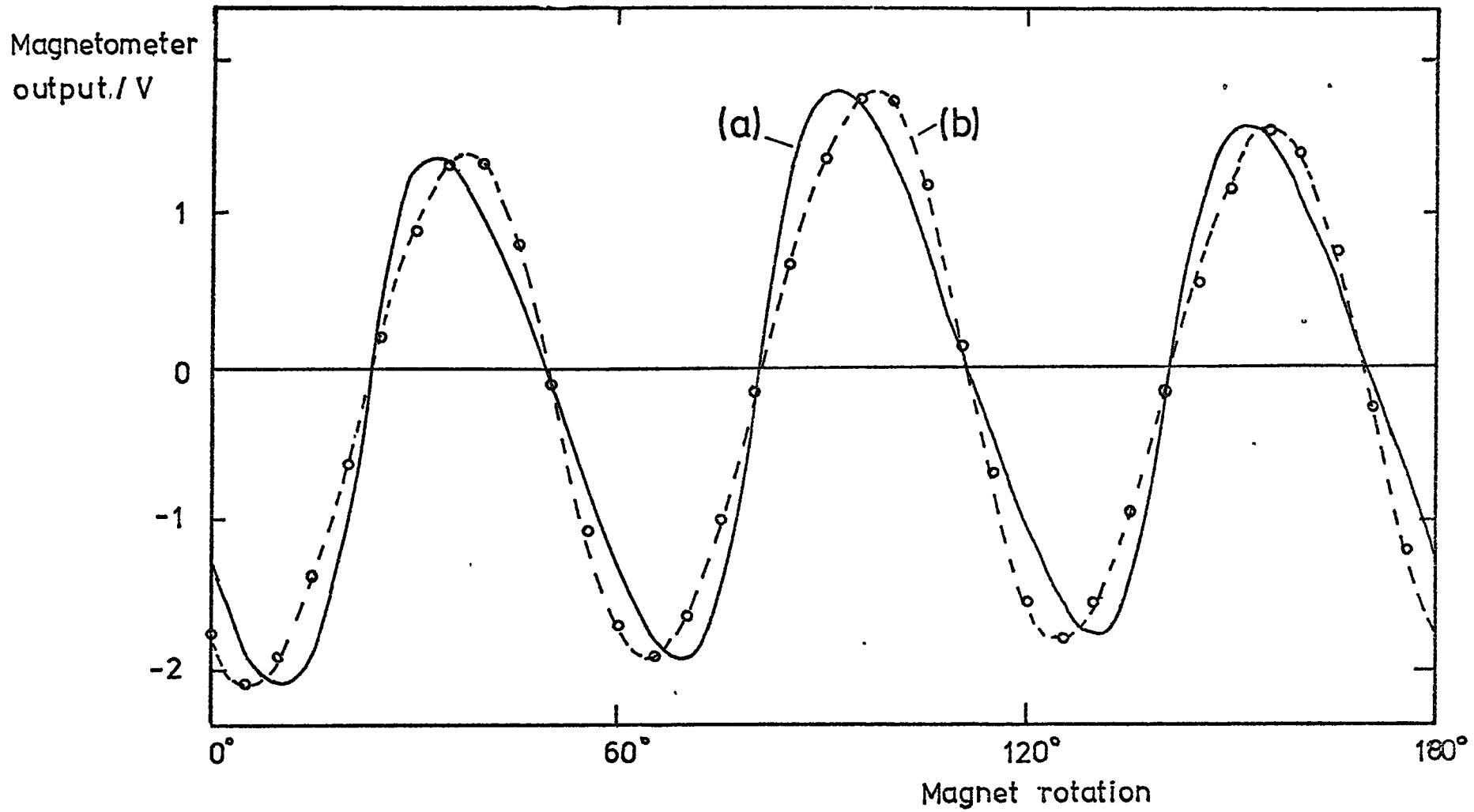

calculation to find the necessary inclination of the graticule. Where the curves are symmetrical the graticule is inclined until the maxima and minima on the torque curve appear to be evenly spaced across the lines on the graticule. In all cases where shearing was significant, the curves proved to be symmetrical enough to allow the use of this simple procedure which reduces the maximum shear below 2 degrees with ease.

Figure 8.6 shows a tracing of a sheared curve and a plot of the points read from it with an inclined graticule and corrected in the above manner.

8.8 Phase Differences between Fourier Components of Clockwise and Anti-Clockwise curves

The phases of the $\sin 2\phi$ and $\sin 6\phi$ terms were found to differ with the direction in which the torque curve was plotted. These differences were attributed to an additional angle of lag between the magnetisation vector and the applied field θ_h, which is constant and due to the hysteresis torque. If L_h represents this latter torque then

$$\theta_h = \sin^{-1} \frac{L_h}{M_s B_o}$$

The difference in phase between the two principal component of the curves should be $2\theta_h$ and it was thought possible that given values of the applied field B_o it might be possible to obtain values of M_s the saturation magnetisation. Values were obtained of the correct order of magnitude thus supporting the view of the origin of the phase differences given above; the values were however too scattered to be of much use in plotting magnetisation against temperature, presumably because of the errors in θ_h which is a small quantity.

One important result of the difference in phase between the clockwise and anticlockwise curves is that it is invalid to calculate K_4 from the mean of corresponding values on the CW and ACW curves. The value of K_4 so obtained is generally less than that obtained from the individual curves. It is necessary to find separate values of K_4 for the CW and the ACW curves and find the mean of these. In several cases the values of K_4 obtained by the two averaging processes turn out to be nearly equal. This point was noted by Bly (1967). These cases however are ones exhibiting large rotational hysteresis where the drag is not constant over the first few degrees of the torque curves and this effect depresses the individual values of K_4 to the level of the invalid mean. A correction for this effect is discussed in the next section.

8.9 Distortion of Torque Curves due to Variable Hysteresis Torques and its Correction

It was found with some specimens that the vertical displacement of the torque curves increased over the first 30 to 40 degrees rotation of the magnet. The effect was reduced but not eliminated by giving a 'run-in' to the curve since hoses and wires restricted the 'run-in' to about 15 degrees. A calculated correction was therefore sought.

Acting on the assumption that the CW and ACW curves should have the same form, the first 12 readings in each curve were replaced by the last 12 readings of the curve taken in the opposite direction, each reading being displaced by a distance equal to the mean distance between the central 12 readings. This procedure is only strictly valid if the Fourier components of the two curves are in phase but its use is encouraged by the following features of the combined curves.

Figure 8.7 Improvement to Computer Fit after Exchanging First and Last 12 Readings of each Curve ($Tb_{.825}Sc_{.175}$, 92K , B_o= 0.425 T) Clockwise Curve
(a) Before exchanging readings (b) After exchanging readings

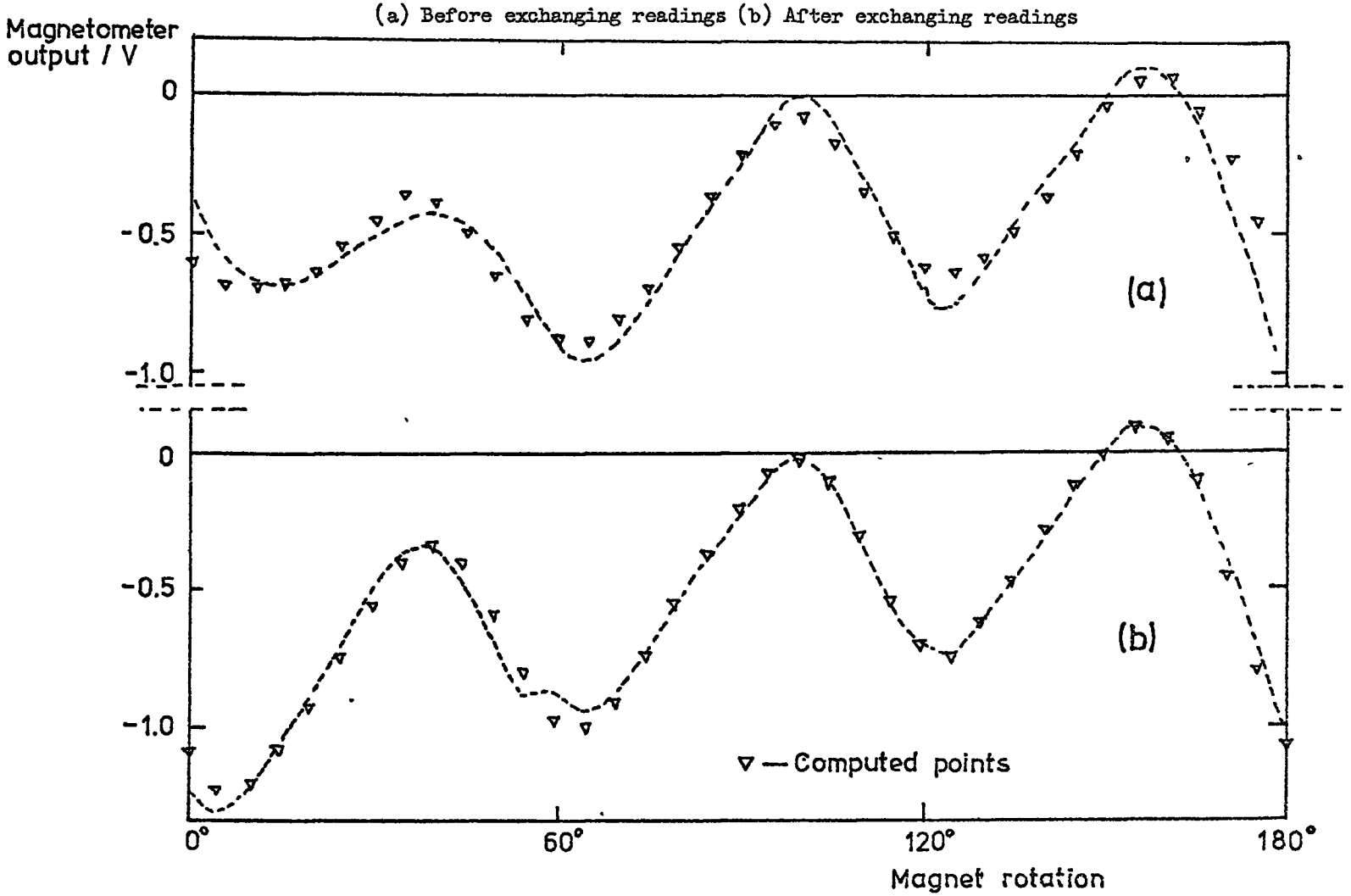

Figure 8.8 Further Illustrating the Computer Fit
($Tb_{.825}Sc_{.175}$, 134K , B_o= 1.173 T)

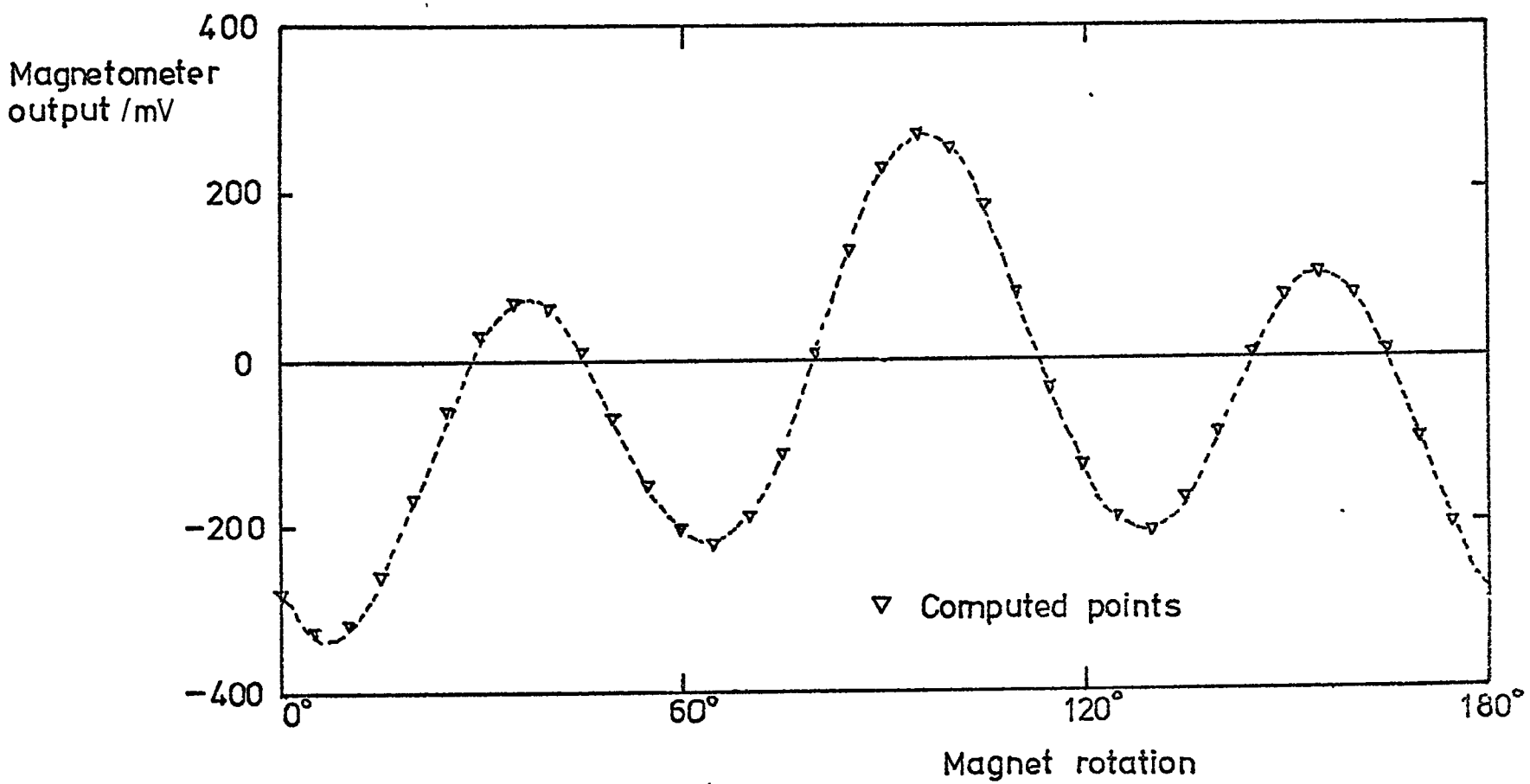

(a) They had the same value and slope at 0 degrees and 180 degrees. This is an essential condition for the valid application of the Euler-Maclaurin expansion in the numerical integration.

(b) They could be more closely fitted by calculated curves Figures 8.7 and 8.8 show the improvements obtained.

8.10 Estimate of Errors

The limits of error for various parts of the experimental work have been estimated in other sections and are summarised below.

Section 6.2	Masses of specimens: Dysprosium and Terbium	1%
	Other specimens	0.5%
Section 7.5	Calibration of torque magnetometer	1.2%
Section 8.5	Reading graphs	1.1%
Section 6.4.1	Temperatures	1K
Section 6.4.5	Magnetic Fields	2%

It is estimated that the relative uncertainty in K_4' values is $\sim 4\%$

The source of the greatest uncertainty in the results is the extrapolation procedure to find K_4 at infinite field, (Section 9.2.4). This extrapolation increases the highest measured value of K_4' by 15 to 20%. Experience with other magnetic materials and the arguments of section 9.2.4 suggest strongly that if a linear portion is reached in the graph of K_4' against $\frac{1}{\mu_o H}$, then the linear relationship will persist up to very high magnetic field values. If the extrapolations are valid they are accurate within 4%. The K_4 values are therefore claimed to be within 8% of the true values. In performing extrapolations, judgment was

aided by the gradual change in the slopes of the lines from one temperature to the next (Figures 9.4 and 9.5). Errors in the values of $K_4(0)$, (the values of K_4 at OK) are likely to be larger since they depend on the correct choice of function for renormalisation (Sections 9.2.7; 9.3.2). The choice was however always clear and in the case of Terbium (section 9.4) gave a value of $K_4(0)$ in good agreement with the results of Rhyne and Clark which were obtained much nearer to absolute zero. It is felt that $K_4(0)$ values obtained for the alloys (sections 9.2.7; 9.3.2) are reliable within 20%.

Table 9.1

K_4' values for $Tb_{0.695}Sc_{0.305}$

	$\mu_o H$ (T)	K_4' (Jkg^{-1})	Phase (^{o}) CW ACW	Hysteresis Arbitrary Units
77K	0.99	0.0004113	7,9	1000
	1.14	0.000996	26,29	1976
	1.173	0.005871	15,15	2617
	1.205	0.0143	15,15	2953
	1.238	0.02387	15,15	3513
	1.27	0.0368	13,13	4165
	1.28	0.03	13,14	6281
	1.29	0.036	13,13	4877
83.6K	1.173	0.0021	17,16	1927
	1.173	0.0032	17,17	2240
	1.205	0.01196	40,40	2725
	1.238	0.01663	16,16	3177
	1.27	0.0235	15,16	3857
	1.285	0.0277	13,14	5177
91K	1.14	0.00086	35,38	1471
	1.173	0.00085	35,39	1533
	1.205	0.004878	14,13	2207
	1.238	0.01175	14,14	2877
	1.275	0.01947	14,14	3364
	1.28	0.02948	12,15	4697
102K	1.173	0.000711	6,7	1107
	1.205	0.00395	12,14	1828
	1.238	0.007619	12,12	2255
	1.27	0.0204	12,13	3377
113K	1.173	0.00111	9,12	1768
	1.205	0.004157	11,13	2873
	1.23	0.00694	14,15	2869
	1.27	0.01137	11,13	3477
117K	1.173	0.0028	0,3	5073
	1.205	0.0042	23,24	6433
	1.238	0.0054	13,13	4813
	1.27	0.0056	16,16	2669
126K	1.045	0.00138	43,11	568
	1.205	0.00107	43,14	544
	1.275	0.001449	11,12	524

Fig.9.1 Measured K_4' Values for $Tb_{0.695}Sc_{0.305}$

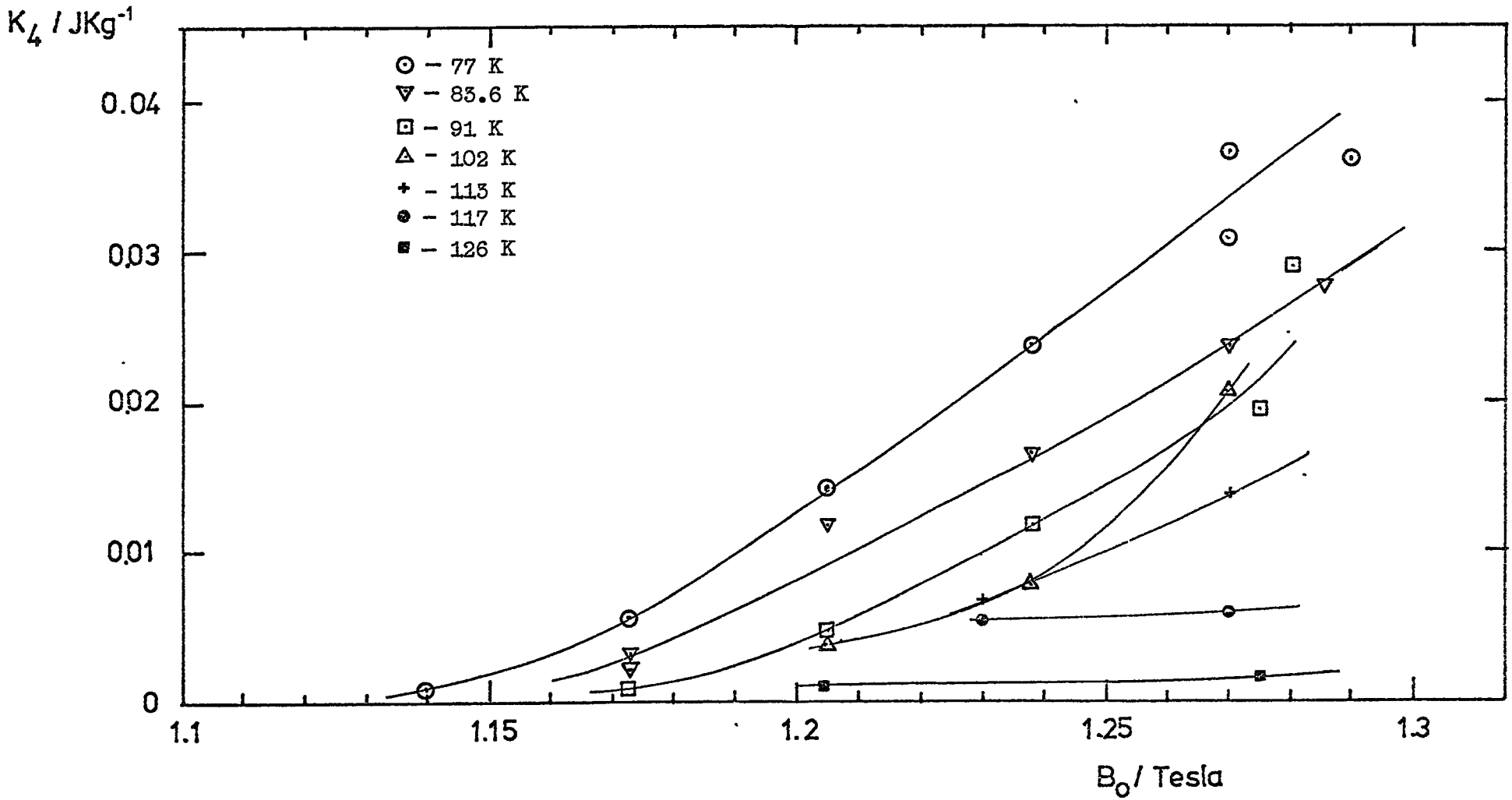

CHAPTER 9

RESULTS AND DISCUSSION

9.1 The $Tb_{0.695}Sc_{0.305}$ Basal Plane Disc

9.1.1. Orientation of the Specimen

The angular relationships between the axes of the crystal and magnet scale were determined as described in Section 6.2.3. From the X-ray photograph the angle between one of the "b" axes of the crystal and the normal to the mirror on the specimen holder was 30.75^{o} and the normal to the mirror was found to be normal to the magnetic field when the magnet scale read 79^{o}. Rotating the magnet anticlockwise about the specimen by 30.75^{o} brought the field lines perpendicular to a "b" axis of the crystal and parallel to an "a" axis. The "a" axes were therefore parallel to the field when the scale read $48.25 \pm n\ 60^{o}$, where n is an integer.

9.1.2. The torque measurements

With the maximum field strength available (1.29T) torque curves were obtained between 77K and 126K, while at 77K the lowest applied field which could be used to obtain a curve was 1.173T. Results are given in Table 9.1 and values of K_4' (the effective value of K_4) are plotted against $\mu_o H$ (the applied field strength) in Figure 9.1. It is clear that the values of K_4' show no tendency to saturate and that any extrapolation to infinite field would be invalid. Tests for agreement with theory are therefore impossible.

The results do however serve to show that the "b" axis is the easy axis of magnetisation as in pure Terbium. Phase angles of 12 to 15

Fig.9.2 Critical Field Versus Temperature for Three Tb/Sc Alloys

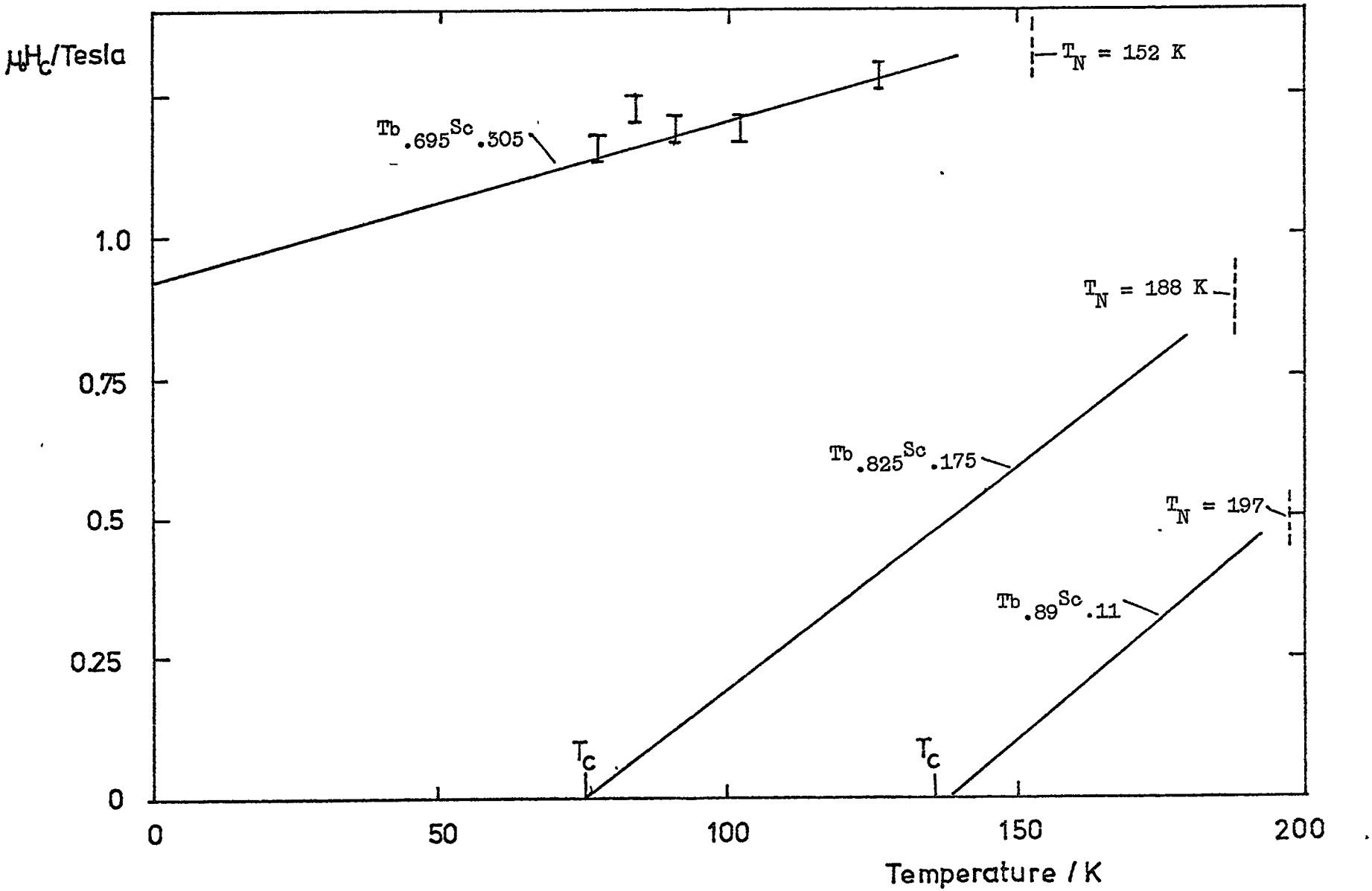

degrees were obtained for the sin6ϕ component of the torque, indicating that the torque on the specimen is changing from negative (clockwise) to positive (anti-clockwise) as the magnet turns clockwise past scale readings of -12, +48, +108°, etc. At these settings the "a" axis is parallel to the field and the torque on the crystal is such as to increase the angle between the "a" axis and the field lines. The "a" axis is therefore the hard direction of magnetisation and the "b" axis is easy. The above phase angle was roughly the same for all torque curves obtained with this specimen except for those measured at field strengths near the critical field. In those cases the phase angles varied in an unsystematic manner and could show differences of up to 30° between values obtained with the magnet turning clockwise and turning anticlockwise.

The results also indicate the approximate value of the critical field through the temperature range used. The values are plotted in Figure 9.2 which also shows the values for crystals of greater Terbium content from Chatterjee (1972). The line for the $Tb_{0.695}Sc_{0.305}$ would not intersect the temperature axis if extended, in agreement with the observation that there is no ferromagnetic phase for alloys of Terbium and Scandium with less than 70-80 at % of Terbium, (Child and Koehler, 1968).

9.2 The $Tb_{0.825}Sc_{0.175}$ Basal Plane Disc

9.2.1 Orientation and determination of the easy axis of magnetisation

The angle between the "b" axis and the normal to the mirror on the specimen holder was 53.2° and the mirror normal was perpendicular to the magnetic field when the scale on the magnet read 74.5°. The field

Table 9.2

K_4' values for $Tb_{0.825}Sc_{0.175}$

	$\mu_o H$ (T)	K_4' Jkg^{-1}	Phase (°)	Hysteresis Arbitrary Units
77K	0.09	0.01428	39	2859
	0.115	0.01793	39	2914
	0.3	0.04189	39.5	4957
	0 3	0.06267	39	5723
	0.525	1 426	39	31520
	0.525	1.473	39	29710
	0.525	1.46	39	32090
	0.645	2.189	39	26000
	0.645	2.192	39.5	23090
	0.765	2 488	39	25480
	0.91	2.616	39	23800
	1 045	2.68	39	25410
	1.14	2.717	38 5	21630
	1.255	2.756	39	23100
85K	0.35	0.4191	39	60580
	0.425	0.8973	39	43220
	0 525	1.35	39.5	35550
	0 645	1 836	39 5	29050
	0 712	1.922	39.5	26420
	0.815	2.01	39	25730
	0.91	2 045	39	26240
	1 045	2.076	39	26590
	.205	2.058	39.5	31290
92K	0.13	0 00537	39.5	1486
	0.22	0.01271	39.5	1610
	0.3	0.01819	38	1890
	0 425	0.5698	39	77760
	0.525	1.15	39	41180
	0 525	1 097	39	42660
	0.645	1.46	39	26130
	0.815	1.596	38.5	22680
	0.95	1 627	38.5	22950
	1.045	1.643	39	21380
	1.14	1.668	38	18820
96.5K	0.36	0.02393	39	3980
	0.41	0.04814	39 2	8225
	0.43	0.2999	39	92/00

	$\mu_o H$ (T)	K_4' Jkg^{-1}	Phase (°)	Hysteresis Arbitrary Units
96.5K	0.44	0 5166	38 5	69270
	0 51	0.7328	39	56580
	0 545	0 9736	39	41590
	0 596	1.105	39	31580
	0 645	1 19	39.5	25910
	0 815	1 297	38	22260
	0.99	1 325	38 5	17430
	1 08	1 362	38 8	17990
	1.173	1 348	37.8	15540
	1 25	1 407	38.5	18230
104.3K	0 47	0 3855	38	79030
	0 48	0 2736	38	90960
	0.515	0 5228	39.5	65980
	0.6	0 7847	39	38000
	0 648	0.8492	39.5	28600
	0 815	0.9087	39	18530
	0.95	0 9632	39	16030
	1.045	0 979	39	15850
	1.14	0 9834	38.5	13770
117K	0.525	0 04278	39,40	10870
	0.585	0.3613	38,39	43690
	0 645	0 4952	38,39	28710
	0 712	0.5361	39,40	21200
	0.765	0 5507	39	17970
	0.91	0.5771	39	13520
	1.02	0 5956	39	12580
	1 11	0.6077	38,39	11500
	1.205	0.6131	38,39	12540
	1.285	0.6174	38,39	12480
128K	0.59	0 0423	38,39	7453
	0.645	0.1723	39,40	19330
	0.712	0 254	39	13220
	0.86	0.3173	39,40	9841
	0.99	0.3355	39,40	8936
	1.08	0.3482	39	8790

	$\mu_o H$ (T)	K_4' (Jkg^{-1})	Phase (°)	Hysteresis Arbitrary Units
128K	1 173	0 3564	38,39	9255
	1 173	0 3502	38,40	8384
	1.285	0 3663	38,40	9180
134.3K	0 61	0 01702	38,39	5353
	0 645	0.07019	38,39	9760
	0 712	0 1259	39	9969
	0 765	0 1583	39	8532
	0 815	0 1818	39	7614
	0.9	0 2097	39	6894
	1.045	0.2374	38,39	7369
	1.173	0.246	39	7247
	1 285	0 2572	38,39	7277
145.5K	0.6	0.005318	37,39	2722
	0.645	0.01678	39,40	4529
	0 712	0 03573	39	5999
	0.815	0.05643	39	3991
	0.91	0 07423	39	3434
	1 045	0 1003	38,39	3881
	1.173	0 1143	38,39	4258
	1 28	0 1213	37,39	4897
151K	0 645	0 01113	39	3954
	0.675	0 01627	39	4927
	0 712	0 01726	39	4223
	0.815	0 02526	39	2253
	0.91	0.03448	39	1922
	1 045	0 05351	38	2436
	1.14	0 05952	39	2449
	1.28	0 06491	39	2926
159.5K	0.712	0 001857	39	1215
	0.815	0.00672	38,39	929
	0 91	0.01192	39	1096
	1 045	0.01983	38,39	1320
	1.173	0.02478	38,39	1665
	1.275	0.02686	38	2059

Fig.9.3 Measured K_4' Values for $Tb_{0.825}Sc_{0.175}$ Versus Applied Field

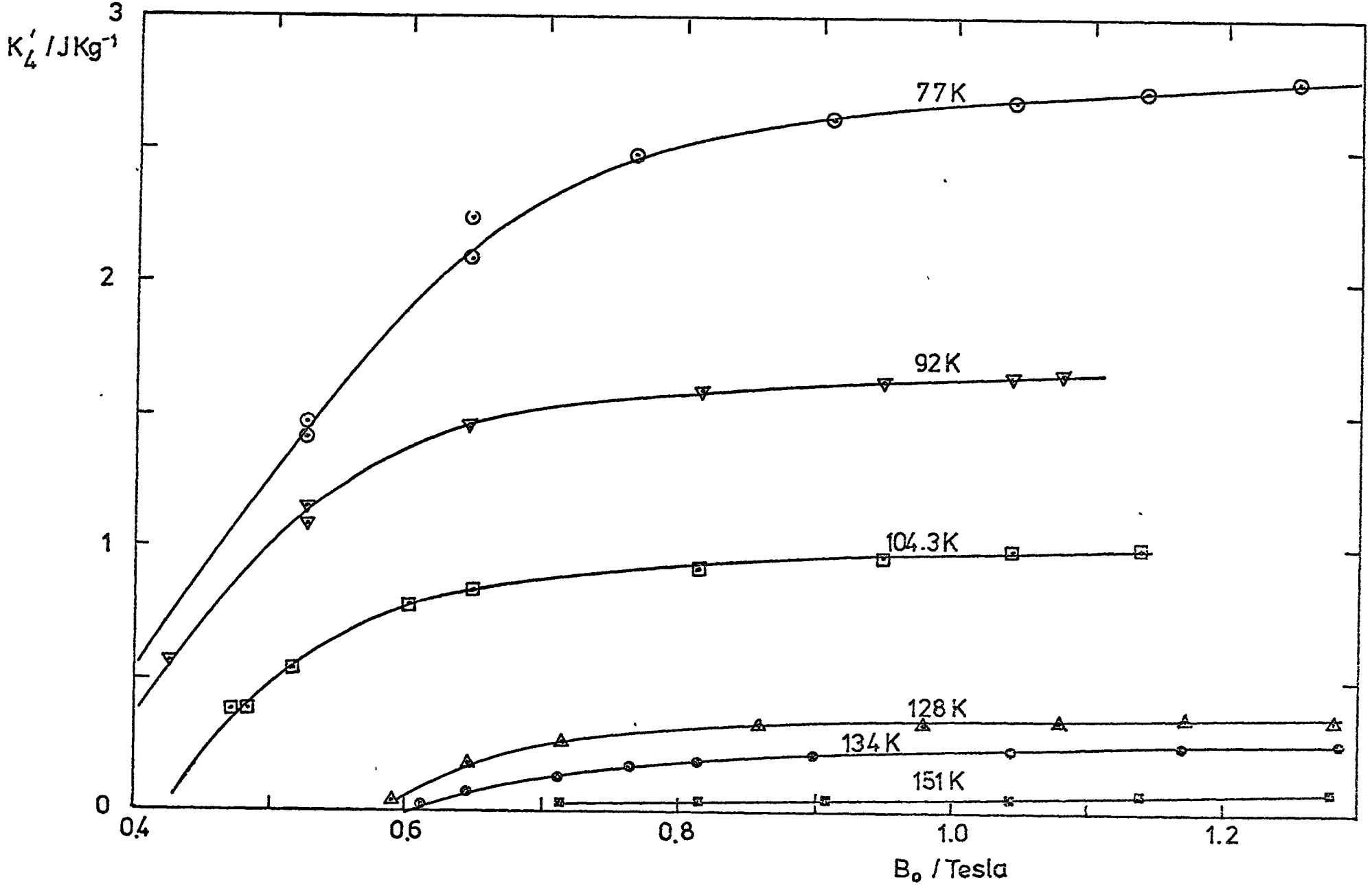

was therefore perpendicular to the "b" axis and parallel to an "a" axis at scale readings of $21.3 \pm n\ 60^{o}$.

Table 9.2 summarises the results for this specimen and it can be seen that the phase angles for the $\sin 6\phi$ components of the torque lie very close to 39^{o} for all the curves. There is thus a hard axis at -39^{o}, $+21^{o}$ etc. The "a" axis is therefore hard and the "b" axis easy.

9.2.2 Obtaining the curves

It was verified that the form and amplitude of the curves did not depend on the previous magnetic history of the specimen by obtaining curves with ascending and descending values of applied field strength. At any particular field strength, the curves obtained by both methods were very closely similar.

9.2.3 The results

Values of K_4' for six temperatures are shown plotted against applied field strength in Figure 9.3. There it can be seen that the graphs flatten off at higher values of applied field strength. It was therefore felt to be legitimate to extrapolate the values to find the value of K_4 at infinite field for each temperature.

9.2.4 Extrapolation to infinite field

The procedure usually adopted has been to plot values for anisotropy constants against 1/H. (For example: Bozorth (1951) page 566; Tarasov (1939)). A straight line graph is usually obtained and the intercept at $1/H = 0$ is read off.

Symbolising by Δ the difference between the extrapolated value of an anisotropy constant and its value at 1.25T, Corner et al (1962) found

that graphs of Δ against temperature for Gadolinium were smooth curves and could be used to correct values of the constants obtained at other temperatures.

Kouvel and Graham (1957) however found for discs of 3¼% Silicon-iron that K_1 plotted against $\sqrt{H}$ from 0.1 to 2T gave straight lines while K_2 appeared to have no simple relationship with 1/H at all. They attributed the field dependance of the anisotropy constants to the lack of saturation at the edges of the discs that they used, even in high fields.

Birss and Wallis (1964), measuring the torques on a (111) Nickel crystal disc found that the amplitude of the sine6ϕ term did not have a simple relationship with 1/H but could be represented over part of the range of values by

$$A_6 = \frac{K_2}{18} - \frac{[K_1 + 1/6K_2]^2}{3(HM_s + k)} \qquad (9.1)$$

They proposed the use of terms in higher powers of 1/H as a means of getting a fit over a wider range of values.

Phillips and Shephard (1970) found for materials of low magneto-crystalline anisotropy that graphs of the anisotropy constants against 1/H were fitted very well by expressions including terms in $1/H^2$. Terms in $1/H^3$ were not needed. They attributed the field dependance of the apparent values of the anisotropy constants to elevation of the magnetisation vector out of the plane of the disc and also to the fact that the applied field and the magnetisation are not parallel. They gave an expression for the torque L,

Fig.9.4 Extrapolation of K_4' to Infinite Field for $Tb_{0.825}Sc_{0.175}$

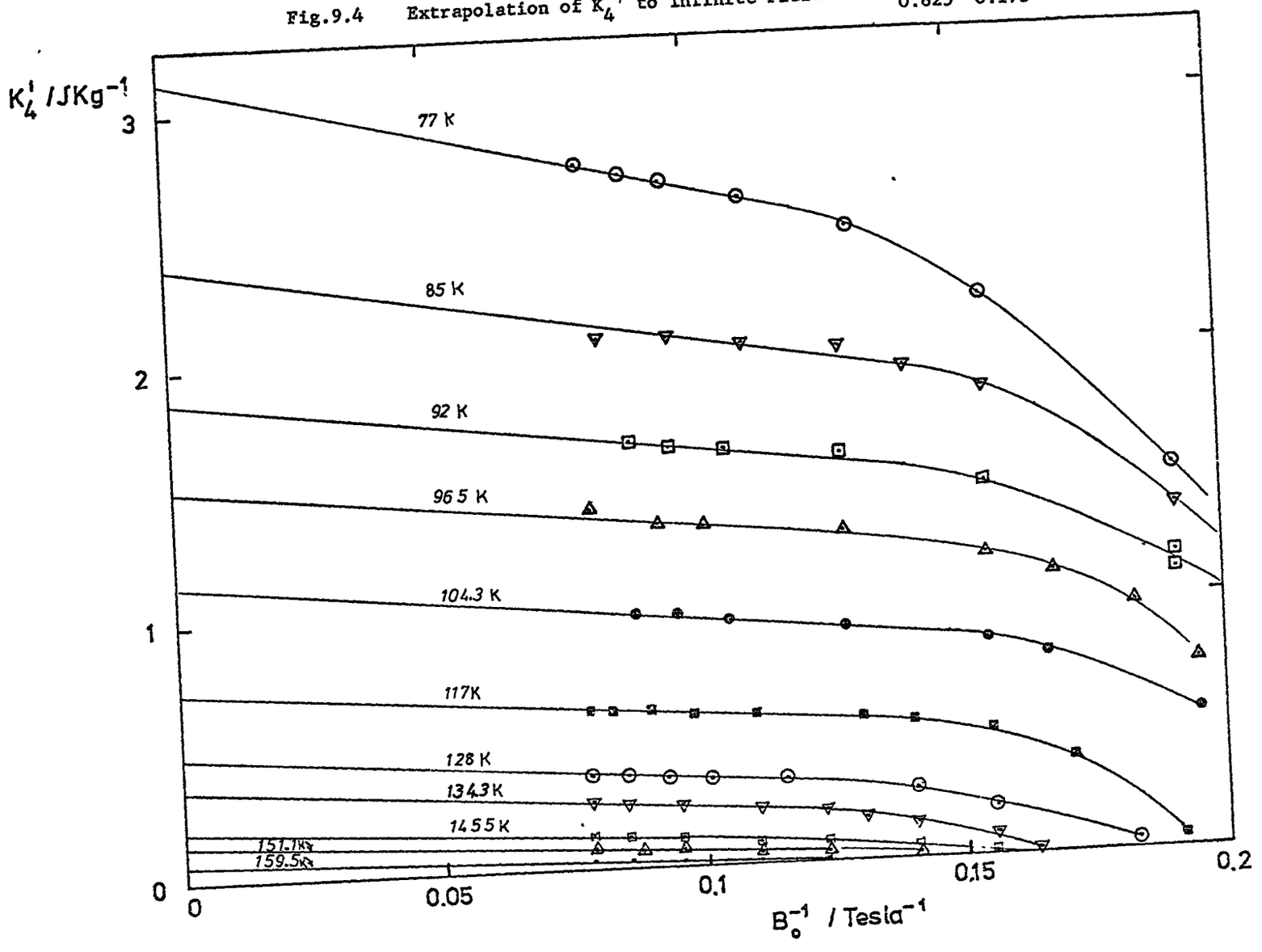

Fig.9.5 ΔK_4 as a Function of Temperature

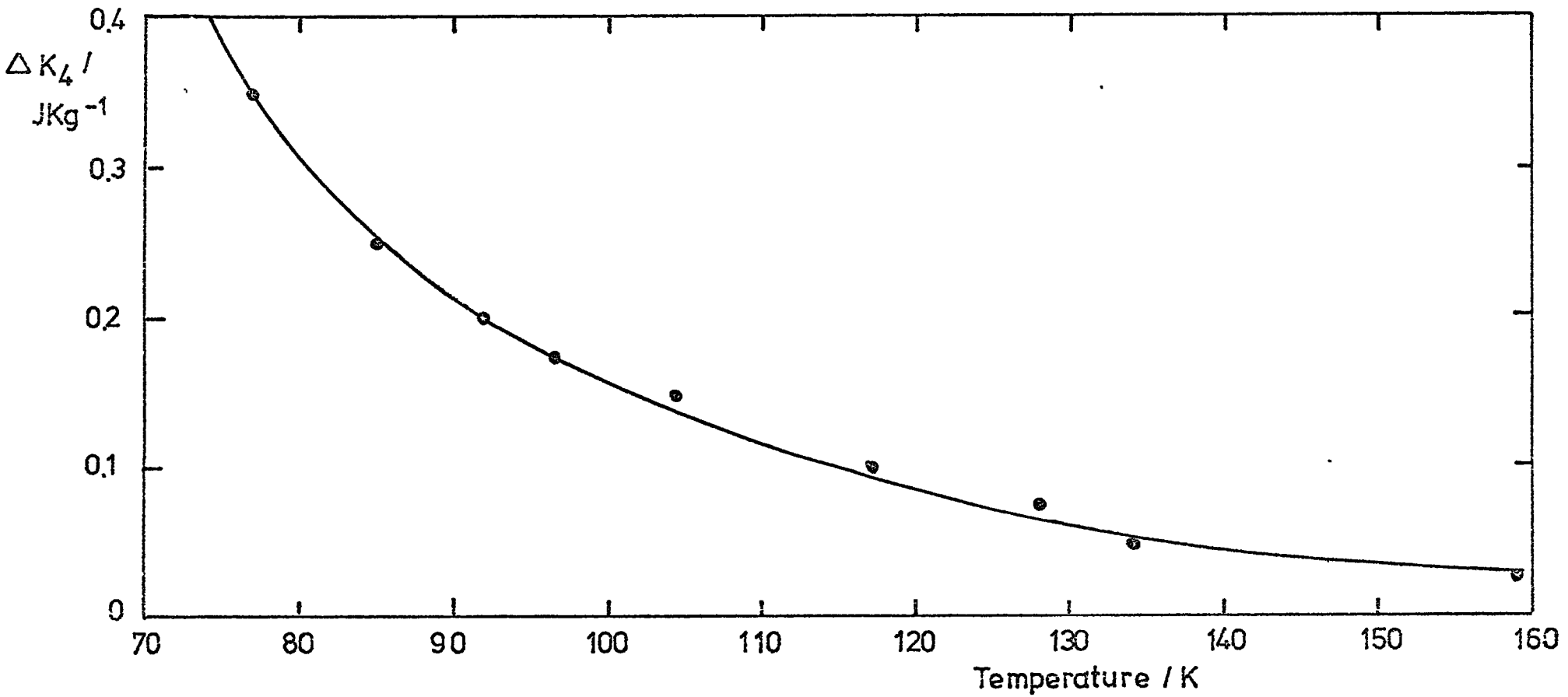

$$L = R - \frac{SP}{Q + HM_s + \frac{M_s^2(1-3N_D)}{\mu_o}} \qquad (9.2)$$

P,Q,R,S are quantities which depend only on the direction of the magnetisation vector relative to a set of axes fixed to the disc and the remaining symbols have their usual meaning. Clearly as H increases, the expression for the torque becomes more nearly linear in 1/H.

Figure 9.4 shows the values of K_4' plotted against $\frac{1}{\mu_o H}$. (or $\frac{1}{B_o}$) Graphs for the lower temperatures become straight at higher values of $\mu_o H$ and on the basis of the experience described it was assumed that they would continue so to $H = \infty$ and they were accordingly extrapolated as straight lines. The curves for the three highest temperatures when plotted on a large scale show a slight change in curvature from concave upwards to a concave downwards as H increases and 1/H decreases. This may indicate that the graphs are just beginning to flatten out as those above them and in this case the linear extrapolations give an upper limit to K_4; the lower limit being the value of K_4' at 1.28T.

Attempts were made to fit quadratic expressions in 1/H to these curves but this was not satisfactory. Because of the small numbers of points used, expressions fitted by the least squares method tended to project the upward curvature of the graphs and give very high values. But some extrapolation gave infinite field values equal to or even less than the values of K_4' at 1.28T. For temperatures above 145K therefore the limits of the uncertainty in the infinite field value are wide.

The difference Δ between the infinite field value and the value of K_4' at 1.28T gives a smooth curve (Figure 9.5) when plotted against temperature. The value of Δ falls off almost exponentially with rising temperature.

Fig.9.6 Amplitude of sin2ϕ Components at Various Applied Fields

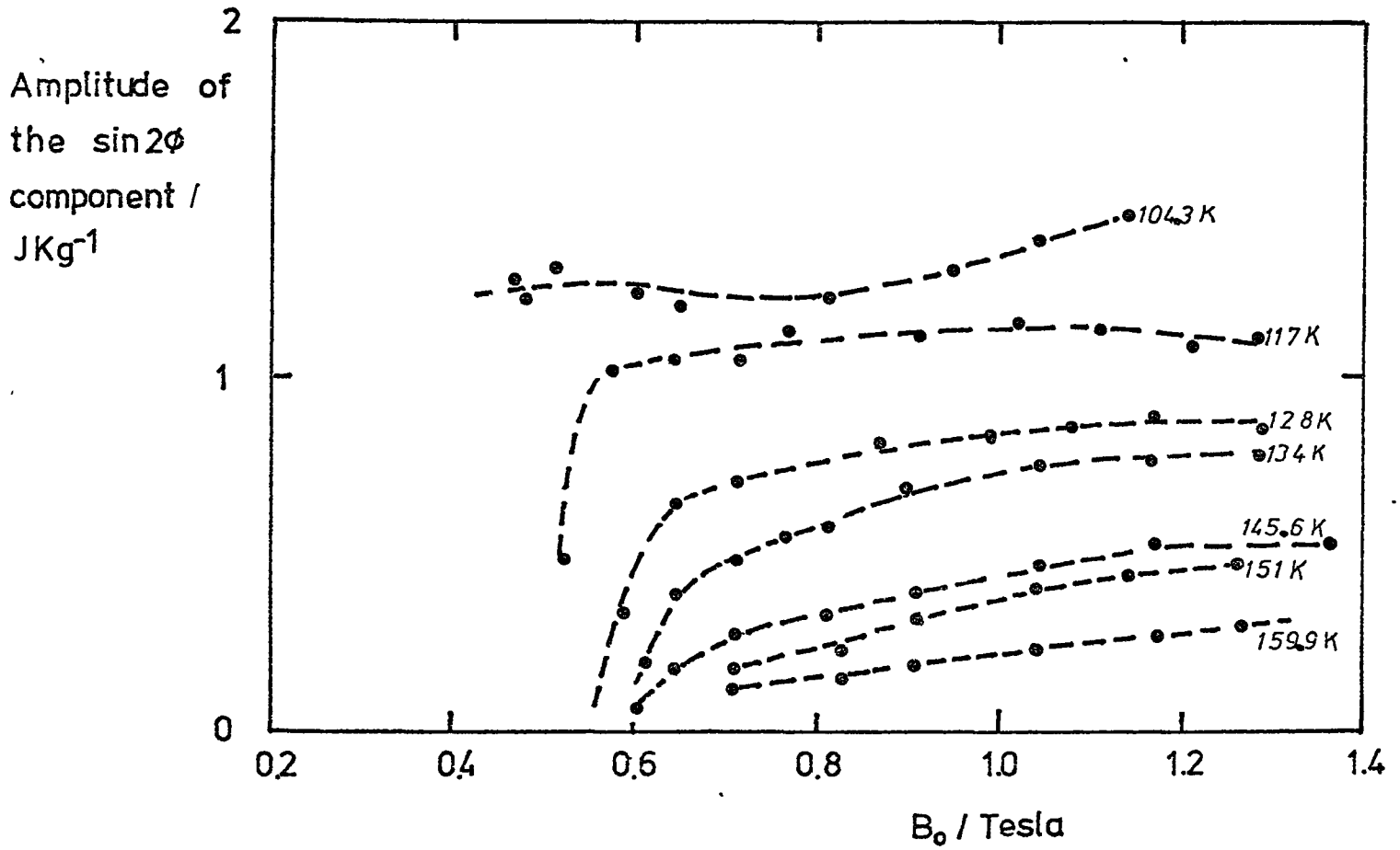

Fig.9.7 Variation of Rotational Hysteresis with Applied Field

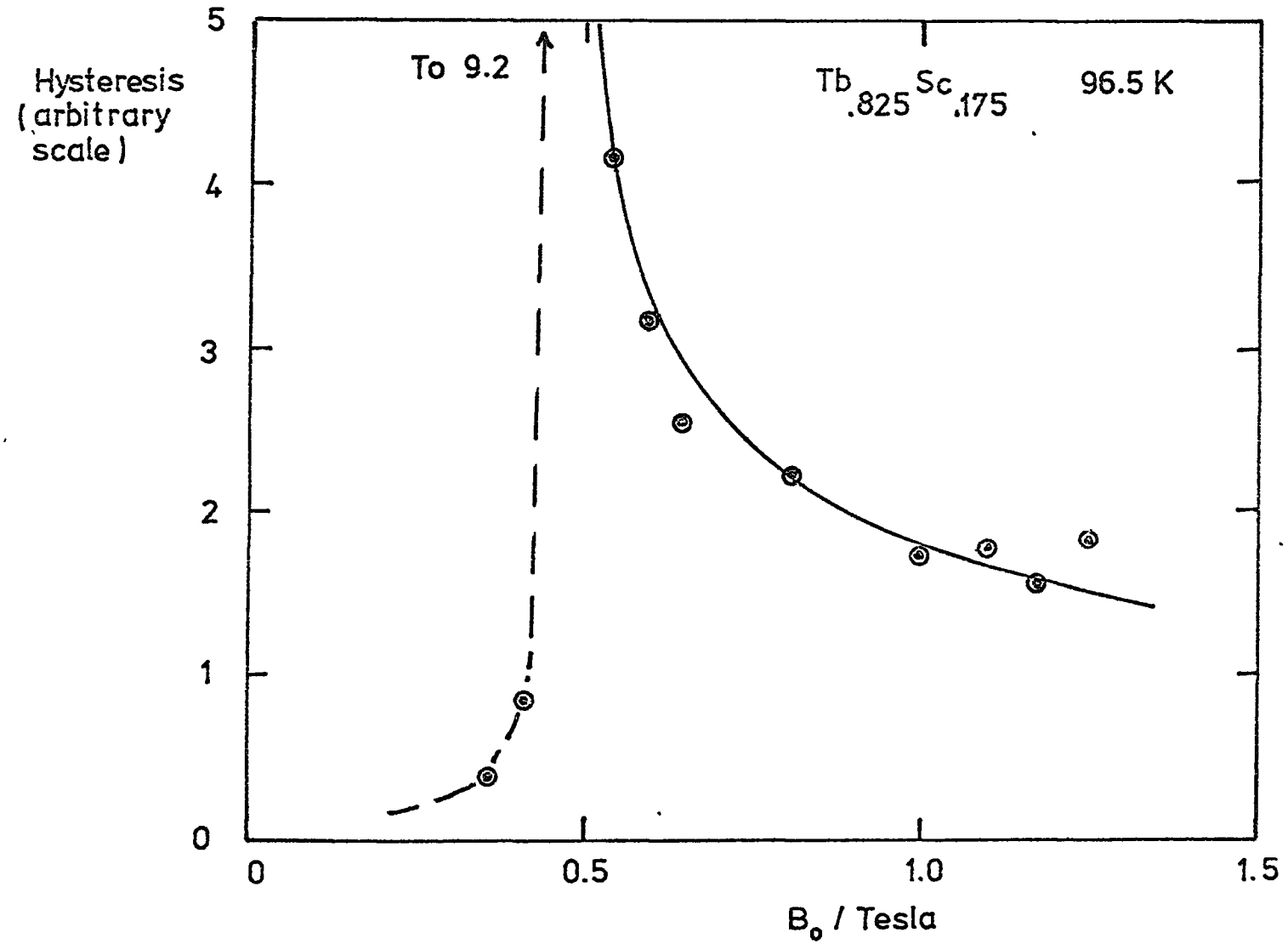

9.2.5 Variation in the amplitude of the sine2ϕ component

The amplitudes of the sine2ϕ components of the torque curve at each temperature were plotted against applied field strength. Values rise to a broad plateau except in the case of results obtained at 151K and 159.5K where it seemed that the applied field strength was too low to produce the plateau. (Figure 9.6).

9.2.6. Variation in rotational hysteresis

The area enclosed between the clockwise and anticlockwise torque curves was recorded for each temperature and field value and multiplied by the scale factor of the XY recorder. This gave a measure of the rotational hysteresis in arbitrary units. Figure 9.7. shows this quantity plotted against applied field strength for a temperature of 96.5K. As the field strength increases there is first of all a gentle rise in the hysteresis and then a very sharp peak. After this the hysteresis falls rapidly and becomes more or less constant. Bozorth (1951, page 516) describes similar effects in nickel and other materials, the gentler shape of his curves being accounted for by the fact that he shows rotational hysteresis plotted against magnetic induction rather than applied field strength.

The state of magnetisation of the specimen may be judged from the behaviour of the rotational hysteresis. On the initial gentle rise the magnetisation is very low and the specimen may not even have been driven past the metamagnetic transition. The peak occurs when the specimen is on the "knee" of the magnetisation curve. Readings are only suitable for extrapolation if the hysteresis is clearly falling with increase of applied field strength.

Table 9.3

K_4 and single-ion functions for $Tb_{0.825}Sc_{0.175}$

T (K)	(a) K_4 Jkg^{-1}	$\hat{I}_{5/2}(L^-(m_T))$	(b) $\hat{I}_{13/2}(L^-(m_T))$	$\hat{I}_{5/2}(Z).I_{9/2}(z)$	log (a)	log (b)	log (c)
77	3.12	0.9007	0.4824	0.63604	0.4942	-0.31661	-0.19652
85	2.4	0.8756	0.3970	0.56308	0.3802	-0.4012	-0.24943
92	1.88	0.8513	0.3272	0.4986	0.2742	-0.48517	-0.30225
96.5	1.55	0.8322	0.2807	0.45252	0.1903	-0.55174	-0.34437
104.3	1.16	0.7865	0.1925	0.3555	0.0645	-0.71546	-0.44911
117	0.75	0.6945	0.08725	0.21093	-0.1249	-1.0592	-0.67586
128	0.475	0.6868	0.0814	0.20125	-0.3233	-1.0894	-0.69626
134.3	0.36	0.5732	0.02881	0.09698	-0.4437	-1.5405	-1.0133
145.5	0.2	0.5000	0.01426	0.05742	-0.6990	-1.8457	-1.2409
151.5	0.125	0.3720	0.00365	0.019396	-0.9031	-2.4377	-1.7123
159.5	0.05	0.2085	0.000385	0.002737	-1.3	-3.4144	-2.5627

Fig.9.8 $Tb_{0.825}Sc_{0.175}$ K_4 Versus Single-Ion Functions, logarithmic plot

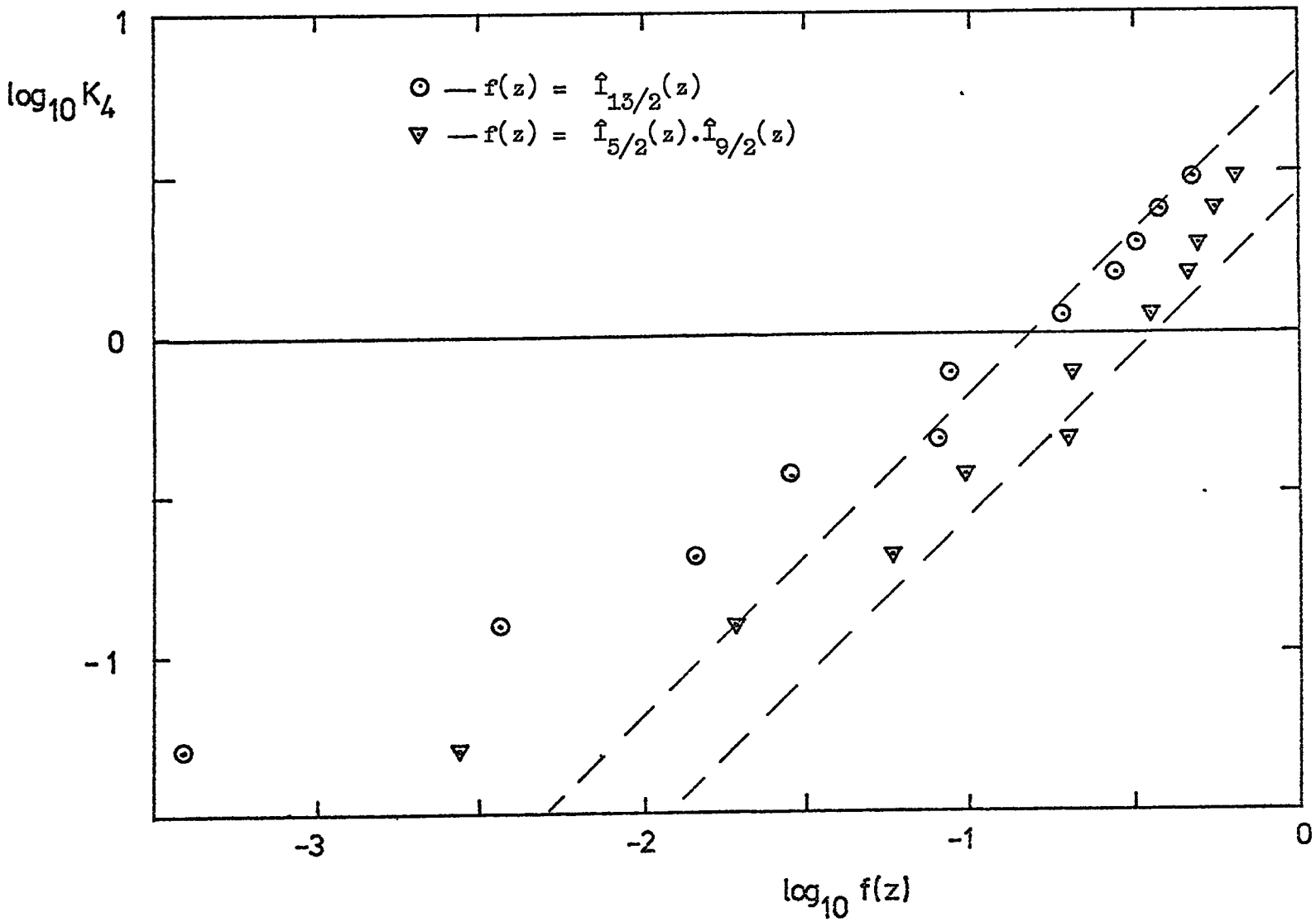

On this criterion the readings at 159.5K for this specimen and all the readings for the $Tb_{0.695}Sc_{0.305}$ specimen are shown to be taken at too low an applied magnetic field.

9.2.7 Comparison of results with theory

The predictions of the single-ion theory (section 3.52) concerning the variation of K_4 with temperature were compared with the values of K_4 obtained by extrapolation to infinite field.

For anisotropy of sixfold symmetry orginating in the crystal field, theoretically the value of K_4 should vary as

$$\hat{I}_{13/2}(z) \quad \text{where } m_T = I_{3/2}(z)$$

Anisotropy of sixfold symmetry can also arise in the basal plane from purely magnetoelastic effects in which case the constant K_4 has a component varying as $\hat{I}_{9/2}(z).\hat{I}_{5/2}(z)$ where the symbols have the meaning assigned to them in section 3.52. Values of $\hat{I}_{5/2}(z)$ were obtained from the thesis of D. Chatterjee and from them were calculated values of z and of the two functions given above, (Table 9.3), using the recurrence relation given in Abramovitz and Stegun (1965)

Log K_4 was then plotted in turn against the logs of the values of the two functions. This is shown in Figure 9.8.

For proportionality the slopes of these graphs should equal 1. Neither function satisfies this criterion very well or even gives a straight line. The best fit is obtained graphically with $\hat{I}_{9/2}(z).\hat{I}_{5/2}(z)$, but taking even the extreme lower limits of the uncertainty in the K_4' values it is not possible to make points corresponding to the higher temperatures fit a straight line. A similar conclusion was reached by numerical tests using the method of least squares.

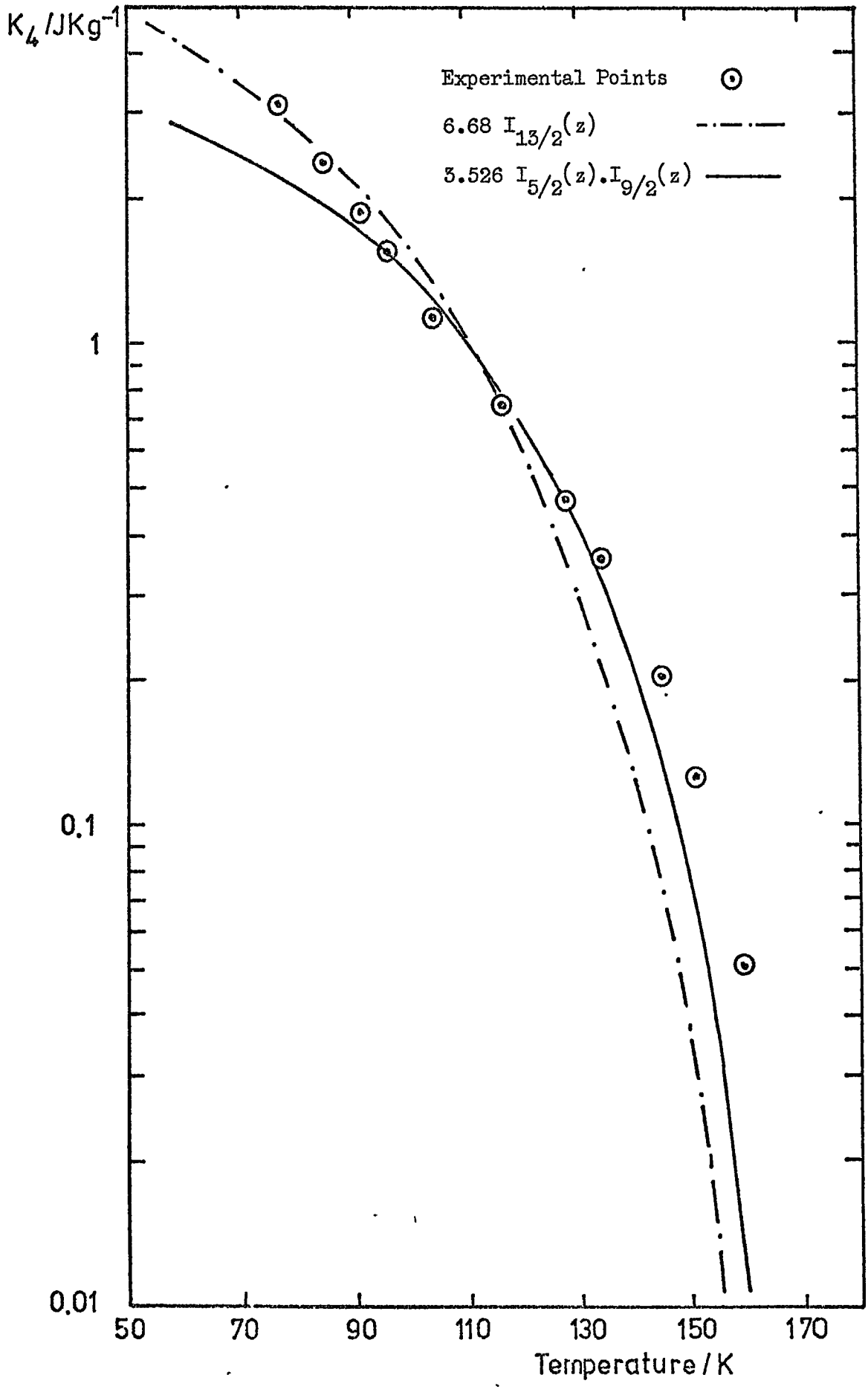

Fig.9.9 $Tb_{0.825}Sc_{0.175}$ Temperature Variation of K_4

Fig.9.10 $Tb_{0.825}Sc_{0.175}$ Log K_4 Versus log m_T

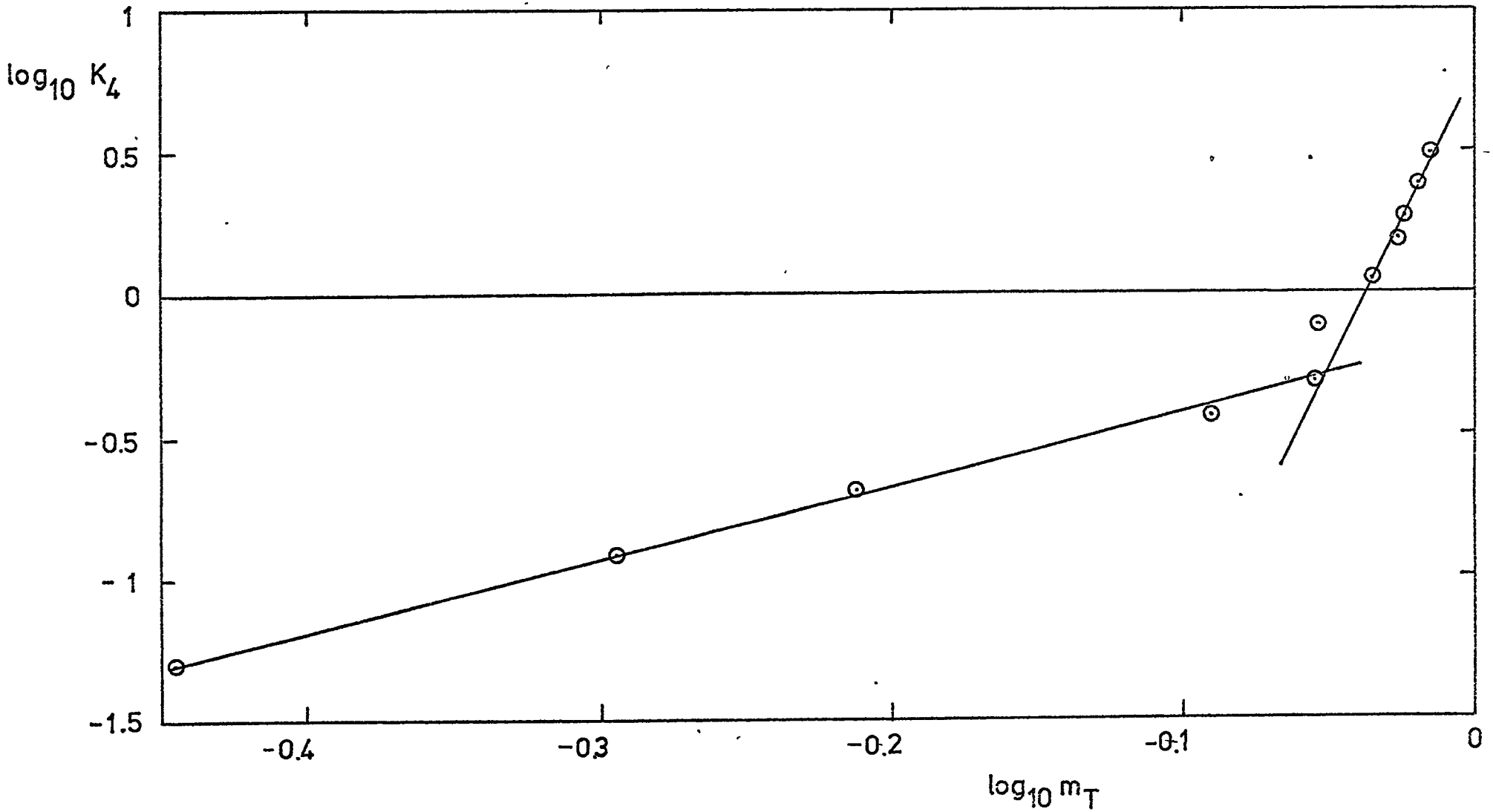

Combinations of the two functions were tried and it was found that the error of the fit decreased steadily as the combination changed from 100% of $\hat{I}_{13/2}(z)$ to 100% of $\hat{I}_{9/2}(z).\hat{I}_{5/2}(z)$. $(m_T = \mathcal{L}(z))$.

Figure 9.9 shows the experimental K_4' values plotted on a logarithmic scale against temperature together with the two theoretical curves.

$$6.68\ \hat{I}_{13/2}(\mathcal{L}^{-1}(m_T)) \tag{9.3}$$

$$3.526\ (I_{5/2}(\mathcal{L}^{-1}(m_T)).(I_{9/2}(\mathcal{L}^{-1}(m_T)) \tag{9.4}$$

In Figure 9.10 the logarithm of K_4 is plotted against the logarithm of the reduced magnetisation. The slope changes from approximately 21 at low temperatures to approximately 2.6 at the higher temperatures. According to Callen and Callen (section 3.53), two-ion terms in the basal plane anisotropy vary according to the $l(l+1)/2$ power of the reduced magnetisation at the low temperature limit and soon go over to an lth power law. For anisotropy of magnetostrictive origin the low and high temperature limits would be 13th and 6th power laws, while for the crystal field effects they would be 21st and 6th power laws respectively.

Examining further the possibility that the variation of K_4 for this specimen might indicate the appearance of two-ion interactions, a function of the following form was fitted to the results.

$$(A\hat{I}_{9/2}(z) + (1-A)(\hat{I}_{5/2}(z))^2).(B\hat{I}_{5/2}(z) + (1-B)(\hat{I}_{3/2}(z))^2)$$

where $\hat{I}_{3/2}(z) = m_T$ and A and B are adjustable constants. The form of this function was suggested by the work of Yang (section 3.53). The best fit was obtained when A and B were both unity. The function in equation 9.4 therefore represents the best fitting single ion function.

Table 9.4

$Tb_{0.89}Sc_{0.11}$:K_4' values

	$\mu_0 H$ (T)	K_4' Jkg^{-1}	Phases(°)
77K	0.35	0.0368	31,37
	0.385	0.0706	28,40
	0.42	0.1094	25,44
	0.47	0.1697	9,6,0
	0.525	0.9504	4.8
	0.56	1.658	3.9
	0.62	2.855	-2
	0.645	3.57	5,6
	0.712	4.987	4,5
85.5K	0.35	0.044	14,22
	0.42	0.1047	-1,20
	0.495	0.459	5,4
	0.54	1.4417	4
	0.585	2.18	4
	0.645	3.489	4
	0.712	4 685	4
93K	0.275	0.0207	6,-8
	0.385	0.0781	24,-12
	0.495	0.635	5.5
	0.56	1.90	3.7
	0.625	3.048	4.86
	0.712	4.258	4.36
	0.74	4.585	4.54
	0.815	5.267	4.78
109K	0.275	0.03126	9,-14
	0.385	0.07289	17,-10
	0.42	0.1108	10,-4
	0.495	0.7672	5
	0.56	0.8926	4.5
	0.645	2.566	4.5
	0.765	3.084	4.7
	0.86	3.227	4.8
	0.95	3.394	4.5
	1.045	3.541	4.4
	1.14	3.625	4.5
	1.238	3.743	3.5
122.5K	0.275	0.07539	34
	0.495	0.8898	5
	0.56	1.403	4,5
	0.645	1.67	4
	0.712	1.787	5
	0.815	1.906	4,5
	0.95	2.022	4,5
	0.99	2.033	4.5
	1.045	2.076	2,6
	1.14	2.138	2,8
	1.238	2.173	3,7
129.5K	0.3	0.03515	32,36
	0.425	0.2418	6,3
	0.525	0.9517	5
	0.645	1.232	5
	0.765	1.366	5
	0.86	1.44	5
	0.95	1.487	5
	1.064	1.562	4,5
	1.14	1.607	4,5
	1.205	1.625	3,5
	1.27	1.645	3,5

	$\mu_0 H$ (T)	K_4' Jkg^{-1}	Phases(°)
138.5K	0.3	0.0145	15,-8
	0.425	0.2617	5,3
	0.525	0.6415	5
	0.645	0.7957	5
	0.765	0.8741	5
	0.873	0.9437	5
	0.95	0.9840	5
	1.045	1.020	5,6
	1.14	1.074	5
	1.205	1.096	4,5
	1.28	1.1245	3,5
149K	0.425	0.1797	4
	0.525	0.3234	5
	0.645	0.4279	5,4
	0.765	0.5044	5,4
	0.86	0.54	4
	0.95	0.5587	4
	0.995	0.5674	4,5
	1.08	0.5954	4
	1.173	0.6029	4,5
	1.275	0.6139	-5,-3
	1.29	0.5987	2,5
155.5K	0.525	0.1727	5
	0.712	0.2984	4,5
	0.86	0.3448	4,5
	0.99	0.3751	4,5
	1.08	0.4	4,5
	1.173	0.4167	4,5
	1.27	0.4152	3,7
165K	0.525	0.05433	
	0.712	0.1317	4
	0.815	0.1603	5
	0.92	0.1793	4,5
	0.99	0.1901	5
	1.02	0.1976	4,6
	1.11	0.2019	4,5
	1.173	0.211	4,5
	1.27	0.2174	3,4
174.5	0.525	0.002046	7,6
	0.645	0.02909	4
	0.815	0.05839	4,5
	0.99	0.07364	4,5
	1.08	0.0801	4,5
	1.173	0.08594	4,5
	1.27	0.09059	3,4
181K	0.525	0.006132	33,34
	0.815	0.02582	4,4
	0.86	0.0285	4,5
	0.99	0.03241	2,3
	1.08	0.0378	4,4
	1.173	0.03621	3,4
	1.27	0.041	3,4
	1.29	0.041	3,7

Fig.9.11 $Tb_{0.89}Sc_{0.11}$ Measured K_4' Values Versus Applied Field

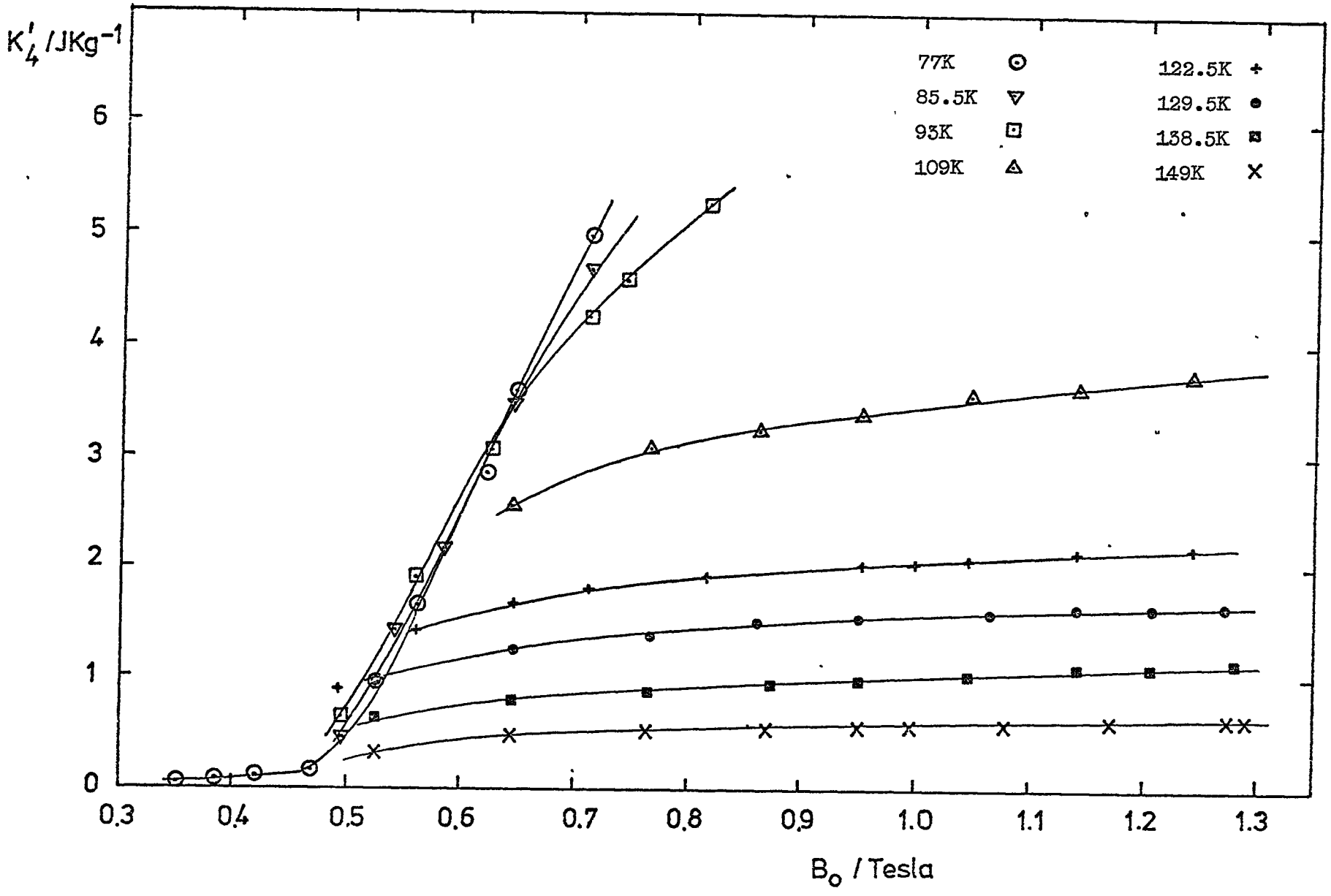

Fig 9.12 $Tb_{0.89}Sc_{0.11}$ Measured K_4' Values Versus Applied Field

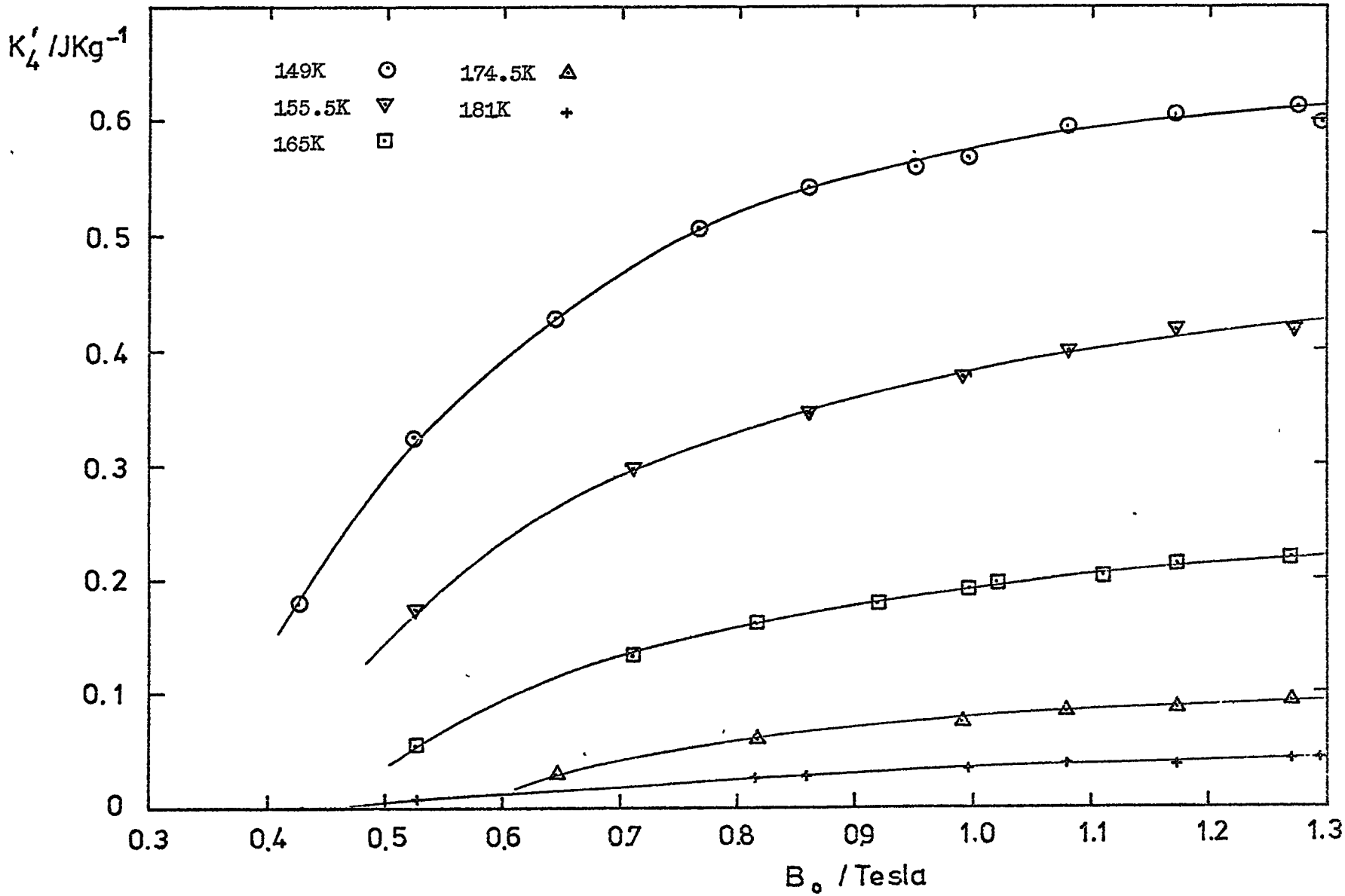

The dependence of K_4 on m_T is nearly as m_T^3 at high temperatures. This suggests that the origin of these small K_4' values is in fact the twofold component in the curves, (Figure 9.6). Distortion in this component will produce a spurious sixfold amplitude in the analysis.

At applied fields just above the critical field a 'creeping' of the pen on the X-Y recorder was observed; i.e. if the magnet was stopped the pen would move slowly to a lower value of torque. In one very bad case the movement amounted to 1 cm in about 15 seconds. It was however verified that the curve obtained by waiting for the pen to settle was parallel to that obtained by moving the magnet at a steady speed. At the higher values of applied field, where the specimen was nearly saturated, the form of the curves obtained was independent of the speed of the magnet.

9.3 The $Tb_{0.89}Sc_{0.11}$ Basal Plane Disc

This specimen was orientated in the same manner as the others and from the phase angle of the sine6ϕ component of the torque, the "b" axis was found to be the easy axis of magnetisation over the whole range of temperature and field strength used. Results are given in Table 9.4.

9.3.1 The Results

At temperatures below 109K the torques on the crystal specimen exceeded the maximum counter-torque obtainable from the apparatus and it was only possible to make measurements up to applied fields of 0.712T. Figures 9.11 and 9.12 show the measured K_4' values plotted against applied field strength, and it is clear that the values obtained at the three lower temperatures are not saturating.

Table 9.5

$Tb_{0.89}Sc_{0.11}$: K_4 values and single-ion functions

T	K_4	$\log_{10} K_4$	$\hat{I}_{5/2}(z)$	$\hat{I}_{13/2}(z)$	$\log_{10}\hat{I}_{13/2}(z)$	$\hat{I}_{5/2}(z).\hat{I}_{9/2}(z)$	$\log_{10}\hat{I}_{5/2}(z).\hat{I}_{9/2}(z)$	$\log_{10}12.59\ \hat{I}_{5/2}(z).\hat{I}_{9/2}(z)$	$\log_{10}30.2\ \hat{I}_{13/2}(z)$
77	18.6/6.8	1.2695/0.8325	0.9318	0.6104	-0.21452	0.73627	-0.133	0.967	1.265
85.5	16/6.4	1.2068/0.8062	0.9058	0.5017	-0.29956	0.6518	-0.1859	0.9141	1.1804
93	12.6/6.8	1.1004/0.8325	0.8806	0.41268	-0.3844	0.5769	-0.2389	0.8611	1.0956
109	4.76	0.6776	0.8090	0.2322	-0.63414	0.401	-0.3968	0.7032	0.8458
122.5	2.71	0.4330	0.7287	0.11765	-0.92941	0.25764	-0.589	0.511	0.55059
129.5	2.08	0.3181	0.6829	0.0786	-1.1043	0.19661	-0.7064	0.3936	0.3757
138.5	1.43	0.1553	0.6099	0.0406	-1.3915	0.12416	-0.906	0.194	0.0885
149	0.8	-0.0969	0.5221	0.01766	-1.753	0.06751	-1.1706	-0.0706	-0.273
155.5	0.6	-0.2218	0.4730	0.010821	-1.9657	0.0464	-1.3333	-0.2333	-0.4857
165	0.325	-0.4881	0.3881	0.00438	-2.3583	0.02255	-1.647	-0.547	-0.8783
174.5	0.152	-0.8182	0.3052	0.001618	-2.791	0.00976	-2.0107	-0.9107	-1.311
181	0.066	-1.2805	0.2505	0.0007555	-3.1218	0.00501	-2.3	-1.2	-1.6418

Fig 9.13 $Tb_{0.89}Sc_{0.11}$ Extrapolation of K_4' Values to Infinite Field

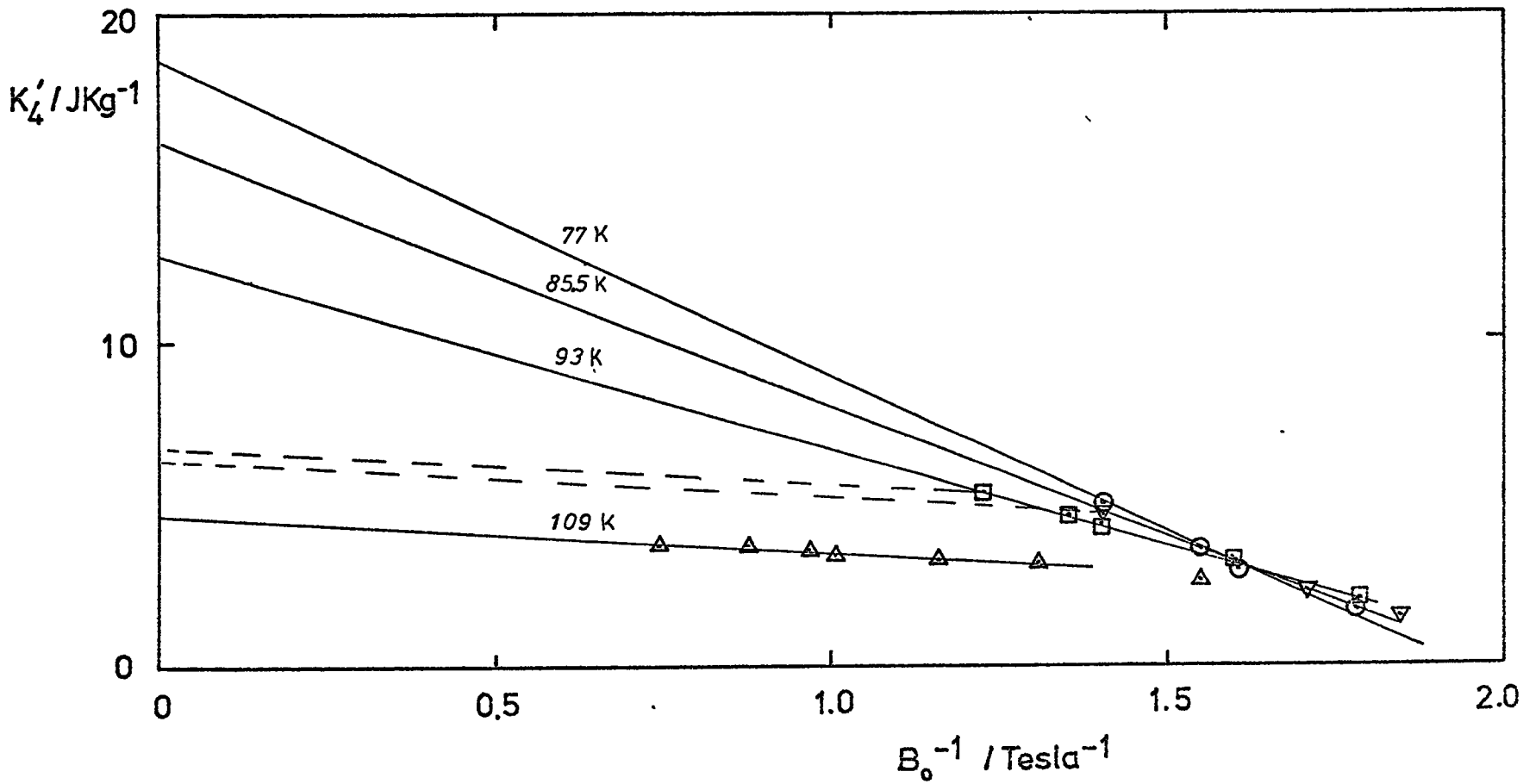

Fig 9.14 $Tb_{0.89}Sc_{0.11}$ Extrapolation of K_4' Values to Infinite Field

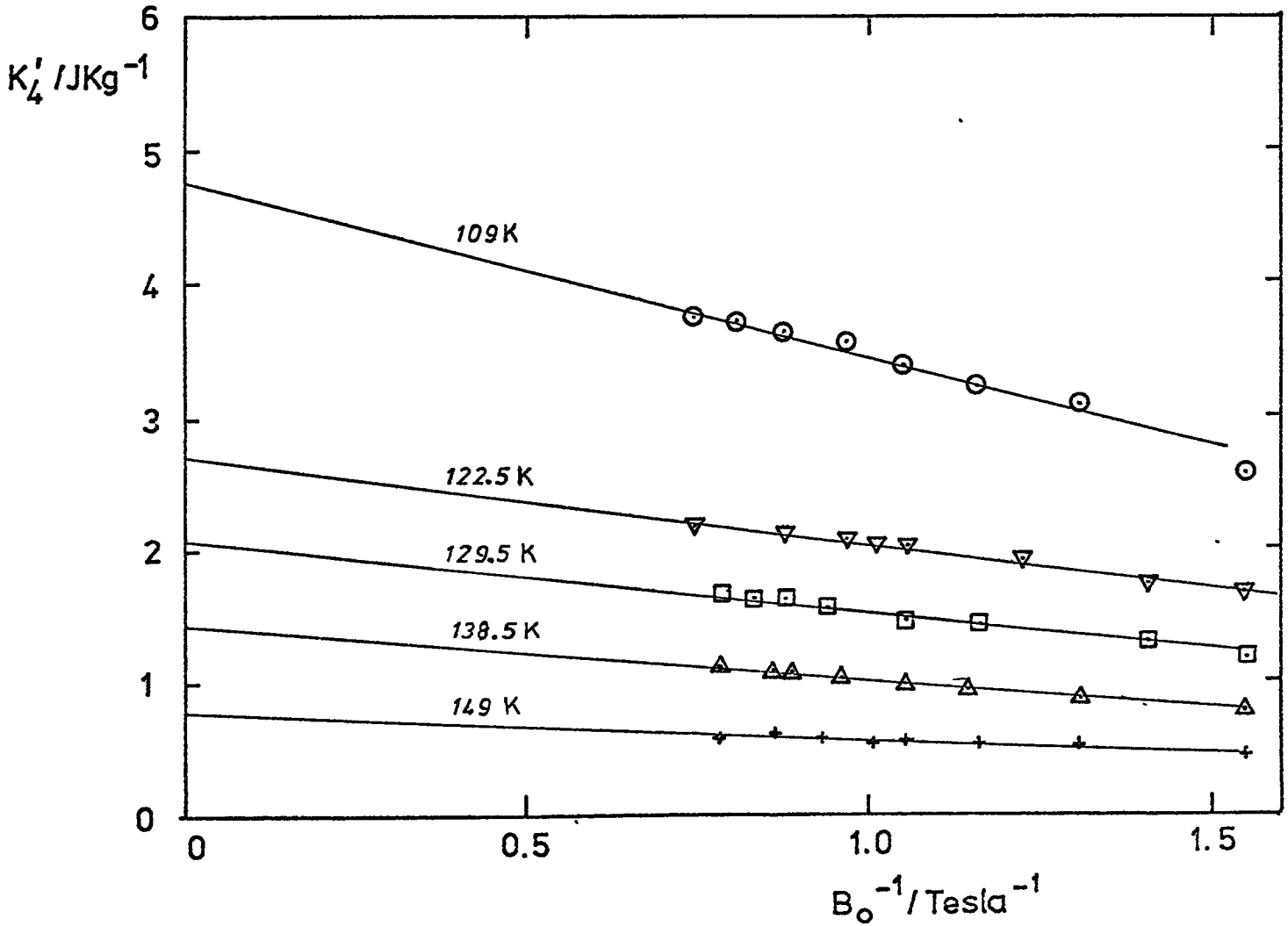

Fig 9.15 $Tb_{0.89}Sc_{0.11}$ Extrapolation of K_4' Values to Infinite Field

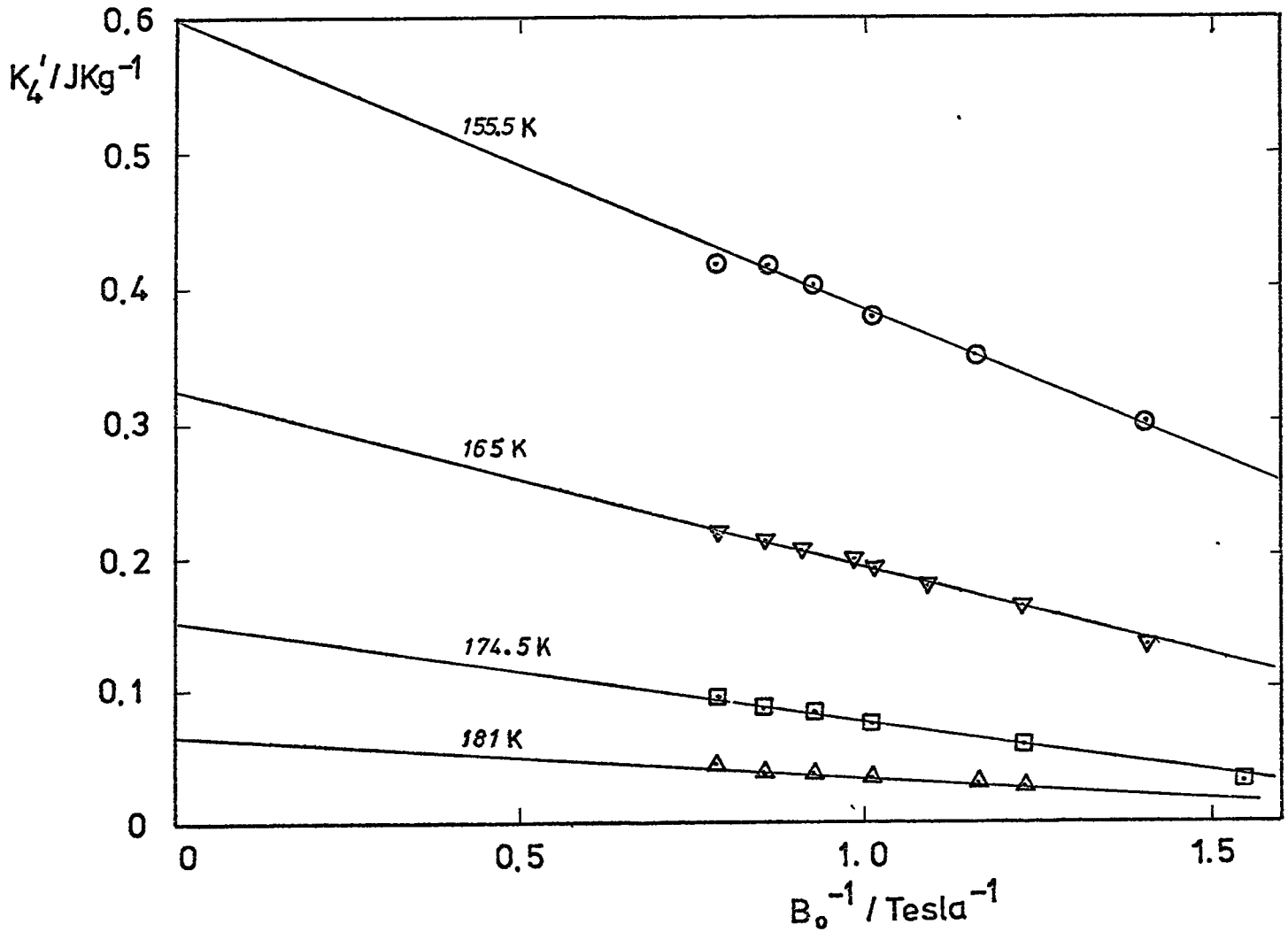

Fig 9.16 $Tb_{0.89}Sc_{0.11}$ K_4 Values Versus Single-Ion Functions, logarithmic plot

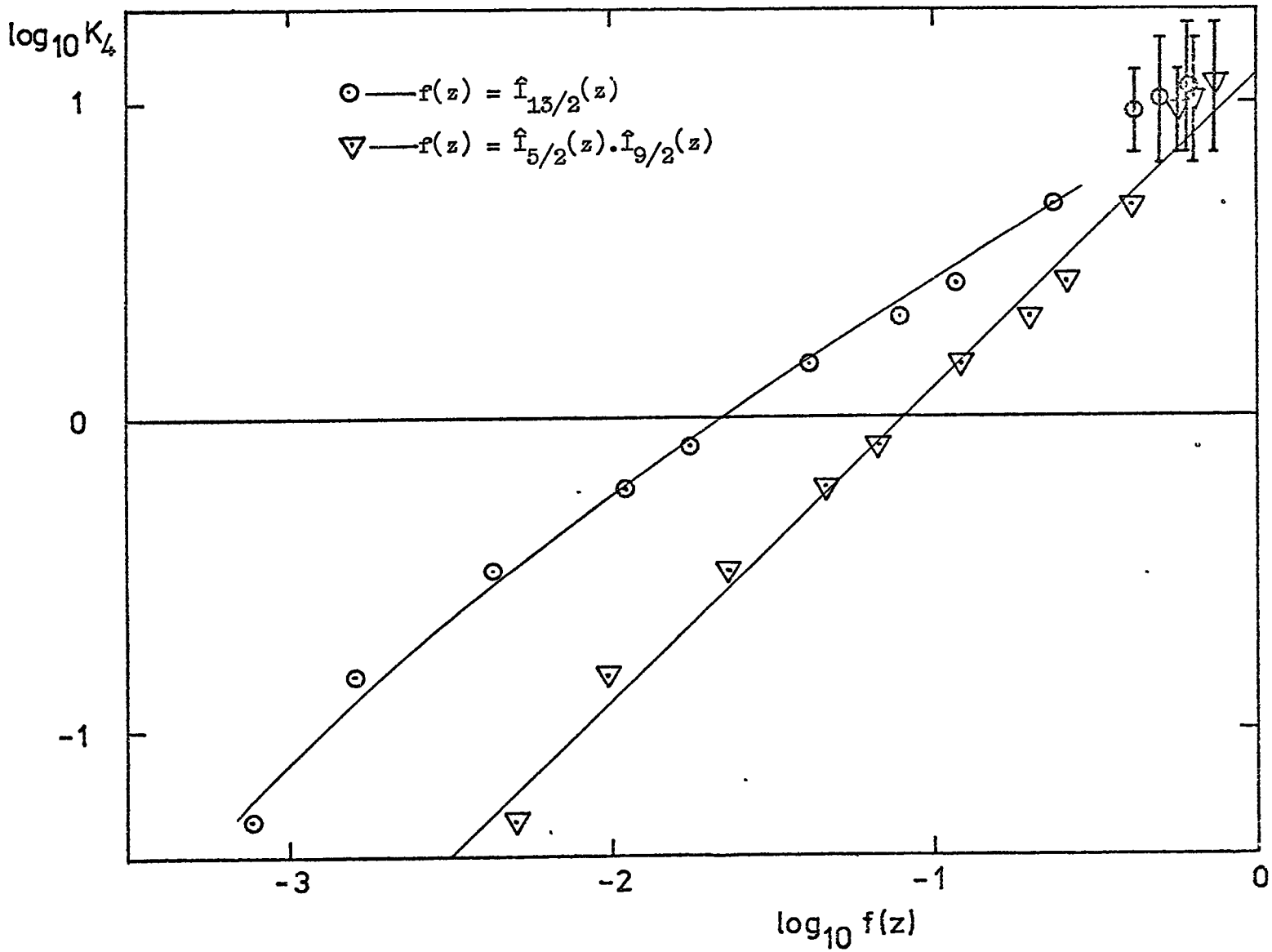

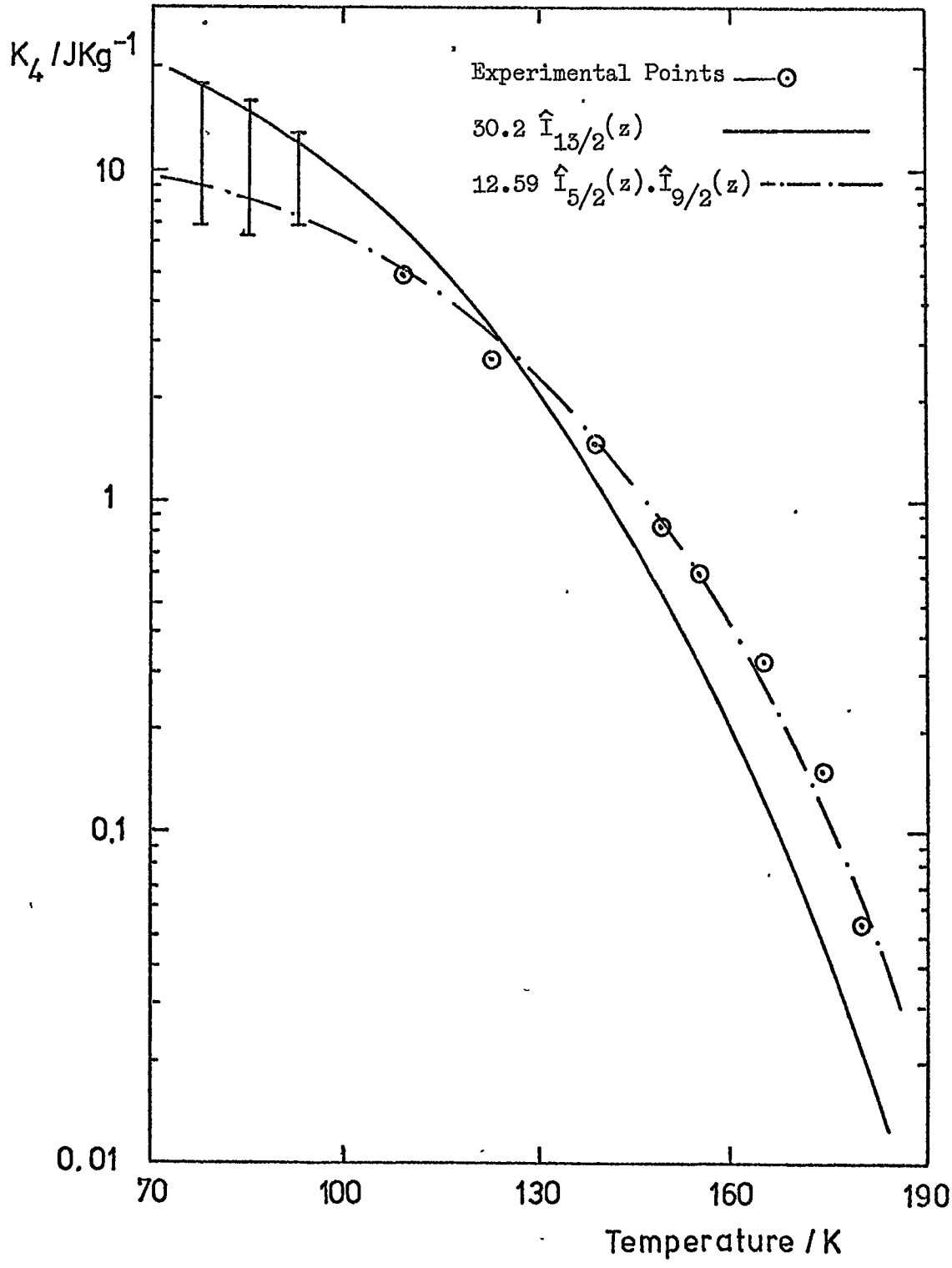

Fig 9.17 $Tb_{0.89}Sc_{0.11}$ Temperature Variation of K_4

Figures 9.13, 9.14 and 9.15 show graphs of K_4' against $\frac{1}{B_o}$. For most of the temperature range the graphs are linear and were extrapolated by continuing the best straight line to $1/B_o = 0$. At the three lower temperatures however extrapolation is extremely uncertain and it is only possible to give a range of values within which K_4 will most probably lie.

The upper end of each range is obtained by extrapolating a straight line through the points which were obtained. Since all the other graphs show a reduction in slope below $\frac{1}{B_o} = 1.55T^{-1}$ it is assumed that the slope of lines passing through points where $\frac{1}{B_o} = 1.55T^{-1}$ would be higher than the correct value. The lower limit was obtained by extrapolating with a line of the same slope as the line for 109K from the highest value of K_4' obtained. Since the negative slopes of the lines increase with decreasing temperature this extrapolation should be below the correct value.

9.3.2 Comparison with theory

Extrapolated values of K_4 are gathered in Table 9.5. Using magnetisation data from D. Chatterjee (1972) the values of $\hat{I}_{13/2}(z)$ and $\hat{I}_{9/2}(z).\hat{I}_{5/2}(z)$ were computed and the logarithms of the K_4 values were plotted in turn against the logarithms of each of these functions. (Figure 9.16).

The second graph is very close to a straight line of slope = 1 so that K_4 is closely proportional to the second function. This is illustrated further in Figure 9.17 where the functions

$$30.2\ \hat{I}_{13/2}(z) \tag{9.5}$$

$$12.59\ \hat{I}_{5/2}(z).\hat{I}_{9/2}(z) \tag{9.6}$$

Table 9.6

Terbium: K_4 values and single-ion functions

T (K)	(a) K_4 Jkg^{-1}	m_T	(b) $\hat{I}_{13/2}(z)$	(c) $\hat{I}_{9/2}(z).\hat{I}_{5/2}(z)$	log (a)	log (b)	log (c)	$71.75\hat{I}_{13/2}(z)$	$24.75\hat{I}_{9/2}(z).\hat{I}_{5/2}(z)$
55	17.1	0.967	0.4956	0.6468	1.233	-0.3049	-0.1892	35.56	16.01
77	11.9	0.932	0.234	0.4027	1.075	-0.6312	-0.395	16.77	9.96
96	8.4	0.907	0.1348	0.2818	0.924	-0.8703	-0.55	9.672	6.976
113	5	0.872	0.06712	0.1764	0.699	-1.17312	-0.7534	4.8162	4.367
135	2.7	0.826	0.0276	0.0941	0.431	-1.56	-1.026	1.9826	2.329
150	1.15	0.795	0.01579	0.06205	0.0607	-1.8	-1.207	1.133	1.536
175	0.444	0.73	0.00534	0.02649	-0.353	-2.27	-1.58	0.3832	0.6557
197	0.222	0.648	0.001524	0.009265	-0.654	-2.82	-2.033	0.10935	0.22934

Fig.9.18 Terbium: K_4 Versus Single-Ion Functions
logarithmic plot

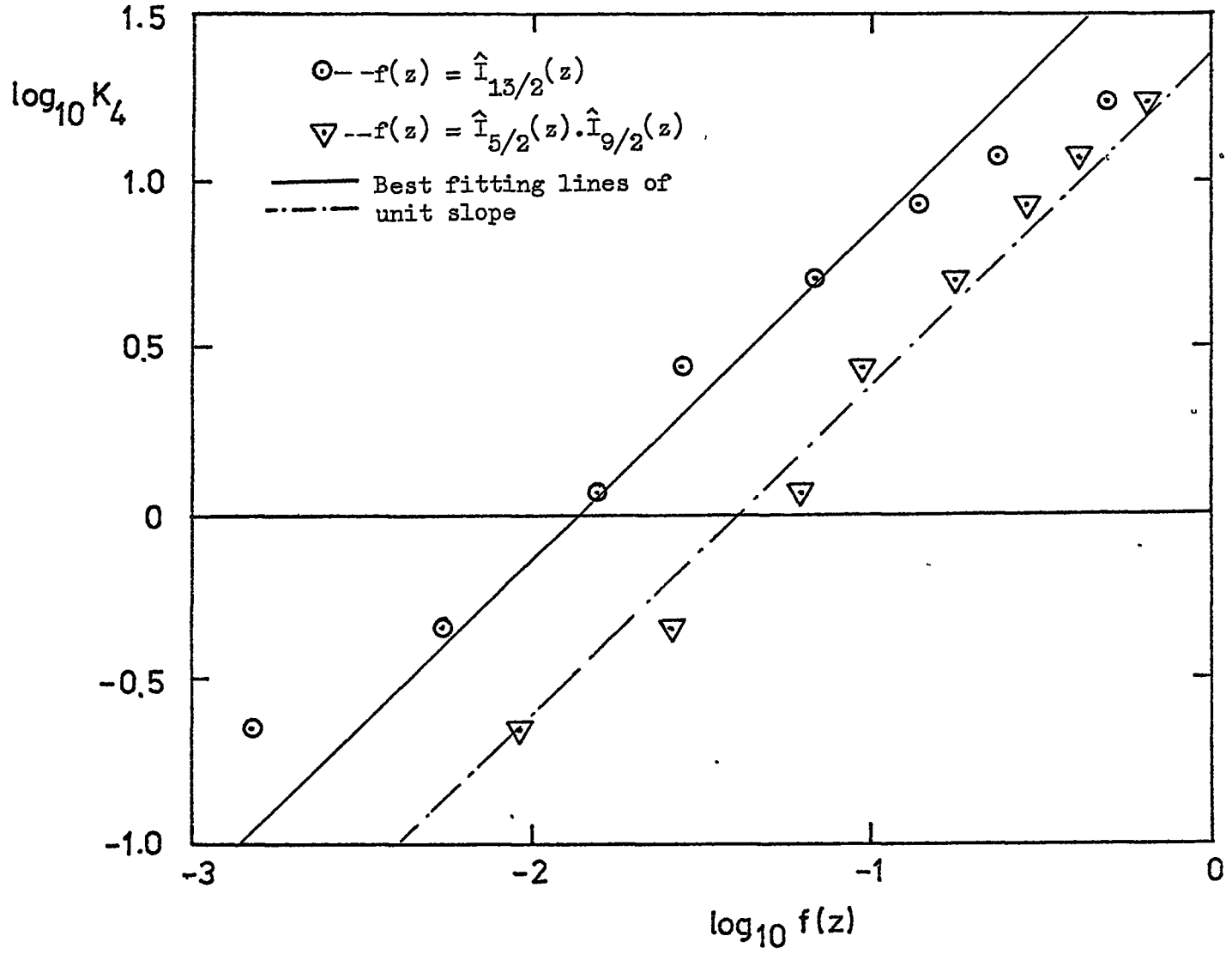

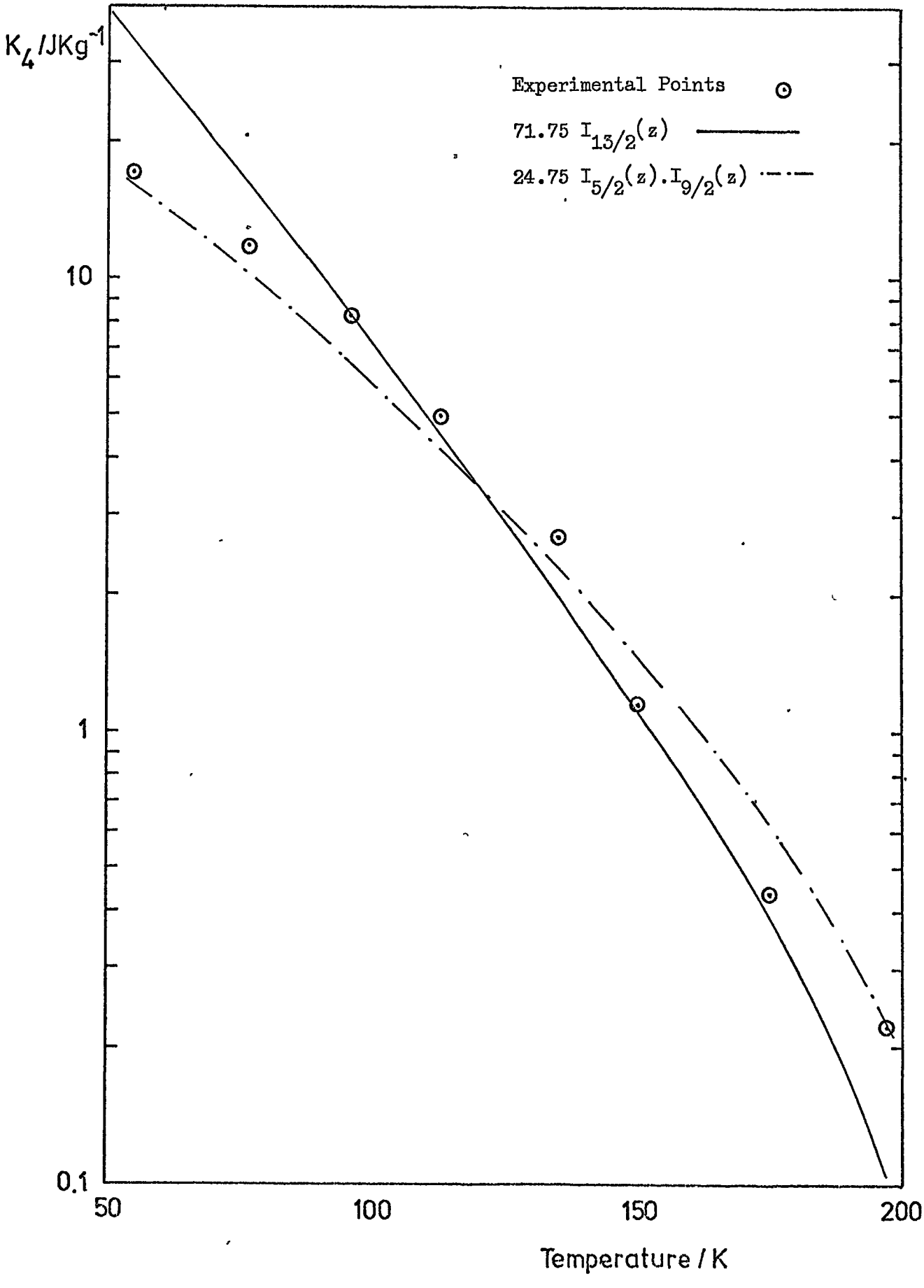

Fig.9.19 Terbium: Temperature Variation of K_4

are plotted on a logarithmic scale against temperature, the experimental value of K_4 also being indicated.

Using a least squares method of curve fitting, the errors were found to be least with a function of the form of equation 9.6 above and they increased with as little as 1% admixture of a function of the form of equation 9.5.

9.4 Terbium Basal Plane Disc

The graphical and numerical treatment used with the previous specimens was repeated for pure Terbium metal using the magnetisation measurements of Hegland et al. (1963) and values of K_4 from the measurements of Bly (1967). Table 9.6 gives the values and Figure 9.18 shows log K_4 plotted against the logarithms of $\hat{I}_{9/2}(z).\hat{I}_{5/2}(z)$ and of $\hat{I}_{13/2}(z)$. The points are more scattered than in the previous case but the superior fit of the first function is clear.

Figure 9.19 shows the temperature variation of the K_4 values and for comparison the two single-ion functions

$$K_4(T) = 24.75\ \hat{I}_{9/2}(z).\hat{I}_{5/2}(z) \qquad (9.7)$$

$$K_4(T) = 71.75\ \hat{I}_{13/2}(z) \qquad (9.8)$$

From the most closely fitting function of this pair (Eq.9.7) the value of $K_4(0)$ is approximately 25 Jkg^{-1}, which may be compared with the value 29.25 Jkg^{-1} $\pm$ 25% obtained by Rhyne and Clarke (1967).

It may be significant that the R.M.S. error in the curve fitting procedure is a minimum for the following function:

$$K_4(T) = 30.5\ \hat{I}_{5/2}(z).\hat{I}_{9/2}(z) - 5.4\ \hat{I}_{13/2}(z) \qquad (9.9)$$

Fig 9.20 Variation of the Magnetostriction Energy for Terbium-Scandium Alloys
(a) The Cylindrical Component (from Chatterjee 1971)
(b) The Hexagonal Component obtained by renormalisation using the Single-Ion Function $\hat{I}_{5/2}(z).\hat{I}_{9/2}(z)$

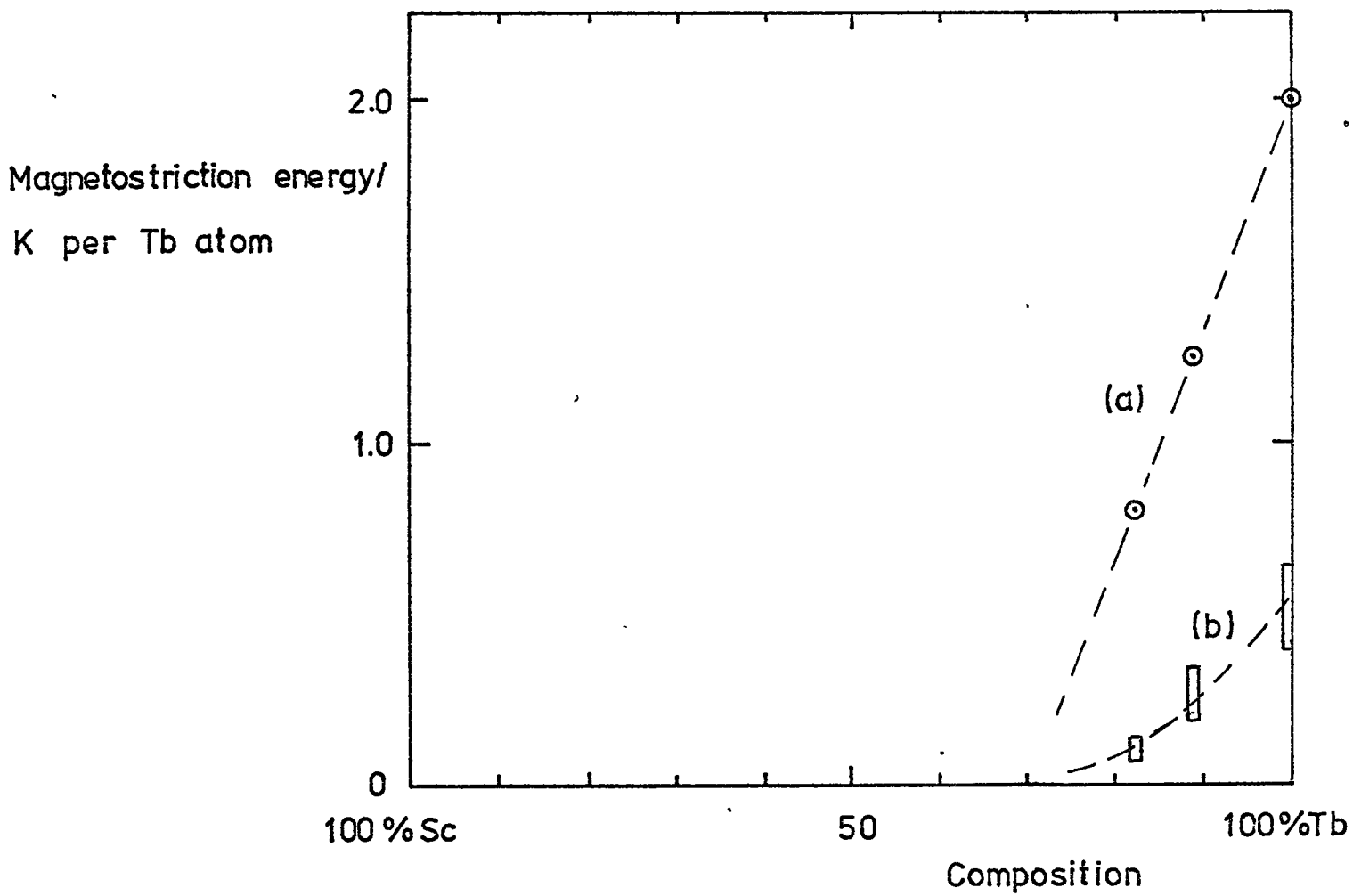

If so, this could be taken as confirmation that the crystal field contribution is of opposite sign to the contribution from the second order hexagonally symmetrical magnetostriction energy (Cooper 1968 I)

9.5 Terbium-Scandium Alloys and Terbium. Conclusions

Both graphical and numerical methods of curve fitting indicate clearly the superiority of the function $\hat{I}_{9/2}(z).\hat{I}_{5/2}(z)$ for describing the variation of the basal plane anisotropy of the two richer alloys and pure Terbium. The origin of this anisotropy is therefore almost entirely the second order magnetostriction of hexagonal symmetry.

Using the function above to estimate the value of K_4 at absolute zero, gave a value for Terbium agreeing with the result of (Rhyne and Clarke 1967) within their reported limits of error. This value and the values for the two richer alloys, expressed in Kelvins per Terbium atom, are plotted against composition in Figure 9.20. Also plotted in the figure are the values for the cylindrically symmetrical magnetostriction energy given by Chatterjee (1972).

The expression for the driving energy (Eq.4.10) may be written,

$$F_d = F_{ms} + F_{cf} = F_{cyl} + F_{hex} + F_{cf} \qquad (9.10)$$

The temperature variation of the hexagonal anisotropy indicates that the last term F_{cf} is negligible. From Figure 9.20 it can also be seen that the cylindrical term is far the larger. The hexagonal term is not however negligible in Terbium and the richest alloy and, since it does not fall with temperature much more rapidly than the cylindrical term, still may account for as much as 15% of the driving energy even at 77K. Both F_{hex} and F_{cyl} die away in alloys with between 70 and 80 atomic percent of Terbium.

Table 9.7

Dysprosium. Characteristics of Torque Curves at 77K Illustrating Hysteresis

Applied field/T	Phases of sin6ϕ		Hysteresis $Jkg^{-1}rev^{-1}$	Mean K_4' Jkg^{-1}	Comments
	CW	ACW			
0.145	9	0.6	13.23	0.01457	No six-fold component visible to the naked eye
0.18	8.9	11	20.22	0.03822	Reasonably smooth curves. CW and ACW curves nearly in phase.
0.21	5	15	22.73	0.0716	Reasonably smooth curves. ACW and CW curves more obviously out of phase.
0.24	11.7	19.86	24.04	0.0579	Bumps and peaks in the curves at irregular intervals.
0.27	-19.6	-17.47	26.39	0.069	Irregular curves.
0.31	-25.9	-0.64	35.35	0.094	Sine6ϕ component disappears during the tracing.
0.375	9.6	11.05	25.84	1.559	Good sin6ϕ form, no distortion, after this point the distortions do not reappear on reducing the field.
0.345	9.7	10.39	23.53	1.099	Field decreasing, good form still.
0.30	12.14	8.817	22.48	0.4605	As above.
0.28	13.97	6.244	23.11	0.2428	Rotational hysteresis causes some distortion at the beginning of each curve, otherwise form is good.
0.24	17.66	1.67	23.8	0.1094	A little distortion. Curve is completely different from that obtained at 0.24T above.
0.214	21.91	-1.137	23.88	0.05888	Sine6ϕ component diminishes as the curve is recorded. Hysteresis remains at same level.
0.185	22.11	-3.045	20.42	0.03157	Sine6ϕ component continues to die away as the curve is traced.

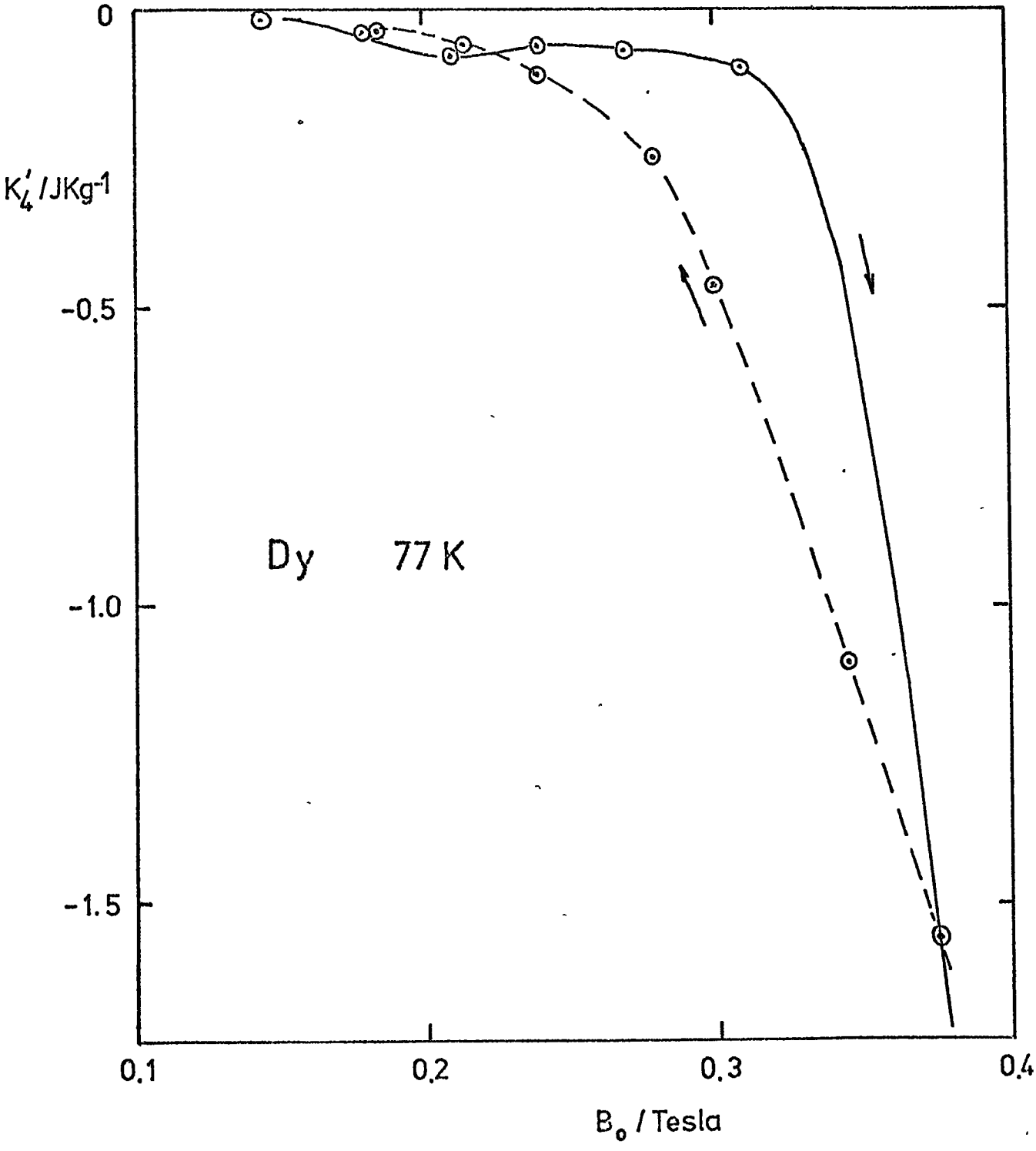

Fig.9.21 Dysprosium: Variation of K_4' with Applied Field at 77K

9.6 Dysprosium Basal Plane Ellipsoid

This investigation was principally concerned with seeking confirmation or otherwise of the changes of easy axis reported by Bly (1967, 1969) (Section 4.4)

A series of about 150 torque curves was obtained at temperatures between 77K and 160K and at fields up to 1.27T. The easy axis was determined in each case either by analysis as for the other specimens or by direct comparison of the curves with those obtained at temperatures and fields where the easy axis was already known.

9.6.1 The Results

(a) At 77K

Table 9.7 gives one of the sets of results obtained at 77K, in the order in which they were measured. Values of K_4', the apparent anisotropy constant, are plotted in Figure 9.21 and can be seen to differ considerably for ascending and descending values of applied magnetic field. The negative values mean that the "a" axis is the easy axis. Irreversible changes, distortions and jumps occur in the curves between 0.23 and 0.31T as B_o is increased. After taking a torque curve at $B_o >$ 0.38T the curves are reproducible and the distortions disappear.

A phase angle of approximately 10 degrees indicates that the 'a' axis is easy and a phase angle of +40 degrees or -20 degrees would indicate that the 'b' axis is easy. The mean phase angle of most of the pairs of curves is about 10 degrees and only for the curves taken at 0.27T is there any indication that the 'b' axis might be easy.

(b) 81,86,92,100 K

Torque curves at these temperatures were similar to those obtained at 77K. When B_o rose above 0.3T the 'a' axis was easy up to the highest value of applied field which could be used.

Fig.9.22 Dysprosium: Changes in Sign of K_4. The Amplitude of the sin6ϕ Component of Torque Curves

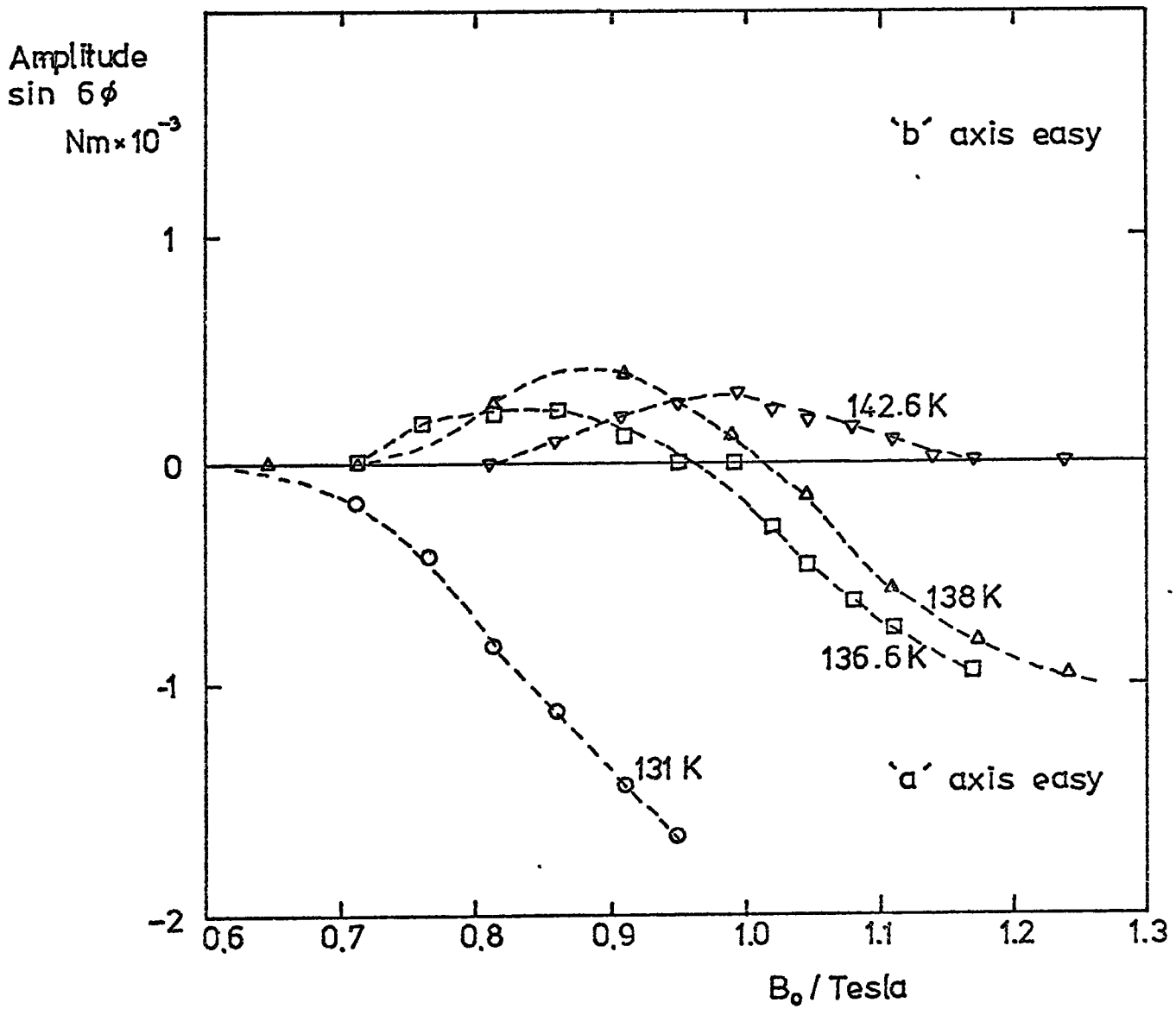

(c) 110K

Curves obtained at 110K differ from those obtained at lower temperatures only in that the distortion of the torque curves reappears when the applied field is lowered, even when curves have been obtained at fields above 0.6T.

(d) 120,124,131K

Torque curves showing a $\sin 6\phi$ component could only be obtained at applied fields in excess of 0.45T, no distortion was observed and 'a' axis was easy up to the highest field used (1.24T). No indication was found of the changes of easy axis at high applied fields which marks the boundary between regions III and I in Figure 4.2.

(e) 136.6, 138, 142.6, 147.6, 156.5K

The amplitudes of the $\sin 6\phi$ component of the curves obtained at 131, 136.6, 138 and 142.6K are shown plotted against applied field in Figure 9.22. The amplitudes are positive when the 'b' axis is easy and negative when the 'a' axis is easy; the field strengths at which the easy axis changes are then easily determined from the points where the graphs cross the field axis. Changes located in this way are plotted on the original figure due to Bly (Figure 4.3) as open circles and agree well with his results for this temperature range. Torque curves obtained at 147.6K showed only the 'b' axis easy and those at 156.5K did not show a clear sixfold component even at the highest field available.

No attempt was made to perform a numerical analysis where a $\sin 6\phi$ component was not clearly visible, since the Fourier analysis calculation can give an amplitude which is merely a component of the noise or the distortions in the curves caused by rotational hysteresis. Direct

inspection was felt to be the best test for the presence of a $\sin 6\phi$ variation in the torque and on this test no trace was found of the change of easy axis between regions II and III in Figure 4.3.

9.6.2 Discussion: Results. 77 to 100K

Apart from the general difficulty in determining the easy axis from torque curves when the specimen is unsaturated (Section 9.6.3), interpretation of the changes of phase occurring in the $\sin 6\phi$ component at low values of applied field between 77K and 100K has the following special difficulties.

i. The curves are distorted through all or part of their length and jumps and abrupt changes of form occur in certain curves.

ii. The amplitude and the phases of the sixfold components are not unique but depend on the previous magnetic history of the specimen.

iii. The rotational hysteresis is still increasing with the applied field and the magnetisation data of Behrendt et al. (1958) confirms that the specimen is still magnetised well below the knee of the magnetisation curve. Domain walls are therefore still present and these appear to behave as if they were pinned in some way, moving only when the applied field exceeds a critical value.

iv. The graphs of K_4' against applied field (Figure 9.21) would have an improbable kink if the single value of K_4' with the appropriate phase (the result for 0.27T, Table 9.7) were to be given a positive value to represent the change of easy axis to 'b'.

Since the curve showing the 'b' axis phase is the most distorted, it is likely that the phase change is a result of the distortion and not of any real change of easy axis. Recent work by Herring et al. (1973) on Dysprosium at 4.2K in zero field showed the existence of small domains and also that the 'a' axis is not easy. This suggests that it is possible that M_s is parallel to the 'b' axis when the specimen is cooled in zero field from above the Curie temperature.

The graphs of K_4' versus applied field in Figure 9.21 exhibit a kind of hysteresis; the values of K_4' do not increase until the applied field passes a critical value, then they increase rapidly and do not fall as far when the field is reduced. Because the distortions in the torque curve are cleared by taking torque curves at higher values of applied field and the clearing process is accompanied by jumps and severe changes of form, it was felt initially that the cause was sticking of the movement of the magnetometer and that the movement was being freed by 'giving it a good run'. Some time was spent in establishing that the magnetometer movement was quite freely suspended and that the changes described were reproducible in a general way.

The hysteresis in the K_4' values appears to be closely related to the hysteresis of the ferromagnetic domain structure in Dysprosium deduced by Rauch and Zeilinger (1972) from neutron depolarisation measurements. For example at 80.2K the mean domain size rises from approximately 18×10^{-6}m at 0.05T to 25×10^{-6}m at 0.12T and remains at about 24×10^{-6}m as the field is again reduced to 0.05T. After taking into account the demagnetising field of the specimen used in the torque measurements, this is very nearly the range of applied field over which the hysteresis in the K_4' value is observed.

The existence of a sort of internal coercive force for the movement of domain boundaries in polycrystalline Dysprosium of about 0.025T at 90K is reported by Löffler and Rauch (1969) and connected by Rauch and Zeilinger (1972) with the high intrinsic coercive force predicted by Egami and Graham (1971). This intrinsic coercive force, which was predicted independently by Van den Broek and Zijlstra (1971) should occur in materials where the ratio of the anisotropy energy to the exchange energy is large. For such materials the angle between adjacent moments in domain walls is large, the wall is thin (of the order of 2nm), the wall energy is high and the movement of the wall involves the movement of individual spins through a metastable state of higher energy. For 180 degree walls in Dysprosium, Egami and Graham estimated a coercive force of about 0.1T at absolute zero, this value falling off rapidly with rising temperature.

Egami (1971) who has measured the coercive force for Dysprosium single crystals at various field sweep rates, has observed that the coercive force rises to a limiting value at sweep rates of about 4 Ts^{-1} and interpreted this limiting value as the intrinsic coercive force of the domain walls. The variation with temperature is great and at 80K the coercive force is only 0.01T at high sweep rates. Since the quasi-static coercive force may be less than this by one or two orders of magnitude, and since this figure is already much lower than the resultant field at which domains start to grow, or at which K_4' rises suddenly (approx. 0.025T) it is unlikely that the hysteresis in K_4' values can be connected with Egami and Graham's intrinsic coercive force.

Near the Curie temperature of Dysprosium, Belov et al. (1969) observed relaxation effects in the magnetisation of polycrystalline

samples with relaxation times of the order of 10 and 10^2 seconds which disappear just below 100K. Rauch and Zeilinger measured even longer relaxation times in the neutron depolarisation factors of single crystals, domain structure continuing to change over times of the order of 10^3 seconds. Belov et al. connect the relaxation with the gigantic magnetostriction of Dysprosium since similar effects are observed in Terbium and Terbium-Yttrium alloys where the magnetostriction is large, but they are not observed in Gadolinium where the magnetostriction is two orders of magnitude less than in the other materials. Rauch and Zeilinger were able to connect the hysteresis effects with magnetostriction by plotting the neutron depolarisation factors for given applied fields against temperature. On these graphs the metamagnetic transition stands out clearly by the large stepwise change in the depolarisation factor. The transition was found to occur at temperatures 2K higher for rising temperatures than for falling temperatures. This is close to the difference in magnetoelastic energies between the ferro- and antiferromagnetic states, calculated to be 2.2K/atom. Similar results for hysteresis of this transition have been obtained by microwave absorption (Rossoll et al. 1965) and neutron diffraction (Wilkinson et al. 1961).

It seems probable therefore that the hysteresis in K_4 values between 77 and 100K can be regarded as one of a series of phenomena attributable to the large magnetostriction of Dysprosium.

9.6.3 Discussion: Results above 136K

In contrast to the results at lower temperatures, the changes of axis obtained above 136K were reproducible and the torque curves show

Fig.9.23 Dysprosium: Established Apparent Changes of Easy Axis

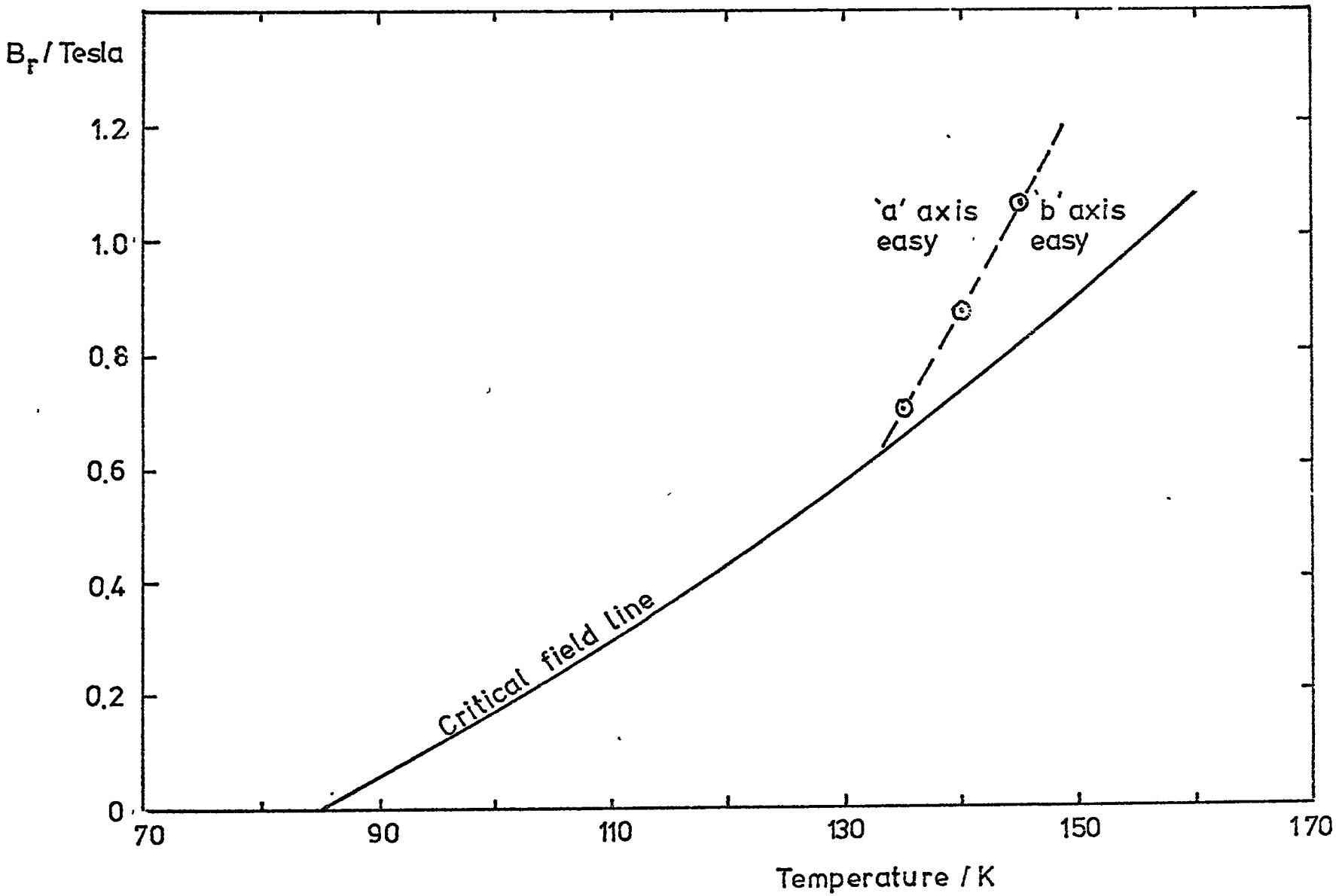

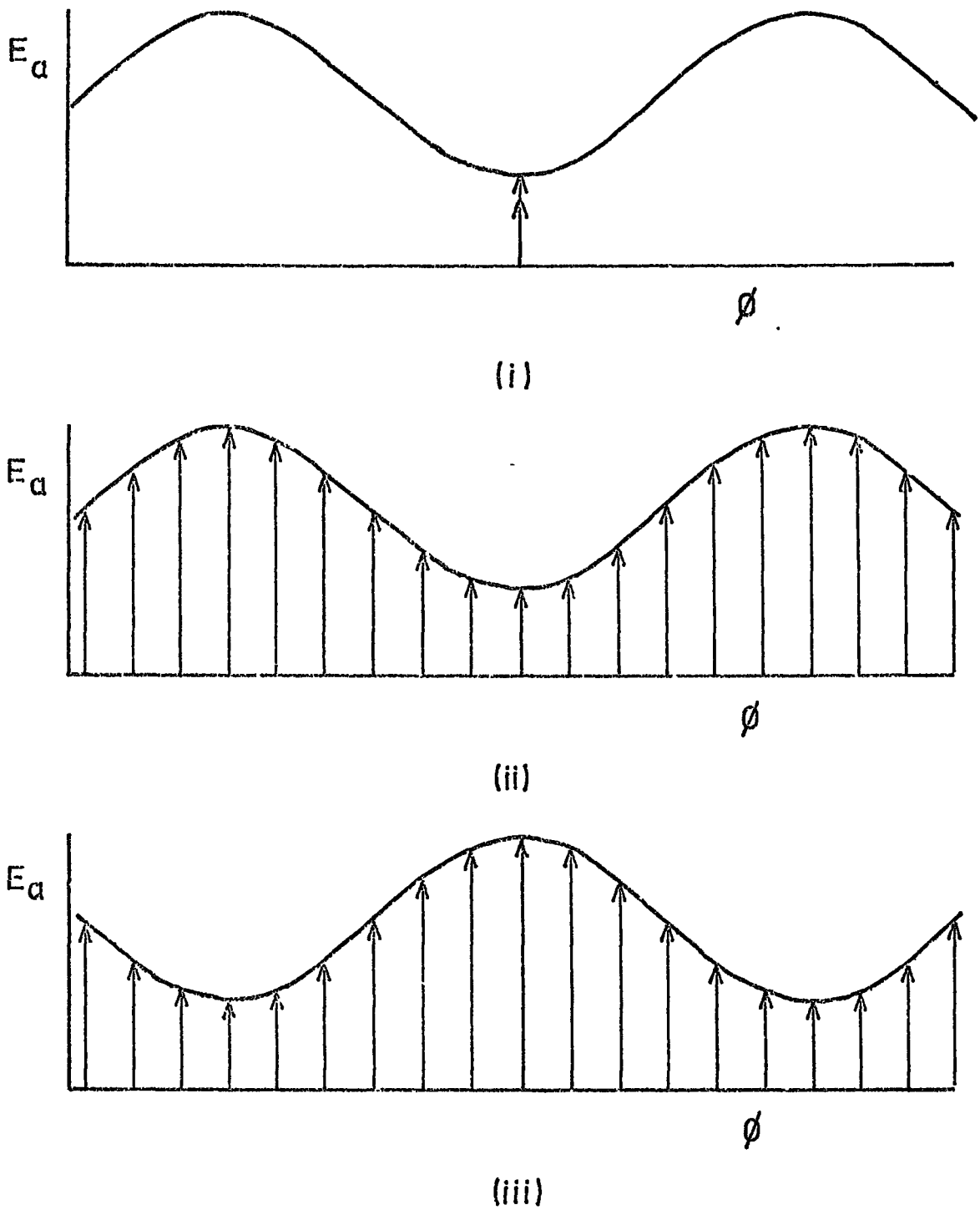

Figure 9.24 Apparent changes in easy axis may be caused by a fanlike spin structure.

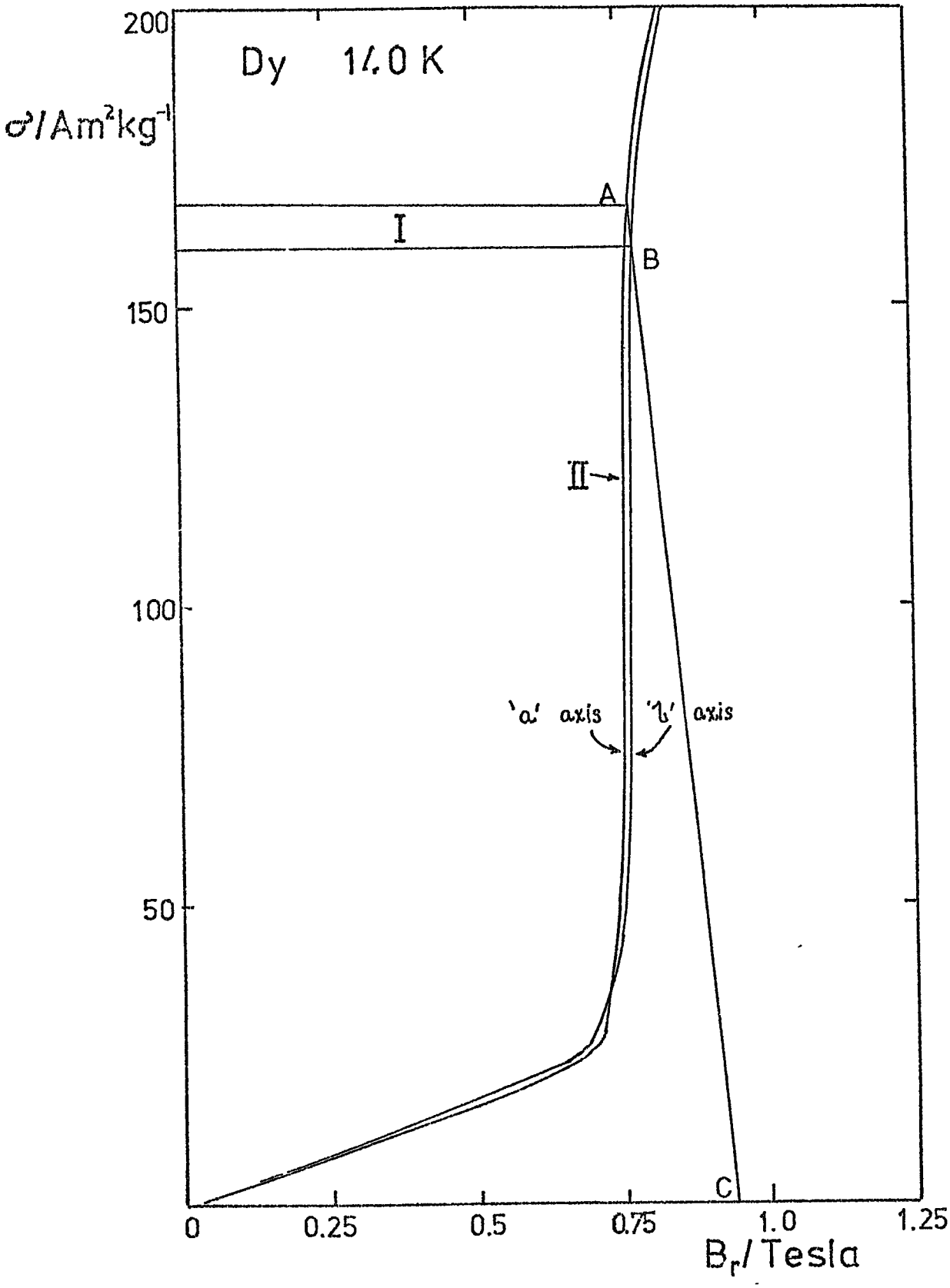

Figure 9.25 To illustrate a possible cause for a change of apparent easy axis.

no distortion and little rotational hysteresis. Graphs of K_4 against applied field are smooth curves which change sign without discontinuities and the changes of easy axis implied by this were regarded with some confidence. These changes are plotted in Figure 9.23. The three points were read from Figure 9.22 and the applied field was adjusted to take account of the demagnetisation field of the Dysprosium ellipsoid. The critical field line in Figure 9.23 was taken from the results of Behrendt et al. (1958). The line marking the change of easy axis cuts the critical field line at about 132K and the validity of this extrapolation is confirmed by the fact that torque curves for 131K show no change of easy axis.

An apparent change of easy axis might be expected if the metamagnetic transition takes place via a series of fan-like moment states in which the directions of the spins are distributed over a sufficiently large angle. Figure 9.24 illustrates in a general way how such a fan-like moment distribution could give an apparent change of easy axis. The graphs represent the anisotropy energy for a single spin, plotted against orientation in the basal plane of the crystal. Thermal effects are taken into account in the amplitude of the curve. In the ferromagnetic state 9.24(i) all the spins are parallel and the observed easy axis is the same as that for a single spin. Figure 9.24(ii) and (iii) represent hypothetical widely divergent fans of spins, centred on an easy and a hard direction respectively. It can be seen that the total anisotropy energy could be greater in the former case than the latter. Thus a change of easy axis might be observed which would not represent any real change in the crystal field.

The existence of an intermediate stage in the approach to saturation is detectable in the rounding of the magnetic isotherms of Dysprosium at temperatures from 130K upwards and at applied fields high enough to eliminate domain effects as an explanation (Behrendt et al 1958). It can be shown theoretically (Enz 1960) that when a field greater than a definite critical value is applied parallel to the basal plane of a helical antiferromagnet such as Dysprosium we can expect the magnetic moments of each ferromagnetic layer to deviate from the direction of the applied field by angles which vary sinusoidally with distance along the "c" axis. Nagamiya et al (1962) deduced the following relationship for the case where there is no anisotropy in the basal plane

$$\text{Sin}\ \frac{\phi_n}{2} = \xi\ \sin(nq_o + \alpha) \qquad (9.11)$$

(Symbols have been altered to agree with later work). ϕ_n is the angle between the field and the magnetisation vector of the nth plane parallel to the basal plane, q_o is the interlayer turn angle of the corresponding helical structure which occurs just below the critical field at the same temperature and α is a phase angle. ξ is an amplitude which is adjusted to minimise the sum of the exchange and Zeeman energies. This structure is illustrated in Figure 2.8.

Kitano and Nagamiya (1964) assumed that the distribution of moments represented by equation 9.11 could also be used in the case where there is anisotropy in the basal plane which is not strong enough entirely to eliminate the fan phase. A term representing the anisotropy energy is derived from 9.11 and included in the expression for the total free energy, which when minimised gives value of ξ.

In Dysprosium the anisotropy in the basal plane will tend to draw the magnetisation vectors nearer to the adjacent easy direction and this will tend to distort the simple sinusoidal fan structure so that additional harmonic terms are required on the right hand side of equation 9.11. For simplicity, Kitano and Nagamiya retained only the single sinusoidal term of 9.11, but for Dysprosium at temperatures near to 140K this is reasonable. The distortion of the sinusoidal distribution is not expected to be great since the anisotropy is small and the interlayer turn angle is not a simple multiple or submultiple of $\pi/3$. Also the neutron diffraction experiments on the helical phase of Dysprosium by Wilkinson et al. (1961) showed very weak additional satellite lines only up to 140K which suggests that the effect of anisotropy on the simple helical structure and also therefore on the sinusoidal fan structure is small above this temperature.

When the applied field is parallel to an easy axis, the anisotropy energy of the n'th atomic plane is

$$e_n = -c.\cos 6\phi_n$$

where c is a constant. The average energy (e_a) is then given by

$$e_a = -\frac{c}{N}\sum_n \mathrm{Cos}6\phi_n = -\frac{c}{N}\sum_n \mathrm{Cos}12\arcsin(\xi \mathrm{Sin}(nq_o + \alpha))$$

where N is the total number of planes.

N is very large in a typical crystal so that nq_o may be regarded as covering the angular range $0\text{-}2\pi$ uniformly and may be replaced by a continuous variable Ψ, hence,

$$e_a = \frac{-c}{2\pi} \int_o^{2\pi} \text{Cos12arcsin}(\xi \text{Sin}\Psi) d\Psi \qquad (9.12a)$$

A numerical evaluation of the integral was performed for a series of values of ξ between 0 and 0.5 which shows that it is negative between $\xi = 0.2$ and $\xi = 0.445$ and positive elsewhere in the range. These two values correspond to fans of total angular width 46^o and 104^o respectively. Thus for spin structures with this angular width the anisotropy energy with the field parallel to an easy axis would be positive and the axis would be apparently hard.

The change of axis would not however be expected when ξ was exactly equal to 0.2 since the expression corresponding to 9.12a when the field is parallel to a hard axis is

$$e_b = \frac{\pm c}{2\pi} \int_o^{2\pi} \cos 6(2\arcsin(\xi \sin\Psi) - \phi) d\Psi \qquad (9.12b)$$

Here it is assumed that the moments oscillate sinusoidally about the direction of the resultant magnetisation which is pulled towards an easy axis and makes an angle ϕ with the applied field. Also the value of ξ which minimises the energy in this case is not necessarily the same as that for the easy axis. Hence the sign of the quantity $e_b - e_a$, which determines the easy axis will not change sign at the same value of ξ as that for the energy e_a alone.

Use was made of the results of calculations for hexagonal crystals given by Kitano and Nagamiya (1964) from which it was determined that ξ just above the critical field would be approximately 0.4 for magnetisation parallel to the hard axis and 0.44 for magnetisation parallel to easy axis. Both fall to zero with increasing applied field and lie

between the limiting values which lead to reversed anisotropy energies together. Thus a change of easy axis is expected on the basis of this theory.

The theory also predicted that the specimen would be in a region where ϕ tended to zero, this being confirmed by the absence of shear from the torque curves.

In order to estimate ξ from the published results it was necessary to obtain values of the quantities

$$X = \frac{V_6}{\{\mathcal{J}(q_o) - \mathcal{J}(o)\}J^2}$$

and

$$\beta_2 = \frac{\mathcal{J}(q_o) - \mathcal{J}(2q_o)}{\mathcal{J}(q_o) - \mathcal{J}(o)}$$

Here V_6 is $\frac{K_4}{m_T^6}$, and $\mathcal{J}(q)$ is the Fourier transformed exchange in the c direction, q_o being the reduced wave vector which makes this function a maximum (section 4.2.1). Values of β_2 (2.125) and $J^2\{\mathcal{J}(q_o) - \mathcal{J}(o)\}$ (0.32×10^{-21}J) were obtained for a temperature of 98K from the results of Nicklow et al (1971) and another value of $J^2\{\mathcal{J}(q_o) - \mathcal{J}(o)\}$ (0.2×10^{-21}J) estimated from the relationship

$$J^2\{\mathcal{J}(q_o) - \mathcal{J}(o)\} \approx n_{sat} m_B \mu_o H_c$$

which holds near the Néel temperature. Even supposing that β_2 should increase threefold and that $\{\mathcal{J}(q_o) - \mathcal{J}(o)\}$ should decrease threefold, values of ξ over 0.3 were obtained at the critical field. These are high enough to account for the change of easy axis. The amplitude ξ was

also estimated directly from the magnetisation above the critical field, making the assumption that the magnitude of the magnetisation of each plane does not change greatly as the moment vectors rotate into line with the applied field. The bulk magnetisation is then proportional to the quantity,

$$m_p \Sigma \cos\phi_n$$

where m_p is the magnetic moment of each plane. Following an argument similar to that leading to equation 9.12, one obtains an expression for the magnetisation at each field value, relative to the magnetisation at a field high enough to cause the collapse of the fan structure.

$$\frac{M(T,H)}{M(T,2H_c)} \approx \frac{1}{2\pi} \int_0^{2\pi} \cos 2(\arcsin(\xi \sin\Psi))\, d\Psi$$

A table of values of this expression was constructed for a range of values of ξ and using the magnetisation data of Jew and Legvold it was confirmed that ξ is approximately 0.45 just above the critical field, falling to zero as the field increases. It was also found that at the field and temperature values where the easy axis is changing, ξ is approximately constant but is nearly 0.3. At this point the integral of equation 9.12 (a and b) is just beginning to increase from its most negative value as the field increases and the amplitude ξ decreases. It is not certain therefore that the sinusoidal fan structure accounts entirely for the change of easy axis.

The change could also be partly due to the fact that the torque magnetometer may give false results for the easy axis when, as in this

case, the specimen is not saturated. This is illustrated in Figure 9.25 which shows the magnetisation curve for 140K from the data of Jew and Legvold. The work needed to magnetise the specimen to any given value of magnetisation is proportional to the area enclosed between the magnetisation curve, the magnetisation axis and a horizontal line through the given magnetisation value. For the part of the curve given, the 'a' axis curve lies to the left of the 'b' axis curve; the work needed to magnetise the specimen to any given intensity of magnetisation is therefore less for magnetisation parallel to the 'a' axis and this axis is therefore easy. The torque magnetometer however indicates as the easy axis the one which requires least work to bring it into line with the applied magnetic field. Using the method described in section 2.3.1 to determine the magnetisation produced by a given applied field, it can be seen in Figure 9.25 that an applied field of 0.95T would produce greater magnetisation when parallel to the 'a' axis than when parallel to the 'b' axis and the work needed to bring the 'a' axis parallel to the magnetic field would exceed that needed to bring the 'b' axis parallel to the field, the extra work being proportional to the difference between the two areas marked I and II in Figure 9.25. Torque magnetometer measurements would therefore show up the 'b' axis as easy. At higher applied fields the area 1 is smaller and the area II is larger, therefore the apparent anisotropy would die away as the applied field increases and would then reappear with the 'a' axis easy. This apparent change of easy axis would not correspond with any change in the specimen. The results of torque measurements cannot therefore be relied on to detect changes of easy axis when the specimen is unsaturated, when the anisotropy is not small and when the steepest part of the magnetisation curve occurs

at high values of applied field, thus increasing areas such as that marked I in Figure 9.24.

In the case of Dysprosium at 140K the measurements of Jew and Legvold do appear to show anisotropy (and changes of easy axis with rising applied fields, although at higher values of applied field than those deduced by Bly who took the crossing of the 'a' and 'b' curves to indicate the change of axis). These authors did not however consider that their results indicated any anisotropy at all above 110K so that it is impossible on this basis to be certain how far the change of axis is affected by the special nature of the measurements with the torque magnetometer. It is thought more probable that the observed changes are due to the angular width of the fan structure of spins.

9.6.4 Temperature variation of K_4 for Dysprosium

It was thought possible at one stage in this investigation that changes of easy axis in Dysprosium near the critical field and at small fields below the Curie temperature might be caused by the different dependence on magnetisation of opposing contributions to the anisotropy from the crystal field and magnetostriction. Thus a small contribution from magnetostriction tending to make the 'b' axis easy would die away more slowly than the crystal field contribution and at low magnetisations might dominate the anisotropy. Accordingly, attempts were made to fit a function of the form given below in equation 9.13 to values of K_4 for Dysprosium.

$$K_4 = K_4(0)\{(1 + x)\hat{I}_{13/2}(z) - x\hat{I}_{5/2}(z).\hat{I}_{9/2}(z)\} \qquad (9.13)$$

Table 9.8

Dysprosium: K_4 values from Féron and single-ion functions

Temp/K	K_4/Jkg^{-1}	$I_{5/2}(z)$	$I_{9/2}(z)$	$I_{13/2}(z)$	$-124.69(0.951I_{13/2}(z) + 0.049I_{9/2}(z).I_{5/2}(z))$
2.45	-128.6	0.998948	0.996499	0.99267	-123.79
4.945	-128.6	0.998159	0.993876	0.98719	-123.12
10.43	-124.4	0.995122	0.983832	0.96635	-120.57
20.24	-98.24	0.982898	0.944123	0.88627	-110.76
30.43	-89.76	0.95996	0.872684	0.75136	-94.21
40	-75.62	0.931676	0.789985	0.60986	-76.8
50.31	-57.25	0.89476	0.69071	0.46069	-58.4
50.31	-55.83	0.89476	0.69071	0.46069	-58.4
55.21	-49.5	0.874961	0.641362	0.39487	-50.25
55.21	-51.6	0.874961	0.641362	0.39487	-50.25
60.123	-42.4	0.851953	0.587322	0.32906	-42.08
60.123	-43.1	0.851953	0.587322	0.32906	-42.08
65.4	-33.9	0.829344	0.537574	0.27422	-35.24
65.4	-36	0.829344	0.537574	0.27422	-35.24
70.06	-29.7	0.802172	0.482029	0.21938	-28.38
72.6	-24.7	0.7895	0.457677	0.19744	-25.62
73	-26.8	0.7895	0.457677	0.19744	-25.62
75.1	-23.3	0.775485	0.431798	0.1755	-22.86
75.1	-26.8	0.775485	0.431798	0.1755	-22.86
77.3	-21.2	0.763819	0.411137	0.159	-20.77
77.3	-24	0.763819	0.411137	0.159	-20.77
80.4	-16.96	0.746468	0.381816	0.1371	-18.00
80.4	-18.09	0.746468	0.381816	0.1371	-18.00
85.3	-13.43	0.718353	0.337752	0.1075	-14.23
85.3	-15.55	0.718353	0.337752	0.1075	-14.23
90.2	-9.47	0.68798	0.294698	0.0823	-11.00
90.2	-10.6	0.68798	0.294698	0.0823	-11.00
95.1	-7.77	0.662902	0.262494	0.0658	-8.86
95.5	-8.48	0.662902	0.262494	0.0658	-8.86
100.6	-5.654	0.623624	0.217681	0.04607	-6.29

If $\frac{1+x}{x}$ is approximately equal to 6, this function would change sign at the appropriate magnetisation. Values of K_4 and $\hat{I}_{13/2}$ were obtained from the results of Feron (1969), the related functions were calculated (Table 9.8) and an attempt was made to fit the experimental values of K_4 to the function above. Fitting was carried out by adjusting the value of $K_4(0)$ to minimise the sum of the squares of the errors, the sum of the squares of the fractional errors and the sum of the products of the errors and fractional errors. In addition the theoretical and experimental values were treated in turn as the independent variable. The results were consistent in showing that the errors in fitting increased with positive values of x. The best fitting equation was

$$K_4 = -124.69\{0.951\ \hat{I}_{13/2}(z) + 0.049\ \hat{I}_{5/2}(z).\hat{I}_{9/2}(z)\}$$

The contribution from magnetostriction is the same sign as that from the crystal field. The hypothesis above is therefore not supported.

9.7 Dysprosium: Conclusions

The changes of easy axis observed by Bly are not confirmed at temperatures near the Curie temperature. Changes do occur at higher temperatures but these may be explained without any real change in the microscopic easy direction as experienced by an individual atomic moment.

Recent observations by Herring et al. (1973) on domain patterns at 4K suggest that in zero field the 'a' axis is not necessarily easy. This is still unexplained.

9.8 Suggestions for Further Work

The present investigation could be extended by making measurements at lower temperatures. This would allow the comparison of theoretical functions with the temperature variation of K_4 and the determination of $K_4(0)$ to be made with greater precision but would involve the use of a larger electromagnet to accommodate the necessary double Dewar vessels. A larger electromagnet is also required to increase the magnetic fields available and to improve the reliability of the extrapolated values of K_4.

The use of lower temperatures and higher magnetic fields would raise the torques to be measured and would involve a radical redesign of the torque magnetometer. The use of a rigid suspension with piezo electric transducers to measure the torque has been attempted by Bly (1967) but was hindered by electrical noise. Modern transducers and signal recovery methods would probably allow the successful construction of such an instrument. It could be made portable and used with a variety of magnets including large fixed magnets. The possibility of using the instrument with a pulsed magnet and very high fields is attractive and would permit the investigation of the constants K_2° and K_4° for the "c" axis anisotropy of the Terbium Scandium alloys.

There is some similarity between the effects on the magnetic properties of Terbium by dilution with Scandium and those produced by hydrostatic pressure (Wollan 1967). It is suggestive that the pressure which causes the same reduction in the Néel temperature as that caused by 30 at.% of Scandium (Bartholin and Bloch 1968; McWhan and Stevens 1967) is of the same order of magnitude as that pressure which

Tatsumoto et al. (1968) estimated would reduce the effective moment of Terbium ions by one Bohr magneton. A fall in the effective moment of Terbium ions is observed as the proportion of Scandium increases from 10 at % to 30 at % (Chatterjee and Corner 1971). It is possible that this shows a loss of large numbers of 4f electrons to the conduction band. The fact that the actual values of effective moment are higher than that for pure Terbium could be accounted for by the high polarisability of the Scandium d electron gas (Wohlleben 1968). The marked drop in anisotropy could be connected with the presence of increasing numbers of Terbium ions having isotropic 4f shells.

Resistivity measurements on Terbium-Scandium alloys might therefore be of interest. Anisotropy, magnetisation, magnetostriction and neutron diffraction experiments on alloys of Scandium with Dysprosium would allow comparison with the behaviour of an ion which does not lose its anisotropic character when it loses a further electron.

ACKNOWLEDGMENTS

My sincere thanks are due to Professor G.D. Rochester and Professor A. Wolfendale, who allowed me the use of the facilities of the Physics Department of the University, and also to the Principal and Governors of Bede College for timetable concessions to allow me to follow a course of advanced study.

I am particularly grateful to Dr. W.D. Corner who suggested the original problem and agreed to supervise my work, for his advice, patience and encouragement.

I would like to thank Dr. K.N.R. Taylor for the loan of papers and for suggesting the possibility of automating the recording of results. I would also like to thank other members of the Ferromagnetism group and the technical staff of the department for their helpfulness to a part-time student, and Mrs. D.M. Armstrong who undertook the task of typing the work.

REFERENCES

Abramovitz M., Stegun I.A. (1965) Eds., Handbook of Mathematical Functions, Dover Publications, New York.

Alberts H.L., Alberts L. (1971) Journal de Physique, supplement to vol 32 C1-110.

Aldenkamp A.A., Marks C.P., Zjilstra H., (1960) Rev. Sci. Instr. 31 544.

Aubert G., (1968) J. App. Phys. 39 504.

Bagguley D.M.S., Liesegang J., (1966) Proc. Roy. Soc. A300 497.

Bagguley D.M.S., Liesegang J., (1967) J. App. Phys. 37 1220.

Baron R., Hoffman R.W., (1970) J. App. Phys. 41 1623.

Bartholin H., Bloch D., (1968) J. App. Phys. 39 889.

Bates L.F., (1970) Contemporary Physics, 11 301.

Becle C., Lemaire R., Paccard D., (1970) J. App. Phys. 41 855.

Becquerel J., Handel J. van den, (1939) J. Physique et Radium, 10 10.

Behrendt D.R., Legvold S., Spedding F.H., (1958) Phys. Rev. 109 1544.

Belov K.P., Nikitin S.A., Gurtovoi K.G., (1969) Sov. Phys. J.E.T.P., 28 84.

Birss R.R., (1964) Symmetry and Magnetism, Vol III of 'Selected Topics in Solid State Physics', Ed E.P. Wohlfarth, North-Holland Publishing Co. Amsterdam.

Birss R.R., Wallis P.M., (1964) Proc. Int. Conf. Magnetism, Nottingham, 744.

Bjerrum-Møller H., Houmann J.C.G., Mackintosh A.R., (1968) J. App. Phys. 39 807.

Bly P.H., (1967) Ph.D. thesis, Durham, unpublished.

Bly P.H., Corner W.D., Taylor K.N.R., Darby M.I., (1968) J. App. Phys. 39 1336.

Bly P.H., Corner W.D., Taylor K.N.R. (1969) J. App. Phys. 40 4787

Booth A.D., (1957) "Numerical Methods" 2nd Edition, Butterworths, London.

Bozorth R.M.,(1951) "Ferromagnetism" Van-Nostrand, Princeton.

Bozorth R.M.,(1954) Phys. Rev. 96 315.

Bozorth R.M., Gambino R.J., (1966) Phys. Rev. 147 487.

Brailsford F., (1966) "Physical Principles of Magnetism", Van-Nostrand, London.

Broek J.J. van den, Zijlstra H., (1971) I.E.E.E. Transactions on Magnetism, Vol Mag-7 226

Brooks M.S.S., (1972) J. Phys. F. 2 978.

Bucher E., Schmidt P.H., Jayaraman A., Andres K., Maita J.P., Nassau K., Dernier P.D., (1970) Phys. Rev. B2 3911.

Callen E., Callen H.B., (1965) Phys. Rev. 139 A455.

Callen E., Callen H.B., (1966) J. Phys. Chem. Solids. 27 1271.

Campbell I.A., (1972) J. Phys. F. 2 L47.

Capellmann H., (1970) J. Low Temp. Phys. 3 189.

Chatterjee D., Corner W.D., (1971) Journal de Physique 32 C I - 243.

Chatterjee D., (1972) Ph.D. thesis, Durham, unpublished.

Chechernikov V.I., Pop I., Naumkin O.P., (1963) Sov. Phys. J.E.T.P. 17 1228.

Child H.R., Koehler W.C., Wollan E.O., Cable J.W., (1965) Phys. Rev. 138 A 1655.

Child H.R., Koehler W.C., (1966) J. App. Phys. 37 1353.

Child H.R., Koehler W.C., (1968) Phys. Rev. 174 562.

Chikazumi S., (1964) "Physics of Magnetism", John Wiley, New York.

Clark A.E., Bozorth R.M., de Savage B.F., (1963) Physics Letters 5 100.

Clark A.E., de Savage B.F., Callen E.R., (1964) J. App. Phys. 35 1028.

Clark A.E., de Savage B.F., Bozorth R., (1965) Phys. Rev. 138 A 216.

Coleman J.E. (1971) Physics Education 6 284.

Collette R., (1962) Rev. Sci. Instr. 33 450.

Cooper B.R., (1967) Phys. Rev. Letters 19 900.

Cooper B.R., (1968 I) Phys. Rev. 169 281.

Cooper B.R., (1968 II) Solid State Physics, Vol 21, Eds. Seitz, Turnbull and Ehrenreich. Academic Press, New York.

Cooper B.R., (1972) Chapter II of Elliott (1972) below.

Corner W.D., Roe W.C., Taylor K.N.R., (1962) Proc. Phys. Soc. 80 927.

Craft G.T., Donahoe F.J., Love W.F., (1955) Rev. Sci. Instr. 26 360.

Darby M.I., Taylor K.N.R., (1964) Proc. Int. Conf. Magnetism, Nottingham, p 742.

Egami T., (1971) American Institute of Physics Conference Proceedings, Vol 5 part 2, 1457.

Egami T., Graham C.D., (1971) J. App. Phys. 42 1299.

Egami T., (1972) J. Phys. C 5 L 85.

Elliott R.J., Stephens K.W.H., (1953) Proc. Roy. Soc. A219 387.

Elliott R.J., (1961) Phys. Rev. 124 346.

Elliott R.J., (1971) Proc. 9th Rare Earth Research Conf. Blacksburg Va. U.S.A. Virginia Polytechnic Institute and State University.

Elliott R.J., Ed (1972) "Magnetic Properties of Rare Earth Metals", Plenum Press, London and New York.

Enz U., (1960) Physica 26 698.

Feron J-L., (1969) Comptes Rendus Acad. Sc. Paris 269B 611

de Gennes P.G., (1962) J. de Physique et le Radium 23 510.

Harnwell G.P., (1949) "Principles of Electricity and Magnetism" 2nd. Edition, McGraw-Hill (New York) p 426.

Harris F.W., (1956) Journ. Sci. Instr. 33 5.

Hart L.W., Stanford J.L., (1971) Phys. Rev. Letters 27 678.

Hegland D.E., Legvold S., Spedding F.H., (1963) Phys. Rev. 131 158.

Herpin A., Meriel P., Villain J., (1959) Comptes Rendus 249 1334.

Herring C.P., Jakubovics J.P., (1973) J. Phys. F, 3 157.

Isaacs L.L., Lam D.J., Ross J.W., (1971) American Institute of Physics Conf. Proc. 5 pt. 2 1488-92.

Ito T., Fujii H., Okamoto T., Tatsumoto E., (1971) J. Phys. Soc. Japan 30 293.

Jew T.T., Legvold S., (1963) U.S. Atomic Energy Commission Reports IS-867

Jouguet M. (1972) Comptes Rendus Acad. Sc. Paris 274 878

Kaplan T.A., (1959) Phys. Rev. 116 888.

Kaplan T.A., (1961) Phys. Rev. 124 329.

Keffer F., (1955) Phys. Rev. 100 1699.

Keffer F.,Oguchi T., (1960) Phys. Rev. 117 718.

King A.P., Robinson G., Cundall J.A., Hight M.J., (1964) J. Sci. Inst. 41 766.

Kitano Y., Nagamiya T., (1964) Progress of Theoretical Physics 31 1.

Kittel C., Van Vleck J.H., (1960) Phys. Rev. 118 1231.

Koehler W.C., (1961) J. App. Phys. 32 20 S.

Koehler W.C., (1965) J. App. Phys. 36 1078.

Kouvel J.S., Graham C.D., (1957) J. App. Phys. 28 340.

Kouvel J.S., Graham C.D., (1959) J. Phys. Chem. Solids 11 220.

Kyllonen E.W., Mamasse F.K., (1972) Rev. Sci. Instr. 43 351.

Levy P.M., (1970) J. App. Phys. 41 902.

Liu S.H., Behrendt D.R., Legvold S., Good R.H., (1959) Phys. Rev. 116 1464.

Löffler E., Rauch H., (1969) J. Phys. Chem. Solids 30 2175.

McWhan D.B., Stevens A.L., (1967) Phys. Rev. 154 438.

Mackintosh A.R., Bjerrum-Møller H., (1972) Chapter 5 in Elliott (1972).

Marsh H.S., Sievers A.J., (1969) J. App. Phys. 40 1563.

Mason W.P., (1954) Phys. Rev. 96 302.

Meiklejohn W.H., Bean C.P., (1957) Phys. Rev. 105 904.

Miyahara S., Miyadai T., Horiuti S., (1971) Journal de Physique 32 C I - 57.

Morrish A.H., (1965) "Physical Principles of Magnetism" John Wiley, New York.

Nagamiya T., Nagata K., Kitano Y., (1962) Prog. Theoretical Physics 27 1253.

Nicklow R.M., Wakabayashi N., Wilkinson M.K., Reed R.E., (1971) Phys. Rev. Letters 26 140.

Nielsen M., Bjerrum-Moller H., Lindgard P.A., Mackintosh A.R., (1970) Phys. Rev. Letters 25 1451.

Nigh H.E., Legovid S., Spedding F.H., Beaudry B.J., (1964) J. Chem. Phys. 41 3799.

Novak P., Roskovec V., Simsa Z., (1971) Journal de Physique 32 C I - 59.

Palmer S.B., Lee E.W., (1972) Proc. Roy. Soc. Lond. A327 519.

Penoyer R.F., (1959) Rev. Sci. Instr. 30 711.

Phillips J.H., Shephard R.G., (1970) J. Phys. D 3 721.

Rauch H., Zeilinger A., (1972) Atomkernenergie 19 167.

Rhyne J.J., Legvold S., (1965) Phys. Rev. 138 507.

Rhyne J.J., Clark A.E., (1967) J. App. Phys. 38 1379.

Rhyne J.J., Foner S., McNiff E.J., Doclo R., (1968) J. App. Phys. 39 892.

Rhyne J.J., (1972) Chapter 4 in Elliott (1972) above.

Rhyne J.J., McGuire T.R., (1972) I.E.E.E. Transactions Magnetics Mag 8 105.

Roe W.C., (1961) Ph.D. Thesis, University of Durham, unpublished.

Ross J.W., Fradin F.Y., Isaacs L.L., Lam D.J., (1969) Phys. Rev. 183 645.

Rossol F.C., Cooper B.R., Jones R.V., (1965) J. App. Phys. 36 1209.

Salamon M.B., (1971) Phys. Rev. Letters 26 704.

Smith D.H., (1970) Contemp. Phys. 11 287.

Sommerfeld A., (1964) "Lectures on Theoretical Physics", Vol III Electrodynamics, Trans. E.G. Ramberg, Academic Press, New York and London.

Spedding F.H., Ito Y., Jordan R.G., (1970) J. Chem. Phys. 53 1455.

Tajima K., (1971) Journal Phys. Soc. Japan 31 441.

Tannenwald P.E., (1955) Phys. Rev. 100 1713.

Tarasov L.P., (1939) Phys. Rev. 56 1224.

Taylor K.N.R., (1970) Contemporary Physics 11 423.

Tatsumoto E., Fujiwara H., Fujii H., Iwata N., Okamato T., (1968) J. App. Phys. 39 894.

Taylor K.N.R., (1971) Adv. Phys. 20 551-660.

Thoburn W.C., Legvold S., Spedding F.H., (1958) Phys. Rev. 110 1298.

Trombe F., (1953) Comptes Rendus 236 591.

Turov E.A., Shavrov V.G., (1965) Sov. Phys. Solid State 7 166.

Van Vleck J.H., (1937) Phys. Rev. 52 1178.

Van Vleck J.H., (1956) Proceedings of the 6th. Conference on Magnetism and Magnetic Materials, Boston, Massachusetts.

Vigren D.T., Liu S.H., (1971) Phys. Rev. Letters 27 674.

Vigren D.T., Liu S.H., (1972) Phys. Rev. B 5 2719.

Villain J., (1959) Chem. Phys. Solids 11 303.

Vonsovskii S.V.,(Ed) (1964) "Ferromagnetic Resonance". Israel Programme for Scientific Translation, Jerusalem.

Weinstein S., Craig R.S., Wollan W.E., (1963) J. Chem. Phys. 39 1449 and J. App. Phys. 34 1354.

Whitworth R.W., Stopes-Roe H.V., (1971) Nature 234 31.

Wilkinson M.K., Koehler W.C., Wollan E.O., Cable J.W., (1961) J. App. Phys. 32 48 S.

Willey R.J., Lanfear A.R., Leak D.A., (1972) J. Phys E 5 305.

Wohlleben D.K., (1968) Phys. Rev. Letters 21 1343.

Wolf W.P., (1957) Phys. Rev. 108 1152.

Wollan E.O., (1967) Phys. Rev. 160 369.

Yafet Y., Kittel C., (1952) Phys. Rev. 87 290.

Yang J.J.H., (1971) Ph.D. thesis, University of California, Los Angeles.

Yang T.T., Yang J.J., Robinson L.B., (1973) Solid State Communications 13 53.

Yoshimori A., (1959) J. Phys. Soc. Japan 14 807.

Yosida K., (1968) J. App. Phys. 39 511.

Zener C., (1954) Phys. Rev. 96 1335.

Zijlstra H., (1967) 'Experimental methods in Magnetism', Vol IX of 'Selected Topics in Solid State Physics' Ed. E.P. Wohlfarth, North-Holland Publishing Co., Amsterdam.

APPENDIX I

```
KAY4:PROCEDURE OPTIONS (MAIN) ; /* ANALYSIS OF TORQUE CURVES */
     DECLARE(A(2,6),AMP(2,6),AO(2),CALIB,DIFF,DY,HYST,K4,LL,PHASE(2,6),
            PRODS(2,2,6),RCRS(2,36),RMS(2),RS(2,36),SCALE,TRIG(2,6,36),
            WT) DEC FLOAT (6)  ,
             (I,J,K,L,NC,SW) BINARY FIXED (15,0),
             (DATE) CHARACTER (15) ;
     /* THIS SECTION STORES THE SINES AND COSINES OF  2,4,6,8,10,12, */
     /* PHI AT FIVE DEGREE INTERVALS OVER THE RANGE 0 TO 180 DEGS.   */
SETUP:   DO L=1 BY 1 TO 6 ;
              DO J=1 BY 1 TO 36 ;
                   TRIG(1,L,J) = SIND(10*L*(J-1)) ;
                   TRIG(2,L,J) = COSD(10*L*(J-1)) ;
              END ;
         END ;
ON CONVERSION PUT LIST(CNSOURCE,CNCHAR) ;
     /*****************************************************************/
     /* DATA CARDS SHOULD BE OF THE FOLLOWING FORM :-                 */
     /* THE FIRST CARD SHOULD CARRY THE CALIBRATION CONSTANT OF THE   */
     /* MAGNETOMETER IN NM PER VOLT AND THE SPECIMEN'S MASS IN KG     */
     /* CARD NO.2    HAS THE DATE IN SINGLE INVERTED COMMAS,THE       */
     /* NUMBER OF THE GRAPH; THE SCALE FACTOR OF THE X-Y RECORDER IN  */
     /* VOLTS PER INCH, THE DISPLACEMENT DY OF THE END OF THE AXIS    */
     /* OF THE GRATICULE AND LL THE LENGTH OF THE AXIS BETWEEN THE    */
     /* ZERO AND 175 DEGREE MARKS, BOTH IN CMS. CARDS 3 TO 5 CARRY    */
     /* 36 CLOCKWISE READINGS AND CARDS 6 TO 8 CARRY 36 ANTICLOCKWISE */
     /* READINGS STARTING AT THE 0 DEG END OF THE GRATICULE. CARD     */
     /* NO.9 IS THE DATE CARD FOR THE NEXT GRAPH  .DATA ITEMS SHOULD  */
     /* BE SEPARATED BY SPACES AND THE LAST ITEM ON A CARD SHOULD BE  */
     /* BE FOLLOWED BY A COMMA .                                      */
     /*****************************************************************/
GET LIST(CALIB,WT) ;
START:  SW=0 ;
        ON ENDFILE(SCARDS) GO TO LAST ;
        GET LIST(DATE,NO,SCALE,DY,LL,((RS(I,J)DO J=1 TO 36)DO I=1,2));
         PUT EDIT(DATE,' NUMBER ',NO,' SCALE ',SCALE, ' V/INCH ',
         'DY= ',DY,' LL= ',LL) (PAGE,A(16),X(2),A(8),     F(4,0),X(2),
         A(7),     F(5,2),X(1),A(9),X(2),A(4),F(6,2),X(2),A(5),
         F(6,2));
PUT EDIT(' MEASURED VALUES')(SKIP,A(18)) ;
         PUT EDIT('CW.RDGS.',RS(1,*),'ACW.RDGS.',RS(2,*))
        (2(SKIP,A(8),12(X(2),F(6,2)),2(SKIP,X(8),12(X(2),F(6,2)))));
     /* THE NEXT DO GROUP CORRECTS FOR SHEAR IN THE CURVE            */
       IF DY>0.01 THEN DO;
              DO I= 1,2 ;
                   DO J=1 BY 1 TO 36 ;
                   RS(I,J)=(COS(ATAN(DY,LL)))*(RS(I,J)+((J-1)*DY/35));
                   END ;
              END ;
         PUT EDIT ('VALUES CORRECTED FOR SHEAR')(SKIP,A(27)) ;
         PUT EDIT('CW.RDGS.',RS(1,*),'ACW.RDGS.',RS(2,*))
```

```
        (2(SKIP,A(8),12(X(2),F(6,2)),2(SKIP,X(8),12(X(2),F(6,2)))));
                        END;
      /* THE NEXT SECTION DOES THE SUMMATION FOR THE FOURIER ANALYSIS */
CALC:     DO I=1,2 ;
               DO K=1,2 ;
                    DO L=1 BY 1 TO 6 ;
                    PRODS(K,I,L)=(SUM(RS(I,*)*TRIG(K,L,*)))/18  ;
                    END ;
               END;
          END;
      /* THE NEXT SECTION FINDS THE MEAN VALUES AND FINISHES OFF THE  */
      /* CALCULATION OF THE AMPLITUDES AND THE PHASES.                */
          DO I=1,2 ;
         AO(I)=(SUM(RS(I,*)))/36 ;
               DO L=1 BY 1 TO 6 ;
               A(I,L) = SQRT((PRODS(1,I,L))**2 + (PRODS(2,I,L))**2) ;
               AMP(I,L) =(A(I,L)*CALIB*SCALE)/(WT*2.54) ;
               PHASE(I,L) = ATAND(PRODS(2,I,L),PRODS(1,I,L))/(2*L);
               END ;
          END ;
      /* THIS NEXT SECTION FINDS THE WORK NEEDED TO ROTATE THE        */
      /* SPECIMEN THROUGH 360 DEGREES AND THE MEAN K4                 */
               HYST = (AC(2)-AO(1))*SCALE*CALIB*6.2832/(WT*2.54) ;
               K4   = (AMP(1,3)+AMP(2,3))/12 ;
      /* THE NEXT SECTION CALCULATES THE VALUES OF THE ORDINATES      */
      /* USING THE AMPLITUDES AND PHASES OF THE 2,4,6,12 FOLD         */
      /* COMPONENTS ONLY.                                             */
          RORS = 0 ;
               DO I = 1,2 ;
               RORS(I,*) = AO(I) ;
                    DO J=1 BY 1 TO 36 ;
                         DO  L=1,2,3,6 ;
          PORS(I,J)=RORS(I,J)+A(I,L)*SIND(2*L*(5*(J-1)+PHASE(I,L)));
                         END ;
                    END ;
               END;
          PUT EDIT('VALUES CALC FROM 2,4,6,12 FOLD COMPONENTS')
                    (SKIP,A(45)) ;
          PUT EDIT('CW.ROS.',RORS(1,*),'ACW.RS.',RORS(2,*))
         (2(SKIP,A(8),12(X(2),F(6,2)),2(SKIP,X(8),12(X(2),F(6,2)))));
      /* THE NEXT SECTION FINDS THE RMS ERROR.                        */
               DO I=1,2 ;
               RMS(I)=0 ;
                    DO J=1 BY 1 TO 36 ;
                    RMS(I)=RMS(I)+(RS(I,J)-RORS(I,J))**2 ;
                    END ;
               RMS(I)= SQRT(RMS(I)/36) ;
               END ;
          PUT EDIT('MEAN','2FOLD','4FOLD','6FOLD','8FOLD','10FOLD',
                    '12FOLD','AMPS(CW)',AO(1),AMP(1,*),'PHASE(CW)',
                     PHASE(1,*),'AMPS(ACW)',AO(2),AMP(2,*),'PHASE(ACW)',
                    PHASE(2,*))(SKIP,X(18),7(X(4),A(7)),2(SKIP,A(18) ,
                    7(X(1),E(10,3)),SKIP,A(18),X(11),6(X(1),E(10,3))));
          PUT SKIP EDIT('HYSTERESIS ESTIMATE = ',HYST,' JKG-1 PER REV ',
                         'MEAN K4= ',K4,' JKG-1','RMS ERROR = ',
                          RMS)(X(5),A(22),E(10,3),X(2),A(14),SKIP,X(17),
                          A(10),E(10,3),X(9),A(7),SKIP,X(16),A(12),
                          E(10,3),X(3),E(10,3));
      /* THIS SECTION EXCHANGES THE FIRST AND LAST  TWELVE  RDGS.     */
      /* OF THE CW. AND ACW. CURVES WITH SUITABLE DISPLACEMENT.       */
```

```
      IF SW=1 THEN GO TC START;
      DIFF = 0 ;
         DO J = 13 BY 1 TO 24 ;
              DIFF = DIFF + (RS(2,J) - RS(1,J)) ;
         END;
         DO J = 1 BY 1 TO 12  ;
              RS(1,J) = RS(2,J) - DIFF/12 ;
              RS(2,(24+J)) = RS(1,(24+J)) + DIFF/12 ;
         END ;
PUT EDIT('VALUES RESHAPED')(SKIP,A(16));
         PUT EDIT('CW.RDGS.',RS(1,*),'ACW.RDCS.',RS(2,*))
        (2(SKIP,A(8),12(X(2),F(6,2)),2(SKIP,X(8),12(X(2),F(6,2)))));
              SW = SW + 1 ;
              GO TO CALC ;
LAST: END KAY4 ;
```

APPENDIX II

NORMALISED HYPERBOLIC BESSEL FUNCTIONS OF Z FROM 0 TO 150

Z	ORDER				
	3/2	5/2	9/2	13/2	(5/2)X(9/2)
0.05	0.016663	0.000166	0.000000	0.000000	0.000000
0.10	0.033311	0.000666	0.000000	0.000000	0.000000
0.15	0.049925	0.001496	0.000000	0.000000	0.000000
0.20	0.066489	0.002656	0.000001	0.000000	0.000000
0.25	0.082988	0.004142	0.000004	0.000000	0.000000
0.30	0.099405	0.005949	0.000008	0.000000	0.000000
0.35	0.115724	0.008072	0.000015	0.000000	0.000000
0.40	0.131932	0.010506	0.000026	0.000000	0.000000
0.45	0.148013	0.013244	0.000042	0.000000	0.000000
0.50	0.163953	0.016279	0.000064	0.000000	0.000001
0.55	0.179739	0.019602	0.000093	0.000000	0.000001
0.60	0.195358	0.023205	0.000131	0.000000	0.000003
0.65	0.210799	0.027079	0.000179	0.000000	0.000004
0.70	0.226050	0.031213	0.000239	0.000000	0.000007
0.75	0.241100	0.035597	0.000313	0.000001	0.000011
0.80	0.255940	0.040222	0.000401	0.000001	0.000016
0.85	0.270561	0.045075	0.000507	0.000002	0.000022
0.90	0.284956	0.050146	0.000631	0.000003	0.000031
0.95	0.299116	0.055422	0.000775	0.000004	0.000042
1.00	0.313035	0.060894	0.000942	0.000006	0.000057
1.05	0.326708	0.066548	0.001132	0.000008	0.000075
1.10	0.340129	0.072373	0.001347	0.000011	0.000097
1.15	0.353296	0.078357	0.001590	0.000014	0.000124
1.20	0.366204	0.084489	0.001861	0.000018	0.000157
1.25	0.378850	0.090757	0.002163	0.000023	0.000196
1.30	0.391234	0.097150	0.002496	0.000028	0.000242
1.35	0.403354	0.103657	0.002863	0.000035	0.000296
1.40	0.415208	0.110266	0.003265	0.000043	0.000360
1.45	0.426798	0.116967	0.003702	0.000053	0.000433
1.50	0.438124	0.123750	0.004177	0.000063	0.000516
1.55	0.449187	0.130604	0.004689	0.000076	0.000612
1.60	0.459988	0.137521	0.005241	0.000091	0.000720
1.65	0.470530	0.144489	0.005834	0.000107	0.000843
1.70	0.480815	0.151501	0.006468	0.000126	0.000979
1.75	0.490846	0.158548	0.007143	0.000147	0.001132
1.80	0.500627	0.165621	0.007861	0.000171	0.001302
1.85	0.510160	0.172713	0.008623	0.000198	0.001489
1.90	0.519449	0.179816	0.009428	0.000228	0.001695
1.95	0.528499	0.186923	0.010277	0.000261	0.001921
2.00	0.537314	0.194027	0.011170	0.000298	0.002167
2.05	0.545899	0.201123	0.012108	0.000338	0.002435
2.10	0.554257	0.208203	0.013091	0.000383	0.002725
2.15	0.562394	0.215264	0.014119	0.000432	0.003039
2.20	0.570314	0.222298	0.015192	0.000485	0.003377
2.25	0.578023	0.229302	0.016309	0.000544	0.003739
2.30	0.585525	0.236271	0.017471	0.000607	0.004127
2.35	0.592825	0.243201	0.018677	0.000676	0.004542
2.40	0.599929	0.250088	0.019927	0.000750	0.004983
2.45	0.606841	0.256928	0.021221	0.000830	0.005452
2.50	0.613567	0.263719	0.022558	0.000917	0.005949

NORMALISED HYPERBOLIC BESSEL FUNCTIONS OF Z FROM 0 TO 15C

Z	ORDER				
	3/2	5/2	9/2	13/2	(5/2)X(9/2)
2.60	0.626478	0.277139	0.025360	0.001108	0.C07028
2.70	0.638703	0.290329	0.028328	0.001328	0.008224
2.80	0.650280	0.303271	0.031459	0.001576	0.009540
2.90	0.661245	0.315952	0.034745	0.001856	0.010977
3.00	0.671636	0.328363	0.038180	0.002169	0.012537
3.10	0.681486	0.340496	0.041759	0.002517	0.014219
3.20	0.690828	0.352348	0.045475	0.002901	0.016023
3.30	0.699694	0.363914	0.049320	0.003324	0.017948
3.40	0.708112	0.375194	0.053287	0.003786	0.019993
3.50	0.716111	0.386190	0.057369	0.004289	0.022155
3.60	0.723716	0.396902	0.061559	0.004834	0.024433
3.70	0.730952	0.407335	0.065849	0.005422	0.026822
3.80	0.737843	0.417491	0.070233	0.006055	0.029321
3.90	0.744409	0.427377	0.074702	0.006732	0.031926
4.00	0.750671	0.436996	0.079252	0.007455	0.034632
4.10	0.756647	0.446355	0.083874	0.008225	0.037437
4.20	0.762354	0.455461	0.088562	0.009041	0.040336
4.30	0.767810	0.464318	0.093310	0.009905	0.043325
4.40	0.773028	0.472934	0.098112	0.010816	0.046400
4.50	0.778024	0.481316	0.102962	0.011775	0.049557
4.60	0.782810	0.489471	0.107854	0.012781	0.052791
4.70	0.787399	0.497404	0.112783	0.013835	0.056098
4.80	0.791802	0.505123	0.117744	0.014937	0.059475
4.90	0.796029	0.512635	0.122731	0.016085	0.062916
5.00	0.800090	0.519945	0.127742	0.017281	0.066418
5.10	0.803995	0.527061	0.132770	0.018523	0.069977
5.20	0.807753	0.533988	0.137811	0.019811	0.073589
5.30	0.811370	0.540733	0.142863	0.021145	0.077251
5.40	0.814855	0.547302	0.147921	0.022523	0.080957
5.50	0.818215	0.553700	0.152981	0.023946	0.084705
5.60	0.821455	0.559934	0.158041	0.025412	0.088492
5.70	0.824583	0.566008	0.163097	0.026921	0.092314
5.80	0.827604	0.571928	0.168146	0.028472	0.096167
5.90	0.830523	0.577699	0.173186	0.030065	0.100049
6.00	0.833345	0.583327	0.178214	0.031697	0.103957
6.10	0.836075	0.588815	0.183228	0.033369	0.107887
6.20	0.838717	0.594168	0.188225	0.035079	0.111837
6.30	0.841276	0.599392	0.193204	0.036827	0.115805
6.40	0.843755	0.604489	0.198163	0.038611	0.119787
6.50	0.846158	0.609465	0.203100	0.040431	0.123782
6.60	0.848488	0.614323	0.208013	0.042285	0.127787
6.70	0.850749	0.619067	0.212901	0.044172	0.131800
6.80	0.852943	0.623701	0.217763	0.046092	0.135819
6.90	0.855074	0.628228	0.222597	0.048044	0.139841
7.00	0.857144	0.632652	0.227402	0.050026	0.143866
7.10	0.859156	0.636976	0.232177	0.052037	0.147891
7.20	0.861112	0.641203	0.236921	0.054077	0.151915
7.30	0.863014	0.645336	0.241634	0.056145	0.155935
7.40	0.864865	0.649378	0.246314	0.058238	0.159951
7.50	0.866667	0.653333	0.250961	0.060357	0.163961

NORMALISED HYPERBOLIC BESSEL FUNCTIONS OF Z FROM 0 TO 150

Z	ORDER				
	3/2	5/2	9/2	13/2	(5/2)X(9/2)
7.65	0.869281	0.659105	0.257869	0.063581	0.169962
7.80	0.871795	0.664694	0.264698	0.066857	0.175943
7.95	0.874214	0.670107	0.271449	0.070181	0.181900
8.10	0.876543	0.675354	0.278118	0.073550	0.187828
8.25	0.878788	0.680440	0.284707	0.076961	0.193726
8.40	0.880952	0.685374	0.291214	0.080412	0.199590
8.55	0.883041	0.690161	0.297638	0.083898	0.205418
8.70	0.885057	0.694807	0.303980	0.087418	0.211207
8.85	0.887005	0.699320	0.310239	0.090969	0.216956
9.00	0.888888	0.703703	0.316415	0.094548	0.222662
9.15	0.890710	0.707963	0.322508	0.098152	0.228324
9.30	0.892473	0.712105	0.328519	0.101780	0.233940
9.45	0.894179	0.716133	0.334449	0.105428	0.239510
9.60	0.895833	0.720052	0.340297	0.109094	0.245031
9.75	0.897435	0.723865	0.346065	0.112776	0.250504
9.90	0.898989	0.727578	0.351752	0.116473	0.255927
10.05	0.900497	0.731194	0.357360	0.120182	0.261300
10.20	0.901960	0.734717	0.362890	0.123901	0.266621
10.35	0.903381	0.738150	0.368342	0.127628	0.271892
10.50	0.904761	0.741496	0.373717	0.131362	0.277110
10.65	0.906103	0.744759	0.379017	0.135101	0.282276
10.80	0.907407	0.747942	0.384241	0.138844	0.287390
10.95	0.908675	0.751047	0.389392	0.142588	0.292452
11.10	0.909909	0.754078	0.394470	0.146332	0.297461
11.25	0.911111	0.757037	0.399476	0.150076	0.302418
11.40	0.912280	0.759926	0.404412	0.153817	0.307323
11.55	0.913419	0.762748	0.409277	0.157555	0.312175
11.70	0.914529	0.765505	0.414074	0.161289	0.316976
11.85	0.915611	0.768199	0.418803	0.165016	0.321724
12.00	0.916666	0.770833	0.423466	0.168737	0.326422
12.15	0.917695	0.773408	0.428063	0.172450	0.331067
12.30	0.918699	0.775927	0.432595	0.176154	0.335662
12.45	0.919678	0.778390	0.437065	0.179849	0.340207
12.60	0.920634	0.780801	0.441471	0.183533	0.344701
12.75	0.921568	0.783160	0.445816	0.187206	0.349146
12.90	0.922480	0.785469	0.450101	0.190867	0.353541
13.05	0.923371	0.787730	0.454327	0.194516	0.357887
13.20	0.924242	0.789944	0.458494	0.198151	0.362185
13.35	0.925093	0.792113	0.462604	0.201773	0.366435
13.50	0.925925	0.794238	0.466657	0.205380	0.370637
13.65	0.926739	0.796320	0.470655	0.208972	0.374792
13.80	0.927536	0.798361	0.474599	0.212549	0.378901
13.95	0.928315	0.800362	0.478489	0.216109	0.382964
14.10	0.929078	0.802323	0.482326	0.219654	0.386982
14.25	0.929824	0.804247	0.486112	0.223181	0.390954
14.40	0.930555	0.806134	0.489847	0.226692	0.394882
14.55	0.931271	0.807985	0.493532	0.230185	0.398766
14.70	0.931972	0.809801	0.497168	0.233660	0.402607
14.85	0.932659	0.811583	0.500755	0.237118	0.406405
15.00	0.933333	0.813333	0.504296	0.240557	0.410160

NORMALISED HYPERBOLIC BESSEL FUNCTIONS OF Z FROM 0 TO 150

Z	ORDER				
	3/2	5/2	9/2	13/2	(5/2)X(9/2)
15.20	0.934210	0.815616	0.508944	0.245113	0.415103
15.40	0.935064	0.817844	0.513512	0.249636	0.419973
15.60	0.935897	0.820019	0.518000	0.254125	0.424770
15.80	0.936708	0.822143	0.522412	0.258579	0.429498
16.00	0.937500	0.824218	0.526748	0.262999	0.434156
16.20	0.938271	0.826245	0.531011	0.267384	0.438745
16.40	0.939024	0.828227	0.535202	0.271733	0.443268
16.60	0.939759	0.830164	0.539322	0.276047	0.447726
16.80	0.940476	0.832057	0.543374	0.280326	0.452119
17.00	0.941176	0.833910	0.547359	0.284569	0.456448
17.20	0.941860	0.835722	0.551278	0.288776	0.460715
17.40	0.942528	0.837496	0.555133	0.292947	0.464921
17.60	0.943181	0.839230	0.558926	0.297083	0.469068
17.80	0.943820	0.840929	0.562657	0.301182	0.473155
18.00	0.944444	0.842592	0.566329	0.305246	0.477184
18.20	0.945054	0.844221	0.569942	0.309275	0.481157
18.40	0.945652	0.845817	0.573498	0.313267	0.485075
18.60	0.946236	0.847381	0.576998	0.317224	0.488937
18.80	0.946808	0.848913	0.580443	0.321146	0.492746
19.00	0.947368	0.850415	0.583835	0.325033	0.496502
19.20	0.947916	0.851888	0.587174	0.328885	0.500207
19.40	0.948453	0.853331	0.590462	0.332701	0.503860
19.60	0.948979	0.854748	0.593701	0.336484	0.507464
19.80	0.949494	0.856137	0.596890	0.340231	0.511019
20.00	0.950000	0.857499	0.600031	0.343945	0.514526
20.20	0.950495	0.858837	0.603125	0.347624	0.517986
20.40	0.950980	0.860149	0.606173	0.351270	0.521400
20.60	0.951456	0.861438	0.609176	0.354882	0.524768
20.80	0.951923	0.862703	0.612136	0.358461	0.528092
21.00	0.952380	0.863945	0.615052	0.362007	0.531371
21.20	0.952830	0.865165	0.617926	0.365520	0.534608
21.40	0.953271	0.866363	0.620758	0.369001	0.537803
21.60	0.953703	0.867541	0.623550	0.372449	0.540956
21.80	0.954128	0.868697	0.626303	0.375866	0.544068
22.00	0.954545	0.869834	0.629016	0.379251	0.547140
22.20	0.954954	0.870952	0.631692	0.382605	0.550173
22.40	0.955357	0.872050	0.634330	0.385928	0.553168
22.60	0.955752	0.873130	0.636932	0.389220	0.556124
22.80	0.956140	0.874192	0.639498	0.392481	0.559044
23.00	0.956521	0.875236	0.642028	0.395712	0.561926
23.20	0.956896	0.876263	0.644525	0.398914	0.564773
23.40	0.957264	0.877273	0.646987	0.402086	0.567585
23.60	0.957627	0.878267	0.649417	0.405229	0.570362
23.80	0.957983	0.879245	0.651814	0.408342	0.573104
24.00	0.958333	0.880208	0.654179	0.411427	0.575814
24.20	0.958677	0.881155	0.656513	0.414484	0.578490
24.40	0.959016	0.882088	0.658816	0.417513	0.581134
24.60	0.959349	0.883006	0.661089	0.420514	0.583746
24.80	0.959677	0.883909	0.663333	0.423487	0.586327
25.00	0.960000	0.884799	0.665548	0.426434	0.588877

NORMALISED HYPERBOLIC BESSEL FUNCTIONS OF Z FROM 0 TO 150

Z	ORDER				
	3/2	5/2	9/2	13/2	(5/2)X(9/2)
25.25	0.960396	0.885893	0.668277	0.430079	0.592022
25.50	0.960784	0.886966	0.670963	0.433682	0.595121
25.75	0.961165	0.888019	0.673606	0.437245	0.598175
26.00	0.961538	0.889053	0.676208	0.440768	0.601185
26.25	0.961904	0.890068	0.678769	0.444251	0.604151
26.50	0.962264	0.891064	0.681291	0.447694	0.607075
26.75	0.962616	0.892042	0.683775	0.451099	0.609957
27.00	0.962962	0.893004	0.686221	0.454466	0.612798
27.25	0.963302	0.893948	0.688629	0.457796	0.615599
27.50	0.963636	0.894876	0.691002	0.461088	0.618361
27.75	0.963963	0.895787	0.693339	0.464344	0.621085
28.00	0.964285	0.896683	0.695642	0.467563	0.623771
28.25	0.964601	0.897564	0.697911	0.470748	0.626420
28.50	0.964912	0.898430	0.700147	0.473897	0.629033
28.75	0.965217	0.899281	0.702351	0.477012	0.631611
29.00	0.965517	0.900118	0.704523	0.480093	0.634154
29.25	0.965811	0.900942	0.706664	0.483140	0.636663
29.50	0.966101	0.901752	0.708774	0.486155	0.639139
29.75	0.966386	0.902549	0.710855	0.489136	0.641582
30.00	0.966666	0.903333	0.712907	0.492086	0.643993
30.25	0.966942	0.904104	0.714930	0.495004	0.646372
30.50	0.967213	0.904864	0.716925	0.497891	0.648720
30.75	0.967479	0.905611	0.718893	0.500747	0.651038
31.00	0.967741	0.906347	0.720834	0.503573	0.653326
31.25	0.967999	0.907071	0.722749	0.506369	0.655585
31.50	0.968253	0.907785	0.724638	0.509135	0.657816
31.75	0.968503	0.908487	0.726502	0.511873	0.660018
32.00	0.968749	0.909179	0.728341	0.514581	0.662192
32.25	0.968992	0.909861	0.730155	0.517262	0.664340
32.50	0.969230	0.910532	0.731946	0.519915	0.666461
32.75	0.969465	0.911193	0.733714	0.522540	0.668555
33.00	0.969696	0.911845	0.735458	0.525139	0.670624
33.25	0.969924	0.912487	0.737180	0.527710	0.672668
33.50	0.970149	0.913120	0.738881	0.530256	0.674687
33.75	0.970370	0.913744	0.740559	0.532775	0.676682
34.00	0.970588	0.914359	0.742216	0.535269	0.678653
34.25	0.970802	0.914966	0.743853	0.537738	0.680600
34.50	0.971014	0.915563	0.745469	0.540182	0.682524
34.75	0.971223	0.916153	0.747065	0.542601	0.684426
35.00	0.971428	0.916734	0.748641	0.544997	0.686305
35.25	0.971631	0.917307	0.750198	0.547368	0.688162
35.50	0.971830	0.917873	0.751736	0.549716	0.689998
35.75	0.972027	0.918431	0.753255	0.552041	0.691813
36.00	0.972222	0.918981	0.754756	0.554343	0.693607
36.25	0.972413	0.919524	0.756239	0.556622	0.695380
36.50	0.972602	0.920060	0.757704	0.558880	0.697133
36.75	0.972789	0.920588	0.759152	0.561115	0.698867
37.00	0.972972	0.921110	0.760583	0.563329	0.700581
37.25	0.973154	0.921625	0.761997	0.565521	0.702276
37.50	0.973333	0.922133	0.763395	0.567692	0.703952

NORMALISED HYPERBOLIC BESSEL FUNCTIONS OF Z FROM 0 TO 150

Z	ORDER				
	3/2	5/2	9/2	13/2	(5/2)X(9/2)
37.80	0.973544	0.922734	0.765051	0.570271	0.705939
38.10	0.973753	0.923326	0.766684	0.572819	0.707899
38.40	0.973958	0.923909	0.768294	0.575339	0.709834
38.70	0.974160	0.924483	0.769883	0.577831	0.711744
39.00	0.974358	0.925049	0.771450	0.580294	0.713630
39.30	0.974554	0.925606	0.772997	0.582730	0.715491
39.60	0.974747	0.926155	0.774522	0.585139	0.717328
39.90	0.974937	0.926696	0.776028	0.587521	0.719142
40.20	0.975124	0.927229	0.777513	0.589876	0.720933
40.50	0.975308	0.927754	0.778979	0.592206	0.722702
40.80	0.975490	0.928272	0.780426	0.594511	0.724448
41.10	0.975669	0.928783	0.781855	0.596790	0.726173
41.40	0.975845	0.929286	0.783265	0.599044	0.727877
41.70	0.976019	0.929782	0.784657	0.601275	0.729560
42.00	0.976190	0.930272	0.786031	0.603481	0.731223
42.30	0.976359	0.930754	0.787388	0.605664	0.732865
42.60	0.976525	0.931230	0.788728	0.607824	0.734488
42.90	0.976689	0.931700	0.790051	0.609960	0.736091
43.20	0.976851	0.932163	0.791358	0.612075	0.737675
43.50	0.977011	0.932619	0.792649	0.614167	0.739241
43.80	0.977168	0.933070	0.793924	0.616237	0.740788
44.10	0.977324	0.933515	0.795184	0.618286	0.742317
44.40	0.977477	0.933954	0.796429	0.620314	0.743828
44.70	0.977628	0.934387	0.797658	0.622320	0.745322
45.00	0.977777	0.934814	0.798873	0.624307	0.746798
45.30	0.977924	0.935236	0.800073	0.626273	0.748258
45.60	0.978070	0.935653	0.801259	0.628219	0.749701
45.90	0.978213	0.936064	0.802432	0.630145	0.751128
46.20	0.978354	0.936470	0.803590	0.632052	0.752539
46.50	0.978494	0.936871	0.804736	0.633940	0.753934
46.80	0.978632	0.937267	0.805868	0.635809	0.755313
47.10	0.978768	0.937658	0.806987	0.637659	0.756677
47.40	0.978902	0.938044	0.808093	0.639492	0.758027
47.70	0.979035	0.938425	0.809186	0.641306	0.759361
48.00	0.979166	0.938802	0.810268	0.643102	0.760681
48.30	0.979296	0.939174	0.811337	0.644881	0.761987
48.60	0.979423	0.939541	0.812394	0.646643	0.763278
48.90	0.979550	0.939904	0.813440	0.648388	0.764556
49.20	0.979674	0.940263	0.814474	0.650115	0.765820
49.50	0.979797	0.940618	0.815497	0.651827	0.767071
49.80	0.979919	0.940968	0.816508	0.653522	0.768308
50.10	0.980039	0.941314	0.817509	0.655201	0.769533
50.40	0.980158	0.941657	0.818498	0.656864	0.770745
50.70	0.980276	0.941995	0.819477	0.658511	0.771944
51.00	0.980392	0.942329	0.820446	0.660143	0.773131
51.30	0.980506	0.942660	0.821404	0.661760	0.774305
51.60	0.980620	0.942987	0.822353	0.663362	0.775468
51.90	0.980732	0.943310	0.823291	0.664949	0.776619
52.20	0.980842	0.943629	0.824219	0.666521	0.777758
52.50	0.980952	0.943945	0.825138	0.668079	0.778885

NORMALISED HYPERBOLIC BESSEL FUNCTIONS OF Z FROM 0 TO 150

Z	ORDER				
	3/2	5/2	9/2	13/2	(5/2)X(9/2)
52.85	0.981078	0.944309	0.826198	0.669878	0.780187
53.20	0.981203	0.944669	0.827245	0.671659	0.781473
53.55	0.981325	0.945023	0.828280	0.673421	0.782744
53.90	0.981447	0.945374	0.829302	0.675164	0.784001
54.25	0.981566	0.945719	0.830312	0.676889	0.785243
54.60	0.981684	0.946061	0.831311	0.678596	0.786471
54.95	0.981801	0.946398	0.832298	0.680286	0.787685
55.30	0.981916	0.946731	0.833273	0.681958	0.788886
55.65	0.982030	0.947060	0.834237	0.683613	0.790073
56.00	0.982142	0.947385	0.835190	0.685251	0.791247
56.35	0.982253	0.947706	0.836133	0.686872	0.792408
56.70	0.982363	0.948023	0.837064	0.688478	0.793556
57.05	0.982471	0.948336	0.837985	0.690067	0.794692
57.40	0.982578	0.948645	0.838896	0.691640	0.795815
57.75	0.982683	0.948951	0.839797	0.693197	0.796926
58.10	0.982788	0.949253	0.840687	0.694739	0.798025
58.45	0.982891	0.949552	0.841568	0.696266	0.799113
58.80	0.982993	0.949847	0.842439	0.697778	0.800189
59.15	0.983093	0.950138	0.843301	0.699275	0.801253
59.50	0.983193	0.950427	0.844153	0.700758	0.802306
59.85	0.983291	0.950712	0.844996	0.702226	0.803348
60.20	0.983388	0.950993	0.845830	0.703680	0.804379
60.55	0.983484	0.951272	0.846656	0.705120	0.805400
60.90	0.983579	0.951547	0.847472	0.706547	0.806410
61.25	0.983673	0.951820	0.848280	0.707959	0.807410
61.60	0.983766	0.952089	0.849079	0.709359	0.808399
61.95	0.983857	0.952355	0.849870	0.710745	0.809378
62.30	0.983948	0.952618	0.850653	0.712119	0.810348
62.65	0.984038	0.952879	0.851427	0.713479	0.811307
63.00	0.984126	0.953136	0.852194	0.714827	0.812257
63.35	0.984214	0.953391	0.852953	0.716162	0.813198
63.70	0.984301	0.953643	0.853704	0.717485	0.814129
64.05	0.984387	0.953892	0.854447	0.718796	0.815051
64.40	0.984472	0.954139	0.855183	0.720095	0.815964
64.75	0.984555	0.954383	0.855912	0.721382	0.816868
65.10	0.984639	0.954624	0.856633	0.722658	0.817763
65.45	0.984721	0.954863	0.857347	0.723922	0.818650
65.80	0.984802	0.955100	0.858054	0.725174	0.819528
66.15	0.984882	0.955334	0.858754	0.726416	0.820397
66.50	0.984962	0.955565	0.859448	0.727646	0.821259
66.85	0.985041	0.955794	0.860134	0.728866	0.822112
67.20	0.985119	0.956021	0.860814	0.730075	0.822957
67.55	0.985196	0.956245	0.861487	0.731273	0.823794
67.90	0.985272	0.956468	0.862154	0.732460	0.824623
68.25	0.985347	0.956688	0.862815	0.733638	0.825444
68.60	0.985422	0.956905	0.863469	0.734805	0.826258
68.95	0.985496	0.957121	0.864117	0.735962	0.827064
69.30	0.985569	0.957334	0.864759	0.737109	0.827863
69.65	0.985642	0.957545	0.865394	0.738246	0.828655
70.00	0.985714	0.957755	0.866024	0.739374	0.829439

NORMALISED HYPERBOLIC BESSEL FUNCTIONS OF Z FROM 0 TO 150

Z	ORDER				
	3/2	5/2	9/2	13/2	(5/2)X(9/2)
70.40	0.985795	0.957991	0.866737	0.740651	0.830327
70.80	0.985875	0.958225	0.867442	0.741915	0.831205
71.20	0.985955	0.958456	0.868140	0.743168	0.832075
71.60	0.986033	0.958685	0.868830	0.744408	0.832935
72.00	0.986111	0.958912	0.869514	0.745637	0.833787
72.40	0.986187	0.959135	0.870190	0.746854	0.834630
72.80	0.986263	0.959357	0.870859	0.748059	0.835465
73.20	0.986338	0.959576	0.871522	0.749253	0.836292
73.60	0.986413	0.959792	0.872177	0.750436	0.837110
74.00	0.986486	0.960007	0.872826	0.751608	0.837920
74.40	0.986559	0.960219	0.873469	0.752770	0.838722
74.80	0.986631	0.960429	0.874105	0.753920	0.839516
75.20	0.986702	0.960636	0.874735	0.755060	0.840302
75.60	0.986772	0.960842	0.875358	0.756189	0.841081
76.00	0.986842	0.961045	0.875975	0.757308	0.841852
76.40	0.986910	0.961246	0.876587	0.758417	0.842616
76.80	0.986979	0.961446	0.877192	0.759516	0.843373
77.20	0.987046	0.961643	0.877791	0.760605	0.844122
77.60	0.987113	0.961838	0.878385	0.761685	0.844864
78.00	0.987179	0.962031	0.878972	0.762754	0.845599
78.40	0.987244	0.962222	0.879555	0.763815	0.846327
78.80	0.987309	0.962412	0.880131	0.764866	0.847049
79.20	0.987373	0.962599	0.880702	0.765907	0.847763
79.60	0.987437	0.962785	0.881268	0.766940	0.848472
80.00	0.987500	0.962968	0.881828	0.767963	0.849173
80.40	0.987562	0.963150	0.882383	0.768978	0.849868
80.80	0.987623	0.963330	0.882933	0.769984	0.850557
81.20	0.987684	0.963509	0.883478	0.770981	0.851239
81.60	0.987745	0.963685	0.884018	0.771970	0.851915
82.00	0.987804	0.963860	0.884553	0.772950	0.852586
82.40	0.987864	0.964034	0.885083	0.773922	0.853250
82.80	0.987922	0.964205	0.885608	0.774885	0.853908
83.20	0.987980	0.964375	0.886128	0.775841	0.854560
83.60	0.988038	0.964544	0.886643	0.776788	0.855207
84.00	0.988095	0.964710	0.887154	0.777728	0.855847
84.40	0.988151	0.964876	0.887661	0.778660	0.856482
84.80	0.988207	0.965039	0.888163	0.779584	0.857112
85.20	0.988262	0.965202	0.888660	0.780500	0.857736
85.60	0.988317	0.965362	0.889153	0.781409	0.858355
86.00	0.988372	0.965521	0.889642	0.782310	0.858968
86.40	0.988425	0.965679	0.890126	0.783204	0.859577
86.80	0.988479	0.965835	0.890606	0.784091	0.860179
87.20	0.988532	0.965990	0.891082	0.784971	0.860777
87.60	0.988584	0.966144	0.891554	0.785843	0.861370
88.00	0.988636	0.966296	0.892022	0.786709	0.861957
88.40	0.988687	0.966447	0.892486	0.787567	0.862540
88.80	0.988738	0.966596	0.892945	0.788419	0.863118
89.20	0.988789	0.966744	0.893401	0.789264	0.863691
89.60	0.988839	0.966891	0.893853	0.790102	0.864259
90.00	0.988888	0.967037	0.894302	0.790934	0.864823

NORMALISED HYPERBOLIC BESSEL FUNCTIONS OF Z FROM 0 TO 150

Z	ORDER				
	3/2	5/2	9/2	13/2	(5/2)X(9/2)
90.45	0.988944	0.967199	0.894801	0.791862	0.865451
90.90	0.988998	0.967359	0.895296	0.792781	0.866074
91.35	0.989053	0.967518	0.895787	0.793693	0.866690
91.80	0.989106	0.967676	0.896273	0.794597	0.867302
92.25	0.989159	0.967832	0.896754	0.795493	0.867907
92.70	0.989212	0.967986	0.897231	0.796381	0.868508
93.15	0.989264	0.968139	0.897703	0.797261	0.869102
93.60	0.989316	0.968291	0.898172	0.798134	0.869692
94.05	0.989367	0.968441	0.898636	0.799000	0.870276
94.50	0.989417	0.968589	0.899095	0.799858	0.870855
94.95	0.989468	0.968737	0.899551	0.800709	0.871428
95.40	0.989517	0.968883	0.900002	0.801552	0.871997
95.85	0.989567	0.969027	0.900450	0.802389	0.872561
96.30	0.989615	0.969170	0.900893	0.803218	0.873120
96.75	0.989664	0.969312	0.901333	0.804041	0.873674
97.20	0.989711	0.969453	0.901769	0.804857	0.874223
97.65	0.989759	0.969592	0.902201	0.805666	0.874767
98.10	0.989806	0.969730	0.902629	0.806469	0.875307
98.55	0.989852	0.969867	0.903053	0.807265	0.875842
99.00	0.989898	0.970003	0.903474	0.808054	0.876372
99.45	0.989944	0.970137	0.903891	0.808837	0.876898
99.90	0.989989	0.970270	0.904304	0.809614	0.877420
100.35	0.990034	0.970402	0.904714	0.810384	0.877937
100.80	0.990079	0.970533	0.905121	0.811149	0.878450
101.25	0.990123	0.970663	0.905523	0.811907	0.878958
101.70	0.990167	0.970791	0.905923	0.812659	0.879462
102.15	0.990210	0.970918	0.906319	0.813405	0.879963
102.60	0.990253	0.971045	0.906712	0.814145	0.880458
103.05	0.990295	0.971170	0.907102	0.814880	0.880950
103.50	0.990338	0.971294	0.907488	0.815609	0.881438
103.95	0.990379	0.971417	0.907871	0.816332	0.881922
104.40	0.990421	0.971539	0.908251	0.817049	0.882402
104.85	0.990462	0.971660	0.908628	0.817761	0.882878
105.30	0.990503	0.971780	0.909002	0.818467	0.883351
105.75	0.990543	0.971899	0.909373	0.819168	0.883819
106.20	0.990583	0.972017	0.909741	0.819863	0.884284
106.65	0.990623	0.972134	0.910105	0.820554	0.884745
107.10	0.990662	0.972250	0.910467	0.821239	0.885202
107.55	0.990701	0.972365	0.910826	0.821918	0.885656
108.00	0.990740	0.972479	0.911182	0.822593	0.886106
108.45	0.990779	0.972592	0.911536	0.823263	0.886553
108.90	0.990817	0.972704	0.911886	0.823927	0.886996
109.35	0.990855	0.972816	0.912234	0.824587	0.887436
109.80	0.990892	0.972926	0.912579	0.825241	0.887872
110.25	0.990929	0.973035	0.912921	0.825891	0.888305
110.70	0.990966	0.973144	0.913261	0.826536	0.888735
111.15	0.991003	0.973252	0.913598	0.827177	0.889161
111.60	0.991039	0.973359	0.913932	0.827812	0.889584
112.05	0.991075	0.973465	0.914264	0.828443	0.890004
112.50	0.991111	0.973570	0.914593	0.829069	0.890421

NORMALISED HYPERBOLIC BESSEL FUNCTIONS OF Z FROM 0 TO 150

Z	ORDER				
	3/2	5/2	9/2	13/2	(5/2)X(9/2)
113.00	C.991150	0.973686	0.914956	0.829760	0.890880
113.50	C.991189	0.973801	0.915316	0.830445	0.891336
114.00	C.991228	0.973915	C.915673	0.831125	0.891787
114.50	C.991266	0.974027	0.916026	0.831799	0.892235
115.00	C.991304	0.974139	0.916377	0.832468	0.892680
115.50	C.991341	0.974250	0.916725	0.833131	0.893120
116.00	0.991379	0.974360	0.917070	0.833790	0.893557
116.50	C.991416	0.974469	C.917412	0.834443	0.893991
117.00	C.991452	0.974578	0.917752	0.835091	0.894421
117.50	0.991489	0.974685	0.918088	0.835734	0.894847
118.00	0.991525	0.974791	C.918422	0.836372	0.895270
118.50	0.991561	0.974897	0.918753	0.837005	0.895690
119.00	C.991596	0.975001	0.919082	0.837634	0.896106
119.50	C.991631	0.975105	C.919408	0.838257	0.896519
120.00	0.991666	0.975208	0.919731	0.838876	0.896929
120.50	0.991701	0.975310	0.920052	0.839490	0.897336
121.00	0.991735	0.975411	C.920370	C.840099	0.897739
121.50	0.991769	0.975511	C.920685	0.840704	0.898139
122.00	0.991803	0.975611	C.920998	0.841305	0.898536
122.50	C.991836	0.975710	0.921309	0.841900	0.898930
123.00	0.991869	0.975808	0.921617	0.842492	0.899321
123.50	0.991902	0.975905	C.921923	0.843079	0.899709
124.00	C.991935	0.976001	0.922226	0.843661	C.900094
124.50	0.991967	0.976097	0.922527	0.844239	0.900476
125.00	0.992000	C.976191	C.922826	C.844813	0.900856
125.50	C.992031	0.976286	0.923123	0.845383	0.901232
126.00	0.992063	0.976379	0.923417	0.845949	0.901605
126.50	C.992094	0.976472	C.923709	0.846510	0.901976
127.00	0.992125	0.976563	0.923998	0.847068	0.902344
127.50	0.992156	0.976655	0.924286	0.847621	0.902709
128.00	C.992187	0.976745	0.924571	0.848171	0.903071
128.50	0.992217	0.976835	0.924855	0.848716	0.903431
129.00	0.992248	0.976924	0.925136	0.849258	C.903788
129.50	C.992277	0.977012	C.925415	0.849796	0.904142
130.00	C.992307	0.977100	0.925692	0.850330	0.904494
130.50	0.992337	0.977187	C.925967	0.850860	0.904843
131.00	0.992366	0.977274	0.926239	0.851387	0.905190
131.50	0.992395	0.977359	0.926510	0.851909	0.905534
132.00	0.992424	0.977444	0.926779	0.852428	0.905876
132.50	C.992452	0.977529	0.927046	0.852944	0.906215
133.00	0.992481	0.977613	C.927311	0.853456	0.906552
133.50	C.992509	0.977696	0.927574	0.853964	0.906886
134.00	0.992537	0.977779	0.927835	0.854469	0.907218
134.50	0.992565	0.977861	0.928095	0.854970	0.907548
135.00	C.992592	0.977942	0.928352	0.855468	0.907875
135.50	0.992619	0.978023	C.928608	0.855963	C.908200
136.00	C.992647	0.978103	C.928862	0.856454	0.908523
136.50	0.992673	0.978182	C.929114	0.856942	0.908843
137.00	0.992700	0.978262	C.929364	0.857427	0.909161
137.50	0.992727	0.978340	0.929612	0.857908	0.909477

NORMALISED HYPERBOLIC BESSEL FUNCTIONS OF Z FROM 0 TO 150

Z	ORDER				
	3/2	5/2	9/2	13/2	(5/2)X(9/2)
138.05	0.992756	0.978426	0.929894	0.858434	0.909822
138.60	0.992784	0.978511	0.930153	0.858956	0.910165
139.15	0.992813	0.978595	0.930420	0.859474	0.910505
139.70	0.992841	0.978679	0.930685	0.859988	0.910842
140.25	0.992869	0.978762	0.930948	0.860498	0.911177
140.80	0.992897	0.978844	0.931209	0.861005	0.911509
141.35	0.992925	0.978926	0.931468	0.861508	0.911839
141.90	0.992952	0.979007	0.931726	0.862008	0.912166
142.45	0.992979	0.979087	0.931981	0.862504	0.912491
143.00	0.993006	0.979167	0.932234	0.862996	0.912814
143.55	0.993033	0.979246	0.932486	0.863485	0.913134
144.10	0.993060	0.979325	0.932736	0.863970	0.913452
144.65	0.993086	0.979403	0.932983	0.864452	0.913767
145.20	0.993112	0.979481	0.933229	0.864931	0.914081
145.75	0.993138	0.979558	0.933474	0.865406	0.914391
146.30	0.993164	0.979634	0.933716	0.865878	0.914700
146.85	0.993190	0.979710	0.933957	0.866347	0.915007
147.40	0.993215	0.979785	0.934196	0.866812	0.915311
147.95	0.993240	0.979859	0.934433	0.867274	0.915613
148.50	0.993265	0.979934	0.934668	0.867733	0.915913
149.05	0.993290	0.980007	0.934902	0.868189	0.916211
149.60	0.993315	0.980080	0.935134	0.868641	0.916507
150.15	0.993339	0.980153	0.935365	0.869091	0.916800